CORRELATING RAMAN SPECTRA WITH CHANGES THAT OCCUR IN THE NORMAL CERVIX: CONFOUNDING FACTORS AND PREGNANCY

By

Elizabeth Ann Vargis

Dissertation

Submitted to the Faculty of the

Graduate School of Vanderbilt University

in partial fulfillment of the requirements

of the degree of

DOCTOR OF PHILOSOPHY

in

Biomedical Engineering

May, 2012

Nashville, Tennessee

Approved:

Professor Anita Mahadevan-Jansen, Chair

Professor Ayman Al-Hendy

Professor Todd D. Giorgio

Professor E. Duco Jansen

Professor Dineo Khabele

In honor of

Sudha John

G. Shyamala

and

Dean Paras

ACKNOWLEDGEMENTS

This work was made possible by the financial support of a National Cancer Institute grant and a Ruth Kirschstein National Institutes of Health fellowship. A fellowship from the Vanderbilt Institute for Integrative Biosystems Research and Education (VIIBRE), a grant from the Vanderbilt Institute for Clinical and Translational Research (VICTR) for patient compensation, funding from the Obstetrics and Gynecology department at Vanderbilt University and the Lai Sulin Scholarship were also all instrumental in the completion of this dissertation.

I would like to thank my advisor Dr. Anita Mahadevan-Jansen for her help and guidance over the last 4 years. My dissertation committee members – Dr. Dineo Khabele, Dr. Ayman Al-Hendy, Dr. Todd Giorgio and Dr. Duco Jansen – were also instrumental in the completion of this work. I would like to thank my committee-like members, Dr. Teresa Byrd, Dr. Jeff Reese and Dr. Kelly Bennett, who took time to discuss my project, let me latch on to their research or their clinics, and consistently steered me in the right direction. I also worked with resident physicians, Drs. Kesha Robertson, Nathan Webb and Quinisha Logan, who found time in their busy schedules to help me with my projects. Lastly, thank you to the staff and nurses at Meharry Medical College and throughout Vanderbilt University who made it possible to obtain measurements in the clinic, from patient samples and from mice.

There are a number of students, postdoctoral scholars and research staff who also helped me throughout my PhD. Amy Rudin, our research nurse, is not only the reason my studies were approved and remained approved, but she is also the reason the human pregnancy data was collected – she consented patients, kept track of their schedules and, in many cases, held the probe to acquire the data. More recently, she has provided me with a home in Nashville,

complete with a couple of parents, a sister that I've always wanted and a wonderful Dalmatian. Isaac Pence is only a second-year graduate student, but his help in thinking about how to collect, analyze and interpret my Raman data has been an immeasurable resource. I truly hope there is someone like Isaac in all my future research endeavors. I also thank Matt Keller who taught me about Raman spectroscopy initially and has continued to advise me, even from Seattle. Receiving an email from him with 20-30 emoticons is something I hope will continue forever. Another thanks goes to Chetan Patil who spent a lot of time assisting me in understanding my data and explaining it to other people. Of course, previous PhD students Elizabeth Kanter and Amy Robichaux-Viehoever were also helpful throughout. Besides those already mentioned, thank you to my office mates, from the Biophotonics and Dr. Rick Haselton's labs who have made my time in graduate school enjoyable and memorable.

Finally, I would like to thank my family, friends and pets for their encouragement during my graduate studies. Thank you to my husband Nick who has been supportive throughout and whose efficiency at performing research is something I strive to emulate. And thank you to my parents who have motivated me and have finally stopped sending me emails about other career options. Lastly, my dog Olivia was often dragged back to the office for late-night work. I appreciate her patience and her constant willingness to run around the hallways of Stevenson with me.

I was initially motivated to pursue graduate work when my dear friend Sudha John passed away at the age of 34 after being diagnosed with breast cancer. During my time in graduate school, my undergraduate research advisor, Dr. G. Shyamala and another close friend, Dean Paras, both passed away, leaving this world entirely too soon. Their memories will continue to inspire my pursuits in biomedical research.

TABLE OF CONTENTS

LIST OF FIGURES

LIST OF TABLES

CHAPTER 1

INTRODUCTION

1.1 Motivation and Objectives

The goal of this PhD is to correlate changes that occur in the uterine cervix to differences seen in Raman spectra. This work shows that the sensitivity of Raman spectroscopy (RS) to cervical changes can be used to detect cervical dysplasia and the changes associated with pregnancy in humans and mice.

In 2012, it is estimated that over 12,170 women will be diagnosed with new cases of invasive cervical cancer and over 4,220 women will die of the disease in the US alone.[1] Worldwide, from statistics gathered in 2010, there are over 529,000 new cases and 275,000 deaths each year resulting from cervical cancer, making it the second most common cancer in women worldwide and the most common cancer in women in developing countries.[1] The use of the Papanicolaou (Pap) smear starting in the early 1950s has led to a large decrease in mortality from this disease.[2] The recent introduction of vaccinations against high-risk strains of human papillomavirus (HPV, the virus that causes over 99% of cervical cancer cases) and HPV DNA testing has the potential to further reduce the incidence and mortality rates of cervical cancer. However, there are disadvantages to both of these advances: The vaccines only protect against 2 of the 15 high-risk strains of HPV and the DNA test requires expensive equipment. Furthermore, these new developments have not been implemented in lower-resource settings. One of the goals of this research is to use RS, an optical technique, to screen for and diagnose cervical dysplasia *in vivo*. Before this application can be implemented in a clinical setting, changes that may occur

due to ethnicity, body mass index (BMI), HPV infection, previous disease, proximity to disease, previous pregnancies or health insurance status (a measure of socioeconomic status), must be investigated; important factors will be identified and studied in this dissertation.

Pregnancy is another event that leads to significant changes in the cervix and preterm labor is a problem associated with abnormal changes of the uterine cervix. One in eight pregnancies is preterm, making preterm birth the leading cause of perinatal morbidity and mortality. Despite significant research funding, the rate of preterm labor has been increasing over the last decade. Preterm labor can cause a myriad of complications for both the mother, such as blood loss and sterility, and the child, such as brain damage, chronic lung diseases, and long-term physical and mental disabilities. The exact causes of preterm birth are largely unknown and while some risk factors exist (i.e. if a woman has had a previous preterm birth), over half of all preterm births fall into no "at-risk" category. Currently, there are no accurate quantitative assessments to determine a woman's risk of developing preterm labor. One goal of this project is to use Raman spectral measurements to identify changes associated with pregnancy in the cervix. As Raman spectra from the cervix of pregnant women have never been acquired, obtaining data from pregnant mice to determine the detailed effects of pregnancy on Raman spectra will be completed first. Finally, a small pilot study acquiring Raman spectra from pregnant women to see if significant changes can be identified prior to the onset of labor will be completed.

Therefore, the overall objective of this doctoral project is to characterize the effects that normal, physiological changes in the cervix have on Raman spectra in order to more accurately distinguish among differences that exist between normal and precancerous tissue and between low- and high-risk pregnancies.

1.2 Specific Aims

Specific Aim (1): Characterize variability of Raman spectra in normal and diseased cervix. Previous studies have shown that classifying Raman spectra based on hormonal status (i.e. ovulation status or menopausal state) before statistical analysis greatly increases the sensitivity and specificity of RS.[3, 4] In this aim, further clinical studies were performed on a diverse population to evaluate the effect of other factors on the cervix and, therefore, the Raman spectra. These spectra were obtained from the cervix of women at Nashville General Hospital at Meharry Medical College undergoing an annual Pap smear exam or a colposcopy-guided biopsy using a fiber-optic probe-based portable RS system. Patients with a history of disease and with a normal cervix were recruited into the study. Factors such as socioeconomic status, BMI, previous pregnancies, and ethnicity were considered. Changes associated with these factors were then correlated to the Raman spectra and their effect on disease classification was evaluated.

Specific Aim (2): Develop Raman microspectroscopy for the detection of HPV, HPV-strain and malignancy. Two high-risk HPV strains (16 and 18) were also examined under a cell culture setting to determine their effect; in this case, spectra were obtained using a Raman microscope system. They were compared to two other cell lines: malignant but HPV-negative and benign (normal). HPV-positive and HPV-negative patient samples were also obtained and examined to determine if RS is sensitive to HPV infection.

Specific Aim (3): Understand the relationship between Raman spectra and pregnancy in normal mice. In this aim, a normal mouse strain was used. Raman spectra were acquired *in vivo* and *ex vivo* from the mouse cervix at various time points before, during, and after pregnancy (19

day gestation) with a portable system similar to the one used in Aim (1). After the cervix was excised from the mouse, biomechanical tests and histological staining were performed to correlate different types of information from the tissue with the differences seen in the Raman spectra. A classification algorithm was also used to classify the Raman data based on the time point within pregnancy.

In Appendix 1, a pilot, *in vivo* study validating the ability of RS to detect changes in the cervix during human pregnancy is discussed. Raman spectra were acquired from the cervix of patients at five time points during their pregnancy and one point six weeks after their pregnancy or weekly during their third trimester using the portable Raman system from Aims 1 and 3. Women experiencing a normal pregnancy were recruited to the study. The feasibility of using a Raman system in the clinic to detect the onset labor was investigated. A classification algorithm was again used to determine if significant changes can be detected in the Raman spectra as a function of pregnancy.

The combination of these three aims and Appendix 1 serves to continue exploring the effects of normal factors, such as ethnicity, BMI, HPV infection, health insurance status, previous disease and pregnancy, on Raman spectra of the cervix. The completion of this project demonstrates that the sensitivity of RS to normal changes in the cervix can be utilized to determine which differences are normal and which are indicative of abnormal changes. Understanding these changes resulted in higher classification accuracies of spectra acquired from areas of cervical dysplasia and in finding spectral differences associated with pregnancy in mice and humans.

1.3 Summary of Chapters

Following this introductory chapter, Chapter 2 contains relevant background information on the biology of the cervix, cervical dysplasia and preterm labor, as well as various types of optical spectroscopy techniques, including RS. Chapter 3 details the preliminary results that were used as the basis of this research.

Chapter 4 provides the first report on the sensitivity of RS from this research, specifically the differences between areas near disease, areas that have had previous disease and a "true normal" area, a region without any previous or current disease.

In Chapter 5, the effect of four normal patient variables (BMI, obstetric history, race/ethnicity, health insurance status) on data obtained from true normal cervical tissue *in vivo* is examined.

Chapter 6 contains the details of ranking normal patient variables listed above, as well as ovulation and menopause (previously examined) to increase the classification accuracy of spectra acquired from areas of cervical disease.

Chapter 7 has the results of a cell culture and patient sample study using Raman microspectroscopy to detect high-risk HPV infection. It also contains the effect of copy number, HPV infection type and malignancy without HPV infection.

Chapter 8 describes the research using RS to monitor biochemical changes that occur during a mouse pregnancy, verifying the Raman data with tissue testing (mechanical testing) and histology.

Chapter 9 provides a summary of the major results presented in this dissertation and potential future directions for this project. It also contains information about the impact of this research on the larger scientific field and society.

Appendix 1 is a short summary of the pilot *in vivo* human pregnancy study using RS to examine the changes in the cervix during and after pregnancy.

Appendix 2 defines and describes the mathematical processes used in these studies.

1.4 References

1. American Cancer Society, "Cancer Facts and Figures 2012," (American Cancer Society, Atlanta, 2011).

2. Anderson, G.H., Boyes D.A., Benedet J.L., Le Riche J.C., Matisic J.P., Suen K.C., Worth A.J., Millner A. and Bennett O.M. "Organisation and Results of the Cervical Cytology Screening-Program in British-Columbia, 1955-85." *Brit Med J* **296**, 975-978 (1988).

3. Kanter, E.M., Majumder, S., Kanter, G.J., Woeste, E.M. and Mahadevan-Jansen, A. "Effect of hormonal variation on Raman spectra for cervical disease detection." *Am J Obstet Gynecol* **200**, 512-512 (2009).

4. Kanter E.M., Vargis E., Majumder S., Keller M.D., Beaven R.B., Rao G.G. and Mahadevan-Jansen A. "Application of Raman spectroscopy for Cervical Dysplasia Diagnosis." *J Biophotonics* **2**, 81-90 (2009).

CHAPTER 2

BACKGROUND

2.1 Normal Cervix

Figure 2.1 Picture of a normal cervix (Courtesy of the University of Washington).

The cervix consists of squamous and columnar epithelium. Multiple layers of squamous epithelia cover most of the ectocervix and are separated from the stroma by the basal layer. A normal cervix is shown in Figure 2.1. The columnar epithelium consists of a single layer of columnar cells, covering the surface of the endocervical canal. The interface of the two epithelia is called the squamo-columnar junction. In a normal cervix, the columnar epithelium is replaced by squamous epithelium, causing the squamo-columnar junction to move towards the opening of the cervix (os). This transitional epithelium is termed squamous metaplasia.[1] Virtually all squamous cervical neoplasias begin at the squamo-columnar junction, with their precursors coming from the transformation zone.[2] An atypical cervix may result from different pathologies. Cervicitis or inflammation, which may or may not be due to infection, is usually the response of tissue to injury and is a by-product of the natural repair mechanism.[2] It is a benign condition.

Squamous metaplasia is also a benign change in the cervix associated with irritation, inflammation, and low vaginal pH.

2.2 Normal Changes in the Cervix Throughout a Woman's Lifetime

Luteinizing hormone (LH) and follicular stimulating hormone (FSH) are two important gonadotropic hormones produced by the anterior pituitary gland (Figure 2.2). They work in tandem during reproduction. Ovulation is induced by a large burst of LH. It also controls the length and sequence of the menstrual cycle, which includes ovulation, preparation of the uterus for implantation of the fertilized egg, and production of estrogen and progesterone from the ovaries. FSH promotes the recruitment and maturation of eggs by the ovaries. It stimulates the production of estradiol during the first half of a woman's menstrual cycle. FSH levels are low during childhood and high after menopause.

During each cycle, the cervix undergoes many changes. One role of estrogen is to regulate the consistency and composition of cervical mucus. Also, as estrogen levels rise, the os gradually opens, softening the cervix and a watery, elastic mucus is produced.[3] From puberty to menopause, these levels fluctuate typically on a 28-day cycle (Figure 2.2). Estrogen is responsible for the maintenance and maturation of the uterus, fallopian tubes, cervix, and vagina.

Progesterone is another important hormone of the female reproductive system. Along with estrogen, it causes the lining of the uterus to thicken, preparing for implantation of the fertilized egg. It is produced by the corpus luteum, which is formed by a ruptured follicle after an egg is released. If the egg is not fertilized, the corpus luteum dissolves, and progesterone is no longer produced. Estrogen levels then decrease, the lining of the uterus breaks down, and a new menstrual cycle begins.[4]

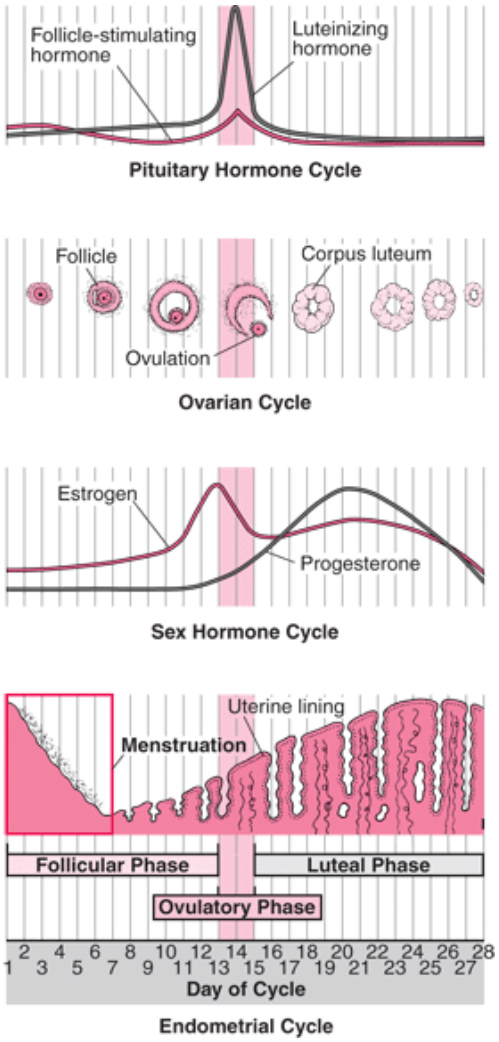

Figure 2.2. The menstrual cycle is regulated by four important hormones: LH, FSH, estrogen, and progesterone (©2003 Merck).

Menopause is defined as the permanent cessation of the menstrual cycle in the female reproductive system. Perimenopause is defined as the transitional period from normal menstrual periods to no periods at all. During menopause, the ovarian source of estrogen disappears and estrogen levels decline rapidly (Figure 2.3). This decrease results in several physiological changes, such as the thinning of the vaginal epithelium, decreased vaginal secretions, and vascular instability.[3] The transition can take up to ten years and is associated with hormonal,

physical, and physiological changes which can affect the spectral signatures of cervical tissue.

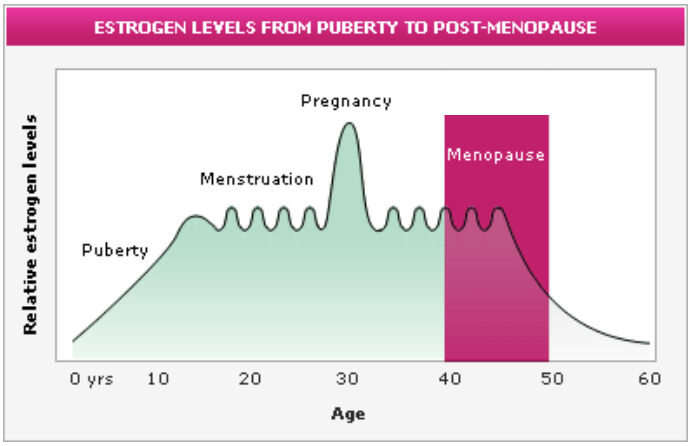

Figure 2.3. Estrogen levels from puberty to menopause (©2006 Promensil)

2.3 Changes During Pregnancy

A wide range of changes occur as a woman progresses through her pregnancy, from an enlarged uterus, an increase in vaginal discharge, larger breasts, and a rising heart rate. These transformations are initiated and promoted by varying hormone levels, regulated by hormones released by the hypothalamus (Figure 2.4). A few of the important hormones are LH, FSH, estrogen, progesterone, and beta-human chorionic gonadotropic hormone (b-HCG). After an egg is fertilized, these hormones promote and regulate the changes that occur.

The first four hormones are also important for menstruation, triggering ovulation and preparing the uterus for implantation of the fertilized egg. The roles of LH and FSH have been discussed above. Progesterone and estrogen are critical during the course of the pregnancy; they are both continuously produced, first by the corpus luteum in the ovaries and then by the placenta, with their levels increasing until right before labor. Estrogen regulates the level of progesterone over the full term of pregnancy and is a key factor in fetal development. Organs such as the lungs, kidneys, liver, and adrenal glands need estrogen in order to mature. It also

plays an important role for the mother, assisting in the lactation process and promoting blood flow within the uterus. Progesterone works in tandem with estrogen, maintaining the functions of the placenta and keeping the endometrium thick. In order to prevent infection, progesterone keeps the cervix covered by strengthening its mucus plug. It also strengthens the pelvic walls in preparation for labor, while at the same time, preventing the uterus from contracting. The decrease in progesterone starts the contractions that eventually lead to labor. b-HCG is released after the fertilized egg is implanted into the uterine wall. Its main role is to stimulate the corpus luteum to produce progesterone and estrogen during the early part of pregnancy (8-9 weeks), before the placenta has matured enough to produce those hormones on its own. Presence of b-HCG is tested in pregnancy tests as well as the "Triple Test," where elevated levels of b-HCG, along with some other factors, can be indicative of neural tube defects or Down syndrome.

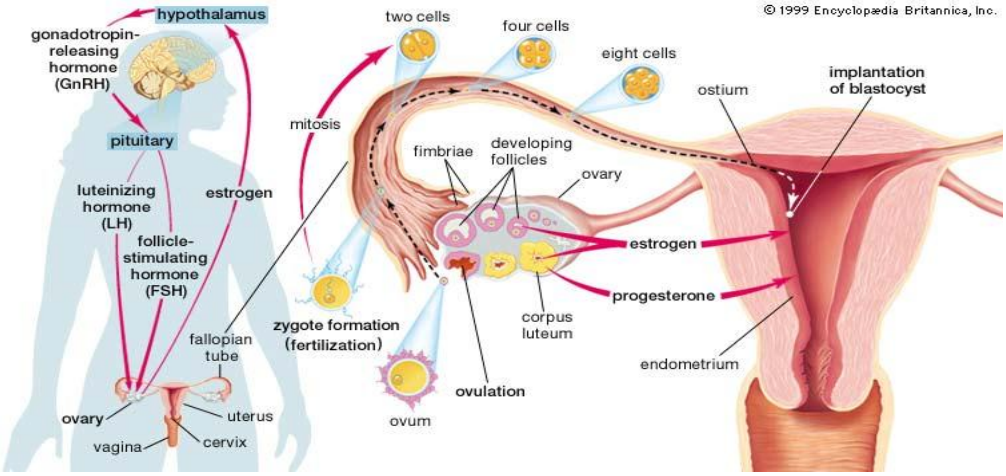

Figure 2.4. A snapshot of the events that occur at the beginning of pregnancy.

The most important event that happens in the cervix during pregnancy is cervical ripening, where the cervix softens, effaces, and dilates to prepare for labor (Figure 2.5). This complicated process is regulated throughout pregnancy by many hormones, specifically relaxin and oxytocin. Relaxin triggers the softening and stretching of the cervix and the relaxing of the

pelvic muscles. Produced by the corpus luteum and the placenta, its level tends to reach its peak during the 14th week of pregnancy and at delivery. While some studies show that the presence of relaxin can lead to decreased collagen accumulation and an increase in cervical cell proliferation, the exact mechanism of its effect on the cervix during pregnancy remains unknown.[5] The second hormone is oxytocin, which acts in response to cervical stretching to make the uterus contract and to stimulate milk production in the mammary glands. The high levels of progesterone throughout pregnancy prevent oxytocin from being effective; progesterone's rapid decrease prior to labor results in oxytocin's effects.

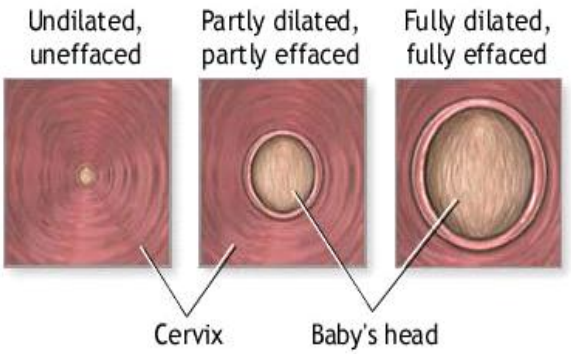

Figure 2.5 Cervical softening, ripening, and effacing occur as a woman's body prepares for birth. (©ADAM)

All of the hormones mentioned above play a vital role in regulating the downstream effects of a wide range of molecules, like collagen, elastin, and aquaporin water channels. Not only do collagen levels decrease during pregnancy, but, based on luminosity measurements, the collagen fibers also become highly unorganized.[6] Elastin has a role in keeping the cervix closed and not dilated during pregnancy.[7] Increasing concentrations of aquaporin channels during pregnancy lead to a higher water content and causes cervical dilation.[8] There are many more hormones and proteins involved in the cervical ripening process than mentioned here. Together, they are responsible for keeping the cervix strong during most of pregnancy, until right before

labor, where a number of changes quickly occur to soften, efface, and dilate the cervix in preparation for labor and birth.

2.4 Other Factors that May Affect the Cervix

A variety of other factors can lead to downstream changes that affect hormone levels and other factors that can then lead to changes in the tissue. Some of these factors are body mass index (BMI), ethnicity, and socioeconomic factors. Many of the studies described below are based on epidemiological data and/or correlative results. Although the mechanisms behind how these factors influence changes that then affect the cervix is not explicitly known or understood, their role in changing the normal, baseline cervix must be considered.

In general, black and Hispanic women have higher cervical cancer rates than white women.[9] Higher BMIs and lower socioeconomic classes may be the cause, but some studies have found that levels of hormones and hormone receptors may vary on the basis of race or ethnicity alone. For example, studies have shown that hormones such as estrogen and testosterone can vary dramatically between white, black, Asian, and Hispanic groups.[10, 11] On the other hand, some studies have found that there are more estrogen-receptor-negative cases of breast cancer in black women, which may mean that even if there are elevated estrogen levels in black women, the more aggressive breast tumor type is found more often.[12] Differences even exist at the gene level, such as increasing levels of estrogen receptor α found in black Americans.[13] Variations with circulating levels of hormones like thyroid-stimulating hormones also exist.[10] Also, there are some cultural activities, like douching, that change the vaginal flora; some studies even report that this can lead to an increased incidence of cervical dysplasia, pelvic inflammatory disease, and Chlamydia infections.[14, 15]

Body mass index (BMI) is a value that estimates a healthy body weight based on how tall the person is; the equation is as follows:

$$\mathrm{BMI} = \frac{\mathrm{weight\,(kg)}}{\mathrm{height}^{2}\,(\mathrm{m}^{2})}.$$

Typical ranges of BMI, as defined by the World Health Organization (WHO), are found in Table 2.1. Many research groups believe that other measurements like waist circumference are more accurate in explaining obesity-related health risks, particularly in Asian populations due to different body proportions.[16] However, BMI is still the most widely used measure of health in terms of weight.

BMI Value (kg/m^2)	**Category**
16.5-18.49	Underweight
18.50-24.99	Normal
25.00-29.99	Overweight
Greater than 30	Obese

Table 2.1. Health categories based on BMI values, as determined by the WHO.

Obesity has been linked to greater risks of heart disease, diabetes, cancer, and Alzheimer's. Many studies have explored the reasoning behind why obesity can lead to increased disease. Some studies postulate that the extra adipose tissue produces additional hormones and other molecules that then lead to these increased risks. For example, research has shown that due to increased amounts of androgens in adipose tissue, aromatized, circulating estrogen levels are usually elevated in people with higher BMIs.[17] Some studies have linked these higher levels of estrogen to an increased risk of breast carcinoma.[18] Fat tissue also may be a storage site for toxins, which could also serve as a continuous, living source of carcinogens.[19] In addition, this

adipose tissue is a source of insulin and insulin-like growth factors, which have been associated with a higher incidence of carcinoma.[20] Finally, women with higher BMIs may have a compromised immune system since androgens appear to suppress it, making the body less capable of recognizing and eliminating neoplastic cells.[17]

In general, most cancers also occur at a higher rate in lower socioeconomic classes due to less access to hospitals, primary care, physicians, and clinics.[21] Lower socioeconomic classes also tend to have a lower level of education. Many factors, such as access to consistent health care, food intake and use of hygiene products may differ within this population compared to the population at large. The combination of these factors, as well as the general psychological distress that can be felt during a medical exam, make health screenings and follow-up appointments a tremendous hurdle within this population.[22] A study by Miller *et al*. found that close to 61% of women from inner cities did not show up for follow-up visits after an abnormal Pap smear.[23] While there may be no physiological mechanism behind the changes that occur in lower socioeconomic classes, there is a need to evaluate how a normal cervix may change under these conditions. Any significant differences between populations need to be determined in order to create a tool for successfully diagnosing malignant changes in the cervix.

2.5 Cervical Cancer

In 2012, it is estimated that over 12,170 women will be diagnosed with new cases of invasive cervical cancer and over 4,220 women will die of the disease in the US alone.[24] Worldwide, from statistics gathered in 2010, there are over 529,000 new cases and 275,000 deaths each year resulting from cervical cancer, making it the second most common cancer in women worldwide and the most common cancer in women in developing countries.[24] Although

early detection of cervical dysplasia has played a key role in reducing the mortality associated with this disease over the last 50 years,[25] the incidence of pre-invasive squamous cervical carcinoma has risen dramatically, especially among women under the age of 50,[26] demonstrating the continued need for an effective diagnostic tool.

Cervical intraepithelial neoplasia (CIN) refers to the development of neoplasia arising from the epithelium of the cervix. CIN refers to the precancerous stages of cervical carcinoma and is often also referred to as cervical dysplasia. The progression can be seen between Figure 2.6a and Figure 2.6b. Precancers may be categorized as mild (Figure 2.6a), moderate, or severe dysplasia or precancer. The next step in the progression of this disease is carcinoma-in-situ CIS) which is one step before the transformation of the dysplasia to cancer (Figure 2.6b).[2, 27, 28] Clinically speaking, cervical lesions can be divided into low-grade lesions (mild dysplasia) and high-grade lesions (moderate or severe dysplasia and CIS). This distinction is important as patients with low-grade lesions usually come more often for Pap smears (i.e. every 6 months), but are not treated. Patients with high-grade lesions are usually treated immediately and go through extended follow-up appointments.

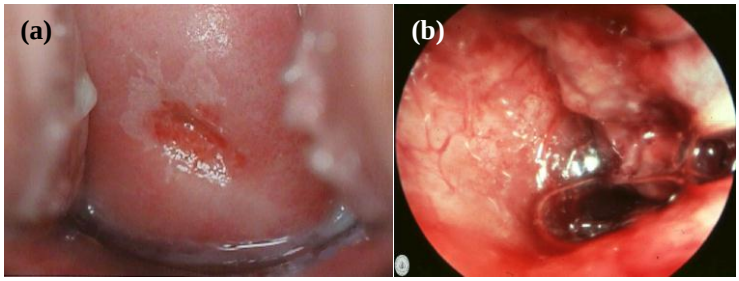

Figure 2.6. Progression of Cervical Disease from (a) mild dysplasia with abnormal area that turned white after application of acetic acid (courtesy of the Military Obstetrics & Gynecology) and (b) cervical cancer (Courtesy of Dr. Alicia Ubeda Hernandez)

Cervical dysplasia can occur any time after a female becomes sexually active since most cases of cervical dysplasia are caused by a sexually transmitted HPV infection. Cervical cancer,

on the other hand, usually occurs in women after the age of 40. In clinical practice, women 65 and older who have had at least three normal Pap tests and no abnormal Pap tests in the last 10 years may stop having annual Pap smears.[29] Therefore, most cervical precancer cases occur before women go through menopause and most cervical cancer develops in women who are either perimenopausal or menopausal. Most likely, this slow progression is due to the normal maintenance that occurs at the sqamo-columnar junction, as cells are dying and being replenished in this region.

2.5.1 HPV Infection

Human papillomaviruses (HPV) predominantly infect skin and mucosal membranes to promote epithelial proliferation. This extraneous proliferation can lead to malignant transformations, even though most HPV infections have no symptoms and go into remission over the course of a few years.[2] A number of studies have determined that certain strains of HPV are involved in the early stages of precancer and other strains may aid in the progression of the disease.[30] Some HPV infections, therefore, are placed in the same category as mild precancers (low-grade lesions) and are clinically treated as such. An HPV vaccine (released in fall 2006), Gardasil™, has been shown to prevent infection from HPV 16 and 18 that together cause 70% of cervical cancer cases worldwide. Gardasil™ also protects against HPV 6 and 11, which account for 90% of genital warts cases. This vaccine, a sequence of 3 shots over a 6-month time period, is available to women ages 9-26. However, females are not protected if they have been infected with HPV prior to the vaccination. Additionally, Gardasil™ does not protect against the other 12 high-risk (but less common) HPV types. Although the vaccination is a huge step towards eradicating cervical cancer, the vaccination is currently voluntary and the other high-risk HPV

strains still pose a great danger, particularly in countries other than the United States.[29, 31]

HPV, identified in humans more than 40 years ago,[32] has a small, circular, double-stranded DNA genome. Even though they are small, with only 8 pairs of genes, they are quite complex. E5, E6, and E7 are three oncogenes found in most high-risk strands of HPV that regulate the transformation process. E6 and E7 proteins cause cell damage and abnormal cell proliferation by cooperatively interfering with functions of cellular tumor suppressor proteins, p53 and pRb, respectively.[33] Two regulatory proteins (E1 and E2) modulate transcription and replication. L1 and L2 are two structural proteins that make up the viral capsid.[34] An infection occurs when the virus infects the basal cells of human epithelial tissues. During cellular reproduction, some infected basal cells reproduce. Infected virions are only produced in terminally differentiated cells, which then shed as squamous cells filled with more viruses. Since HPV only infects cells in the basal layer and replicates only in fully differentiated cells, it can usually remain undetected by the immune system, avoiding a humoral or cell-mediated immune response.[34] HPV infection can lead to chronic inflammation, which may recruit a host of proteins such as chemokines which aid in cell proliferation and growth.[35]

2.5.2 Screening Methods

The primary screening tool for cervical precancer is the Pap smear, where scrapings from the walls of the ecto- and endocervix are examined and diagnosed.[36] Although the widespread application of the Pap smear as a screening tool has greatly decreased the incidence of cervical cancer,[37] sampling and reading errors still lead to high false positive and negative rates. A meta-analysis of the accuracy of Pap smears showed that in low-risk populations, the mean sensitivity and specificity of the Pap smear was 48% and 95%, respectively.[38] Another meta-analysis which

looked at a more diverse population found a mean sensitivity of 58% and a specificity of 69%,.[39] Results from both of these studies suggest that the presence and specific identification of cervical dysplasia is often incorrect. The annual Pap smear is the standard of care amongst women in the developed countries. However, for most women in developing countries, Pap smears are not available. In such areas, if the disease is found, it is often already progressed to a later stage.

When a woman has an abnormal Pap smear result, biopsies are taken from the cervix during a colposcopic exam.[26] A colposcope consists of a fixed focal length microscope with a variable magnification (4-40x) to observe the surface of the cervix. The colposcopic image is produced by illuminating both the surface epithelium and the underlying stroma. To enhance the colposcopic image, 4-6% acetic acid is applied to the cervix to turn abnormal areas white (Figure 2.6a). This process is reversible; as the acetic acid is depleted, the change reverts to normal. This technique can be used repeatedly on the same patient without harm. Acetic acid whitens abnormal areas of the cervix by briefly coagulating proteins and dehydrating intracellular components. Optically, acetic acid causes the cells to become more refractive, which in turn leads to more light being reflected towards the viewer. This amount of coagulation increases if the nuceli are large and the cytoplasm contains more protein, which occurs with metaplasia and dysplasia.

Colposcopy, compared to Pap smear, has a high degree of accuracy in finding the lesion and assessing its grade.[40] However, using a colposcope requires extensive training and even in the hands of expert practitioners, it has a variable accuracy.[41] As a result, colposcopy is limited and it cannot be used as a stand-alone method for diagnosis. If abnormal sites are identified colposcopically, multiple biopsies are taken using standard punch biopsy forceps. These tissue samples are fixed in formalin and then sent for histological examination. Histology then forms

the gold standard for diagnosis and determination of treatment.

Several new techniques for cervical disease detection have been introduced in the past few years, such as wet prep and cervicography. Wet prep, or liquid-based thin-layer slide preparation, modifies conventional Pap smear. This technique rinses the cells into a vial of liquid instead of smearing them onto a slide, reducing cell clumping and making the final slide earlier to read. Results of this method suggest that it may reduce reading error, making it more sensitive than conventional Pap smear for detecting cervical abnormalities.[29] Wet prep is now routinely used in conjunction with the Pap smear. In cervicography, a high-resolution photograph is taken of the cervix after application of acetic acid. This photo is then sent to a laboratory to be read by colposcopists who have received specialized training in interpretation of these photographs. Cervicography would not only eliminate the need for trained colposcopists to look at each individual cervix, but it would also standardize how these images are interpreted.[42] The main disadvantage of this method is the increased amount of time needed for the photographs to be read. HPV-infection is also routinely tested for during Pap smear and colposcopy-guided biopsy; this DNA assay tests for all high-risk HPV types, including 16, 18, and 13 others.[43] A positive result indicates infection with one of those types, without identification of the specific one. A recent FDA-approved study tests for the presence of strains 16 and 18 only (not specifically). However, it is currently not being using in most clinics.[44]

Existing screening and diagnostic techniques for cervical precancers have several deficiencies that prevent efficient management of an otherwise controllable disease. Standard of care ultimately continues to rely on histology for a definitive diagnosis before treatment is planned. An accurate, automated diagnostic method could allow for faster, more effective patient management.

2.6 Preterm Labor

Preterm labor or when birth occurs before week 37 of pregnancy (typical pregnancies last 38-42 weeks), affects 1 in 8 pregnancies. Preterm birth is the second leading cause of infant mortality, causing over 17% of all infant deaths and 75% of infants that have perinatal death are premature.[45] Preterm birth can result in a wide array of complications for the mother and baby (if born), including cerebral palsy, developmental delay, visual and hearing impairment, and chronic lung disease.[46] Even with the current advances in medical knowledge and research, the rate of preterm labor has been steadily increasing over the last few decades. While all races and ethnicities suffer from preterm birth, it is particularly dominant within the black community.[47] Preterm birth is the number one cause of infant mortality in this population, causing over 20% of infant deaths. Infants born to black women have an infant death rate due to preterm birth four times higher than those born to Caucasian women.[48]

The reasons for preterm labor remain largely unknown. Various factors, from a rapid decrease in collagen content[49] to improper hormone levels,[50] have been implicated in occurring during preterm labor, but none have been determined as the sole cause. While some populations are at risk for preterm labor (women who have had a previous preterm birth, are pregnant with more than one child, or have uterine/cervical abnormalities), over half of all women who have preterm births do not fall into any known high-risk category.[51] At this time, there is no way to predict preterm labor, making its prevention and treatment virtually impossible. There are four accepted causes of preterm birth: (1) premature activation of the fetal hypothalamic-pituitary axis, (2) infection/inflammation, (3) hemorrhage/ischemia, and (4) uterine overdistention.[52] Each of these causes may lead to inappropriate uterine contractions and cervical dilation.[53]

Preventing preterm labor even for a day is beneficial. When doctors can diagnose preterm

labor, they have the option of prescribing corticosteroids or tocolytics to increase the time a baby spends in the womb, which can greatly help brain and lung development and improve the odds of survival. These drugs, given at the earliest sign of preterm labor, can delay delivery from 2-7 days and reduce infant death by 30%.[54] They can also reduce the two most serious complications of preterm birth: respiratory distress and bleeding in the brain. Another treatment that has been investigated is catechol-*O*-methyltransferase inhibition, which is the enzyme that catalyzes the methylation of hydroxyestrogens to methoxyestrogens.[55]

2.6.1 Screening Methods

Two clinical tests can be used to identify women at risk for preterm birth. The first method is based on measuring the length of the cervix. At the first prenatal visit, the length of the cervix is measured as a baseline and changes to this measurement are monitored during pregnancy.[56] In subsequent prenatal visits, if the cervix changes by becoming shorter too quickly, this may imply that the cervix is beginning to thin out, which could lead to preterm delivery. If cervical insufficiency (an abnormally short cervix) is suspected, an ultrasound may be performed to measure cervical changes more accurately. However, ultrasound is known to be limited in predicting prematurity, particularly in low-risk populations.

Fetal fibronectin (fFN) screening, the second test, takes 24 hours to complete and is usually performed on women presenting symptoms of preterm labor, such as contractions.[57] fFN is a protein produced by the fetal membranes and found in amniotic fluid. This protein attaches the fetal sac to the uterine lining and is only detected during early pregnancy and about 1-2 weeks before delivery. The presence of fFN during weeks 24-34 (a positive result) may suggest that the fetal sac is separating from the wall and labor may occur in the next 14 days. A negative

result (fFN is not present) means there is a very low risk of delivery within the next two weeks. A negative result is extremely accurate, but the positive result is unreliable and does not always lead to preterm labor. Thus, the two tests described above have many limitations that make them either subjective or inaccurate, restricting their effectiveness.

Detecting preterm labor is difficult because initial symptoms and signs are often mild and can occur in normal pregnancies. Many women who report symptoms during prenatal visits do not end up experiencing preterm labor, while others dismiss early warning signs as normal in pregnancy. By definition, a physician will diagnose preterm labor if there are persistent contractions accompanied by progressive cervical dilatation and effacement. This diagnosis is most accurate when contraction frequency is six or more per hour, cervical dilatation is 3 cm or more, effacement is 80% or more, membranes rupture, and/or bleeding occurs.[46] When digital examination is used to monitor cervical change, in correlation with lower thresholds for contraction frequency, both sensitivity and positive predictive value for actual preterm labor decrease, with the rate of false positives increasing to almost 40%. Even with combining the different screening tests, their maximum sensitivity is 50% and the maximum specificity is 95%.[46] However, currently, these are the only options available to doctors for monitoring their pregnant patients.

2.7 Optical Spectroscopy

Light-based methods have the potential to provide automated, fast determination of the types of changes that are occurring in the cervix without disrupting or removing any tissue for such analysis. Although there are several techniques that have been used to investigate cervical pathology in dysplasia and preterm labor, these techniques have limited applicability in detecting

normal or abnormal transformations of the cervix.[28] This doctoral project used Raman spectroscopy (RS) to achieve the stated aims. The physical principles of various optical spectroscopy modalities are shown in the Jablonski diagram in Figure 2.7. A few of these methods and their role within the cervix are described below.

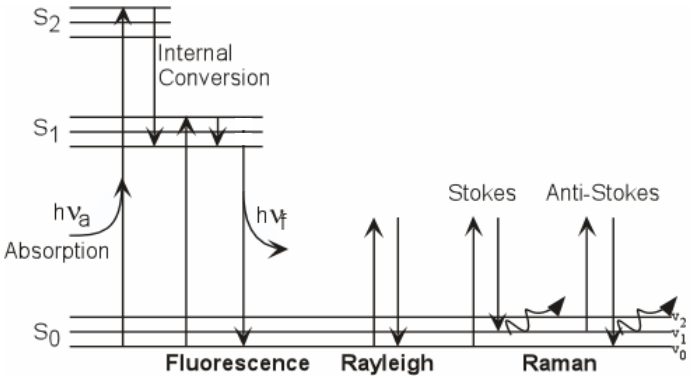

Figure 2.7. Jablonski diagram illustrating physical principles of common optical spectroscopic modalities. S_x refers to electronic energy levels; v_i to vibrational levels

2.7.1 Optical Coherence Tomography (OCT) for Cervical Dysplasia

OCT is a high resolution, cross sectional imaging modality analogous to ultrasound, except it is based on elastic light scattering. It uses a low coherence near-infrared light source to obtain depth-resolved images of tissue microstructure. Even in highly scattering tissues, structures up to 2 mm deep (2-3 cell layers) can be imaged.[58] OCT has high spatial resolution (~11 μm, depending on the source) and images can be taken in real-time. A recent study done by the Cleveland Clinic recruited 220 patients with a history of an abnormal Pap smear (in the US and Dominican Republic). For each patient, a visual exam, a colposcopic exam, and OCT measurements were completed. Using visual inspection, combining colposcopy and OCT on abnormal tissue has a sensitivity of 46% and a specificity of 69%.[59] Figure 2.8 shows an OCT image of an abnormal cervix with high-grade dysplasia (a) and of a normal cervix (b). To the untrained eye, there seem to be very few differences between these two OCT images.

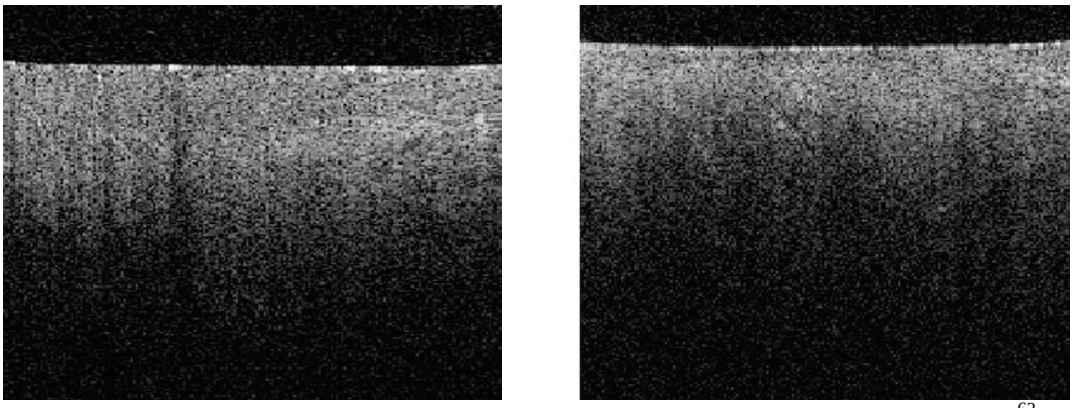

Figure 2.8. OCT images of a cervix with high-grade dysplasia (a) and of a normal cervix (b).[62]

OCT is ultimately dependent on structural changes that occur in small areas of the tissue. The biggest drawback of OCT is its lack of sensitivity since many situations, normal and abnormal, lead to similar architectural disruptions and, therefore, similar OCT images. The study from Escobar *et al*., indicates that OCT alone does not have a sensitive enough performance to improve the detection of cervical dysplasia.[62]

2.7.2 Fluorescence for Cervical Dysplasia

Fluorescence spectroscopy is the most commonly tested optical technique for the *in vivo* detection of diseases in general and cancers in particular. Fluorescence spectroscopy of both exogenous and endogenous chromophores has been successfully used to identify neoplastic cells and tissues in a variety of organ systems.[60] The modality has been studied extensively for diagnosing and screening cervical precancers.[61-64] The first *in vitro* studies for assessing the potential of fluorescence spectroscopy for cervical dysplasia was performed by Mahadevan *et al*.[65] The results from this study highlighted the inter-patient variability of fluorescence signals, suggesting the need for comparisons of abnormal sites to normal areas from the same patient.

Richards-Kortum *et al*. have extensively developed and evaluated fluorescence spectroscopy for detecting cervical precancers *in vivo*.[66] Most efforts have focused primarily on

applying single-point fluorescence spectra, acquired at multiple excitation wavelengths, for detecting cervical lesions.[67] Multivariate discriminations algorithms were developed based on fluorescence spectra acquired from 95 patients at three excitation wavelengths (337, 380 and 460 nm). The prospective sensitivity and specificity of the multivariate algorithms based on paired fluorescence information for distinguishing between cervical dysplasia from normal tissues was 82% and 73% respectively. These studies described above also show that the specificity in discriminating precancers from non-precancerous tissues is 68%.[68] Subsequent studies by this group have moved to measuring entire excitation-emission matrices to improve the diagnostic performance of the technique. More recently, the use of diffuse reflectance has been included to enhance the performance of fluorescence spectroscopy for cervical precancer detection.[62]

Another group from the University of Alabama discriminated between high-grade lesions and all other tissue types with a sensitivity of ~90% and a specificity of 50%.[69] This result in the cervix, along with similar observations made in the colon, indicate that fluorescence spectra of dysplastic and cancerous tissues are similar in many patients to the fluorescence spectra of benign abnormalities such as inflammation, hyperplasia and metaplasia.[68, 70] Fluorescence-based diagnosis yields an unacceptably high false positive rate in distinguishing cancers and dysplasia from all other tissues. It should also be noted that clinically it is extremely important to detect every high-grade lesion. The sensitivities and specificities found with fluorescence-based diagnosis of cervical dysplasia are not sufficient to change the current standard of care.[68]

2.7.3 Raman for Cervical Dysplasia

Raman spectroscopy is based on the Raman Effect, which occurs when an incident photon causes a scattering molecule to enter a virtual excited state, and then return to a ground

state either higher or lower than the original through the emission of another photon, as seen on the right side of Figure 2.7. It is named after the Indian physicist Sir C.V. Raman, who first observed the Raman effect in 1928 and was awarded the Nobel Prize in 1930. Raman Stokes scattering occurs when the scattered photon has less energy than the incident photon, while Raman anti-Stokes scattering occurs when the scattered photon has more energy than the incident photon. In contrast to fluorescence, which involves transitions between electronic energy levels, Raman scattering exploits smaller transitions between vibrational energy levels. This less intense signal requires a more powerful laser source as well as a sensitive detector. Furthermore, fluorescence, much brighter than the Raman signal, is inevitably generated when collecting Raman signal and must be dealt with by subtracting it from the raw spectrum.

A Raman spectrum is a plot of scattered light intensity versus the frequency shift of the scattered photon, making it independent of excitation wavelength. The frequency shift is expressed in units of wavenumber or Raman shift, which is the reciprocal of the wavelength, making it proportional to frequency. The spectrum consists of a series of peaks, each of which represents a different vibrational mode of the scattering molecule. These peaks are narrow and highly specific to a particular chemical bond, so each molecule has a unique spectrum or "fingerprint" associated with it from about 600 to 1800 cm^{-1}. Many biological molecules have unique and distinguishable spectra, so one can determine the gross biochemical composition of a tissue from its Raman spectrum. One particularly relevant biochemical change for cancer cells is an increase in the nucleic acid content correlated with increased proliferation and genetic instability. These changes, among others, can be detected with RS.[68, 71] Another important factor is the amide-III mode that appears when studying collagen. These amide-III peaks are found at 1271 and 1248 cm^{-1}, and the ratio of peaks at 1303 and 1260 cm^{-1}.[72] It is not trivial to determine

from where Raman peaks originate. Therefore, the Raman spectra of cervical tissue must be extensively studied to determine the differences between various states and what factors are contributing to the differences.[71]

Raman spectroscopy was historically used in analytical chemistry to determine chemical structures or the presence of certain molecules. It has only been in the last ten or twelve years that it has become a more popular choice for studying tissue. Many early studies were performed *in vitro*, attempting to distinguish normal from cancerous tissue in areas like cervix,[74] bladder and prostate,[75, 76] lung,[77] and GI tract.[75] Recent studies have used Raman for *in vivo* applications,[78, 79] with successful application to many organs, such as the breast[80] and GI tract.[81, 82] As seen in Figure 2.7, Raman spectra results from different electronic processes compared to fluorescence. Only a limited number of biological molecules can contribute to tissue fluorescence, most with broadband emission. On the other hand, several biological molecules such as nucleic acids, proteins and lipids, have distinctive Raman features that yield molecular specific structural and environmental information.[83]

2.7.4 Fluorescence for Preterm Labor

In 2005, Maul *et al*., found decreases in collagen content during pregnancy by measuring collagen autofluorescence (390 nm) with a collascope, an instrument that measures cervical ripening by analyzing the light-induced fluorescence of collagen in the cervix (Figure 2.9).[84, 85] In this study, they were able to obtain measurements from 40 non-pregnant and pregnant patients. For the pregnant patients, seven measurements were taken over the course of their pregnancy, as well as one post-partum measurement. While this instrument provides a good measure of the collagen content, there are many other processes that are happening during

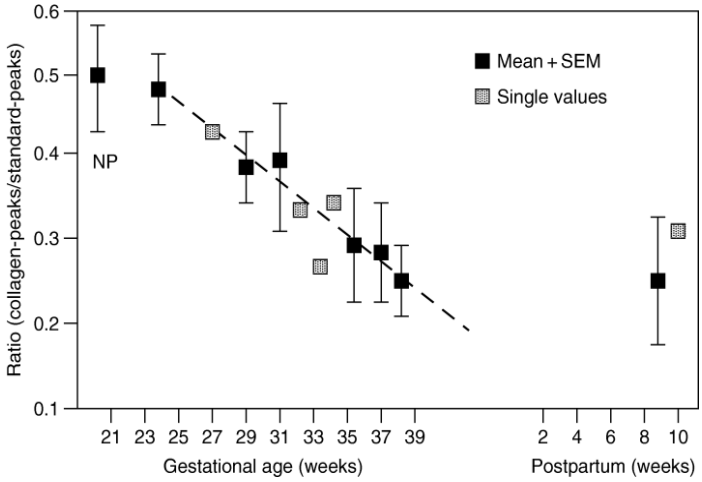

Figure 2.9. Decreases in collagen found by a collascope during pregnancy.[87]

pregnancy that are not solely reflected in collagen content or organization. Therefore, the largest drawback of this study is that they were only able to focus on one substance. Although fluorescence signal is greater than Raman signal, its lack of surveying the entire cervix is the greatest disadvantage of this technique.

2.8 Significance and Impact

We hypothesize that understanding the effects of changes in the cervix on Raman spectra will improve the application of RS to diagnose cervical dysplasia and preterm labor. Cervical cancer is the second leading cause of female mortality worldwide. With Pap smears and colposcopy-guided biopsy, its prevalence in developed countries has greatly diminished over the last 40 years. However, these same techniques cannot be used in settings that do not permit cell fixing and transporting, follow-up visits, and highly-trained clinicians. Optical techniques can potentially be used in lower-resource settings to diagnose abnormalities in real-time.

The use of RS for identifying patients at risk for preterm labor has never been investigated. It follows that if Raman spectra are sensitive to the subtle, normal changes in the

cervix due to menstrual cycle and menopausal status, it would certainly be sensitive to the large changes that occur during pregnancy. Understanding which changes happen normally will result in a method of detecting when labor is about to begin. Knowing which differences, if they occur at inappropriate times, are abnormal will lead to a method of detecting when preterm labor is about to begin.

The thesis has determined which variations in the cervix and other confounding factors significantly impact the Raman spectra. This work will serve as an important base for researchers considering this problem or similar ones that require looking at various, normal factors and their effects on spectral measurements. These changes, if significant enough, may be masking the Raman data, making it more difficult to determine which changes are due to cancer or preterm labor. This work has identified those changes in order to increase the feasibility of using RS in the clinic for detecting cervical dysplasia and the onset of labor.

2.9 References

1. Krantz, K.E. The Biology of the Cervix (The University of Chicago Press, Chicago, 1973).

2. Wright, T., Kurman, R.J. and Ferenczy, A. Blaustien's Pathology of the Female Genital Tract (Springer-Verlag, New York, 1994).

3. Castanzo, L.S. (ed.) 2nd Edition Physiology (Saunders, Philadelphia, 2002).

4. Beers, M.H. and Fletcher, A.J. The Merck Manual of Medical Information (Merck and Company, Inc., Whitehouse Station, 2003).

5. Petersen, L., Skajaa, K. and Uldbjerg, N. "Serum relaxin as a potential marker for preterm labour." *Obstet Gynecol Surv* **47**, 727 (1992).

6. Marx, S.G., Wentz, M. J., Mackay, L. B., Schlembach, D., Maul, H., Fittkow, C., Given, R., Vedernikov, Y., Saade, G. R. and Garfield, R. E.. "Effects of progesterone on iNOS, COX-2, and collagen expression in the cervix." *J Histochem Cytochem* **54**, 623-39 (2006).

7. Leppert, P.C., Yu, S.Y., Keller, S., Cerreta, J. and Mandl, I. "Decreased elastic fibers and desmosine content in incompetent cervix." *Am J Obstet Gynecol* **157**, 1134-9 (1987).

8. Anderson, J., Brown, N., Mahendroo, M.S. and Reese, J. "Utilization of different aquaporin water channels in the mouse cervix during pregnancy and parturition and in models of preterm and delayed cervical ripening." *Endocrinology* **147**, 130-40 (2006).

9. Chu, K.C., Miller, B.A. and Springfield, S.A. "Measures of racial/ethnic health disparities in cancer mortality rates and the influence of socioeconomic status." *J Natl Med Assoc* **99**, 1092-100-1102-4 (2007).

10. Hill, P., Wynder, E. L., Helman, P., Hickman, R., Rona, G. and Kuno, K. "Plasma hormone levels in different ethnic populations of women." *Cancer Res* **36**, 2297-301 (1976).

11. Rose, D.P., Haffner, S.M. and Baillargeon, J. "Adiposity, the metabolic syndrome, and breast cancer in African-American and white American women." *Endocr Rev* **28**, 763-77 (2007).

12. Stanford, J.L. and Greenberg, R.S. "Breast cancer incidence in young women by estrogen receptor status and race." *Am J Public Health* **79**, 71-3 (1989).

13. Al-Hendy, A. and Salama, S.A. "Ethnic distribution of estrogen receptor-alpha polymorphism is associated with a higher prevalence of uterine leiomyomas in black Americans." *Fertil Steril* **86**, 686-93 (2006).

14. Wolner-Hanssen, P., Eschenbach, D. A., Paavonen, J., Stevens, C. E., Kiviat, N. B., Critchlow, C., DeRouen, T., Koutsky, L. and Holmes, K. K. "Association between vaginal douching and acute pelvic Inflammatory disease." *JAMA-J Am Med Assoc* **263**, 1936-41 (1990).

15. Scholes, D., Stergachis, A., Ichikawa, L. E., Heidrich, F. E., Holmes, K. K. and Stamm, W. E. "Vaginal douching as a risk factor for cervical Chlamydia trachomatis infection." *Obstet Gynecol* **91**, 993-7 (1998).

16. Janssen, I., Katzmarzyk, P.T. and Ross, R. "Waist circumference and not body mass index explains obesity-related health risk." *Am J Clin Nutr* **79**, 379-84 (2004).

17. McTiernan, A. "Associations between energy balance and body mass index and risk of breast carcinoma in women from diverse racial and ethnic backgrounds in the U.S." *Cancer* **88**, 1248-1255 (2000).

18. Dorgan, J.F., Longcope, C., Stephenson, H. E., Jr., Falk, R. T., Miller, R., Franz, C., Kahle, L., Campbell, W. S., Tangrea, J. A. and Schatzkin, A. "Relation of prediagnostic

serum estrogen and androgen levels to breast cancer risk." *Cancer Epidem Biomar* **5**, 533-9 (1996).

19. Kohlmeier, L. and Kohlmeier, M. "Adipose tissue as a medium for epidemiologic exposure assessment." *Environ Health Perspect* **103 Suppl 3**, 99-106 (1995).

20. Hankinson, S.E., Willett, W.C., Colditz, G.A., Hunter, D.J., Michaud, D.S., Deroo, B., Rosner, B., Speizer, F.E. and Pollak, M. "Circulating concentrations of insulin-like growth factor-I and risk of breast cancer." *Lancet* **351**, 1393-6 (1998).

21. Baquet, C.R., Horm, J.W., Gibbs, T. and Greenwald, P. "Socioeconomic factors and cancer incidence among blacks and whites." *J Natl Cancer Inst* **83**, 551-7 (1991).

22. Shinn, E., Basen-Engquist, K., Le, T., Hansis-Diarte, A., Bostic, D., Martinez-Cross, J., Santos, A. and Follen, M. "Distress after an abnormal Pap smear result: scale development and psychometric validation." *Prev Med* **39**, 404-12 (2004).

23. Miller, S.M., Siejak, K.K., Schroeder, C.M., Lerman, C., Hernandez, E. and Helm, C.W. "Enhancing adherence following abnormal Pap smears among low-income minority women: a preventive telephone counseling strategy." *J Natl Cancer Inst* **89**, 703-8 (1997).

24. American Cancer Society, "Cancer Facts and Figures 2012," (American Cancer Society, Atlanta, 2011).

25. Anderson, G.H., Boyes D.A., Benedet J.L., Le Riche J.C., Matisic J.P., Suen K.C., Worth A.J., Millner A. and Bennett O.M. "Organisation and Results of the Cervical Cytology Screening-Program in British-Columbia, 1955-85." *Brit Med J* **296**, 975-978 (1988).

26. Burke, L., Antonioli, D.A. and Ducatman, B.S. (eds.) Colposcopy, text and atlas (Appleton and Large, Norwalk, 1991).

27. Ramzy, I. (ed.) Essentials of Gynecologic and Obstetric Pathology. (Appleton - Century - Crofts, Norwalk, 1983).

28. Evers, J.L.H. and Heineman, M.J. (eds.) Gynecology - A Clinical Atlas (CV Mosby Co, St.Louis, 1990).

29. Jemal, A. Siegel, R., Xu, Jiaquan, and Ward, E. "Cancer statistics, 2009." *CA Cancer J Clin* **59**, 225-49 (2011).

30. Coleman, D.V., Wickenden, C. and Malcolm, A.D.B. "Association of Human Papillomavirus with Squamous Carcinoma of the Uterine Cervix." *Ciba F Symp* **120**, 175-189 (1986).

31. Au, W.W., Abdou-Salama, S., Sierra-Torres, C.H. and Al-Hendy, A. "Environmental risk factors for prevention and molecular intervention of cervical cancer." *Int J Hyg Environ Health* **210**, 671-8 (2007).

32. Rowson, K.E. and Mahy, B.W. "Human papova (wart) virus." *Bacteriol Rev* **31**, 110-31 (1967).

33. Brokaw, J.L., Yee, C.L. and Munger, K. "A mutational analysis of the amino terminal domain of the human papillomavirus type 16 E7 oncoprotein." *Virology* **205**, 603-7 (1994).

34. Walboomers J.M.M., Jacobs M.V., Manos M.M., Bosch F.X., Kummer J.A., Shah K.V., Snijders P.J.F., Peto J., Meijer C.J.L.M. and Munoz N. "Human papillomavirus is a necessary cause of invasive cervical cancer worldwide." *J Pathol* **189**, 12-19 (1999).

35. Son, D.S., Parl, A.K., Rice, V.M. and Khabele, D. "Keratinocyte chemoattractant (KC)/human growth-regulated oncogene (GRO) chemokines and pro-inflammatory chemokine networks in mouse and human ovarian epithelial cancer cells." *Cancer Biol Ther* **6**, 1302-12 (2007).

36. Bates, B. (ed.) A Guide to Physical Examination (J.B. Lippincott Co, Philadelphia, 1974).

37. Myers, E.R., McCrory, D. C., Subramanian, S., McCall, N., Nanda, K., Datta, S. and Matchar, D. B. "Setting the target for a better cervical screening test: Characteristics of a cost-effective test for cervical neoplasia screening." *Obstet Gynecol* **96**, 645-652 (2000).

38. Nanda, K., McCrory, D.C., Myers, E.R., Bastian, L.A., Hasselblad, V., Hickey, J.D. and Matchar, D.B. "Accuracy of the Papanicolaou test in screening for and follow-up of cervical cytologic abnormalities: A systematic review." *Ann Intern Med* **132**, 810-819 (2000).

39. Fahey, M.T., Irwig, L. and Macaskill, P. "Metaanalysis of Pap Test Accuracy." *Am J Epidemiol* **141**, 680-689 (1995).

40. Minoru, U. (ed.) Cervical Adenocarcinoma: A Colscopic Atlas (Ishiyaku - EuroAmerica Inc, St Louis, 1985).

41. Ramanujam N., Mahadevan A., Mitchell M.F., Thomsen S., Silva E., and Richards-Kortum R. "Fluorescence Spectroscopy of the Cervix." *Clin Obstet Gynecol* **6**, 62-69 (1994).

42. Bomfim-Hyppolito, S., Franco, E.S., Franco, R.G.D., de Albuquerque, C.M. and Nunes, G.C. "Cervicography as an adjunctive test to visual inspection with acetic acid in cervical cancer detection screening." *Int J Gynecol Obstet* **92**, 58-63 (2006).

43. Cox, J.T., Lorincz, A. T., Schiffman, M. H., Sherman, M. E., Cullen, A., and Kurman, R. J. "Human papillomavirus testing by hybrid capture appears to be useful in triaging women with a cytologic diagnosis of atypical squamous cells of undetermined significance." *Am J Obstet Gynecol* **172**, 946-54 (1995).

44. Peyton, C.L., Schiffman, M., Lorincz, A.T., Hunt, W.C., Mielzynska, I., Bratti, C., Eaton, S., Hildesheim, A., Morera, L.A., Rodriguez, A. C., Herrero, R., Sherman, M.E. and Wheeler, C. M. "Comparison of PCR- and hybrid capture-based human papillomavirus detection systems using multiple cervical specimen collection strategies." *J Clin Microbiol* **36**, 3248-54 (1998).

45. Goldenberg, R.L. and Rouse, D.J. "Prevention of premature birth." *N Engl J Med* **339**, 313-20 (1998).

46. Iams, J.D. "Prediction and early detection of preterm labor." *Obstet Gynecol* **101**, 402-12 (2003).

47. Schempf, A.H., Branum, A.M., Lukacs, S.L. and Schoendorf, K.C. "The contribution of preterm birth to the black-white infant mortality gap, 1990 and 2000." *Am J Public Health* **97**, 1255 (2007).

48. Mathews, T.J. and MacDorman, M.F. "Infant mortality statistics from the 2005 period linked birth/infant death data set." *Natl Vital Stat Rep* **57**, 1-32 (2008).

49. Parry, S. and Strauss, J.F. "Premature rupture of the fetal membranes." *N Engl J Med* **338**, 663-670 (1998).

50. Guendelman, S., Kosa, J.L. and Pearl, M. "Exploring the relationship of second-trimester corticotropin releasing hormone, chronic stress and preterm delivery." *J Matern-Fetal Neo M* **21**, 788-795 (2008).

51. Mercer, B.M., Goldenberg, R.L., Das, A., Moawad, A.H., Iams, J.D., Meis, P.J., Copper, R.L., Johnson, F., Thom, E., McNellis, D., Miodovnik, M., Menard, M.K., Caritis, S.N., Thurnau, G.R., Bottoms, S.F. and Roberts, J. "The preterm prediction study: a clinical risk assessment system." *Am J Obstet Gynecol* **174**, 1885-95 (1996).

52. Kiefer, D.G. and Vintzileos, A.M. "The Utility of Fetal Fibronectin in the Prediction and Prevention of Spontaneous Preterm Birth." *Rev Obstet Gynecol* **1**, 106 (2008).

53. Peltier, M.R. "Immunology of term and preterm labor." *Reprod Biol Endocrinol* **1**, 122 (2003).

54. Gyetvai, K., Hannah, M.E., Hodnett, E.D. and Ohlsson, A. "Tocolytics for preterm labor: A systematic review." *Obstet Gynecol* **94**, 869-877 (1999).

55. Wentz, M.J., Shi, S.Q., Shi, L., Salama, S.A., Harirah, H.M., Fouad, H., Garfield, R. E. and Al-Hendy, A. "Treatment with an inhibitor of catechol-O-methyltransferase activity reduces preterm birth and impedes cervical resistance to stretch in pregnant rats." *Reproduction* **134**, 831-9 (2007).

56. Arulkumaran, S., Symonds, I.M. and Fowlie, A. Oxford handbook of obstetrics and gynecology (Oxford University Press, Oxford; New York, 2004).

57. Faron, G., Boulvain, M., Lescrainier, J.P. and Vokaer, A. "A single cervical fetal fibronectin screening test in; population at low risk for preterm delivery: an improvement on clinical indicators?" *Brit J Obstet Gynaec* **104**, 697-701 (1997).

58. Huang, D. Swanson, E.A., Lin, C.P., Schuman, J.S., Stinson, W.G., Chang, W., Hee, M.R., Flotte, T., Gregory, K., Puliafito, C.A. and Fujimoto J.G. "Optical coherence tomography." *Science* **254**, 1178-81 (1991).

59. Escobar, P.F., Rojas-Espaillat, L., Tisci, S., Enerson, C., Brainard, J., Smith, J., Tresser, N.J., Feldchtein, F.I., Rojas, L.B. and Belinson, J.L. "Optical coherence tomography as a diagnostic aid to visual inspection and colposcopy for preinvasive and invasive cancer of the uterine cervix." *Int J Gynecol Cancer* **16**, 1815-1822 (2006).

60. Ramanujam, N. "Fluorescence spectroscopy of neoplastic and non-neoplastic tissues." *Neoplasia* **2**, 89-117 (2000).

61. Chang, S.K., Pavlova, I., Marin, N.M., Follen, M. and Richards-Kortum, R. "Fluorescence spectroscopy as a diagnostic tool for detecting cervical pre-cancer." *Gynecol Oncol* **99**, S61-S63 (2005).

62. Chang, S.K., Mirabal, Y. N., Atkinson, E. N., Cox, D., Malpica, A., Follen, M. and Richards-Kortum, R. "Combined reflectance and fluorescence spectroscopy for *in vivo* detection of cervical pre-cancer." *J Biomed Opt* **10** (2005).

63. Utzinger, U., Trujillo, E.V., Atkinson, E.N., Mitchell, M.F., Cantor, S.B., and Richards-Kortum, R. "Performance estimation of diagnostic tests for cervical precancer based on fluorescence spectroscopy: Effects of tissue type, sample size, population, and signal-to-noise ratio." *IEEE T Bio-med Eng* **46**, 1293-1303 (1999).

64. Lee, J.S., Shuhatovich, O., Price, R., Pikkula, B., Follen, M., McKinnon, N., MacAulay, C., Knight, B., Richards-Kortum, R. and Cox, D. D. "Design and preliminary analysis of a study to assess intra-device and inter-device variability of fluorescence spectroscopy instruments for detecting cervical neoplasia." *Gynecol Oncol* **99**, S98-S111 (2005).

65. Mahadevan, A., Mitchell, M.F., Silva, E., Thomsen, S. and Richards-Kortum, R.R. "Study of the Fluorescence Properties of Normal and Neoplastic Human Cervical Tissue." *Laser Surg Med* **13**, 647-655 (1993).

66. Mitchell, M.F., Cantor, S.B., Ramanujam, N., Tortolero-Luna, G. and Richards-Kortum, R. "Fluorescence spectroscopy for diagnosis of squamous intraepithelial lesions of the cervix." *Obstet Gynecol* **93**, 462-470 (1999).

67. Milbourne, A., Park, S.Y., Benedet, J.L., Miller, D., Ehlen, T., Rhodes, H., Malpica, A., Matisic, J., Van Niekirk, D., Atkinson, E.N., Hadad, N., Mackinnon, N., Macaulay, C., Richards-Kortum, R. and Follen, M. "Results of a pilot study of multispectral digital colposcopy for the *in vivo* detection of cervical intraepithelial neoplasia." *Gynecol Oncol* **99**, S67-75 (2005).

68. Ramanujam, N., Mitchell, M.F., Mahadevan-Jansen, A., Thomsen, S.L., Staerkel, G., Malpica, A., Wright, T., Atkinson, N. and Richards-Kortum, R. "Cervical precancer detection using a multivariate statistical algorithm based on laser-induced fluorescence spectra at multiple excitation wavelengths." *Photochem Photobiol* **64**, 720-735 (1996).

69. Huh, W.K., Cestero, R.M., Garcia, F.A., Gold, M.A., Guido, R.S., McIntyre-Seltman, K., Harper, D.M., Burke, L., Sum, S.T., Flewelling, R.F. and Alvarez, R.D. "Optical detection of high-grade cervical intraepithelial neoplasia *in vivo*: Results of a 604-patient study." *Am J Obstet Gynecol* **190**, 1249-1257 (2004).

70. Schomacker, K.T., Frisoli, J.K., Compton, C.C., Flotte, T.J., Richter, J.M., Nishioka, N. S. and Deutsch, T.F. "Ultraviolet Laser-Induced Fluorescence of Colonic Tissue - Basic Biology and Diagnostic Potential." *Laser Surg Med* **12**, 63-78 (1992).

71. Mahadevan-Jansen, A. in Biomedical Photonics Handbook (ed. Vo-Dinh, T.), 30-1 (CRC Press, Washington DC, 2003).

72. Frushour, B.G. & Koenig, J.L. "Raman scattering of collagen, gelatin, and elastin." *Biopolymers* **14**, 379-91 (1975).

73. Vo-Dinh, T. and Cullum B.M. in Biomedical Photonics Handbook (ed. Vo-Dinh, T.), 28-1 (CRC Press, Washington DC, 2003).

74. Mahadevan-Jansen, A., Mitchell, M.F., Ramanujam, N., Malpica, A., Thomsen, S., Utzinger, U. and Richards-Kortum, R. "Near-infrared Raman spectroscopy for *in vitro* detection of cervical precancers." *Photochem Photobiol* **68**, 123-32 (1998).

75. Alfano, R.R. Tang, G.C., Pradhan, A., Lam, W., Choy, D.S.J. and Opher, E.. "Fluorescence-Spectra from Cancerous and Normal Human-Breast and Lung Tissues." *IEEE J Quantum Elect* **23**, 1806-1811 (1987).

76. Crow, P. Molckovsky, A., Stone, N., Uff, J., Wilson, B., and Wong Kee Song, L.M. "Assessment of fiberoptic near-infrared Raman spectroscopy for diagnosis of bladder and prostate cancer." *Urology* **65**, 1126-30 (2005).

77. Huang, Z., McWilliams, A., Lui, H., McLean, D.I., Lam, S., and Zeng, H. "Near-infrared Raman spectroscopy for optical diagnosis of lung cancer." *Int J Cancer* **107**, 1047-52 (2003).

78. Choo-Smith, L.P., Edwards, H.G., Endtz, H.P., Kros, J.M., Heule, F., Barr, H., Robinson, J.S., Jr., Bruining, H.A. and Puppels, G.J. "Medical applications of Raman spectroscopy: from proof of principle to clinical implementation." *Biopolymers* **67**, 1-9 (2002).

79. Hanlon, E.B., Manoharan, R., Koo, T.W., Shafer, K.E., Motz, J.T., Fitzmaurice, M., Kramer, J.R., Itzkan, I., Dasari, R.R. and Feld, M.S. "Prospects for *in vivo* Raman spectroscopy." *Phys Med Biol* **45**, R1-R59 (2000).

80. Keller, M.D., Majumder, S.K. and Mahadevan-Jansen, A. "Spatially offset Raman spectroscopy of layered soft tissues." *Opt Lett* **34**, 926-928 (2009).

81. Shim, M.G., Song, L., Marcon, N.E. and Wilson, B.C. "*In vivo* near-infrared Raman spectroscopy: Demonstration of feasibility during clinical gastrointestinal endoscopy." *Photochem Photobiol* **72**, 146-150 (2000).

82. Molckovsky, A., Song, L.M., Shim, M.G., Marcon, N.E. and Wilson, B.C. "Diagnostic potential of near-infrared Raman spectroscopy in the colon: differentiating adenomatous from hyperplastic polyps." *Gastrointest Endosc* **57**, 396-402 (2003).

83. Twardowski, J. and Anzenbacher, P. (Ellis Horwood, New York, 1994).

84. Maul, H., Saade, G. and Garfield, R.E. "Prediction of term and preterm parturition and treatment monitoring by measurement of cervical cross-linked collagen using light-induced fluorescence." *Acta Obstet Gynecol Scand* **84**, 534-6 (2005).

85. Fittkow, C.T., Maul, H., Olson, G., Martin, E., MacKay, L.B., Saade, G.R., and Garfield, R.E. "Light-induced fluorescence of the human cervix decreases after prostaglandin application for induction of labor at term." *Eur J Obstet Gynecol* **123**, 62-66 (2005).

CHAPTER 3

PRELIMINARY STUDIES

The work described below represents preclinical studies utilizing Raman spectroscopy to diagnose cervical dysplasia and to understand variations that occur in the cervix. The results below were obtained by two previous PhD students (Amy Robichaux-Viehoever (ARV) and Elizabeth Kanter (EK)) and me (EV). These studies laid the foundation for the rest of this dissertation.

This majority of this chapter has been published as the following:

Robichaux-Viehoever A, Kanter EM, Shappell H, Billheimer D, III Jones H, A Mahadevan-Jansen. Characterization of Raman Spectra Measured *In vivo* for the Detection of Cervical Dysplasia. *Applied Spectroscopy*, 61: (9), 986-993, 2007

Kanter EM, Vargis E, Majumder S, Keller MD, Beaven RB, Rao GG, A Mahadevan-Jansen. Application of Raman spectroscopy for Cervical Dysplasia Diagnosis. *Journal of Biophotonics*, 2: (1-2), 81-90, 2009

Kanter EM, Majumder S, Vargis E, Robichaux-Viehoever A, Kanter G, Shappell H, III Jones H, A Mahadevan-Jansen. Multiclass Discrimination of Cervical Precancers using Raman Spectroscopy. *Journal of Raman Spectroscopy*, 40: (2), 205-211, 2009

Kanter EM, Majumder S, Kanter GJ, Woeste EM, A Mahadevan-Jansen. Effect of Hormonal Variation on Raman Spectra for Cervical Disease Classification. *American Journal of Obstetrics and Gynecology*, 200: (5), 512e1-5, 2009

3.1 Characterization of the Normal Cervix

Raman spectroscopy has the potential to provide non-invasive, real-time diagnosis of different pathologies in the cervix. Yet the sources and relative contributions of spectral variability for a given pathology must be understood to accurately predict its effectiveness. To

begin studying this, Raman spectra were collected *in vivo* from 35 patients undergoing hysterectomy with no evidence of cervical dysplasia. The effects of signal collection, time, and acetic acid on the measured spectra were examined in the first few patients. The remaining patient data was used to quantify the spectral variance within a site, within a patient, and between different patients. Further analysis of the sources of inter-patient variability included menopausal status, smoking history, and overall patient diagnosis.

Thirty-five patients undergoing total abdominal or vaginal hysterectomies were recruited to participate in the study as approved by the Vanderbilt Institutional Review Board (IRB). After the patient was placed under anesthesia, but before the hysterectomy procedure began, a colposcopic examination of the cervix was performed and Raman spectra were measured. Four percent acetic acid was applied to the cervix to visually enhance any abnormal areas of the epithelium by inducing aceto-whitening. Colposcopy was performed for two reasons: to ensure the measured areas were colposcopically normal and to maintain consistency with the current study of dysplasia patients. Multiple Raman spectra of colposcopically normal appearing sites were measured *in vivo* using the portable RS system (Figure 3.1).

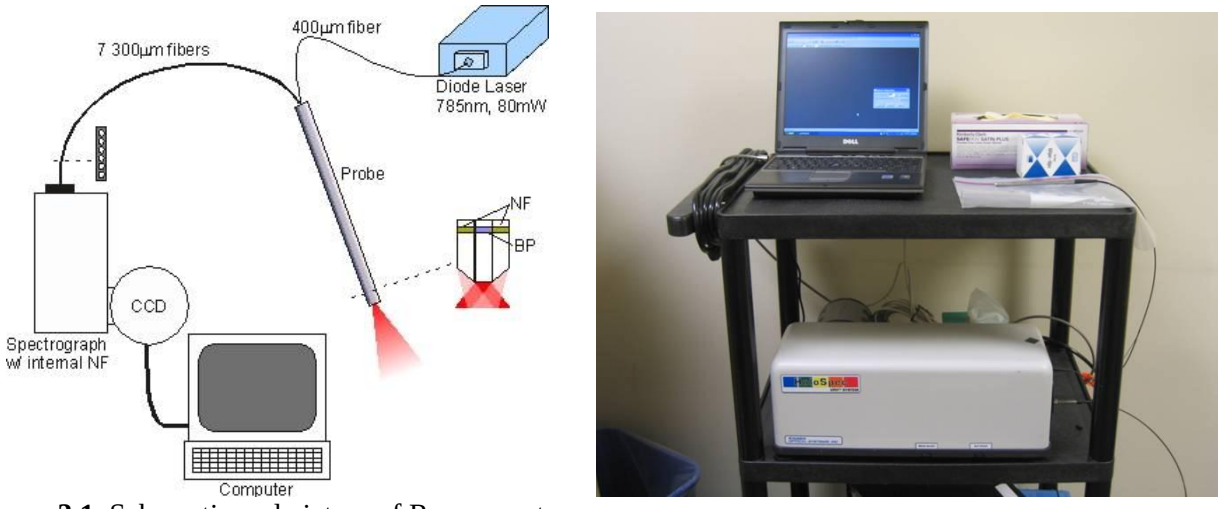

Figure 3.1. Schematic and picture of Raman system.

Raman spectra were acquired using a portable RS system consisting of a 785 nm diode laser (Process Instruments, Inc., Salt Lake City, UT), custom fiber optic probe (Visionex, Inc.), imaging spectrograph (Kaiser Optical Systems, Inc., Ann Arbor, MI), and back-illuminated, deep-depletion, charge coupled device (CCD) camera (Princeton Instruments, Princeton, NJ) which were all controlled with a laptop computer (Figure 3.1). For this study, the fiber optic probe delivered 80 mW of incident light onto the tissue and collected the scattered light for 3-5 seconds. In all cases, the overhead fluorescent and colposcope lights were turned off during the measurements. Any luminescent lights were left on but turned away from the measurement site.[1] The measured sites were subsequently marked with a methylene blue. The hysterectomy procedure proceeded according to standard clinical protocol. Upon removal of the cervix, histological analysis was performed.[1]

Studies on the first five patients were designed to determine the optimal signal collection time. In these patients, three sites on the cervix were chosen. Five spectra were acquired at each site with a different integration time: 1, 3, 5, 8 seconds, or 3 accumulations of 5 seconds for a total of 15 seconds. The fiber optic probe was kept in contact with the tissue throughout the five measurements. Studies on 2 other patients examined the effect of applying acetic acid to cervix. In this study, three sites were chosen for measurements. All spectra were collected using a 5 second signal collection time. Spectra were acquired at each site prior to applying acetic acid and at various time intervals ranging from 0-180 seconds after the application of acetic acid to determine its effect on the Raman spectra. Studies on the remaining subjects (subjects 8-35) were designed to examine the sources of variation. In this study, 3 sites were chosen for measurements and 3 spectra were collected at each site: the first two were collected without moving the fiber optic probe, and the last was acquired after removing the probe and placing it at the same site.

These differences allowed for determination of the relative variability due to user error of probe placement versus intrinsic variability of the Raman spectra. Measurements at different locations within the normal ectocervix of a given patient provided the calculation of variation due to different locations. The comparison of spectra between different patients allowed for the calculation of inter-patient variation.[1]

Prior to each day of measurements, the system was calibrated using a neon-argon lamp and a naphthalene standard to correct for system wavenumber, laser excitation, and throughput variations. Raman spectra from the cervix were noise smoothed using a Savitzky-Golay filter and fluorescence was subtracted using the modified polyfit technique with a 5^{th} degree polynomial developed within our lab.[2] The resulting spectra were then correlated with the corresponding histopathologic diagnosis to characterize the differences between various diagnostic categories.

A study of the optimal integration time showed that signal to noise ratio (SNR) increases linearly with an increase in integration time until 5 seconds. Further increase in the integration time did not proportionally improve SNR and, as such, subsequent spectra were acquired using a 5-second integration time. The acetic acid analysis showed two small, non-significant spectral changes arising after the application of acetic acid; no time-dependent changes were noted. Thus it was determined that applying acetic acid did not affect Raman spectra from cervical tissue regardless of how long after application the Raman measurement was taken.[1] The variability due to probe placement was quantified by calculating the mean spectral difference between an initial measurement and a subsequent measurement in which the probe was either kept in place or removed and replaced at the initial site.

The remaining components of variance, defined in this study as inter-patient (between different patients), intra-patient (between different locations within a given patient), and intrinsic

measurement error were calculated using analysis of variance (ANOVA) and Henderson's method.[3] Henderson's method is a commonly used statistical method for unbalanced data that estimates the variance due to each component. The analysis was done at each wavenumber in the spectrum. In using this method, an ANOVA table was constructed and the observed mean squared error for each category was set equal to its expected value, as defined by Henderson's method.[3] A series of three equations (for each component of variance) with three unknowns (variance due to each component) can then be solved to determine the variance due to each component. Using this method, the main source of variability within normal ectocervix was identified to be due to inter-patient variations, contributing 73% of the total variance. Variability from the same site as well as from the same patient was found to be minimal. Since there is little variation in the Raman spectra from normal tissue within a given patient, it was determined that a single measurement from the normal cervix is sufficient to characterize the normal signature of that patient (ARV).

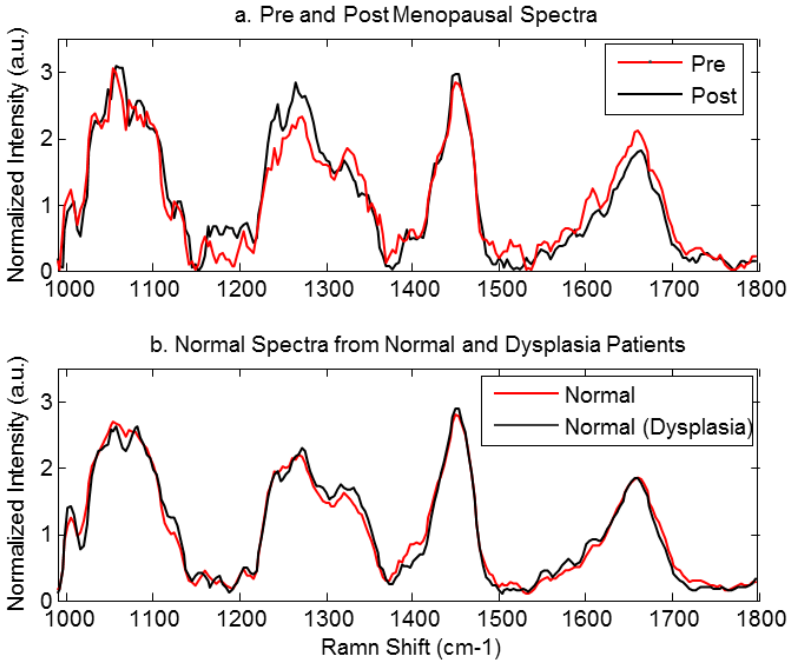

Figure 3.2. Mean Raman spectral overlays for the following categories: (a) Premenopausal spectra and postmenopausal and (b) normal from normal and normal for dysplasia.

In order to characterize inter-patient variability, spectral differences were compared based on menopausal status, smoking, and disease state. Spectral differences between smokers and non-smokers were negligible. Spectral differences were found between premenopausal and postmenopausal normal spectra (Figure 3.2a). The peak at 1324 cm^{-1} and the region around 1600 cm^{-1} are all areas of statistically significant differences. In comparing the normal spectra from normal patients (with no cervical disease) to normal spectra from cervical dysplasia patients, interesting differences were observed (Figure 3.2b). Although, the normal ectocervix from normal and dysplasia patients appear identical histologically, there are spectroscopic differences between them. The most notable visual distinctions appear in the peaks at 1006, 1055, 1244 and 1450 cm^{-1}. This finding indicates that RS may be able to detect differences in tissue biology that are not evident by histological examination. It is possible that RS can detect malignancy-associated changes, perhaps occurring at the sub-cellular level. These changes have been documented using high resolution image analysis of cervical smear specimens.[4] The observed malignancy-associated changes increased in intensity with higher grades of dysplasia.

3.2 Characterization of Cervical Dysplasia

In the first attempt to determine if Raman spectroscopy (RS) could be used to distinguish between normal and dysplasia, spectra were measured *in vivo* from 110 patients undergoing diagnostic or therapeutic procedures which involved the removal of cervical tissue. Written informed consent was obtained from each patient prior to spectral measurements. Two to six Raman spectra were acquired from both colposcopically normal and abnormal areas after the application of 4% acetic acid prior to tissue excision. Following spectral measurements, the measured sites were marked with a methylene blue paste. The tissue was then excised according

to standard clinical protocol and the histological analysis was performed. All normal locations were assumed to be normal unless pathological evaluation indicated otherwise (ARV and EK).[1]

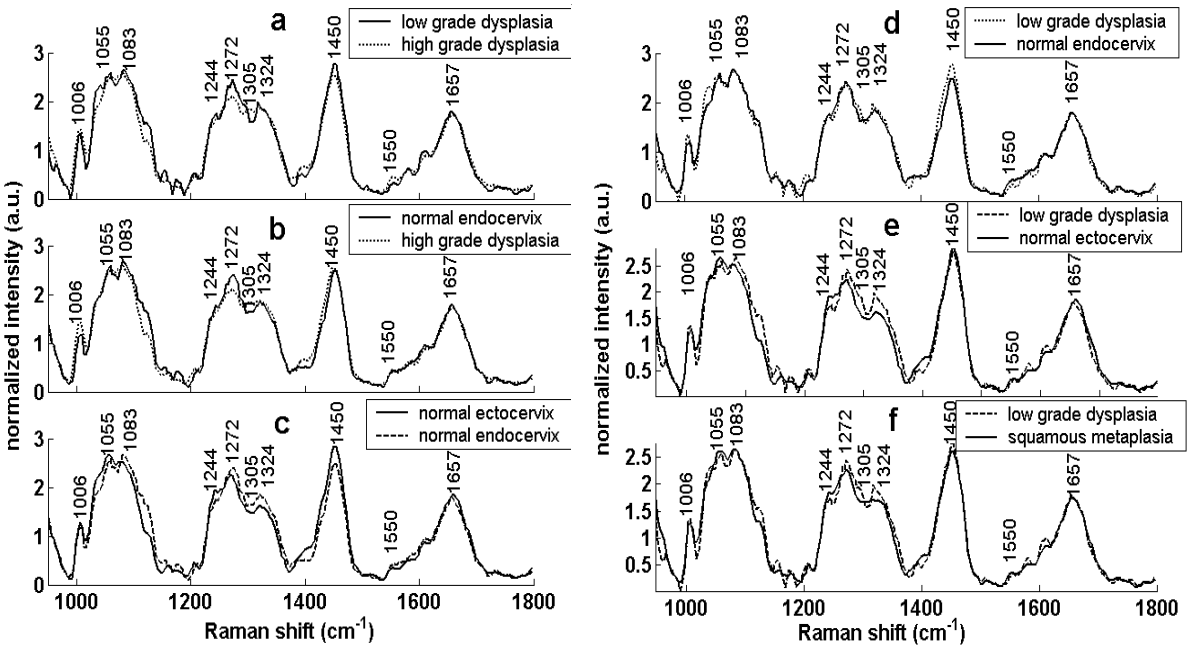

Figure 3.3. Mean Raman spectral overlays for the following categories: (a) high-grade dysplasia (n=29 spectra) and low-grade dysplasia (n=6 spectra), (b) normal endocervix (n=8 spectra) and high-grade dysplasia, (c) normal ectocervix (n=100 spectra) and normal endocervix, (d) low-grade dysplasia and normal endocervix, (e) low-grade dysplasia and normal ectocervix, (f) low-grade dysplasia and squamous metaplasia (29 spectra).[1]

Figure 3.3 shows the mean spectra (for 79 patients) comparing two different categories for easy comparison (ARV). The most consistent peaks are labeled and found at 1006, 1058, 1086, 1244, 1270, 1324, 1450, 1550, 1655 cm^{-1}. Several spectral regions show statistically significant differences in comparing high-grade dysplasia from the normal ectocervix. Even with only 6 low-grade dysplasia spectra in the analysis, interesting trends are still observed. There is an increase in the 1324 cm^{-1} peak as compared with normal ectocervix, which matches comparisons between high-grade dysplasia and normal ectocervix. Yet the intensity of the 1272 and 1450 cm^{-1} peaks in the low-grade dysplasia spectra seems to remain similar to those seen in normal ectocervix, unlike high-grade dysplasia spectra. The comparison of high-grade dysplasia

with normal endocervix spectra in Figure 3.3b shows a decrease in intensity at the 1272 cm^{-1} peak compared to the high-grade dysplasia spectra. This change is also seen when comparing normal ectocervix and squamous metaplasia spectra. The normal endocervix spectra also appear to retain the valley seen at 1305 cm^{-1}, similar to the normal ectocervix spectra. However, a comparison of normal endocervix and ectocervix spectra surprisingly shows some striking differences. Most notably, there is an increase in the intensity of the 1272 and 1324 cm^{-1} peaks in the endocervix spectra as compared with ectocervix spectra, while the 1450 cm^{-1} peak shows a decrease in intensity.[1]

Based on these differences observed and using histology as the gold standard, logistic regression discrimination algorithms were developed to distinguish between normal ectocervix, squamous metaplasia, and high-grade dysplasia using independent training and validation sets of data. Low-grade dysplasia was not classified due to the low number of samples. The classification model was constructed to automatically classify spectra into one of two categories - high-grade dysplasia or benign cervix - using a two-tiered logistic regression model. The first algorithm was trained to classify a spectrum as either normal ectocervix (score=0) or high-grade dysplasia (score =1) and was developed using independent training and validation sets that were randomly generated by dividing the normal ectocervix and high-grade dysplasia data sets into a training set (two-thirds of the patients) and a validation sets (one-third of the patients). Any major peak that showed statistical difference at the level of $p< 0.01$ between normal ectocervix spectra and high-grade dysplasia spectra were chosen as an input for the algorithm. Thus, the inputs to the algorithm are the normalized intensity values at 1006, 1058, 1240 1305 1324, 1450, 1550, 1655 cm^{-1} and the logistic regression equation. A two-tiered algorithm was developed to separate high-grade dysplasia from everything else and to remove any misclassified squamous

metaplasia samples. An unbiased estimate of the model's accuracy indicates that RS was able to distinguish between high-grade dysplasia and benign areas of the cervix (normal ectocervix and squamous metaplasia) with a sensitivity of 89% and a specificity of 81%. Colposcopy, in expert hands, can discriminate such areas with a sensitivity of 87% and a specificity of 72% (ARV).[1]

The limitation of this particular study is that the discrimination algorithms developed above were binary and therefore did not allow for multi-class discrimination. Thus, a new discrimination algorithm was developed based on novel statistical methods: Maximum representation and discrimination feature (MRDF) combined with sparse multinomial logistic regression (SMLR).

MRDF is a method of feature extraction that maximally extracts the diagnostic information that tends to be hidden in a set of measured spectral data. It achieves this by reducing its dimensionality through a set of mathematical transforms. Given a set of input data with spectra from different tissue types, MRDF will try to find a set of nonlinear transforms (restricted order polynomial mappings) of the input data that optimally discriminate between the different classes in a reduced dimensionality space. This occurs in two steps. In the first stage, the input spectral data $\mathbf{x} = [x_1, x_2, ...x_N]^T$ (intensities corresponding to wavenumbers of the spectra) from each tissue type are raised to the power p' to produce the associated nonlinear input vectors $\mathbf{x}_{p'} = [x_1^{p'}, x_2^{p'}, ..., x_N^{p'}]$, which are then subject to a transform Φ'_M such that $\mathbf{y}'_M = \Phi'^T_M \mathbf{x}_{p'}$ are the first stage output features in the nonlinear feature space of reduced dimension $M << N$. In the second stage, the reduced M-dimensional output features $\mathbf{y}'_M$ for each tissue type are transformed nonlinearly to the power p to produce higher order features $\mathbf{y}'_{Mp} = [y'^p_1, y'^p_2, ..., y'^p_M]$, and a second transform Φ_K is computed so as to yield the final output features $\mathbf{y}_K = \Phi^T_K \mathbf{y}'_{Mp}$ in the

nonlinear feature space of dimension K ($K \leq M$).[5]

SMLR, a method of supervised classification, is the second stage of this statistical analysis. It is a probabilistic multi-class model based on a sparse Bayesian machine-learning framework of statistical pattern recognition. SMLR's goal is to separate a set of labeled input data into its classes by predicting the posterior probabilities of their class-membership. It computes the posterior probabilities using a multinomial logistic regression model and constructs a decision boundary that separates the data into its constituent classes based on the computed posterior probabilities following Bayes' rule. Data is assigned to a class for which its posterior probability is the highest.[5]

In order to determine the effectiveness of this new discrimination algorithm as compared to the one used previously,[1] Raman spectra from the same 79 patients were classified using an algorithm based on MRDF and SMLR. This algorithm is capable of discriminating *in vivo* Raman spectra acquired from the human cervix simultaneously into various pathological categories using leave-one-spectra-out cross validation. The results indicate that RS can distinguish high-grade dysplasia from normal ectocervix and squamous metaplasia with a similar sensitivity of 92% and much higher specificity of 96% than colposcopy performed by experts (EK, EV, ARV).[6] The posterior probability output by the algorithm is also clinically-relevant since clinicians can recheck any sample having lower posterior probabilities of belonging to a category using the traditional biopsy method. However, further clinical studies were needed to increase the number of tissue spectra, especially from low-grade dysplasia, so independent training and test sets can be used to optimize the algorithm for discriminating all pathology categories of cervix.[5]

Additional data was collected to increase the number of samples within each category with particular emphasis on low-grade lesions. Low-grade patients were primarily collected from

		Raman Classification, output of MRDF and SMLR			
		High-grade	Low-grade	Metaplasia	Normal
Pathology	High-grade	**95%**	0	0	5%
	Low-grade	0	**74%**	0	26%
	Metaplasia	0	0	**90%**	10%
	Normal	0	0	4%	**96%**

Table 3.1. Confusion matrix showing classification of Raman spectra based on MRDF-SMLR

Tri-State Women's Health in Florence, KY during colposcopy-guided biopsies, so as to increase the likelihood of studying such patients.[6] A total of 110 patients were recruited and analyzed using the algorithm based on MRDF and SMLR. Due to the similarities found between spectra from the same patient,[1] leave-one-patient-out cross validation was performed, instead of leave-one-spectra-out as in the analysis above. The performance of spectra that were classified correctly into each category is reported as percentages in Table 3.1. The high-grade spectra classified correctly 95% of the time, and only one misclassified as normal. Low-grade data never classified as high-grade, but it did misclassify 26% of the time.[6] Even though emphasis was placed on the collection of low-grade spectra, only 23 low-grade spectra were obtained in this study, which may account for the higher misclassification rate. However, at this point, it also became clear that even with an increase in low-grade spectra, the spectra were still being misclassified at rates that would not be acceptable in a clinical setting. A different approach needed to be taken to see if the diagnostic algorithm and Raman spectra are sensitive enough to distinguish between normal and low-grade cervix.

In the next study, 133 patients undergoing either colposcopy-guided biopsy or Pap smear were recruited from either Vanderbilt University or Tri-State Women's Health. The same protocol and system (Figure 3.1) were used to acquire Raman spectra from diseased and normal cervix. First, the effect of location within menstrual cycle and menopausal state were investigated by using MRDF-SMLR to classify spectra into four categories: premenopausal proliferative phase (days 1-14 of the menstrual cycle) or premenopausal before ovulation (PBO); premenopausal secretory phase (days 15-28 of the menstrual cycle) or premenopausal after ovulation (PAO); perimenopausal (PERI); and postmenopausal (POST). Perimenopausal patients were defined as women between 45 and 55 years of age or with any symptoms of menopause, such as irregular periods or hot flashes. MRDF-SMLR was used to classify Raman spectra from normal cervix based on the four categories.

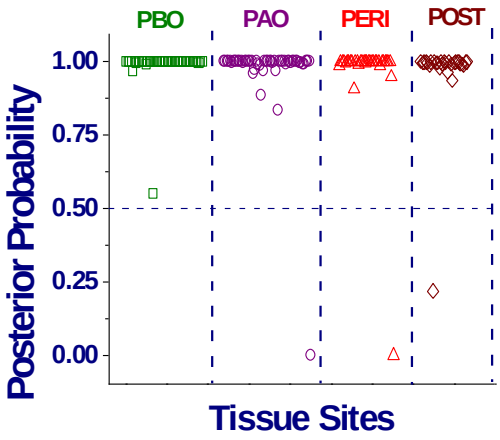

Figure 3.4. Posterior probabilities (chance that the spectrum belongs to a certain category) for spectra when classified based on menstrual cycle or menopausal status.

Out of the 156 spectra obtained from normal patients, only 3 misclassified or had posterior probabilities less than 0.5 (Figure 3.4) when classified as PBO, PAO, PERI, or POST. These results showed that the normal fluctuations caused by varying hormonal levels affects the Raman spectra, even if it does not affect the pathology of the cervix.[7, 8] From these results, we determined that normal variations may be masking the low-grade dysplasia spectra and hindering

MRDF-SMLR's ability to correctly classify such spectra. Our previous results with low-grade data classifying correctly only 74% of the time (Figure 3.5) is not feasible for use in clinical applications. By adding more patients into this study, we could begin stratifying data based on menstrual cycle and menopausal state. As seen in Figure 3.5, classifying data based on menopausal state before running statistical analysis results in not only a higher classification rate, from 88% to 94%, but also posterior probabilities that are closer to 1. Furthermore, low-grade spectra classified with 97% accuracy (EK and EV), proving that Raman spectra are indeed affected by normal changes that occur in the cervix.[7, 8]

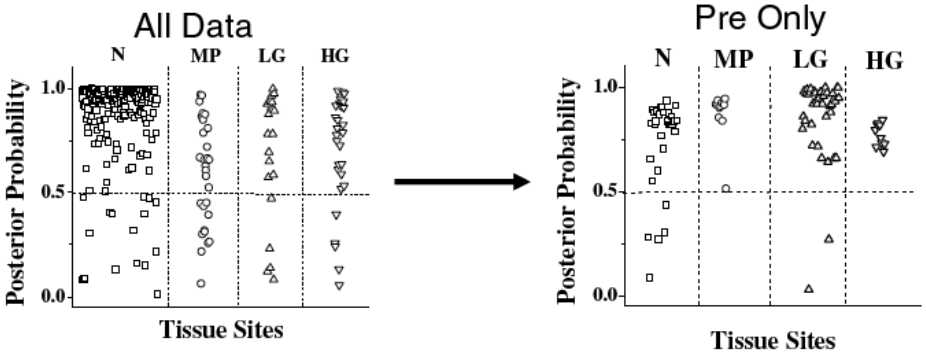

Figure 3.5. Posterior probabilities of classification as normal ectocervix (N), metaplasia (MP), low-grade (LG) and high-grade (HG) from the entire data set and the premenopausal data only.[3]

3.3 Understanding the Basis of Spectral Signatures

Organotypic raft cultures were used as a controlled *in vitro* model of *in vivo* tissue conditions to understand how alterations in tissue biology affect RS. Organotypic cultures are multilayer, three dimensional cultures designed to reproduce the *in vivo* structure and function of tissue. Raft cultures represent a specific type of organotypic cultures that reconstruct epithelial tissue types consisting of avascular epithelium attached via the basement membrane to a supporting connective tissue stroma. Three different types of rafts were constructed representing normal squamous tissue, squamous cell carcinoma (SCC) of skin and SCC of the cervix using

protocols developed in our lab.[9] Raman spectra were measured from multiple samples of each type of raft culture and compared with spectra acquired from intact cervical tissue *in vivo* (ARV).

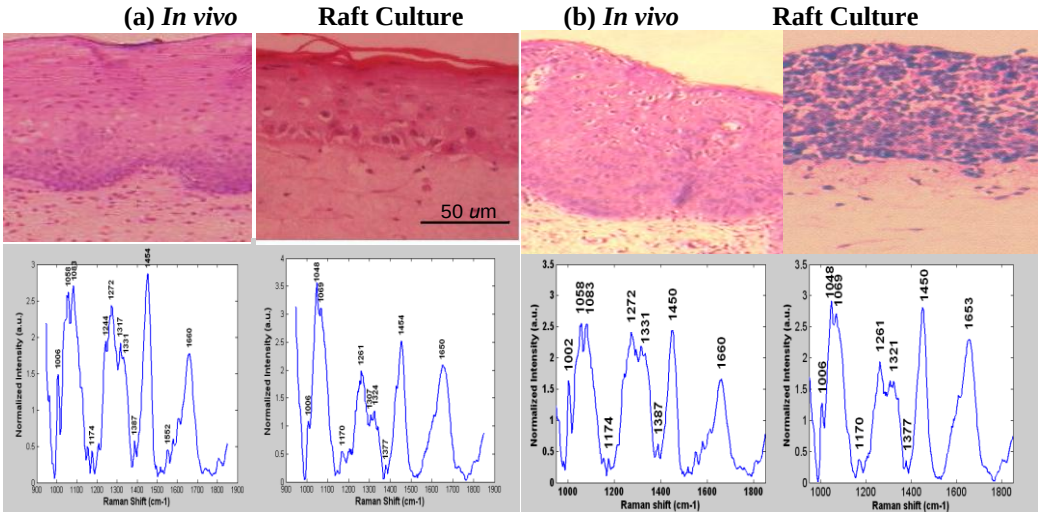

Figure 3.6. Comparison of *in vivo* vs. raft culture histology and Raman spectra. (a) Left panel shows histology (top) from an area of normal cervix squamous epithelium and the corresponding Raman spectra (bottom). Right panel shows results from raft cultures constructed using normal keratinocytes from neonatal foreskin with histology from a representative raft culture (top) and the corresponding Raman spectra (bottom). (b) Left panel shows histology (top) from a cervix with high-grade dysplasia and the corresponding Raman spectra (bottom). Right panel shows results from raft cultures constructed using SiHa (cervical squamous cell carcinoma cells). The top panel shows histology from a representative raft culture; the bottom panel is the Raman spectra.

Figure 3.6 shows histological and spectral comparison of raft cultures compared to intact tissues. Other studies in the breast have indicated that raft cultures are an accurate model for morphologic and biochemical representation of *in vivo* tissue.[10] The spectral differences seen between the dysplastic cultures and normal cultures parallel those seen between high-grade cervical dysplasia and normal ectocervix *in vivo*. The spectral contribution of the two layers of the cervix (epithelium and stroma) were analyzed in normal and dysplastic rafts and compared to *in vivo* tissue spectra. Results indicate that the key spectral differences observed *in vivo* arise primarily from the epithelial layers of the tissue. The 1325 cm^{-1} peak originates primarily from the epithelial layer in contrast to the 1272 cm^{-1} peak which has almost no contribution from the

epithelial layer and can be associated with the type I collagen in the stromal layer. Other peaks in the spectra were found to have equal contributions from the epithelial and stromal layers. This technique can be useful in perfecting the discrimination algorithm and in determining the effect of other components such as HPV infection on tissue Raman spectra.

3.4 References

1. Robichaux-Viehoever, A., Kanter E.M., Shappell H., Billheimer D., III Jones H., and Mahadevan-Jansen A. "Characterization of Raman spectra measured *in vivo* for the detection of cervical dysplasia." *Appl Spectrosc* **61**, 986-93 (2007).

2. Lieber, C.A. and Mahadevan-Jansen, A. "Automated method for subtraction of fluorescence from biological Raman spectra." *Appl Spectrosc* **57**, 1363-1367 (2003).

3. Neter J., e.a. (ed.) Applied Linear Statistical Models. 4th ed. (Irwin, Chicago, 1996).

4. Guillaud, M., Doudkine, A., Garner, D., MacAulay, C. and Palcic, B. "Malignancy associated changes in cervical smears: systematic changes in cytometric features with the grade of dysplasia." *Anal Cell Pathol* **9**, 191-204 (1995).

5. Talukder A. and Casasent D. "General methodology for simultaneous representation and discrimination of multiple object classes," *Opt Eng* **37**, 904-913 (1998).

6. Kanter, E.M., Majumder S., Vargis E., Robichaux-Viehoever A., Kanter G., Shappell H., III Jones H., and Mahadevan-Jansen A. "Multiclass discrimination of cervical precancers using Raman spectroscopy." *J Raman Spectrosc* **40** (2009).

7. Kanter, E.M., Majumder, S., Kanter, G.J., Woeste, E.M. and Mahadevan-Jansen, A. "Effect of hormonal variation on Raman spectra for cervical disease detection." *Am J Obstet Gynecol* **200**, 512-512 (2009).

8. Kanter E.M., Vargis E., Majumder S., Keller M.D., Beaven R.B., Rao G.G. and Mahadevan-Jansen A. "Application of Raman spectroscopy for Cervical Dysplasia Diagnosis." *J Biophotonics* **2**, 81-90 (2009).

9. Viehoever, A.R., Anderson, D., Jansen, D. and Mahadevan-Jansen, A. "Organotypic raft cultures as an effective *in vitro* tool for understanding Raman spectral analysis of tissue." *Photochem Photobiol* **78**, 517-524 (2003).

10. Shafer-Peltier, K.E., Haka, A.S., Fitzmaurice, M., Crowe, J., Myles, J., Dasari, R.R. and Feld, M.S. “Raman microspectroscopic model of human breast tissue: implications for breast cancer diagnosis *in vivo*.” *J Raman Spectrosc* **33**, 552-563 (2002)

CHAPTER 4

EFFECT OF NORMAL VARIATIONS ON DISEASE CLASSIFICATION OF RAMAN SPECTRA FROM CERVICAL TISSUE

This first step of this dissertation was to study the effect of proximity to disease and previous disease on correctly classifying spectra from diseased areas of the cervix. It corresponds to work performed prior to the development of the Specific Aims obtained from patients at Vanderbilt University and Tri-State Women's Health (Florence, KY). This chapter was published in the *Analyst*, a multidisciplinary journal that reports the development of analytical methods for clinical diagnostics.

Vargis E, Kanter EM, Majumder S, Keller MD, Beaven RB, Rao GG, A Mahadevan-Jansen. Effect of Normal Variations on Classification of Raman Spectra of Cervical Tissue. *Analyst*, 136: (14), 2981-2987, 2011

4.1 Abstract

In this paper, we examine how variations in normal tissue can influence classification of Raman spectra acquired from areas of disease. Raman spectra from normal areas may be affected by previous disease or proximity to areas of dysplasia. Spectra were acquired *in vivo* from 172 patients and classified into five tissue categories: true normal (no history of disease), previous disease normal (history of disease, current normal diagnosis), adjacent normal (disease on cervix, spectra acquired from visually normal area), low-grade disease, and high-grade disease. Taking into account the various ‘‘normal’’ states of the tissue before statistical analysis led to a disease classification accuracy of 97%. These results indicate that abnormal changes significantly affect Raman spectra, even when areas are histopathologically normal. The sensitivity of Raman

spectroscopy to subtle biochemical differences must be considered in order to successfully implement it in a clinical setting for diagnosing cervical dysplasia and cancer.

4.2 Introduction

Cervical cancer is the second most common malignancy among women worldwide, with over 529,000 new cases diagnosed and 275,000 deaths yearly.[1] Fortunately, cervical cancer takes years to progress from an intraepithelial lesion to an invasive disease, making screening and diagnostic tests successful in detecting early malignancies. In particular, the Papanicolaou (Pap) smear introduced in the 1950s has played a major role in reducing mortality from cervical cancer by up to 70%.[2] During this test, cells are exfoliated from the cervix, stained with the Papanicolaou stain, and examined visually under a light microscope to detect any abnormal morphological changes.[3] Recently, the presence of high-risk strains of the human papilloma virus (HPV) has been associated with the incidence and progression of cervical cancer.[4-6] Oncogenes found in these high-risk strains of HPV can block tumor suppressor gene products, such as p53 and pRb, which can cause cell proliferation and tumor formation.[7] The American College of Obstetrics and Gynecologists recommends that in conjunction with high-risk HPV testing, most women should undergo a Pap smear exam to screen for cervical dysplasia every 1 to 3 years.[8, 9] If abnormal cells are found during the Pap smear, a colposcopy-guided biopsy is required for a definitive diagnosis to determine the severity of the disease. From the diagnosis, the medical provider can decide on an appropriate treatment from a few choices: screen at a later date for follow-up or perform a loop electrosurgical excision procedure (LEEP) to remove disease areas of the cervix or perform a hysterectomy to remove the entire cervix.

However, up to 61% of women with abnormal Pap smears do not return for follow-up testing.[10, 11] This large number is due in part to a lack of access to easy, affordable healthcare for women.[12] Colposcopy-guided biopsies, although widely used, have been shown in some studies to have a low sensitivity and colposcopists have difficulty visually differentiating among tissue areas with different levels of malignancy.[13, 14] Even though many tools[15, 16] have been developed to aid colposcopists in choosing the best site to biopsy, they still rely on a biopsy which is painful, costly, and incompatible with delivering a real-time diagnosis.

A tool for screening and diagnosing cervical cancer in a single visit would have a tremendously positive impact on both the patients and the medical community by reducing the number of unnecessary biopsies, ameliorating the patient's stress, and eliminating the possibility of patients failing to present for follow-up evaluation.[17] Such a tool must be sensitive enough to differentiate among various benign and malignant histopathological categories of cervical tissue, including normal, inflammation, metaplasia, low-grade squamous intraepithelial lesion (LGSIL), high-grade squamous intraepithelial lesion (HGSIL), and cancer.

Optical techniques have the potential to fill the need for "see and treat" procedures due to their noninvasive nature and short measurement times, allowing for near-real-time diagnosis. In this study, we continue our research on using Raman spectroscopy (RS) for rapid cervical tissue discrimination.[18-21] Raman spectroscopy is a molecular-specific technique that provides detailed information about the biochemical composition of a sample by probing vibrational or rotational transitions in chemical bonds.[22]

Raman spectroscopy has been shown by multiple groups to be an effective method for cervical dysplasia detection.[20, 23-25] Previous studies in our lab and other labs have shown that spectroscopic techniques, including Raman, can be used to differentiate among normal, LGSIL,

and HGSIL.[19, 21] However, with a classification accuracy of only 88%, the full clinical potential of this method has not been achieved. During these prior studies, it became apparent that misclassifications of low-grade and normal spectra were one of the main reasons for the lower classification rates. Furthermore, the spectra from these two groups had more variance compared to the high-grade spectra. In order to understand a cause of this variance, the effect of hormonal (before and after ovulation) and menopausal status of the patients was determined.[21] Our previous results show that if we look at normal spectra alone, they classify according to hormonal and menopausal status with an accuracy of over 98%. Considering only spectra obtained from premenopausal women in the disease analysis led to a classification accuracy of normal, metaplasia, LGSIL, and HGSIL groups of over 94%, compared to the previous 88%. Other research groups have used similar optical techniques and found variability due to normal differences, such as hormonal levels, age, and type of cell population.[26-28] While these accuracies are higher than what is used currently, maximizing the classification accuracy of a new technology is necessary to increase its chance of becoming a part of routine medical care.

In order to implement this optical method in a clinical setting, further evaluation of the types of variations among normal spectra must be considered. Specifically, prior disease or presence of disease near a normal area of the cervix may alter those regions and consequently the Raman spectra obtained from them. Separating "true normal" data (no history of cervical disease) from "previous disease normal" data (history of abnormal cervix, currently histologically normal) and "adjacent normal" (histologically normal areas of cervix with current presence of disease) may reduce the variance in the normal data by accounting for any permanent changes caused by disease.

The goal of this research is to characterize normal variations and their effect on disease classification. In this paper, we present results from 2 clinical studies in which Raman spectra have been acquired from 165 patients undergoing either a routine annual screening consisting of a Pap smear or following up an abnormal Pap smear result with a colposcopy-guided biopsy. In the first study, Raman spectra were acquired from Pap smear patients to understand the impact of previous disease. In the second study, measurements were taken from patients coming in for screening and for biopsy to see how proximity to disease affects the classification of spectra. Next, a multivariate statistical algorithm has been used to classify Raman measurements of cervical tissue as either true normal or previous disease in the first study or true normal, adjacent normal, LGSIL, or HGSIL in the second study. From these results, we conclude that previous disease and proximity to disease significantly affect the Raman spectra acquired from histopathologically normal areas of the cervix. When the normal spectra are separated into different categories, the variance among the spectral classes decreases while the disease classification accuracy increases, demonstrating that this methodology is very sensitive to subtle biochemical changes that occur in or adjacent to tissue. These changes must be characterized before RS can be used clinically as a screening and diagnostic tool for cervical dysplasia.

4.3 Experimental Methods

Raman spectra were obtained from two sets of patients, Pap smear patients for study 1 and 2 and dysplasia patients for study 2. Pap smear patients are patients coming in for a routine annual screening for cervical cancer. These patients may have had an abnormal Pap smear result in the past, but any cervical disease has been treated and recent Pap smears have all been within normal limits. Dysplasia patients have had an abnormal Pap smear and are returning for a follow

up exam to visualize and biopsy (if necessary) specific diseased sites of the cervix. During this exam, acetic acid is placed on the cervix to whiten any abnormal areas. A colposcope is then used to visualize the cervix and a biopsy is taken from any abnormal area and examined by a pathologist to determine a diagnosis.

These studies were approved by the Copernicus Group and Vanderbilt Institutional Review Boards. To be eligible for enrollment, the patient must be undergoing a Pap smear or colposcopy-guided biopsy, be between the ages of 18-75, and still have a cervix (i.e. no history of a hysterectomy). Informed consent was obtained from each patient. The patient's age, last period date (for menstrual cycle), use of artificial hormones, menopausal status, and any previous abnormal Pap smears were all noted upon chart review. These two patient groups were designed in order to obtain data from true normal, previous disease normal, adjacent normal, LGSIL, and HGSIL areas of the cervix. These areas will be defined in greater detail below. Three to five Raman measurements were taken from each patient using a portable RS system and each measurement had an integration time of 3 seconds. A multivariate statistical algorithm (MRDF-SMLR) was then used to classify the data into one of the tissue categories.[20]

4.3.1 Clinical study design 1: Previous disease

In order to study the effect of previous disease on the classification of Raman spectra, we recruited patients during their annual cervical cancer screening. A total of 93 patients undergoing a routine Pap smear were recruited to this study. With an effect size of 1, the power of this study was over 90% (two-sample t-test, α=0.05). The following protocol was used to acquire the Raman spectra. The cervix was exposed and visually examined by the attending physician. The cervix was wiped clean with a dry cotton swab and then with a saline solution, after which

Raman measurements were taken from two to three locations on the ectocervix. The Pap smear procedure was done according to standard clinical protocol. If the patient's Pap smear was negative for disease and she had no history of abnormal Pap smears, the spectra were considered true normal. If she was negative for disease, but had a history of abnormal Pap smears, the spectra were considered previous disease normal. See Table 4.1 for the complete set of definitions. A total of 163 spectra were used in this study. Only spectra from women with a currently normal Pap smear result were used for further analysis.

Description	**True Normal**	**Previous Disease Normal**	**Adjacent Normal**	**LGSIL**	**HGSIL**
History of Abnormal Pap smear (i.e. one or more)	No	Yes	Yes	Yes	Yes
Evidence of Current Disease on the cervix regardless of location	No	No	Yes	Yes	Yes
Evidence of disease where measurement is taken	No	No	No	Yes	Yes
Presence of acetic acid	No (Study 1) Yes (Study 2)	No	Yes	Yes	Yes
Pathology results	normal	normal	N/A – No biopsy	Cervical intraepithelial neoplasm (CIN) I, HPV cellular effects	CIN II, CIN III, carcinoma in situ

Table 4.1 Summary of the categories used to describe the data sets.

4.3.2 Clinical study design 2: Adjacent normal

To study the effect of proximity to disease on classification accuracy, spectra were acquired from patients coming in for a routine cervical screening and from patients referred for biopsy following an abnormal Pap smear. Twenty-nine patients undergoing a routine Pap smear

and 43 patients who were referred for a colposcopy-guided biopsy following an abnormal Pap smear were recruited to participate in the study. With an effect size of 1, the power of this study was over 80% (two-sample t-test, α=0.05). To compare these two groups, acetic acid was applied to each patient. Specifically, for the Pap smear patients, the Pap smear was performed first, according to standard protocol as described above, prior to obtaining the Raman measurements so there were no changes to the Pap smear samples sent to the pathology lab due to the application of acetic acid. Next, the cervix was wiped clean with a dry cotton swab, a saline solution, and then with acetic acid. The Raman measurements were then taken from two to three locations on the ectocervix. For the colposcopy-guided biopsy patients, acetic acid was applied to the cervix to turn abnormal areas white for visualization and spectra were acquired from multiple areas of abnormal tissue that were to be biopsied and 1-2 visually normal areas. Abnormal tissue was then removed and placed in fixative solution for pathological examination.

Based on the pathology results from the Pap smear or the biopsy, spectra were placed into five categories for analysis: true normal, previous disease normal, adjacent normal, LGSIL, and HGSIL. True normal and previous disease normal were described above. Adjacent normal spectra were acquired from patients who were coming in for a biopsy and had abnormal areas on their cervix that were biopsied; these spectra were taken from the visually normal areas of the cervix. LGSIL and HGSIL spectra were acquired from areas of the cervix that were biopsied and diagnosed as such in the pathology report. Table 4.1 describes the five tissue categories within the two studies. A total of 146 spectra were used for further analysis. Only spectra from patients with no history of disease or current disease were used for the true normal samples. There were some cases where adjacent normal measurements were not acquired from the colposcopy-guided biopsy patient group.

4.3.3 Data Collection

Raman spectra were collected *in vivo* using a portable RS system consisting of a 785 nm diode laser (Process Instruments, Inc., Salt Lake City, UT), a beam-steered fiber optic probe (Visionex, Atlanta, GA), an imaging spectrograph (Kaiser Optical Systems, Ann Arbor, MI), and a back-illuminated, deep-depletion, thermo-electrically cooled CCD camera (Princeton Instruments, Princeton, NJ), all controlled with a laptop computer. Details of the system have been previously reported.[29] The fiber optic probe delivered 80 mW of incident light onto the tissue at an integration time of 3 seconds with all room lights turned off. The system provided a spectral resolution of 8 wavenumbers (cm^{-1}).

Spectral calibration of the system was performed each day using a neon-argon lamp and naphthalene and acetaminophen standards to correct for day-to-day variations. A National Institute of Standards and Technology (NIST)-calibrated tungsten lamp was also used to account for the wavelength dependent response of the system. The spectra were processed for fluorescence subtraction and noise smoothing using the modified polynomial fit and Savitzky-Golay methods, described previously.[29] Following data processing, each spectrum was normalized to its mean spectral intensity across all Raman bands to account for intensity variability.

4.3.4 Statistical Analysis

A multivariate statistical analysis method was used to classify the spectra as true normal or previous disease normal for the first study or as true normal, previous disease normal, adjacent normal, LGSIL, or HGSIL for the second study. Briefly, the process consists of two steps – first, nonlinear maximum representation and discrimination feature (MRDF) is used to extract

diagnostic features and reduce the dimensionality of the spectra; second, a probabilistic, multi-class scheme of classification based on sparse multinomial logistic regression (SMLR) is developed for classifying the MRDF output into corresponding tissue categories. This analysis outputs posterior probabilities that a given spectrum belongs to each histopathology class; the spectrum is then placed into the class corresponding to its highest probability of membership. All classification was performed using leave-one-patient-out cross-validation. Further details of this multivariate statistical analysis technique have been published previously.[30]

4.4 Results and Discussion

To understand the effect of normal variations on disease classification, Raman spectra were acquired and separated into the following categories: true normal – no history of cervical disease, previous disease normal – history of abnormal cervix, currently histologically normal, adjacent normal – histologically normal areas of cervix with current presence of disease, low-grade dysplasia – LGSIL, and high-grade dysplasia – HGSIL (Table 4.1). For this study, we were unable to collect enough data from patients who had areas of metaplasia and inflammation. In previous studies, statistically significant amounts of data from these two groups have been collected; spectra acquired from those areas classified correctly with over 90% accuracy.[19, 21]

4.4.1 Spectral difference – previous disease

The average Raman spectra from true normal ectocervix and previous disease normal ectocervix are shown in Figure 4.1. The area of the largest qualitative differences is in the 1200-1400 cm^{-1} range, indicated by the dashed box. The peak around 1250 cm^{-1}, associated with proteins like collagen type I, is higher in the true normal spectra compared to the previous

disease spectra.[31] The peak around 1330 cm^{-1}, which is usually associated with DNA and glycogen, is higher in the previous disease spectra compared to the normal spectra.[32, 33]

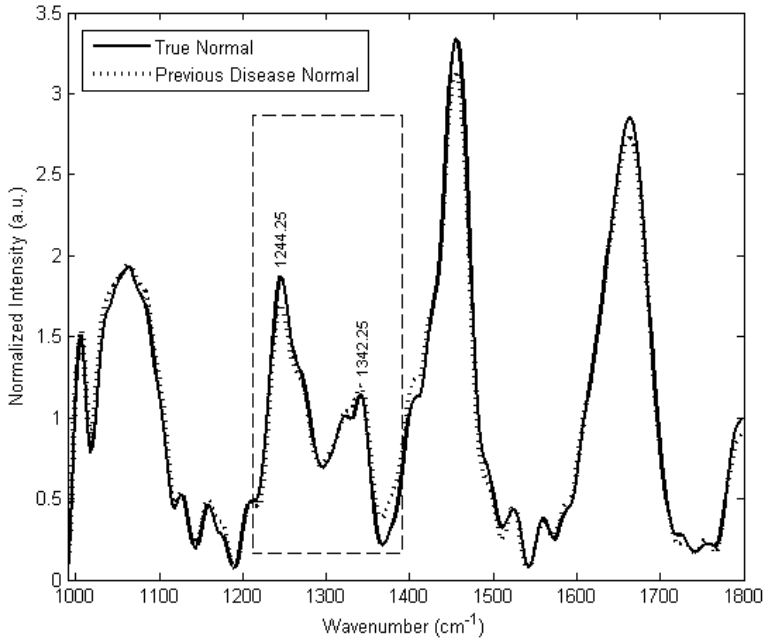

Figure 4.1 Average Raman spectra for true normal ectocervix and previous disease normal ectocervix. The area within the dashed box has the highest variability.

Even though these two groups would both be diagnosed as normal by a pathologist, there are areas of variation found in the spectra. These results suggest that the presence of any disease on the cervix may permanently change the biochemical and optical properties of the cervical tissue. Similar results have been found in breast tissue, where even the presence of benign disease (fibrocystic change) has a significant impact on normal optical properties of the breast.[28] Likewise, cervical disease is typically correlated with HPV infection. While the tissue may have either been treated for the disease or may no longer be diagnosed as abnormal, the HPV infection may have led to permanent changes in, for example, the amount and arrangement of DNA, collagen, and glycogen of the cervix.[34, 35]

4.4.2 Spectral differences – adjacent normal

A pilot study was first performed to investigate the effect of acetic acid on spectra acquired from the cervix. Average Raman spectra from normal ectocervix before and after the application of acetic acid are displayed in Figure 4.2 in 10 patients. Two areas of visual difference (1006 cm^{-1} and 1305 cm^{-1}) are seen in the spectra. However, these areas were highly variable and analyzing the spectra with the MRDF-SMLR algorithm described above yielded low classification rates, suggesting that the application of acetic acid does not significantly change the spectra to affect its classification. Acetic acid may increase the overall signal obtained from the cervix, but not enough to affect the classification accuracy of algorithms used for detecting normal differences or disease.

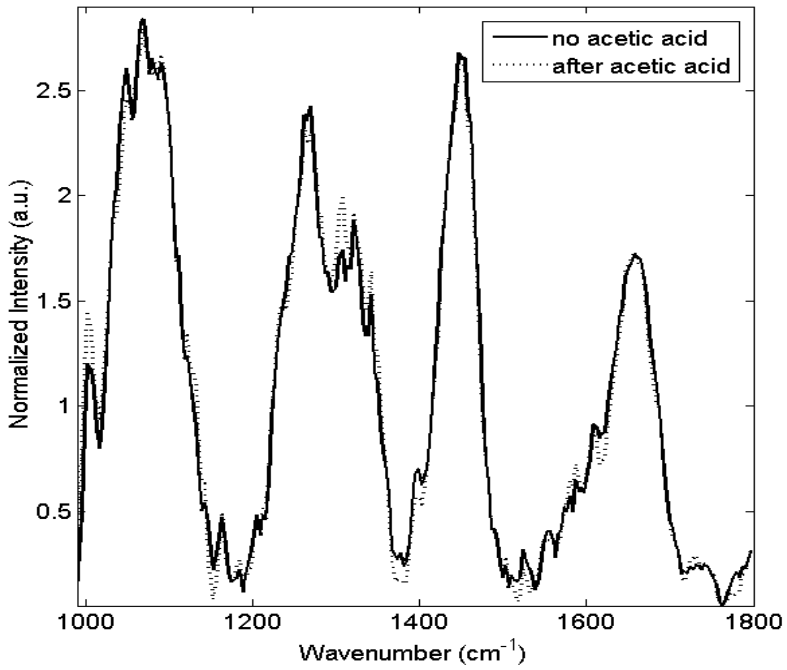

Figure 4.2. Average Raman spectra from high-grade dysplasia ectocervix before and after application of acetic acid. No significant differences were observed.

The average Raman spectra from true normal ectocervix, adjacent normal ectocervix, LGSIL, and HGSIL are shown in Figure 4.3. Due to the smaller patient population of this study,

the number of previous disease spectra acquired was not statistically significant. The spectra in this group are more varied compared to the previous group, which were both pathologically normal. Similar to the spectra in Figure 4.2, the largest qualitative difference between dysplasia and normal spectra occur in the 1200-1400 cm^{-1} range, highlighted by a dashed box. The peak around 1250 cm^{-1} (associated with collagen) is higher in both true normal and adjacent normal spectra. The relative amount of collagen decreases as the tissue becomes more dysplastic and disorganized. Similar changes occur as a woman becomes older, but this data has been obtained from a group of premenopausal women, between the ages of 18-45. Conversely, the peak around 1330 cm^{-1} (associated with glycogen and DNA) is higher in the LGSIL and HGSIL spectrum. This difference is consistent with changes that occur in dysplastic tissue. Specifically, the amount of DNA increases in dysplastic tissue due to rapid cell dividing and irregular growth.

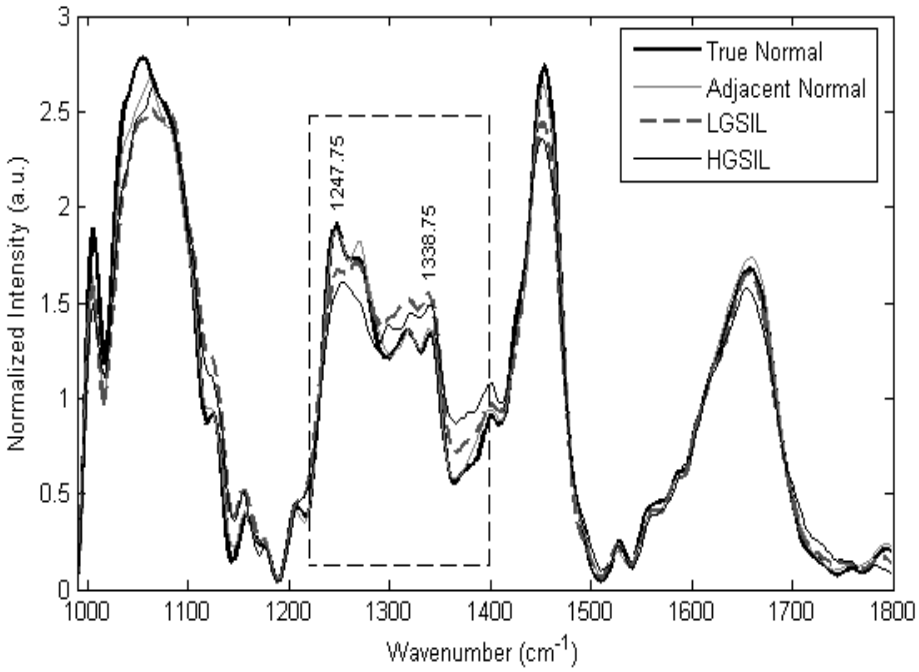

Figure 4.3. Average Raman spectra for true normal ectocervix, adjacent normal ectocervix, LGSIL, and HGSIL. Acetic acid was applied to all tissue prior to acquisition of the spectra. The area within the dashed box has the highest variability.

While the shape of the previous disease normal spectra does not appear to differ significantly from the true normal spectra (Figure 4.1), the adjacent normal appears more similar to the LGSIL spectra compared to the true normal spectra. The presence of disease on the cervix may affect the "normal" areas more adversely than a prior presence of abnormal cervical cells, making the adjacent normal spectra qualitatively resemble LSGIL spectra more than true normal spectra. Similar results have been reported with breast tissue.[28]

This concept has previously been described as malignancy associated changes (MACs) or field effect.[36, 37] MACs are defined as biochemical changes, such as chromatin rearrangement or a lower number of cell surface binding sites, which may be seen in histologically normal cells adjacent to a tumor.[38, 39] These subtle changes in areas near malignancy are typically only observed using high resolution techniques, like cytometry and fluorescence endoscopy.[40, 41] This idea was proposed in the 1950s and has been validated by studies in tissues such as the lung, cervix, blood, and breast.[40-43] A few studies using optical techniques have also found results that suggest their sensitivity to detecting MACs.[44-46]

4.4.3 Multivariate Statistical Analysis

Based on these and other spectral differences, a multivariate algorithm was used to classify the data into the aforementioned tissue classes (true normal, previous disease normal, adjacent normal, LGSIL, and HGSIL). Data acquired from premenopausal women alone was used in the analysis, based on results discussed previously.[19] The overall results using MRDF and SMLR can be seen for the study 1 and 2 in Table 4.2 and Table 4.3, respectively. In the first study, the algorithm classified the two tissues types with an accuracy of over 99%. Only 1 previous disease normal spectrum misclassified as true normal (out of 163, Table 4.2). For the

second study, the MRDF-SMLR algorithm classified the four tissue types with 97% accuracy. Its best performance was with true normal and HGSIL, where all spectra were classified correctly. Four of the 146 spectra from this study misclassified (Table 4.3).

Classification Accuracy: 99%		Raman Classification	
		True Normal	Previous Disease Normal
Histological Classification	True Normal ($n_{spectra}$=110)	**109**	1
	Previous Disease Normal ($n_{spectra}$=53)	0	**53**

Table 4.2. Classification of true normal and previous disease normal spectra using MRDF and SMLR with leave-one-patient-out cross-validation.

Classification Accuracy: 97%		Raman Classification			
		True Normal	Adjacent Normal	LGSIL	HGSIL
Histological Classification	True Normal ($n_{spectra}$=52)	**52**	0	0	0
	Adjacent Normal ($n_{spectra}$=37)	1	**35**	0	1
	LGSIL ($n_{spectra}$=45)	1	1	**43**	0
	HGSIL ($n_{spectra}$=12)	0	0	0	**12**

Table 4.3. Classification of true normal, adjacent normal, LGSIL, and HGSIL spectra using MRDF and SMLR with leave-one-patient-out cross-validation.

In Figure 4.4, posterior probabilities are shown from the classifications from Table 4.3 to demonstrate how correct and incorrect classifications are generated. Furthermore, it shows the probabilistic nature of the technique could help a medical provider decide on a diagnosis, based on the spectra alone. The provider could acquire the Raman spectra, use MRDF-SMLR to classify them, and then based on the posterior probability generated by the algorithm, decide on the appropriate course of action. If spectra have a posterior probability close to 1, the provider

can rely on the spectra belonging to that classification group with a high amount of accuracy without the need for a Pap smear or a colposcopy-guided biopsy to confirm (spectrum highlighted with dashed box, Figure 4.4). However, for example, if the algorithm calculates the posterior probability of a normal spectrum as approximately 0.6 (spectrum highlighted by dashed circle, Figure 4.4), the provider can always continue with the current clinical protocol to verify the diagnosis. For the spectra represented in Figure 4.4, the probabilities for LGSIL spectra are all near 1, indicating that there is a very high chance that the spectra belong within that category. There is a larger variation in the probabilities of the other tissue categories, though many of the correct classifications still display probabilities close to 1, which is a result that may help RS become clinically relevant to positively affect patient care.[47]

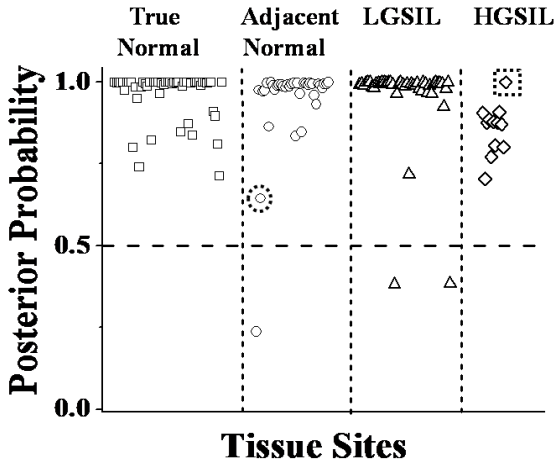

Figure 4.4. Posterior probabilities of classification as true normal ectocervix, adjacent normal ectocervix, LGSIL, and HGSIL. The dashed box has a spectrum with a posterior probability close to 1; the dashed circle has a spectrum with a posterior probability close to 0.6.

In the previous disease study, 1 out of 163 spectra misclassified as true normal. This 1 spectrum was from an inflamed area of the cervix. In the adjacent normal study, 4 out of 146 spectra were misclassified. Two adjacent normal samples were misclassified: one as true normal and one as HGSIL. The first sample was from a patient who was returning for her first follow-up

after her first abnormal Pap exam. The spectrum that incorrectly classified as HGSIL was diagnosed as intense chronic endocervicitis, a benign inflammatory condition usually resulting from a pathogenic bacteria.[48] Two LGSIL spectra misclassified, one as true normal and the other as adjacent normal. The first misclassification correlated with biopsy results of mild HPV changes (LGSIL) in the tissue but no dysplasia. For the second misclassification, the abnormal area may have been at the very early stages of disease or with cervical biopsy error rates between 12-15%, the pathologic result may be incorrect.[49] Although these 5 misclassifications only represent 1.6% of the data acquired, some conclusions can be drawn from them. First, disease may take a longer time to affect nearby normal areas. Other diagnostic categories, such an inflammation, to account for areas of endocervicitis, and early HPV effects, may need to be incorporated in future implementations of the statistical algorithm for RS to be used clinically. For example, florid cervicitis may need to be a separate classification category or may just simply as inflammation. Finally, there can be small differences between where the Raman measurement was acquired from and what area was excised for pathology, which could specifically account for the errors in LGSIL classifications.

4.4.4 Clinical Impact and Future Considerations

The ultimate goal of this research is to use RS for real-time diagnosis of cervical precancers, effectively eliminating the majority of Pap smears, follow up exams, and colposcopy-guided biopsies, widening the success of early screening.[17] The focus of this paper, however, is on normal tissue and its variations, which may seem contradictory to diagnosing disease. Yet, before RS can move from the lab to the clinic, we have to understand the effect of normal physiological variability on Raman spectral signatures. Once the normal variations are

understood, we can continue to understand the effect of disease on RS to improve diagnosis.[28] The results of this study show that variations in normal spectra are statistically significant. Furthermore, incorporating normal variations into the disease classification algorithm results in better classification overall, including within the disease groups.

The current standard of care dictates that acetic acid is applied to patients coming in for a colposcopy-guided biopsy. Therefore, for the adjacent normal study, acetic acid was applied to both normal and dysplasia patients in order to compare and classify spectra acquired from each group. The initial study, looking for any statistically significant effects on the Raman spectra after applying acetic acid, suggests that its application does not change the accuracy or performance of classifying Raman spectra (Figure 4.2). This result has been found in similar studies looking at fluorescence spectra acquired from the cervix, with or without the presence of acetic acid.[50] both groups of this study, results shown in Figure 4.2 and Figure 4.3 confirm that RS can be used to detect disease, with or without acetic acid. In future applications, it will be possible to implement RS for disease classification whether acetic acid is used or not.

Other variations may need to be considered to fully characterize the sensitivity of RS and optimize it for disease classification. While age and hormonal changes have already been considered,[19, 21] previous disease and proximity to disease were the focus of this paper. Ethnicity, socioeconomic status, and body mass index are other factors that may also have an effect on the normal cervix and therefore the Raman spectra.[28] From the posterior probabilities shown in Figure 4, it also seems that there is a high variance among HGSIL spectra. As Table 4.1, row 6 shows, HGSIL corresponds to a number of pathological results; the HGSIL category may potentially need to be separated into subcategories so the spectra classify with a posterior

probability closer to 1. A restrospective analysis, where a few patients were followed after a diagnosis of HGSIL may to fully characterize the sensitivity of Raman spectroscopy.

The results from our previous studies demonstrated that RS can classify spectra from normal, LGSIL, and HGSIL areas of the cervix with 94% accuracy.[19] This previous analysis only included premenopausal women, which improved upon the prior 88% classification rate. However, the normal category from that study included women who may have had a previous abnormal Pap smear. In this paper, we have demonstrated that by accounting for normal variations, the classification accuracy of cervical disease increases from 94% to 97%.

4.5 Conclusions

This paper describes the continued development of RS to discriminate between normal, benign and malignant areas of the cervix. The results of this paper demonstrate the significant sensitivity inherent in RS, suggesting it can be successfully implemented in clinical applications for diagnosing disease. Teasing out these subtleties will improve the sensitivity and specificity of disease classification, leading to the use of RS for the diagnosis of cervical malignancies *in vivo*.

4.6 Acknowledgements

The authors acknowledge the financial support of the NCI/NIH (R01-CA95405). We would also like to thank the doctors and staff at Vanderbilt University Medical Center and Tri-state Women's Health for all of their help.

4.7 References

1. Ferlay, J., Shin, H.R., Bray, F., Forman, D., Mathers, C., and Parkin, D.M. "Estimates of worldwide burden of cancer in 2008: GLOBOCAN 2008." *Int J Cancer* **127**, 2893–2917 (2010).

2. Williams, G.H., Romanowski, P., Morris, L., Madine, M., Mills, A.D., Stoeber, K., Marr, J., Laskey, R.A., and Coleman, N. "Improved cervical smear assessment using antibodies against proteins that regulate DNA replication." *Proc Natl Acad Sci U S A* **95**, 14932-7 (1998).

3. Wood, B.R., Chiriboga, L., Yee, H., Quinn, M.A., McNaughton, D., and Diem, M. "Fourier transform infrared (FTIR) spectral mapping of the cervical transformation zone, and dysplastic squamous epithelium." *Gynecol Oncol* **93**, 59-68 (2004).

4. Schiffman, M.H., Bauer, H.M., Hoover, R. N., Glass, A.G., Cadell, D.M., Rush, B.B., Scott, D. ., Sherman, M.E., Kurman, R.J. and Wacholder, S. "Epidemiologic evidence showing that human papillomavirus infection causes most cervical intraepithelial neoplasia." *J Natl Cancer Inst* **85**, 958-64 (1993).

5. Manos, M.M., Kinney, W.K., Hurley, L.B., Sherman, M.E., Shieh-Ngai, J., Kurman, R.J., Ransley, J.E., Fetterman, B.J., Hartinger, J.S., McIntosh, K.M., Pawlick, G.F. and Hiatt, R.A. "Identifying women with cervical neoplasia: using human papillomavirus DNA testing for equivocal Papanicolaou results." *JAMA-J Am Med Assoc* **281**, 1605-10 (1999).

6. Furumoto, H. and Irahara, M. "Human papilloma virus (HPV) and cervical cancer." *J Med Invest* **49**, 124-33 (2002).

7. Scheffner, M., Münger, K., Byrne, J.C. and Howley, P.M. "The state of the p53 and retinoblastoma genes in human cervical carcinoma cell lines." *P Natl Acad Sci U S A* **88**, 5523 (1991).

8. Elfgren, K., Jacobs, M., Walboomers, J.M., Meijer, C.J. and Dillner, J. "Rate of human papillomavirus clearance after treatment of cervical intraepithelial neoplasia." *Obstet Gynecol* **100**, 965-71 (2002).

9. ACOG Practice Bulletin no. 109: Cervical cytology screening. *Obstet Gynecol* **114**, 1409-20 (2009).

10. Khanna, N. and Phillips, M.D. "Adherence to care plan in women with abnormal Papanicolaou smears: a review of barriers and interventions." *J Am Board Fam Pract* **14**, 123-30 (2001).

11. Miller, S.M., Siejak, K.K., Schroeder, C.M., Lerman, C., Hernandez, E., & Helm, C.W. "Enhancing adherence following abnormal Pap smears among low-income minority women: a preventive telephone counseling strategy." *J Natl Cancer Inst* **89**, 703-8 (1997).

12. Lindau, S.T., Tomori, C., McCarville, M.A. & Bennett, C.L. “Improving rates of cervical cancer screening and Pap smear follow-up for low-income women with limited health literacy.” *Cancer Invest* **19**, 316–32 (2001).

13. Wright, T.C., Jr., Cox, J.T., Massad, L.S., Carlson, J., Twiggs, L.B., andWilkinson, E.J. “2001 consensus guidelines for the management of women with cervical intraepithelial neoplasia.” *Am J Obstet Gynecol* **189**, 295-304 (2003).

14. Massad, L.S. and Collins, Y.C. “Strength of correlations between colposcopic impression and biopsy histology.” *Gynecol Oncol* **89**, 424-8 (2003).

15. Ferris, D.G., Lawhead, R. A., Dickman, E. D., Holtzapple, N., Miller, J. A., Grogan, S., Bambot, S., Agrawal, A. and Faupel, M.L. “Multimodal hyperspectral imaging for the noninvasive diagnosis of cervical neoplasia.” *J Low Genit Tract D* **5**, 65-72 (2001).

16. Balas, C., Papoutsoglou, G. and Potirakis, A. “*In vivo* molecular imaging of cervical neoplasia using acetic acid as biomarker.” *IEEE J Quantum Elect* **14**, 29 (2008).

17. Shinn, E., Basen-Engquist, K., Le, T., Hansis-Diarte, A., Bostic, D., Martinez-Cross, J., Santos, A. and Follen, M. “Distress after an abnormal Pap smear result: scale development and psychometric validation.” *Prev Med* **39**, 404-12 (2004).

18. Robichaux-Viehoever, A., Kanter E.M., Shappell H., Billheimer D., III Jones H., and Mahadevan-Jansen A. “Characterization of Raman spectra measured *in vivo* for the detection of cervical dysplasia.” *Appl Spectrosc* **61**, 986-93 (2007).

19. Kanter E.M., Vargis E., Majumder S., Keller M.D., Beaven R.B., Rao G.G. and Mahadevan-Jansen A. “Application of Raman spectroscopy for Cervical Dysplasia Diagnosis.” *J Biophotonics* **2**, 81-90 (2009).

20. Kanter, E.M., Majumder S., Vargis E., Robichaux-Viehoever A., Kanter G., Shappell H., III Jones H., and Mahadevan-Jansen A. “Multiclass discrimination of cervical precancers using Raman spectroscopy.” *J Raman Spectrosc* **40** (2009).

21. Kanter, E.M., Majumder, S., Kanter, G.J., Woeste, E.M. and Mahadevan-Jansen, A. “Effect of hormonal variation on Raman spectra for cervical disease detection.” *Am J Obstet Gynecol* **200**, 512-512 (2009).

22. Mahadevan-Jansen, A. in Biomedical Photonics Handbook (ed. Vo-Dinh, T.), 30-1 (CRC Press, Washington DC, 2003).

23. Utzinger, U., Heintzelman, D. L., Mahadevan-Jansen, A., Malpica, A., Follen, M., and Richards-Kortum, R. “Near-Infrared Raman Spectroscopy for *in vivo* Detection of Cervical Precancers.” *Appl Spectrosc* **55**, 955-959 (2001).

24. Krishna, C.M., Prathima, N. B., Malini, R., Vadhiraja, B. M., Bhatt, R. A., Fernandes, D. J., Kushtagi, P., Vidyasagar, M.S. and Kartha, V.B. “Raman spectroscopy studies for diagnosis of cancers in human uterine cervix.” *Vib Spectrosc* **41**, 136-141 (2006).

25. Jess, P.R.T., Smith, D.D.W., Mazilu, M., Dholakia, K., Riches, A.C., and Herrington, C.S. "Early detection of cervical neoplasia by Raman spectroscopy." *Int J Cancer* **121**, 2723-2728 (2007).

26. Chang, S.K., Dawood, M.Y., Staerkel, G., Utzinger, U., Atkinson, E.N., Richards-Kortum, R.R and Follen M. "Fluorescence spectroscopy for cervical precancer detection: Is there variance across the menstrual cycle?" *J Biomed Opt* **7**, 595-602 (2002).

27. Walsh, M.J., Singh, M.N., Stringfellow, H.F., Pollock, H.M., Hammiche, A., Grude, O., Fullwood, N.J., Pitt, M.A., Martin-Hirsch, P.L. and Martin, F.L. "FTIR Microspectroscopy Coupled with Two-Class Discrimination Segregates Markers Responsible for Inter- and Intra-Category Variance in Exfoliative Cervical Cytology." *Biomark Insights* **3**, 179-189 (2008).

28. Thomsen, S. and Tatman, D. "Physiological and Pathological Factors of Human Breast Disease That Can Influence Optical Diagnosis." *Ann N Y Acad Sci* **838**, 171-193 (1998).

29. Lieber, C.A. and Mahadevan-Jansen, A. "Automated method for subtraction of fluorescence from biological Raman spectra." *Appl Spectrosc* **57**, 1363-1367 (2003).

30. Majumder, S.K., Gebhart, S., Johnson, M.D., Thompson, R., Lin, W.C., and Mahadevan-Jansen, A.. "A probability-based spectroscopic diagnostic algorithm for simultaneous discrimination of brain tumor and tumor margins from normal brain tissue." *Appl Spectrosc* **61**, 548-57 (2007).

31. Goheen, S.C., Lis, L.J. and Kauffman, J.W. "Raman spectroscopy of intact feline corneal collagen." *BBA Protein Struct* **536**, 197-204 (1978).

32. Kendall, C., Stone, N., Shepherd, N., Geboes, K., Warren, B., Bennett, R., and Barr H. "Raman spectroscopy, a potential tool for the objective identification and classification of neoplasia in Barrett's oesophagus." *J Pathol* **200**, 602-9 (2003).

33. Nijssen, A., Bakker Schut, T.C., Heule, F., Caspers, P.J., Hayes, D.P., Neumann, M.H., and Puppels, G.J. "Discriminating basal cell carcinoma from its surrounding tissue by Raman spectroscopy." *J Invest Dermatol* **119**, 64-9 (2002).

34. McCance, D.J., Kopan, R., Fuchs, E. and Laimins, L.A. "Human papillomavirus type 16 alters human epithelial cell differentiation *in vitro*." *Proc Natl Acad Sci U S A* **85**, 7169 (1988).

35. Schneider, A. "Pathogenesis of genital HPV infection." *Br Med J* **69**, 165 (1993).

36. Nieburgs, H.E. "Recent progress in the interpretation of malignancy associated changes (MAC)." *Acta Cytol* **12**, 445-53 (1968).

37. Slaughter, D.P., Southwick, H.W. and Smejkal, W. "Field cancerization in oral stratified squamous epithelium; clinical implications of multicentric origin." *Cancer* **6**, 963-8 (1953).

38. Inbar, M., Ben-Bassat, H. and Sachs, L. "Membrane changes associated with malignancy." *Nat New Biol* **236**, 3-4 passim (1972).

39. Susnik, B., Worth, A., LeRiche, J. and Palcic, B. "Malignancy-associated changes in the breast. "Changes in chromatin distribution in epithelial cells in normal-appearing tissue adjacent to carcinoma." *Anal Quant Cytol Histol* **17**, 62 (1995).

40. Ikeda, N., MacAulay, C., Lam, S., LeRiche, J., Payne, P., Garner, D., Konaka, C, Kato, H and Palcic, B. "Malignancy associated changes in bronchial epithelial cells and clinical application as a biomarker." *Lung cancer* **19**, 161 (1998).

41. Mommers, E. and Poulin, N. "Malignancy-associated changes in breast tissue detected by image cytometry." *Anal Cell Pathol* **20**, 187-195 (2000).

42. Guillaud, M., Doudkine, A., Garner, D., MacAulay, C. and Palcic, B. "Malignancy associated changes in cervical smears: systematic changes in cytometric features with the grade of dysplasia." *Anal Cell Pathol* **9**, 191 (1995).

43. Nieburgs, H.E., Goldberg, A. F., Bertini, B., Silagi, J., Pacheco, B., and Reisman, H. "Malignancy associated changes (MAC) in blood and bone marrow cells of patients with malignant tumors." *Acta Cytol* **11**, 415-23 (1967).

44. Keller, M.D., Kanter, E.M., Lieber, C.A., Majumder, S.K., Hutchings, J., Ellis, D.L., Beaven, R.B., Stone, N. and Mahadevan-Jansen, A. "Detecting temporal and spatial effects of epithelial cancers with Raman spectroscopy." *Dis Markers* **25**, 323-37 (2008).

45. Lieber, C., Majumder, S., Ellis, D., Billheimer, D. and Mahadevan Jansen, A. "*In vivo* nonmelanoma skin cancer diagnosis using Raman microspectroscopy." *Laser Surg Med* **40**, 461-467 (2008).

46. Arndt, R., Briscoe, W., Strakovsky, I. and Workman, R. "Partial-wave analysis and baryon spectroscopy." *Eur Phys J A* **35**, 311-316 (2008).

47. Choo-Smith, L.P., Edwards, H.G., Endtz, H.P., Kros, J.M., Heule, F., Barr, H., Robinson, J.S., Jr., Bruining, H.A. and Puppels, G.J. "Medical applications of Raman spectroscopy: from proof of principle to clinical implementation." *Biopolymers* **67**, 1-9 (2002).

48. ACOG committee opinion No. 431: routine pelvic examination and cervical cytology screening. *Obstet Gynecol* **113**, 1190-3 (2009).

49. Barker, B., Garcia, F., Lozevski, J., Warner, J. and Hatch, K. "The Correlation between Colposcopically Directed Cervical Biopsy and Loop Electrosurgical Excision Procedure Pathology and the Effect of Time on That Agreement." *Gynecol Oncol* **82**, 22-26 (2001).

50. A. R. Viehoever, PhD Thesis, Vanderbilt University (2004).

CHAPTER 5

SENSITIVITY OF RAMAN SPECTROSCOPY TO NORMAL PATIENT VARIABILITY

This chapter describes the first study of this PhD dissertation, looking at the effect of normal variables on Raman spectra acquired from the normal cervix. It corresponds to Specific Aim 1. The Raman data was acquired from patients at Meharry Medical College. This chapter was published in the *Journal of Biomedical Optics.*

Vargis E, Byrd T, Logan Q, Khabele D, A Mahadevan-Jansen. Sensitivity of Raman Spectroscopy to Normal Patient Variability. *Journal of Biomedical Optics* 16 (11): 117004-1-9, 2011

5.1 Abstract

Many groups have used Raman spectroscopy for diagnosing cervical dysplasia, however there have been few studies looking at the effect of normal physiological variations on Raman spectra. This study assesses four patient variables that may affect normal Raman spectra: Race/ethnicity, body mass index (BMI), parity, and socioeconomic status. Raman spectra were acquired from a diverse population of 75 patients undergoing routine screening for cervical dysplasia. Classification of Raman spectra from patients with a normal cervix was performed using SMLR to determine if any of these variables had a significant effect. Results suggest that BMI and parity have the greatest impact, while race/ethnicity and socioeconomic status have a limited effect. Incorporating BMI and obstetric history into classification algorithms may increase sensitivity and specificity rates of disease classification using Raman spectroscopy. Studies are underway to assess the effect of these variables on disease.

5.2 Introduction

Multiple research groups have taken advantage of the extreme sensitivity of Raman spectroscopy (RS) to detect subtle changes in a variety of samples. Raman spectroscopy has been used to solve many types of problems, from detecting malignant areas in various sites, such as the cervix,[1] bladder,[2, 3] colon,[4, 5] breast,[6, 7] and esophagus[8, 9] *in vivo* and *in vitro*, detecting controlled substances,[10] and authenticating works of art.[11] Raman spectroscopy is useful for multiple applications because it is a molecular-specific technique that provides detailed information about the biochemical composition of a sample by probing vibrational or rotational transitions in chemical bonds. Therefore, a Raman spectrum consists of a series of spectrally-narrow peaks and valleys which represent the different vibrational modes of specific scattering molecules. These peaks are associated with specific bonds, such that a Raman spectrum may be referred to as a biochemical fingerprint of a molecule, tissue or sample. Changes in peaks may be related to differences in the concentration of glycogen or collagen,[12] which is useful in cancer detection, benzoic acid rings for detecting illegal drugs,[13] and natural or synthetic stains to decipher ages of works of art.[14]

Although RS is inherently a sensitive technique, previous studies using Raman to detect cervical dysplasia both *in vivo* and *in vitro* have reported a wide range of sensitivity (70-100%) and specificity (70-100%) rates.[1, 15-19] Krishna *et al.* used a bench top RS system to acquire information from cervical samples *ex vivo* and classified normal compared to malignant samples at sensitivity and specificity rates of 75% to 99.5%.[19] Since infection with certain strains of human papillomavirus (HPV) is the cause of cervical dysplasia in over 99% of cases worldwide,[20-22] certain research groups have used RS to identify differences between HPV types. Jess *et al.* used a confocal Raman microscope system and were able to discriminate varying HPV

types in live and fixed cells with sensitivity and specificity rates of 70% to 100%.[15] Our research group has used a portable probe-based RS system to distinguish between normal and malignant cervical samples in cell culture, *in vitro* and *in vivo*. The sensitivity and specificity rates of this work have ranged between 81% and 97%.[1, 16, 17]

Variations in classification rates that are observed when using RS to detect malignant areas of the cervix are a hurdle that must be overcome in order for this technology to benefit clinical practice. Fortunately, as more research into using RS to diagnose cervical dysplasia has been conducted, it has become apparent that by accounting for normal patient variations, the sensitivity and specificity of Raman for diagnosing disease can increase.[23, 24] Similar research on inherent normal patient variability has been seen when using Raman on other tissue sites, such as the colon and the breast.[25-27] In many cases, accounting for these normal differences has led to an increase in both the sensitivity and specificity rates of classifying normal spectra compared to disease.

Specifically, research from our lab has shown that both hormonal differences due to menstrual cycles and menopause[23] and previous disease or presence near disease[24] have a significant impact on the Raman spectra acquired from benign areas of the cervix *in vivo* as well as the classification of spectra acquired from metaplastic and dysplastic sites. During a menstrual cycle and menopause, varying levels of hormones are released throughout the body that can cause changes in the cervix, including softening, drying or thinning.[28, 29] Permanent field effects or malignancy-associated changes that result from the presence or prior history of disease may account for the significant effect of such differences on Raman spectra.[30, 31] Accounting for hormonal levels and history of disease prior to disease classification resulted in sensitivity and specificity rates of over 95%. By recognizing and accounting for these normal variations prior to

disease classification, better training sets were used for the classification algorithms, and therefore, differences among spectra were more likely to result from malignancy than normal variations. Other factors may further improve cervical disease classification with RS.

Race and ethnicity, for example, as well as socioeconomic status are all correlated with different incidences of cervical malignancies.[32] In 2010, black and Hispanic populations had the highest incidence of and mortality rates from cervical dysplasia in the US (11.1 cases and 4.6 deaths and 12.7 cases and 3.1 deaths per 100,000 women, respectively, compared to 7.9 cases and 2.2 deaths per 100,000 white women).[33, 34] Worldwide, cervical cancer is the fifth most common cancer for women and the most common cancer for women in Central America and southern Africa.[35] These differences are likely correlated with less access to routine care and screening. Obesity is also associated with higher rates of cancer, including cervical cancer.[22, 36, 37] There are many potential reasons for the contribution of obesity to cervical cancer, including differences in vaginal flora patterns, steroid hormone and cholesterol levels, cultural norms and bacterial or viral infections.[36] HPV could also be a potential factor in the differences in incidence and mortality rates since several high-risk strains are more prevalent in certain racial and ethnic populations.[20-22] Any of these characteristics may significantly influence the biochemical makeup of the cervix and thus the Raman spectra acquired from the cervix. Such important variables must be accounted for prior to disease classification to increase classification accuracy rates.

It is interesting to explore whether other optical techniques are similarly influenced by normal patient variables. Studies have shown that fluorescence spectroscopy is not significantly influenced by changes that occur during a woman's menstrual cycle or menopause as it only causes a variation of 8-16% in normal spectra.[38, 39] This result suggests that fluorescence

spectroscopy is not sensitive to the small biochemical changes that occur as a result of the fluctuations in normal hormonal levels. Biochemical changes due to hormonal fluctuations, age, and parity have been observed in the breast using reflectance and transmittance spectroscopy,[40, 41] however their effect on disease classification has yet to be determined. Similar results have been found in the cervix,[42] but these results are controlled by levels of hemoglobin, water and lipids, instead of the broader biochemical fingerprint obtained with RS. Kelly *et al*. used infrared (IR) spectroscopy to separate samples based on HPV infection and age and was able to show separation of samples using principal component analysis followed by linear discriminant analysis (PCA-LDA), but this *in vitro* study was performed on cells grown in culture.[43] IR spectroscopy, analogous to RS, may perform with similar sensitivity rates. However, the water content found in bulk tissue may inhibit IR spectra, thereby reducing its utility as a tool for *in vivo* detection. To our knowledge, there are no published reports that consider the effect of race/ethnicity, BMI, obstetric history or socioeconomic status on optical measurements.

The goal of this study is to examine the significance of such normal variations on the classification of Raman spectra. Implementing RS in a clinical setting will require it to be successfully applied to any patient population, regardless of race or ethnicity, body mass index (BMI), parity, or socioeconomic status. To accomplish this goal, Raman measurements were acquired from a diverse patient population without current or previous disease. A classification algorithm (SMLR) was then used to determine if the Raman spectra were significantly affected by race/ethnicity, BMI, obstetric history or socioeconomic status.

5.3 Materials and Methods

In our lab, previous studies were performed on a predominantly white population with BMI levels of normal to overweight.[1, 17, 23, 24] For this study, patients were recruited from the county hospital in Nashville, TN (Nashville General Hospital at Meharry Medical College) to acquire data from patients of varying racial/ethnic background, BMI, obstetric history and socioeconomic status. This study was approved by the Meharry Medical College Institutional Review Board.

5.3.1 Patient Enrollment

A total of 75 adult, female patients undergoing a routine Pap smear were consented to participate in the study. With an effect size of 1, the power of this study was over 80% (two-sided statistical test, α=0.05). The patient's age, date of last menstrual period, use of artificial hormones, menopausal status, height, weight, obstetric history, ethnicity, address, insurance, relevant medical history and any previous abnormal Pap smears were all noted upon chart review. After the cervix was exposed and visually examined by the attending physician, the cervix was wiped clean with a dry cotton swab followed by saline. Raman measurements were then taken from two to three locations on the ectocervix. Next, the Pap smear procedure was done according to standard clinical protocol. The spectra were correlated with histological results and considered normal if the Pap smear was negative.

5.3.2 Patient Information

Patients were stratified according to four sets of data to determine the sensitivity of RS: 1) Race/ethnicity (white, black and Hispanic); 2) BMI category: (normal, overweight and obese);

3) parity (no pregnancies or 1 or more) and 4) socioeconomic status (uninsured or insured, determined by whether the patient had government-subsidized or private health insurance). Racial or ethnic group was determined by what the patient identified as. Body mass index (BMI) was calculated using the formula below from the height and weight measured the same day when Raman spectra were acquired.[44]

$$BMI = \frac{mass(lb) \times 703}{(height(in))^2}$$

BMI values that define specific categories used in this study, normal, overweight and obese, are in Table 5.1. Obstetric history was determined from a chart review.

Category	BMI Range
Normal	18.50 – 24.99
Overweight	25.00 – 29.99
Obese	$\geq$ 30.00

Table 5.1. BMI categories.

5.3.3 Instrumentation and Data Processing

Raman spectra were collected *in vivo* using a portable RS system consisting of a 785 nm diode laser (PI-ECL-785-350, Process Instruments, Inc., Salt Lake City, UT), a beam-steered fiber optic probe (Visionex, Atlanta, GA), an imaging spectrograph (Holospec f/1.8i-NIR, Kaiser Optical Systems, Ann Arbor, MI), and a back-illuminated, deep-depletion, thermo-electrically cooled CCD camera (Pixis 256BR, Princeton Instruments, Princeton, NJ), all controlled with a laptop computer. Details of the system have been reported previously.[45] The fiber optic probe delivered 80 mW of incident light onto the tissue at an integration time of 2-3 seconds with all room lights and the computer monitor turned off. The system provided a spectral resolution of 8 wavenumbers (cm^{-1}).

Spectral calibration of the system was performed each day using a neon-argon lamp and naphthalene and acetaminophen standards to correct for day-to-day variations. A NIST-calibrated tungsten lamp was also used to account for the wavelength-dependent response of the system. The spectra were processed for fluorescence subtraction and noise smoothing using the modified polynomial fit and Savitzky-Golay methods, described previously.[45] Following data processing, each spectrum was normalized to its mean spectral intensity across all Raman bands to account for intensity variability.

5.3.4 Data Analysis

As previously reported, menopausal status and history of cervical disease affects Raman spectra.[23] For this reason, only premenopausal patients with no history of cervical disease were used in this analysis. A composite spectrum averaging Raman measurements from each patient was used as it would contain the effects of any significant patient variations. Discrimination was performed with sparse multinomial logistic regression (SMLR), a Bayesian machine-learning framework that computes the posterior probability of a spectrum belonging to each tissue class based on a labeled training set.[24, 46] For this analysis, whichever class had the higher probability of membership was the one to which the spectrum was classified. Since only one composite spectrum per patient was used, SMLR was run with leave-one-patient-out cross-validation. A range of input parameters to SMLR have been tested previously and these tests revealed that the combination of parameters that provide the most accurate classification, while also maximizing sparsity, was using a Laplacian prior, direct kernel, lambda value of 0.01, with no additional bias term (see Appendix 2 for a complete explanation).

5.4 Results

The epidemiologic makeup (race/ethnicity groups, BMI category, obstetric history and socioeconomic status) of the entire cohort of 75 patients recruited to this study is shown in Table 5.2. In the analyses below, only Raman spectra from premenopausal women with no history or current presence of cervical disease were used. Due to lower recruitment numbers, patients of Arabic descent or underweight BMI were excluded. Some spectra could not be classified into appropriate categories, such as those from women with spontaneous abortions and from women whose health insurance status was different at their previous medical appointment (for example, they were uninsured the last time they came for medical care, but now they are insured). Those spectra were also excluded.

White	23 (31%)
Black	31 (39%)
Hispanic	20 (27%)
Arabic	1 (1%)
Underweight BMI	2 (3%)
Normal BMI	21 (28%)
Overweight BMI	24 (32%
Obese BMI	28 (37%)
No previous pregnancies	33 (44%)
Prior Pregnancy/ies	42 (56%)
Insured	44 (59%)
Not Insured	31 (41%)

Table 5.2. Patient Categories. Total in all categories is 75.

5.4.1 Race and Ethnicity

Raman spectra ($n_{spectra}$=193) were acquired from the cervix of patients from 3 different racial and ethnic groups (white $n_{patients}$=21, black $n_{patients}$=23, Hispanic $n_{patients}$=18, total number of patients=62, excluded=13 if multiple race/ethnicity or Arabic due to low recruitment numbers).

There are many similarities across these spectra throughout the wavenumber range. Figure 5.1A shows difference spectra of Raman measurements from white and black patients and white and Hispanic patients. A few of the small differences between the spectra are shown as the box plots in Figure 5.1B-D, including the peaks that have been assigned in previous studies as lipid and DNA around 1303 cm^{-1}, the phenylalanine and DNA region around 1510-1520 cm^{-1} and the shoulders of the 1656 cm^{-1} amide-I peak.[47-49] Changes in the shoulders of the amide-I peak are usually due to changes in the secondary structures of amide-I, like the β pleated sheet proteins.[49] These peaks that seemed to qualitatively have the most difference in the averaged composite spectra have large areas of overlap. Box plots were used to visualize the data as they provide more detailed information compared to bar graphs. These figures have been explained in detail previously.[50] Generally, the box represents the 25th and 75th percentiles as the bottom and top of the box. The center line is the median, the error bars represent one standard deviation from the mean, and any outliers are represented by a +.

A

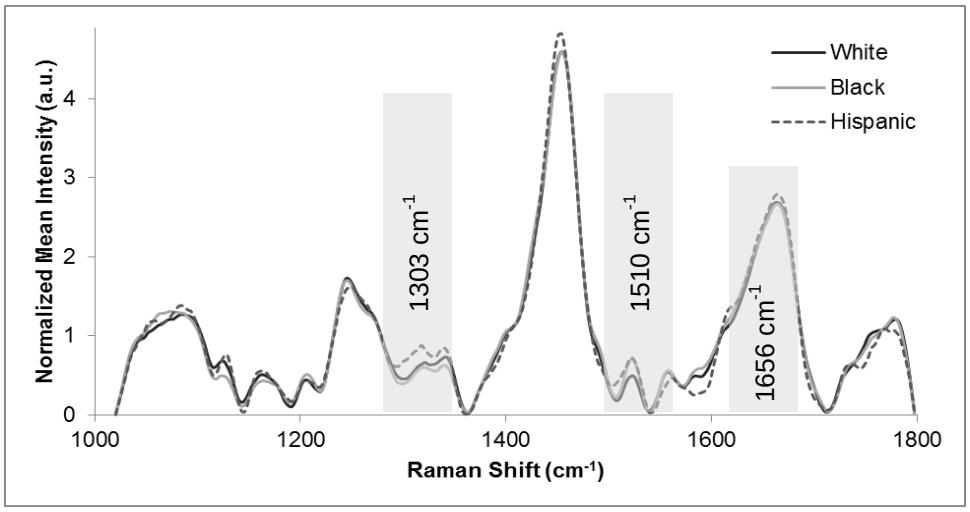

B

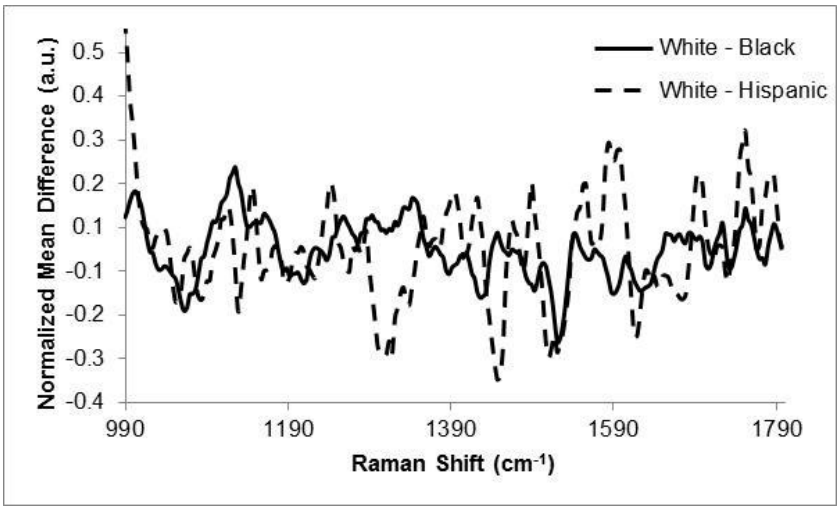
White - Black
White - Hispanic
Normalized Mean Difference (a.u.)
0.5
0.4
0.3
0.2
0.1
-0.1
-0.2
-0.3
-0.4
990
1190
1390
1590
1790
Raman Shift (cm-1)

C

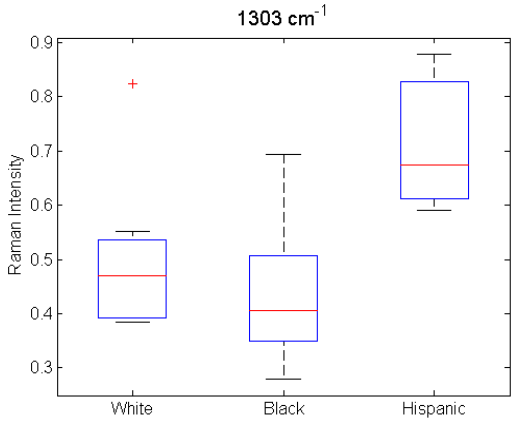
1303 cm-1
Raman Intensity
0.9
0.8
0.7
0.6
0.5
0.4
0.3
White
Black
Hispanic

D

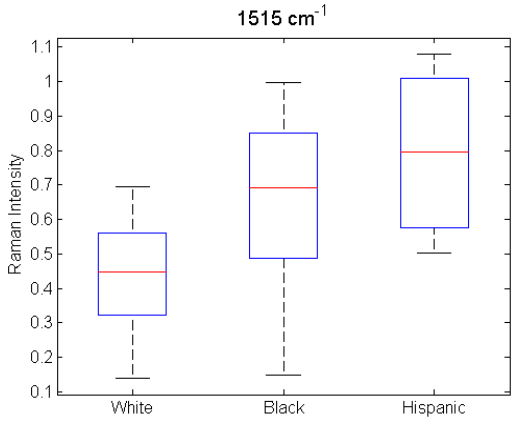
1515 cm-1
Raman Intensity
1.1
1
0.9
0.8
0.7
0.6
0.5
0.4
0.3
0.2
0.1
White
Black
Hispanic

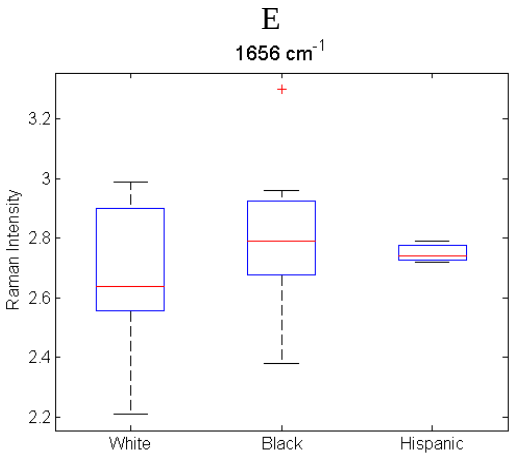

Figure 5.1 A) Normalized average Raman spectra of white, black and Hispanic patients. Highlighted regions are displayed in C-E. B) Difference spectra between measurements from white and black patients and white and Hispanic patients. C-E) Box plots of specific peaks of Raman spectra from normal cervix of patients who described themselves as white, black, or Hispanic. Potential peak assignments: Lipid & DNA (C), Phenylalanine & DNA (D), Amide-I shoulder (E). The box contains data between the 25th and 75th percentile, with the center line representing the median. The error bars are ±1 S.D. about the mean. Outliers are represented by the +.

5.4.2 BMI

Raman measurements ($n_{spectra}$=187) from 3 different BMI categories (normal $n_{patients}$=19, overweight $n_{patients}$=21, obese $n_{patients}$=23, total number of patients=63, excluded=12 if no patient history or underweight due to low recruitment numbers) were acquired and averaged. The spectra among these 3 categories appear similar in most areas, but a few significant differences occur in the peaks at 1010 cm^{-1}, 1656 cm^{-1} and 1750 cm^{-1}. Difference spectra have been plotted in Figure 5.2A showing differences between patients of normal BMI and overweight BMI, as well as normal and obese. To visualize important areas of the spectra, box plots for these peaks, which have been assigned by other researchers as phenylalanine, lipid and C=C bonds, respectively, are shown in Figure 5.2B-D.[49, 51, 52]

A

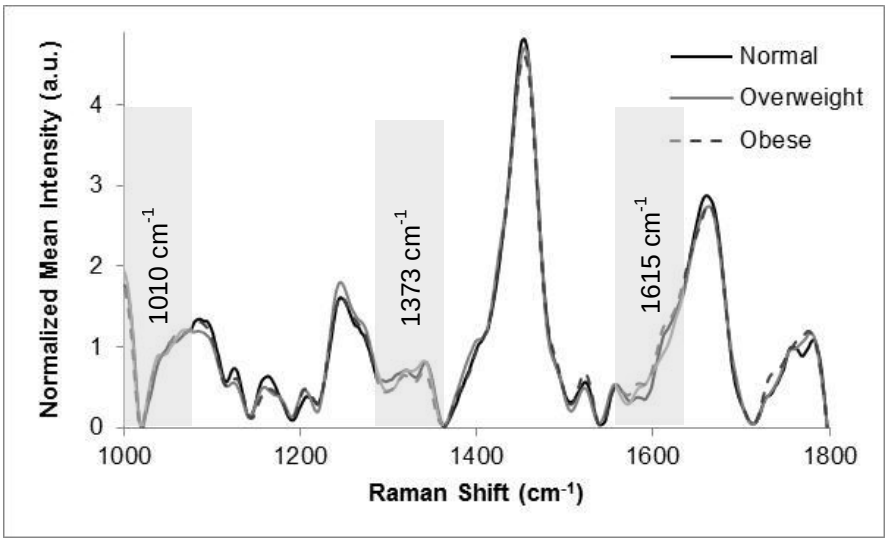
Normalized Mean Intensity (a.u.)
Raman Shift (cm-1)
Normal
Overweight
Obese
1010 cm-1
1373 cm-1
1615 cm-1
0
1
2
3
4
1000
1200
1400
1600
1800

B

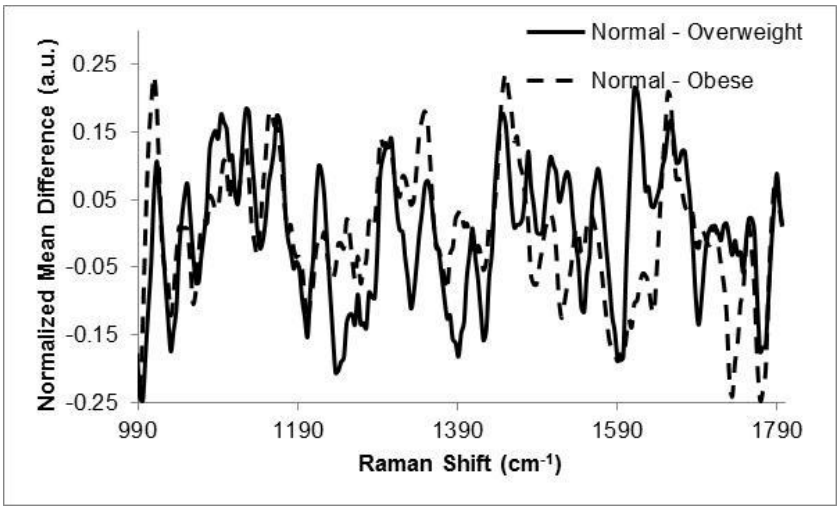
Normalized Mean Difference (a.u.)
Raman Shift (cm-1)
Normal - Overweight
Normal - Obese
0.25
0.15
0.05
-0.05
-0.15
-0.25
990
1190
1390
1590
1790

C

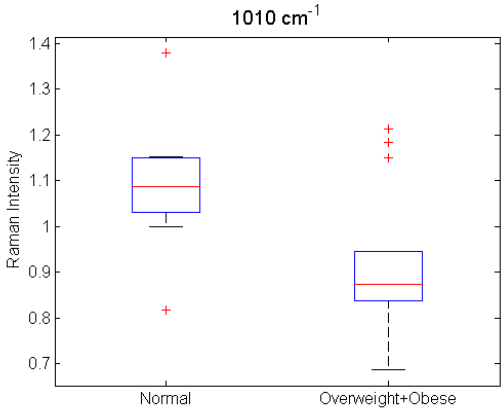
1010 cm-1
Raman Intensity
1.4
1.3
1.2
1.1
1
0.9
0.8
0.7
Normal
Overweight+Obese

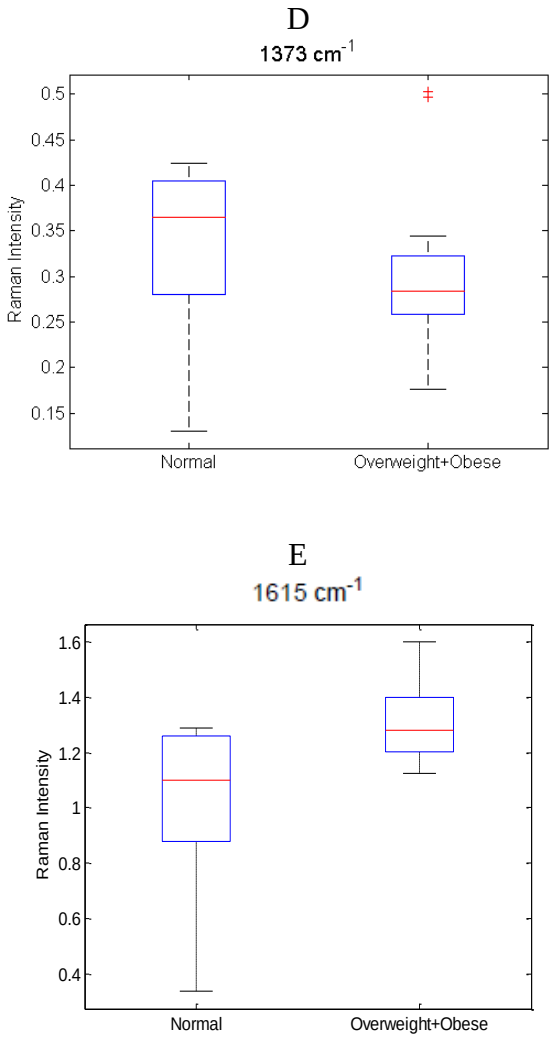

Figure 5.2. A) Normalized average Raman spectra from normal, overweight and obese patients. Highlighted regions are displayed in C-E. B) Difference spectra between measurements from normal and overweight patients and normal and obese patients. C-E) Box plots showing regions of difference between patients with normal and overweight + obese BMI levels. Potential peak assignments: Phenylalanine (C), Lipid (D), C=C bond (E). The box contains data between the 25th and 75th percentile, with the center line representing the median. The error bars are ±1 S.D. about the mean. Outliers are represented by the +.

5.4.3 Parity

Raman measurements ($n_{spectra}$=117) were obtained from two groups of patients, nulliparous ($n_{patients}$=23) and parous ($n_{patients}$=24, total number of patients=47, excluded=28 if prior miscarriage or abortion). Compared to previous spectra, there are variations throughout the entire range. A subtraction spectrum showing the differences between measurements from

women who have and have not been pregnant is in Figure 5.3A. More significant differences are seen in the region of 1050–1130 cm^{-1}, which have been attributed to C-C and C-O stretches, as well as the concentration of collagen, elastin, lipid and proline.[49, 53, 54] Box plots peaks corresponding to some of these differing regions are shown in Figure 5.3B-D.

A

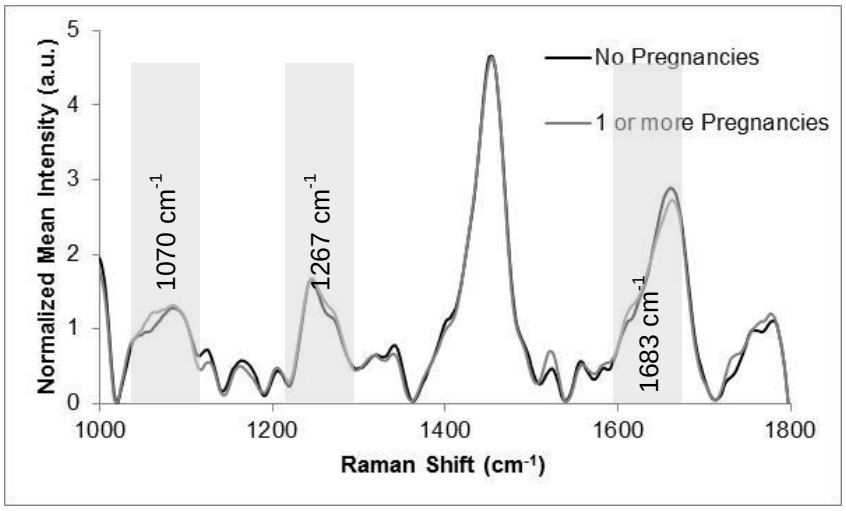

B

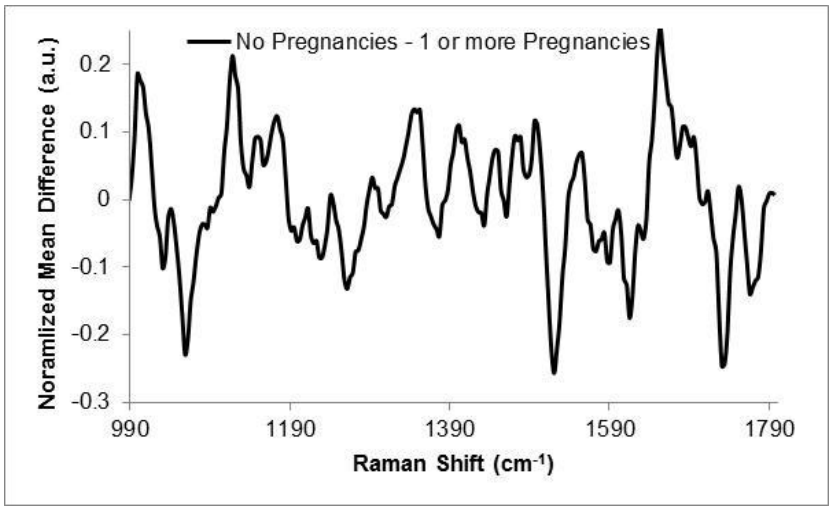

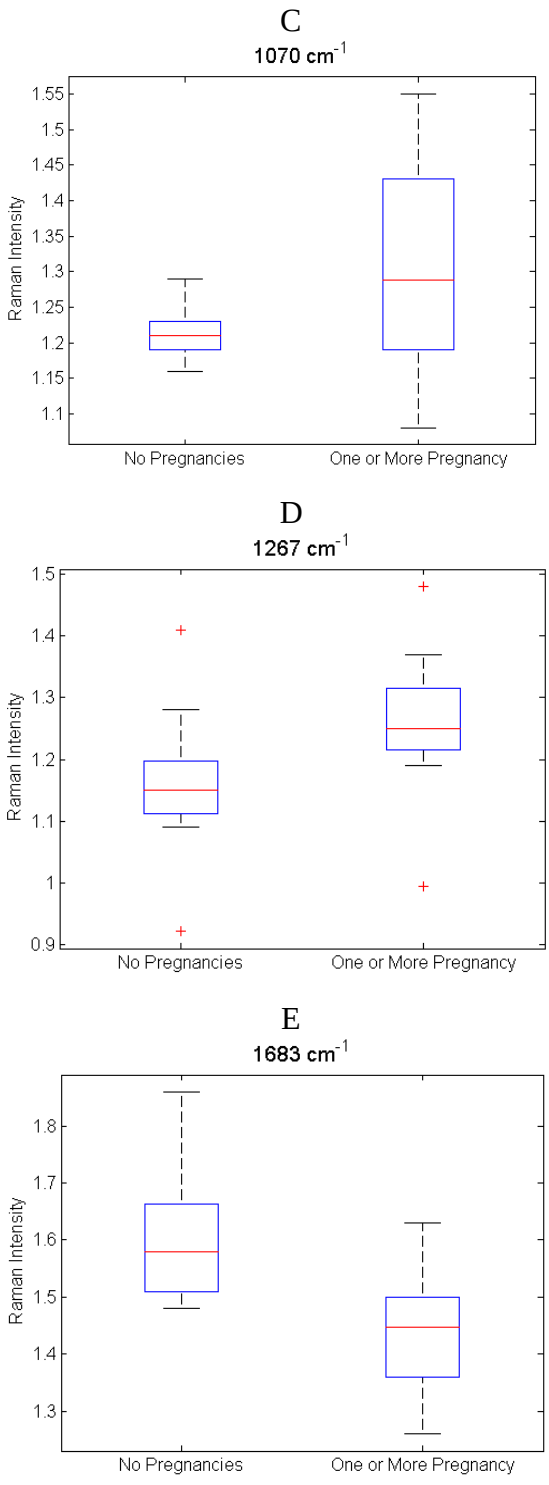

Figure 5.3. A) Normalized average Raman spectra from patients with zero pregnancies and one or more pregnancy. Highlighted regions are displayed in C-E. B) Difference spectra between measurements from patients with and without previous pregnancy. C-E) Box plots showing regions of difference between patients with and without previous pregnancy. Potential peak assignments: Collagen/Elastin (C), Amide-III (D), C-O stretch (E). The box contains data between the 25th and 75th percentile, with the center line representing the median. The error bars are ±1 S.D. about the mean. Outliers are represented by the +.

5.4.4 Socioeconomic Status

For this study, patients' health insurance status was used as an indicator of socioeconomic status. Raman spectra ($n_{spectra}$=123) were obtained from the cervix of patients with or without private health insurance with 26 patients in each category (excluded=23 if health insurance status was unknown or had recently changed). Included in the group of patients without health insurance were women who qualified for the Tennessee Breast and Cervical Cancer Screening (TBCC) program. These patients have health care for mammograms, Pap smears, etc. but the program does not provide comprehensive health care coverage. The spectra from the two groups mostly overlap, with only a few areas of small differences between patients with and without health insurance. This outcome is shown in Figure 5.4A. Figure 5.4B-D contain box plots for the peaks at 1095 cm^{-1}, 1265 cm^{-1} and 1656 cm^{-1}, which correspond to PO_2^{-1}, protein content and the shoulder of the amide-I band.[49, 54-56]

A

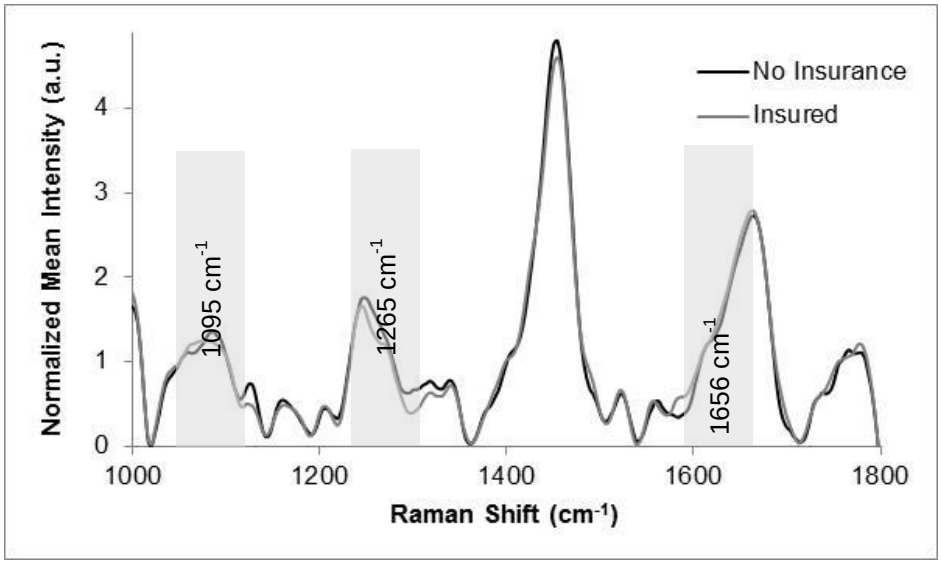

B

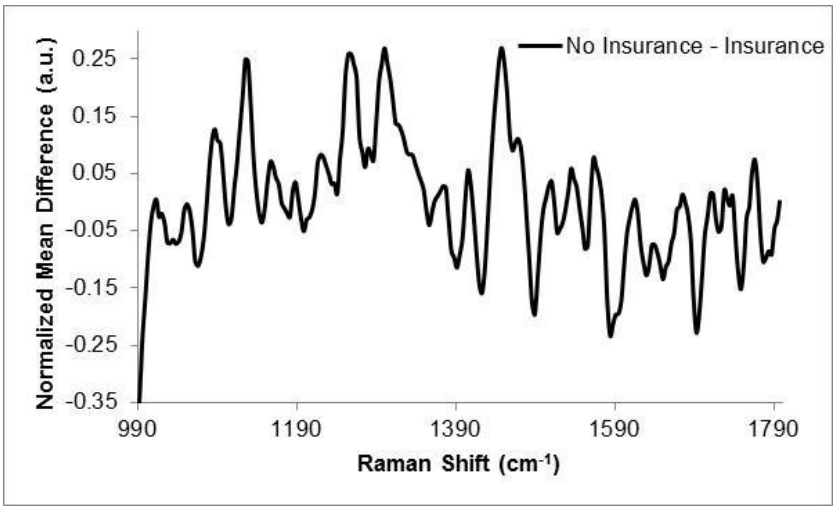
No Insurance - Insurance
Normalized Mean Difference (a.u.)
0.25
0.15
0.05
-0.05
-0.15
-0.25
-0.35
990
1190
1390
1590
1790
Raman Shift (cm-1)

C

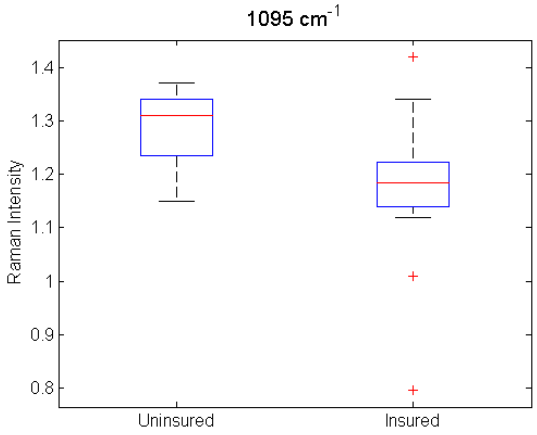
1095 cm-1
Raman Intensity
1.4
1.3
1.2
1.1
1
0.9
0.8
Uninsured
Insured

D

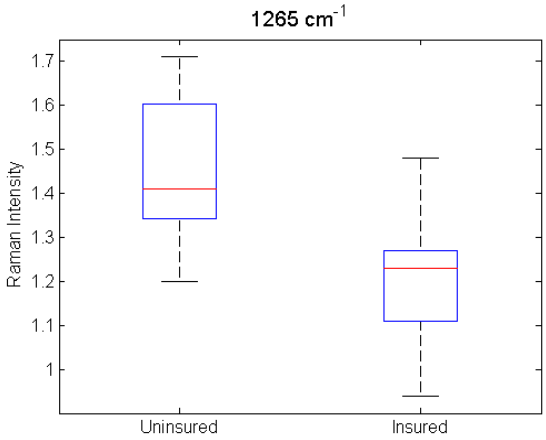
1265 cm-1
Raman Intensity
1.7
1.6
1.5
1.4
1.3
1.2
1.1
1
Uninsured
Insured

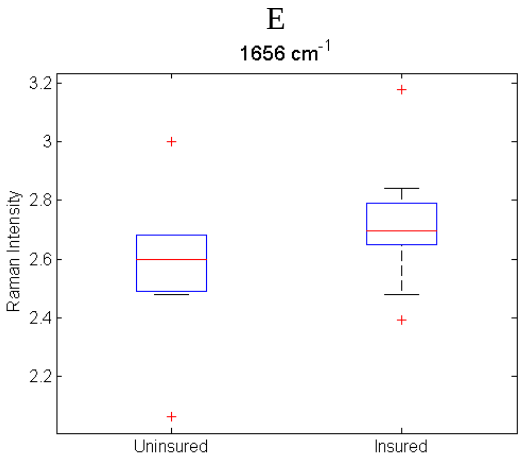

Figure 5.4. A) Normalized average Raman spectra from patients with and without health insurance. Highlighted regions are shown in C-E. B) Difference spectra between measurements from patients with and without health insurance. C-E) Box plots showing regions of difference between patients with and without health insurance. Potential peak assignments: PO_2^{-1} (C), Protein content (D), Amide-I shoulder (E). The box contains data between the 25th and 75th percentile, with the center line representing the median. The error bars are ±1 S.D. about the mean. Outliers are represented by the +.

5.4.5 Statistical Analyses

Although box plots have been used to highlight various regions of the spectrum, the entire normalized spectrum from 990 to 1800 cm^{-1} for each patient within each category was used for this analysis. The first step of this analysis was to classify the spectra according to the previous categories (i.e. white, black, and Hispanic, etc.) to determine if significant differences exist in the Raman spectra acquired from these specific groups of patients. Various iterations of analyses were used to decide how the spectra should be classified, which was determined by finding the greatest classification accuracy of these iterations. For example, for the BMI category, SMLR was first performed to classify the spectra as normal, overweight or obese. However, a higher classification accuracy rate was found when SMLR was performed with only two categories: normal versus a combined category of spectra from overweight and obese patients. Table 5.3 shows the maximum classification accuracy obtained within each patient variability category. The category of race/ethnicity classified with a maximum rate of 58%, BMI

with a maximum rate of 78% when spectra were classified as normal or a combined category of overweight or obese, parity with a rate of 75%, and socioeconomic status with a rate of 61%.

Patient Variable	Optimized Classification Categories (Number of Categories Used)	Maximum Classification Accuracy
Race/Ethnicity	White, Black, Hispanic (3)	58%
BMI	Normal, Overweight+Obese (2)	78%
Obstetric History	No pregnancies, ≥1 Pregnancy (2)	75%
Socioeconomic Status	Uninsured, Insured (2)	61%

Table 5.3. Results from statistical analyses of patient variables

5.5 Discussion

Previous studies using RS to detect cervical dysplasia have shown limited success.[1, 15, 16] We have previously demonstrated that some of these limitations can be overcome by accounting for both normal patient variability, such as hormonal differences and the history or presence of disease.[1, 23, 24] In this paper, we evaluate whether Raman spectra acquired from normal tissue can be separated based on other patient variables, including race/ethnicity, BMI, obstetric history and socioeconomic status.

The spectra used in the analyses presented here were acquired from patients with no history of disease and whose current Pap smear result was within normal limits. When a pathologist examined these cytology specimens, few variations were observed and the clinical diagnosis of each patient was normal. If there are no significant differences due to common patient variations, like ethnicity, height and weight, we expect spectra acquired from the cervix of patients with a normal pathology to also appear similar and have few variations. Furthermore, if these variables, like BMI, parity, etc., have no impact on the spectra, statistical classification

should produce results with accuracy rates around 50%, similar to a coin toss. Previous studies have suggested the patient variables analyzed in this paper may be correlated with higher incidences of cervical dysplasia.[32, 35] While we do not expect a significant impact from these normal physiological and social variables on the biochemical makeup of the cervix or the acquired Raman spectra, investigating the influence of these variables is an important first step in validating the application of RS on a diverse patient population. The results from this study show that some of these variables produce significant changes to Raman spectra that are separable using statistical classification methods.

The two patient variables that resulted in the most separable spectra were BMI and parity, with classification rates of 78% and 75%, respectively. These results suggest that BMI and parity cause significant changes in the cervix and therefore affect any spectra acquired from the cervix. As discussed previously, higher BMI is associated with increased areas of inflammation and higher blood serum hormonal levels.[22, 24, 37] While there are cycling levels of hormones that effect the elasticity and softness of the cervix, varying baseline levels of steroid hormones due to BMI differences may change the cervix as well. Similarly, it is reasonable to believe that parity would influence normal Raman spectra. The cervix is known to change dramatically during pregnancy and labor.[57] These changes appear to be long-term and affect tissue biochemistry significantly enough to be recognizable with RS. Furthermore, accuracy rates may increase by defining narrower classification groups. Figure 5.3B shows a box plot of the peak at 1070 cm^{-1}, correlating to collagen and elastin content. While there is little variance in patients who have not been pregnant, there is a significant amount of variance in the spectra from those who have. This variance may be correlated with number of pregnancies and type of delivery (vaginal or caesarean), both of which may change the concentration and organization of collagen.[58] In the

future, comparing groups of patients with different delivery types and number of pregnancies may increase accuracy rates.

Classification by socioeconomic status and race/ethnicity resulted in accuracy rates of 61% and 58% respectively, suggesting that these variables have a smaller impact on the Raman spectra. While there are small differences in the Raman spectra that lead to a classification rate higher than 50%, socioeconomic status and race/ethnicity are less significant compared to BMI and parity. One possible explanation for the 61% classification accuracy with socioeconomic status may be an increased prevalence of undiagnosed medical problems due to the lack of medical insurance reducing access to comprehensive health care. These results also suggest that the different incidence rates of cervical dysplasia among racial and ethnic groups are not due to fundamental differences in the biochemical makeup of the cervix. Even though there is no physiological evidence that race or ethnicity change the biochemical makeup of the cervix, it was important to investigate these variables to ensure that RS can be applied to detect cervical dysplasia in diverse populations. The low rate of classifying data by race or ethnicity alone suggests that these variations do not significantly affect the cervix or the classification of Raman spectra. This outcome is significant as it indicates RS may be applied in clinical settings on any patient population.

The success of the analyses performed in this study depends on the reliability of the data used to categorize the spectra. For example, the patient reported her own race or ethnicity, but the categories were limited to "white," "black" and "Hispanic" and she may fit into more than one or none of these. BMI is a controversial measure of body fat that may be inaccurate since it does not reflect changes due to age, race, gender, etc.[59] To classify spectra based on parity, higher rates may be achieved by further categorizing previously pregnant patients by number of

pregnancies and number and type of delivery (vaginal or cesarean). In this study, some spectra ($n_{spectra}$=11) were acquired during a patient's post-partum exam, typically 6-10 weeks after delivery. Obtaining data at this point may not only affect spectra acquired from the cervix, but also a patient's BMI. Future studies on patient variability should exclude data from such patients. Finally, whether or not a patient has health care coverage may not be an accurate measure of socioeconomic status or other cultural practices such as dietary and social habits which are associated with different economic levels. To truly investigate the influence of specific variables, surveys of the patients may be more beneficial.

Previous studies from our research group using RS to detect changes in the cervix analyzed the data with a combined algorithm of maximum representation and discrimination feature (MRDF) and SMLR.[1, 23, 24] MRDF is a kernel-based algorithm that extracts important features by reducing the dimensionality of a set of data by performing a number of mathematical transforms. These features were then used by SMLR to classify the data sets. In this study and in chapters 7 and 8 and Appendix 1, SMLR was used on its own to reduce the time and computing power needed to classify the data. SMLR, also a kernel-based algorithm, maximizes the sparsity between separate sets of data by maximizing the sparsity between them. The results from this paper suggest that SMLR may be capable on its own for discriminating between the subtle differences among various data sets.

Studies from our lab and others have looked at the effect of hormonal variations,[28] age,[26] acetic acid,[24] creams and lotions,[27] history or presence of disease,[24, 25] smoking, BMI, obstetric history, insurance status and race/ethnicity on Raman spectra obtained from non-malignant areas of the cervix and other tissues. The results from previous work have shown that, prior to classification, stratifying spectra based on hormonal changes and history or presence of disease

reduces intra-class variability amongst both normal and diseased spectra.[1, 24] Unsupervised classification algorithms were then more likely to account for the variance due to differences from disease instead of the variance due hormonal status or disease history, resulting in improved performance. However, close examination of these results revealed that a significant amount of intra-class variance among the normal spectra remained,[1, 23, 24] which motivated investigating additional factors that could be used to account for the variance among normal spectra and improve classification of disease.

Therefore, the purpose of this paper is to perform the critical intermediate step of identifying the most separable sources of intra-class variation amongst normal spectra. Our results indicate that of the variables investigated, normal spectra are best separated as a function of BMI and parity, which are both easily obtainable from the patient. Based on previous experience with hormonal status and disease history, it is possible that stratification of the spectra by BMI and parity may also improve the accuracy of disease diagnosis using RS. Because an effect of race/ethnicity or socioeconomic status on classification was not identified, there appears to be no benefit to accounting for those variables prior to classification. Consideration of other variables beyond those discussed here may be important and can be determined based on organ sites. However, the cost to benefit ratio of incorporating additional physiological patient variables prior to spectral classification must be considered before further analysis is performed.

Current research is underway in our lab to understand the significance of BMI, parity, race/ethnicity, and socioeconomic status on disease classification and to quantify the relative variance these factors impart on normal spectra compared to diseased spectra. While it may be

possible that BMI and parity do not affect disease spectra as has been demonstrated with normal spectra, they are still important factors to be aware of prior to classification of cervical dysplasia.

The goal of using RS for precancer detection is to provide an automated, real-time method of accurately detecting malignant cells in any patient population, regardless of race, ethnicity, BMI, parity or socioeconomic status. Previous work using RS for *in vivo* screening and diagnosis of cervical dysplasia has shown promising results, with sensitivities and specificities above 90%, however this work was done in a fairly homogenous patient population. In this study, we investigated the spectral variations in a more diverse patient group and found more distinct differences due to BMI and obstetric history compared to race/ethnicity and socioeconomic status. We believe these results suggest that classification algorithms for the detection of cervical dysplasia with RS should be developed to incorporate BMI and obstetric history, but it does not appear necessary to control for race, ethnicity or a patient's socioeconomic status. These results also suggest that normal sources of physiological variability, such as hormone levels, BMI, etc., may affect the inherent baseline Raman spectra acquired from other organ systems as well. For example, skin pigment and dryness may be important variables to account for when using RS for diagnosing melanoma. Age and gender may be significant factors that impact the biochemical makeup of the GI tract. Parity and hormonal fluctuations may affect the classification accuracy of Raman spectra acquired from the ovary. By examining the effect of such normal physiological variables on spectra, the sensitivity of RS will be revealed, as will its effectiveness for detecting and diagnosing disease.

5.6 Acknowledgements

The authors acknowledge the financial support of the National Institute of Health grant R01-CA-095405 and a predoctoral fellowship (T32-HL7751-15) for EV. Special thanks go to the nurses and staff at Meharry Medical College for their help and to Chetan Patil and Amy Rudin for proofreading this paper.

5.7 References

1. Kanter E.M., Vargis E., Majumder S., Keller M.D., Beaven R.B., Rao G.G. and Mahadevan-Jansen A. "Application of Raman spectroscopy for Cervical Dysplasia Diagnosis." *J Biophotonics* **2**, 81-90 (2009).

2. Crow, P. Molckovsky, A., Stone, N., Uff, J., Wilson, B., and Wong Kee Song, L.M. "Assessment of fiberoptic near-infrared Raman spectroscopy for diagnosis of bladder and prostate cancer." *Urology* **65**, 1126-30 (2005).

3. Grimbergen, M.C., van Swol, C.F., van Moorselaar, R.J., Uff, J., Mahadevan-Jansen, A. and Stone, N. "Raman spectroscopy of bladder tissue in the presence of 5-aminolevulinic acid." *Photochem Photobiol B* **95,** 170-6 (2009).

4. Krafft, C., Ramoji, A.A., Bielecki, C., Vogler, N., Meyer, T., Akimov, D., Rosch, P., Schmitt, M., Dietzek, B., Petersen, I., Stallmach, A. and Popp, J. "A comparative Raman and CARS imaging study of colon tissue." *J Biophotonics* **2,** 303-12 (2009).

5. Chowdary, M.V., Kalyan Kumar, K., Mathew, S., Rao, L., Krishna, C.M. and Kurien, J. "Biochemical correlation of Raman spectra of normal, benign and malignant breast tissues: a spectral deconvolution study." *Biopolymers* **91,** 539-46 (2009).

6. M. V. Chowdary, K. Kalyan Kumar, S. Mathew, L. Rao, C.M. Krishna, and J. Kurien, "Biochemical correlation of Raman spectra of normal, benign and malignant breast tissues: a spectral deconvolution study," *Biopolymers* **91**, 539–546 (2009).

7. Majumder, S.K., Keller, M.D., Boulos, F.I., Kelley, M.C. and Mahadevan-Jansen, A. "Comparison of autofluorescence, diffuse reflectance, and Raman spectroscopy for breast tissue discrimination." *J Biomed Opt* **13,** 054009 (2008).

8. Barr, H., Kendall, C., Bazant-Hegemark, F., Moayyedi, P., Shetty, G. and Stone, N. "Endoscopic screening and surveillance for Barrett's esophagus--clinical implications." *Med Gen Med* **8,** 88 (2006).

9. Shetty, G., Kendall, C., Shepherd, N., Stone, N. and Barr, H. "Raman spectroscopy: elucidation of biochemical changes in carcinogenesis of oesophagus." *Br J Cancer* **94,** 1460-4 (2006).

10. Eliasson, C., Macleod, N.A. and Matousek, P. "Non-invasive detection of cocaine dissolved in beverages using displaced Raman spectroscopy." *Anal Chim Acta* **607,** 50-3 (2008).

11. Leona, M., Decuzzi, P., Kubic, T.A., Gates, G. and Lombardi, J.R. "Nondestructive Identification of Natural and Synthetic Organic Colorants in Works of Art by Surface Enhanced Raman Scattering." *Anal Chem* (2011).

12. Kumar V. and Robbins S.L. Robbins Basic Pathology (Saunders/Elsevier, Philadelphia, 2007).

13. Gamot, A.P., Vergoten, G. and Fleury, G. "Etude par spectroscopie raman du chlorhydrate de cocaine." *Talanta* **32,** 363-72 (1985).

14. Feller, R.L., Roy, A., FitzHugh, E.W. and Berrie, B.H. Artists' Pigments: A Handbook of Their History and Characteristics. (National Gallery of Art, Washington 1986).

15. Jess, P.R., Smith, D.D., Mazilu, M., Dholakia, K., Riches, A.C. and Herrington, C.S. "Early detection of cervical neoplasia by Raman spectroscopy." *Int J Cancer* **121,** 2723-8 (2007).

16. Mahadevan-Jansen, A., Mitchell, M.F., Ramanujam, N., Malpica, A., Thomsen, S., Utzinger, U. and Richards-Kortum, R. "Near-infrared Raman spectroscopy for *in vitro* detection of cervical precancers." *Photochem Photobiol* **68,** 123-32 (1998).

17. Robichaux-Viehoever, A., Kanter, E., Shappell, H., Billheimer, D., Jones, H., 3rd and Mahadevan-Jansen, A. "Characterization of Raman spectra measured *in vivo* for the detection of cervical dysplasia." *Appl Spectrosc* **61,** 986-93 (2007).

18. Yazdi, Y., Ramanujam, N., Lotan, R., Mitchell, M.F., Hittelman, W. and Richards-Kortum, R. "Resonance Raman spectroscopy at 257 nm excitation of normal and malignant cultured breast and cervical cells." *Appl Spectrosc* **53,** 82-85 (1999).

19. Krishna, C.M., Prathima, N.B., Malini, R., Vadhiraja, B.M., Bhatt, R.A., Fernandes, D.J., Kushtagi, P., Vidyasagar, M.S. and Kartha, V.B. "Raman spectroscopy studies for diagnosis of cancers in human uterine cervix." *Vib Spectrosc* **41,** 136-141 (2006).

20. Walboomers J.M.M., Jacobs M.V., Manos M.M., Bosch F.X., Kummer J.A., Shah K.V., Snijders P.J.F., Peto J., Meijer C.J.L.M. and Munoz N. "Human papillomavirus is a necessary cause of invasive cervical cancer worldwide." *J Pathol* **189**, 12-19 (1999).

21. Dunne, E.F., Unger, E.R., Sternberg, M., McQuillan, G., Swan, D.C., Patel, S.S. and Markowitz, L.E. "Prevalence of HPV infection among females in the United States." *JAMA-J Am Med Assoc* **297,** 813-819 (2007).

22. Lacey Jr, J.V., Swanson, C.A., Brinton, L.A., Altekruse, S.F., Barnes, W.A., Gravitt, P.E., Greenberg, M.D., Hadjimichael, O.C., McGowan, L. and Mortel, R. "Obesity as a potential risk factor for adenocarcinomas and squamous cell carcinomas of the uterine cervix." *Cancer* **98,** 814-821 (2003).

23. Kanter, E.M., Majumder, S., Kanter, G.J., Woeste, E.M. and Mahadevan-Jansen, A. "Effect of hormonal variation on Raman spectra for cervical disease detection." *Am J Obstet Gynecol* **200**, 512-512 (2009).

24. Vargis, E., Kanter, E. M., Majumder, S. K., Keller, M. D., Beaven, R. B., Rao, G. G., and Mahadevan-Jansen, A. "Effect of normal variations on disease classification of Raman spectra from cervical tissue." *Analyst* **139,** 2981-2987 (2011).

25. Bergholt, M.S., Zheng, W., Lin, K., Ho, K. Y., Teh, M., Yeoh, K. G., So, J. B., and Huang, Z. "Characterizing variability in *in vivo* Raman spectra of different anatomical locations in the upper gastrointestinal tract toward cancer detection." *J Biomed Opt* **16,** 037003 (2011).

26. Haka, A.S., Shafer-Peltier, K. E., Fitzmaurice, M., Crowe, J., Dasari, R. R., and Feld, M.S. "Diagnosing breast cancer by using Raman spectroscopy." *Proc Natl Acad Sci U S A* **102,** 12371-12376 (2005).

27. Chrit, L., Bastien, P., Sockalingum, G.D., Batisse, D., Leroy, F., Manfait, M., and Hadjur, C. "An *in vivo* randomized study of human skin moisturization by a new confocal Raman fiber-optic microprobe: assessment of a glycerol-based hydration cream." *Skin Pharmacol Physio* **19,** 207-215 (2006).

28. Cano, A., Serra, V., Rivera, J., Monmeneu, R. and Marzo, C. "Expression of estrogen receptors, progesterone receptors, and an estrogen receptor-associated protein in the human cervix during the menstrual cycle and menopause." *Fertil Steril* **54**, 1058-1064 (1990).

29. Gould, S.F., Shannon, J.M. and Cunha, G.R. "The autoradiographic demonstration of estrogen binding in normal human cervix and vagina during the menstrual cycle, pregnacy, and the menopause." *Am J Anao* **168**, 229-238 (1983).

30. Thomsen, S. and Tatman, D. "Physiological and Pathological Factors of Human Breast Disease That Can Influence Optical Diagnosis." *Ann N Y Acad Sci* **838**, 171-193 (1998).

31. Nieburgs H. E.. "Recent progress in the interpretation of malignancy associated changes (MAC)." *Acta Cytol.* **12**(6), 445–453 (1968).

32. Mitchell, J.B. and McCormack, L.A. "Time trends in late-stage diagnosis of cervical cancer: Differences by race/ethnicity and income." *Med Care* **35**, 1220-1224 (1997).

33. Jemal, A. Siegel, R., Xu, Jiaquan, and Ward, E. "Cancer statistics, 2009." *CA Cancer J Clin* **59**, 225-49 (2011)

34. Ward, E., Jemal, A., Cokkinides, V., Singh, G.K., Cardinez, C., Ghafoor, A. and Thun, M. "Cancer disparities by race/ethnicity and socioeconomic status." *CA Cancer J Clin* **54**, 78-93 (2004).

35. Ferlay, J., Shin, H.R., Bray, F., Forman, D., Mathers, C., and Parkin, D.M. "Estimates of worldwide burden of cancer in 2008: GLOBOCAN 2008." *Int J Cancer* **127**, 2893–2917 (2010).

36. Calle, E.E. and Kaaks, R. "Overweight, obesity and cancer: epidemiological evidence and proposed mechanisms." *Nat Rev Cancer* **4**, 579-91 (2004).

37. Key, T.J., Allen, N.E., Verkasalo, P.K. and Banks, E. "Energy balance and cancer: the role of sex hormones." *Proc Nutr Soc* **60**, 81-9 (2001).

38. Macaulay, C., Richards-Kortum, R., Utzinger, U., Fedyk, A., Atkinson, E., Cox, D. and Follen, M. "Variation of fluorescence spectroscopy during the menstrual cycle." *Opt Express* **10**, 493-504 (2002).

39. Chang, S.K., Dawood, M.Y., Staerkel, G., Utzinger, U., Atkinson, E.N., Richards-Kortum, R.R and Follen M. "Fluorescence spectroscopy for cervical precancer detection: Is there variance across the menstrual cycle?" *J Biomed Opt* **7**, 595-602 (2002).

40. Cubeddu, R., D'Andrea, C., Pifferi, A., Taroni, P., Torricelli, A. and Valentini, G. "Effects of the Menstrual Cycle on the Red and Near-infrared Optical Properties of the Human Breast." *Photochem Photobiol* **72**, 383-391 (2000).

41. Knight, J.A., Blackmore, K.M., Wong, J., Tharmalingam, S. and Lilge, L. "Optical spectroscopy of the breast in premenopausal women reveals tissue variation with changes in age and parity." *Med Phys* **37**, 419-426 (2010).

42. Chang, V.T., Cartwright, P.S., Bean, S.M., Palmer, G.M., Bentley, R.C. and Ramanujam, N. "Quantitative physiology of the precancerous cervix *in vivo* through optical spectroscopy." *Neoplasia* **11**, 325-32 (2009).

43. Kelly, J.G., Cheung, K.T., Martin, C., O'Leary, J.J., Prendiville, W., Martin-Hirsch, P.L. and Martin, F.L. "A spectral phenotype of oncogenic human papillomavirus-infected exfoliative cervical cytology distinguishes women based on age." *Clin Chim Acta* **411**, 1027-1033 (2010).

44. "Physical status: the use and interpretation of anthropometry. Report of a WHO Expert Committee." *World Health Organ Tech Rep Ser* **854**, 1-452 (1995).

45. Lieber, C.A. and Mahadevan-Jansen, A. "Automated method for subtraction of fluorescence from biological Raman spectra." *Appl Spectrosc* **57**, 1363-1367 (2003).

46. Krishnapuram, B., Carin, L., Figueiredo, M.A. and Hartemink, A.J. "Sparse multinomial logistic regression: fast algorithms and generalization bounds." *IEEE Trans Pattern Anal Mach Intell* **27**, 957-68 (2005).

47. Puppels, G.J., Olminkhof, J.H., Segers-Nolten, G.M., Otto, C., de Mul, F.F. and Greve, J. "Laser irradiation and Raman spectroscopy of single living cells and chromosomes: sample degradation occurs with 514.5 nm but not with 660 nm laser light." *Exp Cell Res* **195**, 361-7 (1991).

48. Lieber, C.A., Molpus, K., Brader, K. and Mahadevan-Jansen, A. "Diagnostic tool for early detection of ovarian cancers using Raman spectroscopy." *Proc SPIE* **3918** 129-130 (2000).

49. Mahadevan-Jansen, A. and Richards-Kortum, R.R. “Raman spectroscopy for the detection of cancers and precancers,” *J Biomed Opt* **1**, 31–70 (1996).

50. Tukey. J.W. Exploratory data analysis. (Addison-Wesley, Reading, 1977).

51. Erckens, R.J., Motamedi, M., March, W.F. and JWicksted, J.P. “Raman spectroscopy for noninvasive characterization of ocular tissue: potential for detection of biological molecules,” *J Raman Spectrosc* **28**, 293–299 (1997).

52. Fendel, S. and Schrader, B. “Investigation of skin and skin lesions by NIR-FT-Raman spectroscopy,” *Fresenius’ J Anal Chem* **360**, 609–613 (1998).

53. Utzinger, U., Heintzelman, D. L., Mahadevan-Jansen, A., Malpica, A., Follen, M., and Richards-Kortum, R. “Near-Infrared Raman Spectroscopy for *in vivo* Detection of Cervical Precancers.” *Appl Spectrosc* **55**, 955-959 (2001).

54. Frank, C.J., Redd, D.C., Gansler, T.S. and McCreery, R.L. "Characterization of human breast biopsy specimens with near-IR Raman spectroscopy." *Anal Chem* **66**, 319-26 (1994).

55. Miura, T. and Thomas, Jr., G.J. “Raman spectroscopy of proteins and their assemblies,” *Subcell Biochem.* **24**, 55–99 (1995).

56. Liu, C.H., Das, B.B., Sha Glassman, W.L., Tang, G.C., Yoo, K.M., Zhu, H.R., Akins, D.L., Lubicz, S.S., Cleary, J. and Prudente, R. "Raman, fluorescence, and time-resolved light scattering as optical diagnostic techniques to separate diseased and normal biomedical media." *Photochem Photobiol B* **16**, 187-209 (1992).

57. Danforth, D.N., Veis, A., Breen, M., Weinstein, H.G., Buckingham, J.C. and Manalo, P. "The effect of pregnancy and labor on the human cervix: changes in collagen, glycoproteins, and glycosaminoglycans." *Am J Obstet Gynecol* **120**, 641-51 (1974).

58. Yu, S.Y., Tozzi, C.A., Babiarz, J. and Leppert, P.C. "Collagen changes in rat cervix in pregnancy--polarized light microscopic and electron microscopic studies." *Proc Soc Exp Biol Med* **209**, 360-8 (1995).

59. Rothman, K.J. "BMI-related errors in the measurement of obesity." *Int J Obes* **32**, S56-S59 (2008).

CHAPTER 6

ANALYSIS OF THE EFFECT OF PHYSIOLOGICAL VARIABLES ON DISEASE CLASSIFICATION OF RAMAN SPECTRA

This chapter demonstrates the effect of the normal variables that were previously studied on the classification of Raman spectra acquired from areas of cervical dysplasia, corresponding also to Specific Aim 1. The data was acquired from patients with current cervical disease at Meharry Medical College. It is being prepared for submission.

Vargis E, Pence IJ, Byrd T, Khabele D, A Mahadevan-Jansen. Analysis of the Effect of Physiological Variables on Disease Classification of Raman Spectra. (In preparation) 2012

6.1 Abstract

Raman spectroscopy is a sensitive technique that has been used to detect and diagnose tissues at multiple sites as normal, inflammatory or diseased. As more research into using Raman spectroscopy to diagnose cervical dysplasia has been conducted, it has become apparent that by accounting for normal patient variations, the sensitivity and specificity of Raman for diagnosing disease can increase. The goal of this research is to use Raman spectroscopy to successfully diagnose abnormal areas of the cervix of any patient independent of other factors. Raman spectra were acquired from a diverse patient population coming in for a colposcopy-guided biopsy. Multiple generalized linear methods were used to determine which variables should be considered and in what order to maximize the classification accuracy of Raman spectra from diseased areas of the cervix. For this data, using menopausal status, parity and BMI were sufficient to achieving 100% classification accuracy.

6.2 Introduction

Raman spectroscopy (RS) is a sensitive technique that has been used to detect and diagnose multiple tissue sites as normal, inflammatory or diseased. This optical method is a molecular-specific technique that probes into the vibrational or rotational transitions of chemical bonds, providing detailed information about the biochemical composition of a sample.[1] In particular, near-infrared RS has been used to detect cancers in many sites, such as the colon,[2] lung,[3] cervix,[4] breast,[5] and skin[6] with varying sensitivity and specificity rates (65%-100%). In this study, we examine normal physiological factors and quantify their effect on Raman spectra acquired from the cervix. Such factors may be inhibiting the success of using RS to correctly diagnose cervical dysplasia.

As more research into using RS to diagnose cervical dysplasia has been conducted, it has become apparent that by accounting for normal patient variations, the sensitivity and specificity of Raman for diagnosing disease can increase.[7, 8] Similar research on inherent normal patient variability has been seen when using Raman on other tissue sites, such as the colon and the breast.[9-11] In many cases, accounting for these normal differences has led to an increase in both the sensitivity and specificity rates of classifying normal spectra compared to disease.

Raman spectra are influenced by many factors, such as the varying levels of hormones released throughout the body during a menstrual cycle which can cause changes in the cervix, including softening, drying or thinning.[12, 13] The presence or prior history of disease may cause permanent field effects or malignancy-associated changes, significantly impacting the Raman spectra.[14, 15] Accounting for these normal variations prior to classification creates more accurate training sets for algorithm development. The variance between spectra from different sites,

therefore, is more likely to result from true malignancy instead of normal differences, resulting in higher classification accuracy rates.

More recently, the effect of other normal physiological variables, including race/ethnicity, body mass index (a measure of body fat, BMI), obstetric history and whether or not a patient has health insurance, has been studied in spectra obtained from the normal, non-diseased cervix.[16] Race and ethnicity and health insurance status are all correlated with different incidences of cervical malignancies,[17] with black and Hispanic populations having the highest incidence of and mortality rates from cervical dysplasia in the US in 2010.[18, 19] These differences are likely correlated with limited access to routine care and screening. Going through pregnancy and parturition can result in permanent changes to the normal cervix. Obesity is also associated with higher rates of cancer, including cervical cancer,[20-22] possibly due to differences in vaginal flora patterns, steroid hormone and cholesterol levels, cultural norms and bacterial or viral infections.[21] The results from our previous studies indicate that BMI and parity both have a slightly significant effect on Raman spectra from the normal, benign cervix, whereas race/ethnicity and health insurance status (an indicator of socioeconomic status) had a minimal effect.

The number of normal physiological variables that may affect Raman spectra and therefore disease classification are limitless. At this time, the impact of six variables on normal Raman spectra acquired from the cervix has been studied. Four of these variables have been determined to have a significant effect. While adding additional variables, such as human papilloma virus (HPV) strain or type of birth control, may increase disease classification accuracy, we must first develop a method for analyzing the effect of such variables in a quantifiable manner. Physiological variables such as these contribute to the variance of the

baseline or normal Raman spectra, which may result in classification algorithms placing an inappropriate significance on those normal differences, instead of focusing on the differences due to disease. Determining the importance of the effect of each variable will help identify the ones that should be considered prior to disease classification.

Other groups have examined the effect of normal variations on Raman spectra. Knudsen *et al*. looked at variations due to measuring spectra from the skin at different times during the day and on different days, from different measurements at the same location, and from persons with differing skin pigmentation.[23] The variability was assessed by comparing relative intensities of peaks; small differences were found in the overall spectral intensity and the amide-I and amide-III peaks. Studies using fluorescence spectroscopy to study the cervix have examined different sources of intra-patient and inter-patient variability including menopausal status, menstrual cycle variations, age, smoking history, the application of acetic acid, and overall diagnosis of the patient, finding that few of these variables affect the fluorescence spectra.[24, 25] Both of these studies, however, had a limited and homogenous group of patients.

In this article, we examine the effect of combining normal physiological variations: menopause, ovulation, race/ethnicity, body mass index (BMI), parity and health insurance status, on the classification of spectra acquired from a diseased cervix. These variables were chosen based on the results of our previous work.[7, 16] The goal of this research is to use RS to successfully diagnose abnormal areas of the cervix of any patient regardless of the above factors. Raman spectra were acquired from a diverse and diseased patient population coming in for a colposcopy-guided biopsy following a previous abnormal Pap smear. Multiple generalized linear methods were used to determine which variables should be considered and in what order to maximize the classification accuracy of Raman spectra from diseased areas of the cervix.

6.3 Materials and Methods

Patients with a previous abnormal Papanicolaou (Pap) result, scheduled for follow-up colposcopy-guided biopsy were recruited to this study. This study was conducted at the county hospital in Nashville, TN (Nashville General Hospital at Meharry Medical College, a hospital in an urban setting) in order to obtain measurements from a diverse set of patients. This study was approved by the Meharry Medical College Institutional Review Board (IRB).

6.3.1 Clinical study design: Patient recruitment

A total of 97 adult, female patients undergoing a colposcopy-guided biopsy were consented to participate in the study. With an effect size of 1, the power of this study is over 80% (two-sided statistical test, α=0.05). The patient's age, date of last menstrual period, use of artificial hormones, menopausal status, height, weight, obstetric history, ethnicity, address, insurance, relevant medical history and any previous abnormal Pap smears were all noted upon chart review with Health Insurance Portability and Accountability Act (HIPAA) authorization. To obtain the Raman measurements, first, the cervix was exposed and visually examined by the attending physician. Acetic acid was applied to the cervix to turn abnormal areas white to enable their visualization. Raman measurements were taken after the application of acetic acid from each area to be biopsied and one or two visually normal areas. Next, abnormal tissues were biopsied according to standard clinical protocol and sent for pathological examination. The spectra were correlated with histological results and considered normal, inflammation (metaplasia or cervicitis), CIN 1/HPV changes, or CIN 2/3, depending on the pathology report.

Patients were stratified according to four sets of variables to determine the effect of normal patient variations on disease classification of RS: 1) menopausal status (pre, peri or post),

2) menstrual cycle (before or after ovulation), 3) Race/ethnicity (white, black, Hispanic, or other); 4) BMI category: (underweight, normal, overweight and obese); 5) parity (never pregnant or 1 or more full-term pregnancies) and 6) insurance status (uninsured or insured). Patients' menopausal status and menstrual cycle were determined by the patient's age and last menstrual period, respectively. The patient identified her own racial or ethnic group. Body mass index (BMI) was calculated using the formula below with height and weight measured the same day that Raman spectra were acquired.[26]

$$BMI = \frac{mass(lb) \times 703}{(height(in))^2}$$

Patients were classified as normal if their BMI was between 18.50–24.99, overweight if it was between 25.00–29.99, and obese if it was equal to or greater than 30.00. Obstetric history was determined by a chart review. Health insurance status was established by whether the patient had private (insured) or government-subsidized health insurance (uninsured).

6.3.2 Instrumentation and Data Processing

The portable RS system used to collect Raman spectra *in vivo* consisted of a 785 nm diode laser (PI-ECL-785-350, Process Instruments, Inc., Salt Lake City, UT), a beam-steered fiber optic probe (Visionex, Atlanta, GA), an imaging spectrograph (Holospec f/1.8i-NIR, Kaiser Optical Systems, Ann Arbor, MI), and a back-illuminated, deep-depletion, thermo-electrically cooled CCD camera (Pixis 256BR, Princeton Instruments, Princeton, NJ), all controlled with a laptop computer (Figure 6.1). The fiber optic device delivered 80 mW of light onto the tissue with an integration time of 2-3 seconds. During the measurements, all room lights and the computer monitor were turned off. A spectral resolution of 8 wavenumbers (cm^{-1}) was achieved with this system.

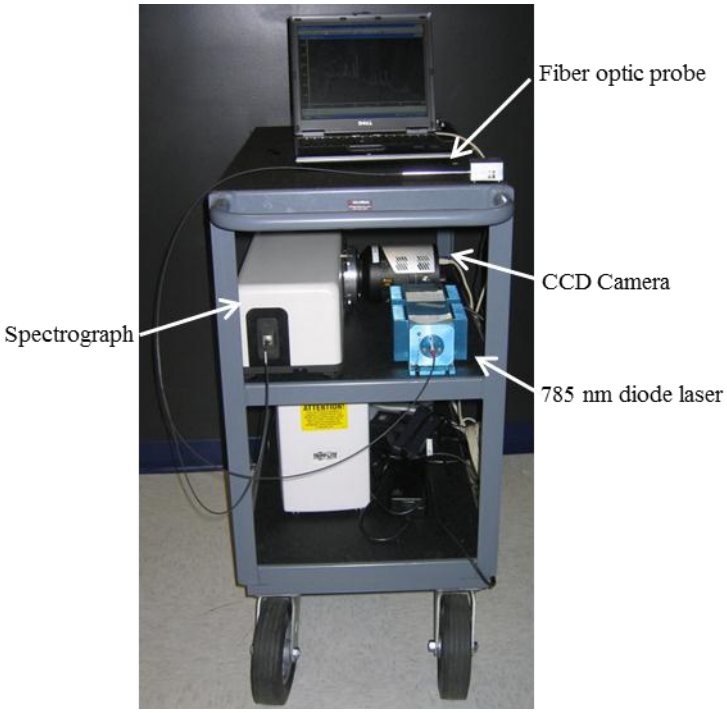

Figure 6.1. Picture of Raman system used for this study.

Spectral calibration of the system was performed daily with a neon-argon lamp and naphthalene and acetaminophen standards to correct for day-to-day variations. A National Institutes of Standards and Technology (NIST)-calibrated tungsten lamp was used to adjust for the wavelength-dependent response of the system. Spectra were processed for fluorescence subtraction and noise smoothing using the modified polynomial fit (9^{th} degree) and Savitzky-Golay methods, described previously.[27] Following data processing, each spectrum was normalized to its mean spectral intensity across all Raman bands to account for intensity variability.

6.3.3 Physiological Variable Ranking and Disease Classification

Ranking of the variables was achieved by analyzing the data considering each variable and combinations of variables. The spectra were first classified into their disease categories,

without accounting for any variable. Then, the spectra were separated by each variable and reclassified. The variable that led to the highest classification accuracy rate was considered to have the greatest effect on the spectra. This process continued until each of the 6 variables was used to separate the data.

The spectra were analyzed using an elastic-net regularized generalized linear model (GLMnet). Briefly, this method uses different methods (linear regression, two-class logistic regression, and multinominal regression) to fit the data and penalties (called the elastic net) while using the elastic net, i.e. the lasso and ridge regression as penalties to reduce the dimensionality of the data.[28, 29] The methods and penalties are combined to handle large data sets while efficiently dealing with sparse features. For this study, leave-one-patient-out cross validation was used to minimize bias. Predicted or posterior probabilities of a spectrum belonging to a specific class were output from this analysis. The posterior probability was set to 0.5 such that if a spectrum's probability for belonging to a certain class was 0.5 or higher, the spectrum was assigned to that class. Four groups were used for disease classification: negative for abnormal changes (negative), benign (cervicitis, metaplasia, etc.), CIN 1/HPV changes, and CIN 2/3. CIN 2 and 3 were combined because they are treated similarly in clinical practice.

The results from these analyses are presented in two ways. A confusion matrix is used to show the algorithm classification compared to the true classification of the sample determined by pathologists. Secondly, the posterior probabilities for each sample in each of the 4 groups are graphed. A posterior probability close to 1 suggests that there is a higher chance that the spectrum has classified correctly.

6.4 Results and Discussion

The types of disease and epidemiologic makeup of the patient group (menopausal status, ovulation, race/ethnicity groups, BMI category, obstetric history and insurance status) in this study are shown in Table 6.1. The entire data set consisted of two-hundred seventy-three spectra (273) acquired from a total of ninety-seven (97) patients. With an effect size of 1, the power of this study is over 80% (two-sided statistical test, α=0.05). Figure 6.2 shows Raman spectra of the four classification groups, regardless of menopause, ovulation, racial/ethnic background, BMI, parity, and insurance status. There are many variations in the spectra found among the different disease types. Some of these differences include the peak around 1070 cm^{-1} and the region between 1230 and 1330 cm^{-1}, which have been found to potentially correspond to collagen, elastin, lipids and DNA.[30-32] While differences in the spectra can be observed based on disease type, there are also underlying sources of variance due to normal patient variation.

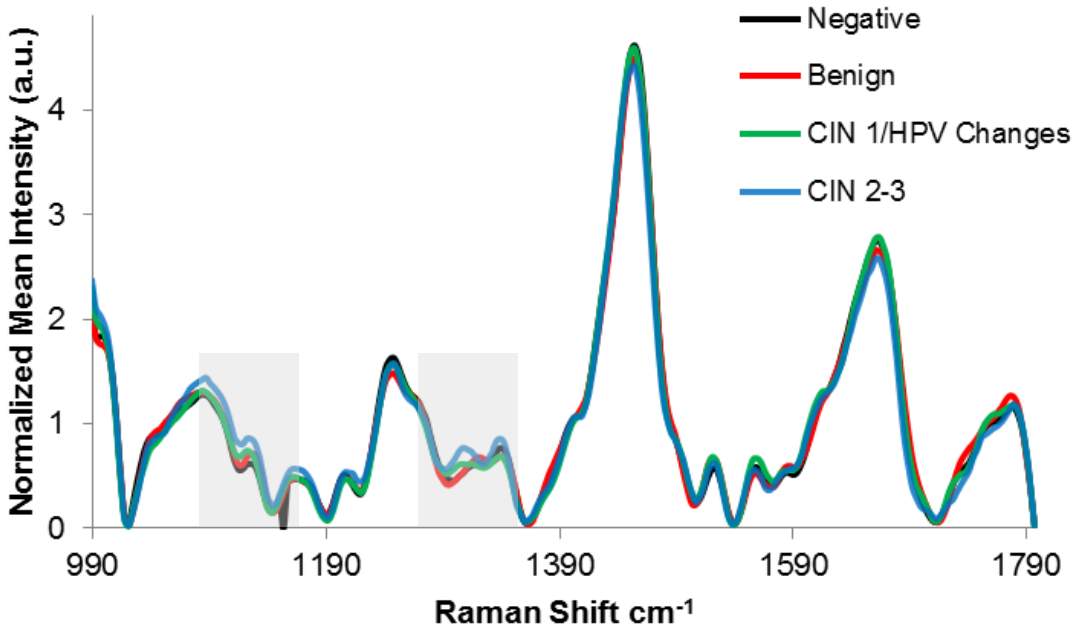

Figure 6.2. All 273 Raman spectra for all disease groups. The most amount of difference occurs in the two highlighted regions.

Negative	105
Inflammation	70
CIN 1/HPV Changes	83
CIN 2/3	15

Premenopausal	209
Perimenopausal	46
Postmenopausal	18

Before ovulation	103
After ovulation	97
No ovulation	73

White	91
Black	106
Hispanic	74
Arabic	2

Underweight BMI	8
Normal BMI	77
Overweight BMI	89
Obese BMI	99

No previous pregnancies	120
Prior Pregnancy/ies	153

Insured	161
Not Insured	112

Table 6.1. Demographic table of all spectra from patients recruited to this study. A total of 273 spectra were used.

Without taking any patient variable into consideration, all of the data ($n_{spectra}$=273) classified with an overall accuracy of 86% using the GLMnet method described above. The classification results are shown in Table 6.2. The maximum accuracy found was 97% for the negative spectra and the lowest classification accuracy was 80% for the CIN 1/HPV spectra. Overall, the spectra classified with an over 94% accuracy rate, however, 20% of the spectra obtained from malignant (CIN 1-3 or HPV) regions of the cervix classified as normal. Although

the accuracy rates are quite high in this first set of analysis, there is a considerably low sensitivity rate or a high false-negative rate which makes using the data unfeasible in a medical setting

		Raman Classification, output of GLMnet			
		Negative	Benign	CIN 1/HPV	CIN 2/3
Pathological Diagnosis	Negative	**97%**	2%	1%	-
	Benign	16.3%	**75.5%**	8.2%	-
	CIN 1/HPV	30.5%	2.8%	**66.7%**	-
	CIN 2/3	22.2%	5.6%	-	**72.2%**

Table 6.2. Confusion Matrix for data classified by disease only.

The variables were then considered in order to determine their influence on disease classification accuracy, especially their effect on reducing the number of false negatives (increasing the specificity). Table 6.3 shows the GLMnet output when the spectra are stratified by specific patient variables. For example, for the menopausal category, GLMnet was first run on the diseased spectra from premenopausal women, then on the spectra from perimenopausal women, etc. The classification accuracy displayed is the average of the groups for each patient variable. The variable that led to the maximum classification accuracy, sensitivity and specificity was menopausal status, followed by parity. BMI and menstrual cycle time point had a minimal impact on the classification accuracy, while health insurance and race/ethnicity had none.

Patient Variable	**Maximum Classification Accuracy**	**Sensitivity**	**Specificity**
None	*86%*	*82%*	*96%*
Menopausal Status	**97%**	**100%**	**99%**
Ovulation	95%	99%	100%
Race/Ethnicity	94%	84%	99%
BMI	95%	94%	98%
Obstetric History	**97%**	**98%**	**99%**
Socioeconomic Status	94%	85%	97%

Table 6.3. First iteration of looking at the effect of 1 patient variable.

Next, the data were classified again by taking multiple variables into consideration. First, the data was stratified by menopausal status. At this point, there were 3 groups of data: premenopausal, perimenopausal and postmenopausal. Each of these three groups was separated by another variable, for example, BMI, creating new groups of patients, such as a set of premenopausal women with a normal BMI. GLMnet was used to reclassify these new groups of data into 4 categories. In this second step, incorporating obstetric history resulted in the highest classification accuracy. This process was repeated and BMI was the next variable that, when incorporated into the analysis to separate the data prior to disease classification, resulted in the maximum classification accuracy. At this point, the classification accuracy, and therefore the sensitivity and specificity, were 100%. Further analyses were performed to consider the effects of menstrual cycle time point, race/ethnicity, and health insurance status. Classification accuracy was no longer used as a metric to determine success. Rather, the graphs of the posterior probabilities were used to measure if more of the spectra were classifying in their correct categories at a posterior probability closer to 1. Incorporating ovulation time point resulted in a small improvement in increasing posterior probability, but race/ethnicity and health insurance status had none (data not shown).

These results are displayed in Figure 6.3 and Figure 6.4. Figure 6.3 shows the posterior probabilities of all the data, before its stratification based on any patient variable. Although all of the data classified with 86% accuracy, there remains a large spread in all of the categories (Figure 6.3). In Figure 6.3, the y-axis corresponds to each of the 273 spectra. The x-axis corresponds to the posterior probability that the spectrum belongs to any of the 4 categories (Negative, Benign, CIN 1/HPV Changes, CIN 2/3). A posterior probability is generated for each spectrum to classify as each pathology (i.e. a posterior probability is calculated that each

spectrum is negative, benign, etc.). Therefore, each spectrum on the x-axis has a corresponding 1, 2, 3, or 4, indicating the posterior probability of classifying the spectrum into a specific group (negative = 1, benign = 2, CIN 1/HPV Changes = 3, CIN 2/3 = 4). If the spectrum has a high chance of belonging to a certain category, the posterior probability will be close to 1. Ideally, the number 1 (corresponding to the negative spectrum classifying correctly as negative) would be seen across the negative section (the first box on the left) with posterior probabilities close to 1; "2" would be seen with high posterior probabilities in the next box, corresponding to benign spectrum correctly classifying as benign, etc. The posterior probability spread is calculated by subtracting lowest posterior probability from the highest within a certain class; the largest spread is reported. A smaller spread suggests that the classification algorithm is successfully differentiating between spectra acquired from various pathology groups.

When menopausal state, parity and BMI are used to separate the data before disease classification, not only does the accuracy increase to 100%, but the posterior probabilities for the samples in all 4 groups increases (Figure 6.4). Only data from premenopausal, overweight women with a history of at least 1 pregnancy was included in this analysis. When the posterior probabilities were displayed when menstrual cycle was also considered, there was a slight increase in the posterior probabilities, especially in the CIN 1 group as well as a decrease in the overall posterior probability spread (Figure 6.5). Incorporating race/ethnicity or health insurance status led to no increase.

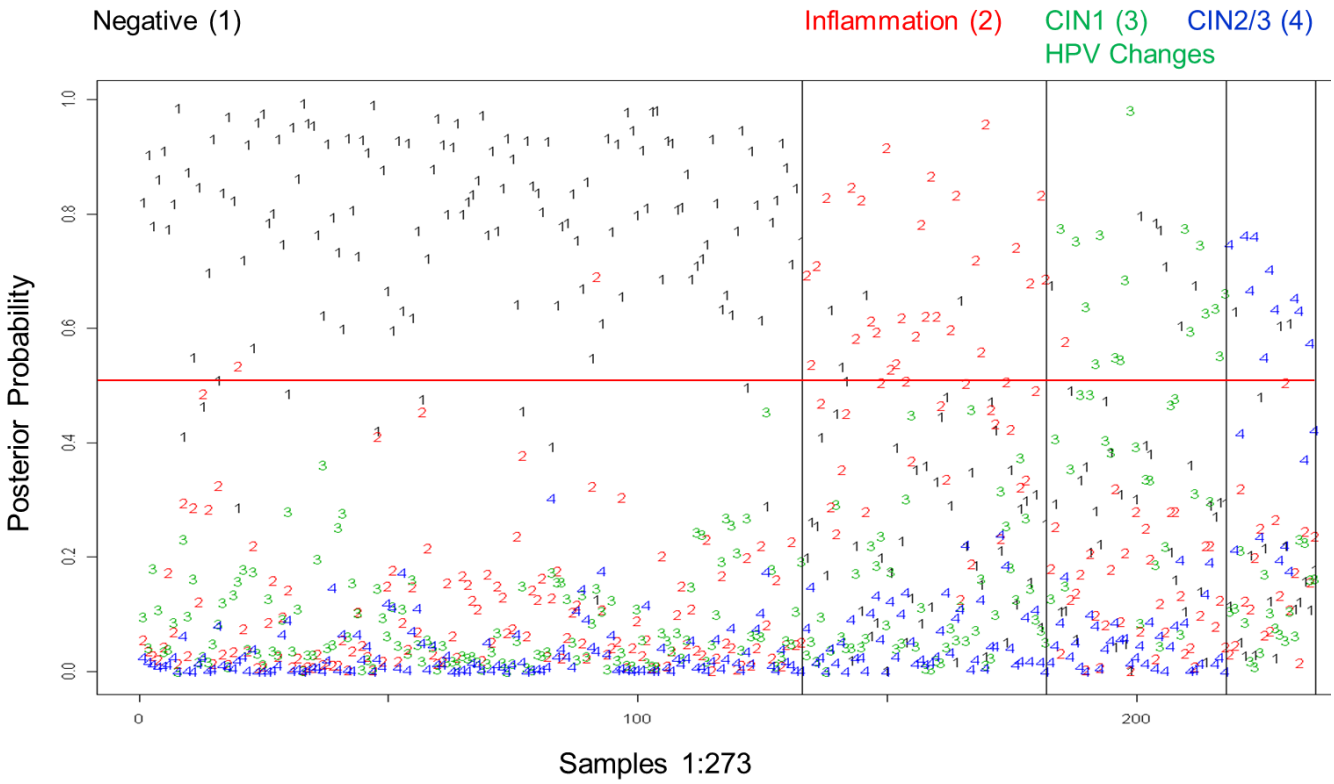

Figure 6.3 Posterior probabilities when classifying all data. Plotted are the posterior probabilities of each spectrum belonging to each of the 4 pathological classes. Classification accuracy: 86%; posterior probability spread: 0.89

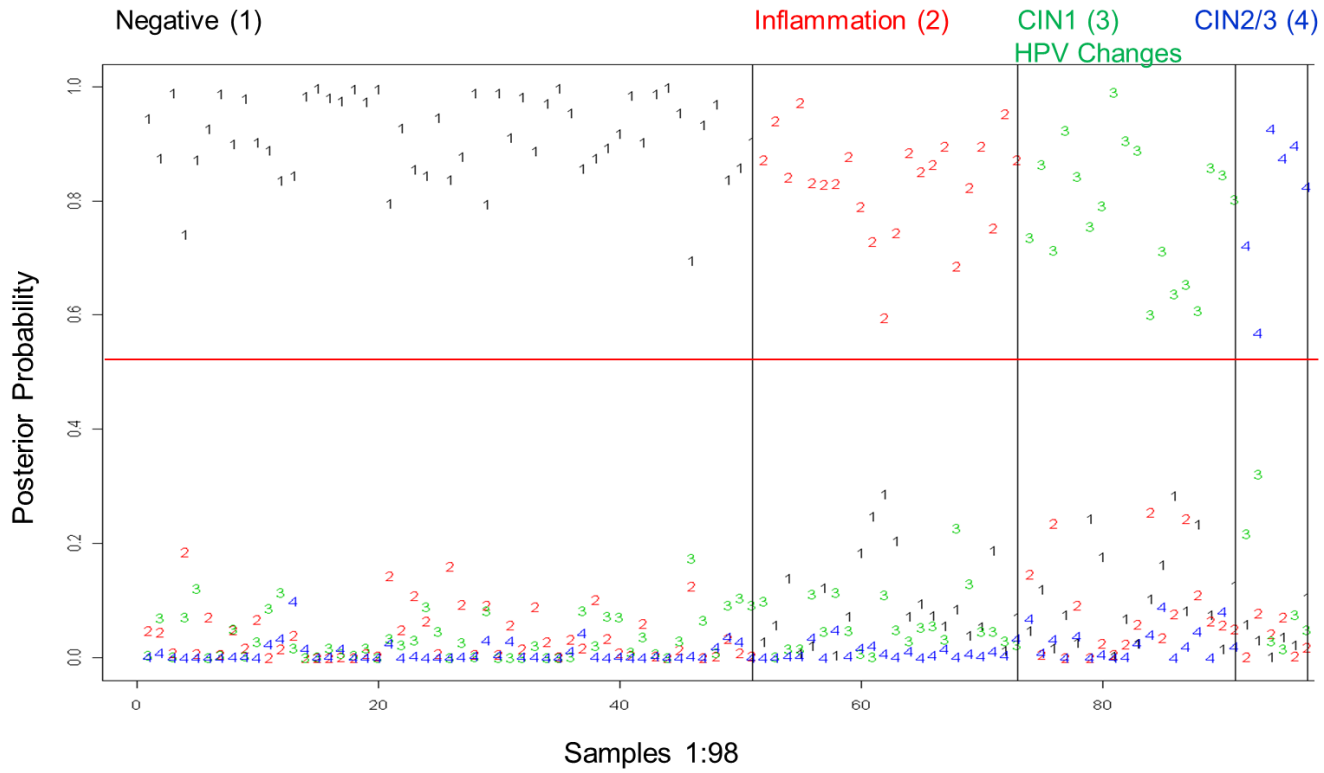

Figure 6.4. Posterior probabilities of 98 samples, taken from the original set of data. This data was obtained from premenopausal, overweight women who had at least 1 pregnancy. Plotted are the posterior probabilities of each spectrum belonging to each of the 4 pathological classes. Classification accuracy: 100%; posterior probability spread: 0.49

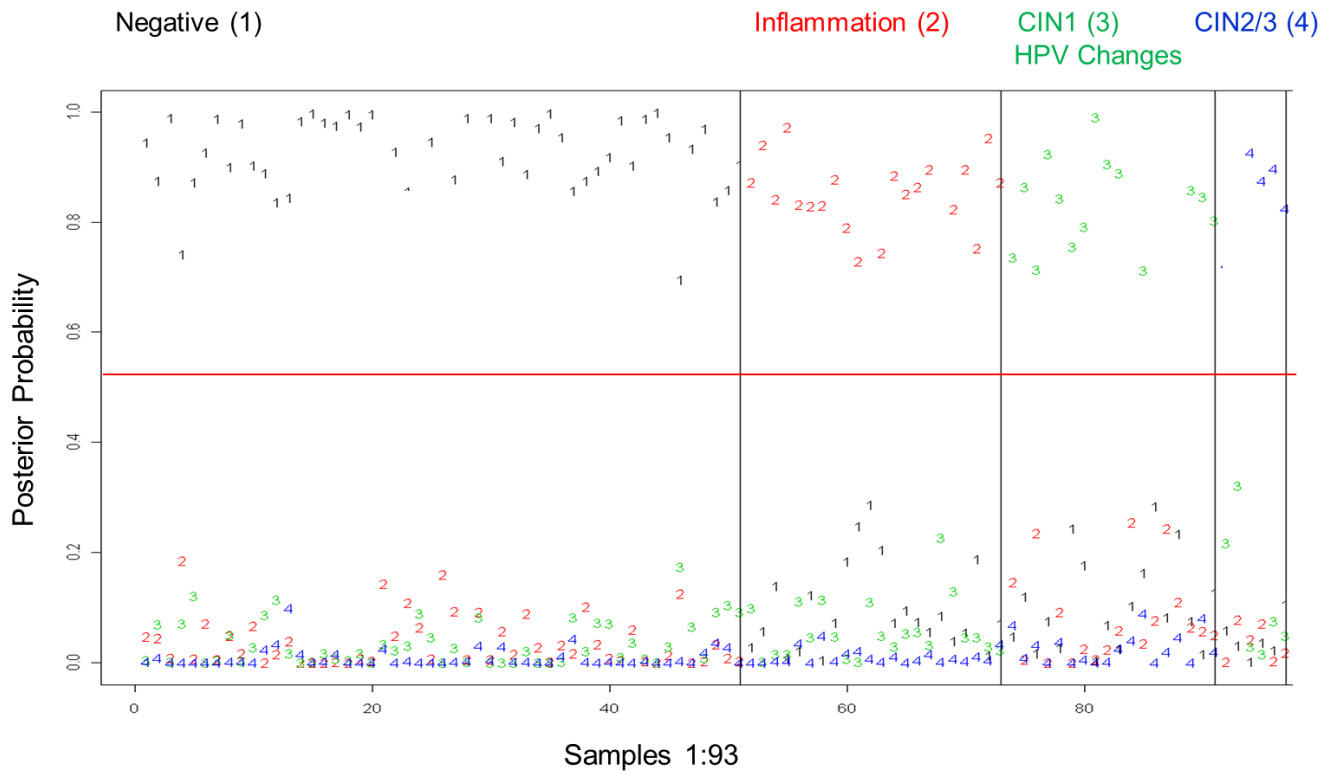

Figure 6.5. Posterior probabilities of 93 samples, taken from the original set of data. This data was obtained from premenopausal, overweight women before ovulation who had at least 1 pregnancy. Plotted are the posterior probabilities of each spectrum belonging to each of the 4 pathological classes. Classification accuracy: 100%; posterior probability spread: 0.39

Raman spectroscopy is a sensitive optical modality, used by many groups to detect abnormal or malignant areas of tissue. Results from previous work have shown that when spectra are stratified based on hormonal changes and history or presence of disease prior to classification, a reduction in intra-class variability was seen in both normal and diseased spectra.[4, 8] When noise from normal differences among patients was considered, unsupervised classification algorithms were then more likely to account for the variance due to differences from disease, resulting in improved performance. However, close examination of these results revealed that a significant amount of intra-class variance in the normal spectra remained,[4, 7, 8]

which motivated investigating additional factors that may account for the variance among normal spectra and improve classification of disease.

The classification accuracies found in this study were based on the posterior probabilities that each spectrum belonged to a specific class. For this work, a threshold of 0.5 was set to determine when a spectrum classified correctly. To increase the accuracy of this system, a higher probability may be set as the threshold. Setting a higher threshold would drastically affect the initial disease classification output, where no patient variables were considered. However, in our later classifications, where normal patient variables were used prior to inputting the data into GLMnet, the majority of the data classified correctly at a threshold above 0.7. This result suggests that by incorporating important variables, our classification algorithm has a better ability to define spectra as being more likely to belong to a specific pathological diagnosis.

In this study, we have demonstrated that the impact of normal patient variations must be accounted for in order to maximize disease classification accuracy of Raman spectra. To our knowledge, this is the first report where normal physiological variables were ranked based on their effect on disease classification. After ranking the variables by their order of importance, classification of disease spectra was then performed. Those results showed that menopausal status, parity and BMI have the greatest effect on correctly classifying Raman data. We have effectively performed a cost-benefit analysis on the basis of disease variables. The small increase in classification accuracy that ovulation time point, race/ethnicity and health insurance status provide are not significant enough to warrant their inclusion in further studies for diagnosing dysplasia in the cervix. However, these variables may be important for other disease sites, such as the skin, and a similar analysis should be conducted prior to using Raman to diagnose disease.

6.5 Acknowledgements

The authors acknowledge the financial support of the National Institute of Health grant R01-CA-095405 and a predoctoral fellowship (T32-HL7751-15) and the Lai Sulin Scholarship for EV. Special thanks go to Dr. Elliott Roberts, the nurses and staff at Meharry Medical College for all of their help, to Ming Li and Mingsheng Guo in the Department of Biostatistics at Vanderbilt University and to Amy Rudin for proofreading this paper.

6.6 References

1. Raman, C. and Krishnan, K. "A new type of secondary radiation." *Nature* **121**, 501-502 (1928).

2. Molckovsky, A., Song, L.M.W.K., Shim, M.G., Marcon, N.E. and Wilson, B.C. "Diagnostic potential of near-infrared Raman spectroscopy in the colon: Differentiating adenomatous from hyperplastic polyps." *Gastroint Endo* **57**, 396-402 (2003).

3. Huang, Z., McWilliams, A., Lui, H., McLean, D.I., Lam, S. and Zeng, H. "Near-infrared Raman spectroscopy for optical diagnosis of lung cancer." *Int J Cancer* **107**, 1047-1052 (2003).

4. Kanter, E.M., Vargis, E., Majumder, S., Keller, M.D., Woeste, E., Rao, G.G. and Mahadevan-Jansen, A. "Application of Raman spectroscopy for cervical dysplasia diagnosis." *J Biophotonics* **2**, 81-90 (2009).

5. Keller, M.D., Vargis, E., de Matos Granja, N., Wilson, R.H., Mycek, M.A., Kelley, M.C. and Mahadevan-Jansen, A. "Development of a spatially offset Raman spectroscopy probe for breast tumor surgical margin evaluation." *J Biomed Opt* **16**, 077006 1-8 (2011).

6. Caspers, P., Lucassen, G., Wolthuis, R., Bruining, H. and Puppels, G. "*In vitro* and *in vivo* Raman spectroscopy of human skin." *Biospectroscopy* **4**, S31-S39 (1998).

7. Kanter, E.M., Majumder, S., Kanter, G.J., Woeste, E.M. and Mahadevan-Jansen, A. "Effect of hormonal variation on Raman spectra for cervical disease detection." *Am J Obstet Gynecol* **200**, 512 e1-5 (2009).

8. Vargis, E., Kanter, E. M., Majumder, S. K., Keller, M. D., Beaven, R. B., Rao, G. G., and Mahadevan-Jansen, A. "Effect of normal variations on disease classification of Raman spectra from cervical tissue." *Analyst* **139**, 2981-2987 (2011).

9. Bergholt, M.S., Zheng, W., Lin, K., Ho, K.Y., Teh, M., Yeoh, K.G., So, J.B. and Huang, Z. "Characterizing variability in *in vivo* Raman spectra of different anatomical locations

in the upper gastrointestinal tract toward cancer detection." *J Biomed Opt* **16**, 037003 (2011).

10. Haka, A.S., Shafer-Peltier, K. E., Fitzmaurice, M., Crowe, J., Dasari, R. R., and Feld, M.S. "Diagnosing breast cancer by using Raman spectroscopy." *Proc Natl Acad Sci U S A* **102**, 12371-12376 (2005).

11. Chrit, L., Bastien, P., Sockalingum, G. D., Batisse, D., Leroy, F., Manfait, M., Hadjur, C. "An *in vivo* randomized study of human skin moisturization by a new confocal Raman fiber-optic microprobe: assessment of a glycerol-based hydration cream." *Skin Pharmacol Physio* **19**, 207-215 (2006).

12. Cano, A., Serra, V., Rivera, J., Monmeneu, R. and Marzo, C. "Expression of estrogen receptors, progesterone receptors, and an estrogen receptor-associated protein in the human cervix during the menstrual cycle and menopause." *Fertil Steril* **54**, 1058 (1990).

13. Gould, S.F., Shannon, J.M. and Cunha, G.R. "The autoradiographic demonstration of estrogen binding in normal human cervix and vagina during the menstrual cycle, pregnacy, and the menopause." *Am J Anat anatomy* **168**, 229-238 (1983).

14. Thomsen, S. and Tatman, D. "Physiological and pathological factors of human breast disease that can influence optical diagnosis." *Ann N Y Acad Sci* **838**, 171-93 (1998).

15. Nieburgs, H.E. "Recent progress in the interpretation of malignancy associated changes (MAC)." *Acta Cytol* **12**, 445-53 (1968).

16. Vargis, E., Byrd, T., Logan, Q., Khabele, D. and Mahadevan-Jansen, A. "Sensitivity of Raman spectroscopy to normal patient variability." *J Biomed Opt* **16**, 117004-1-117004-9 (2011).

17. Mitchell, J.B. and McCormack, L.A. "Time trends in late-stage diagnosis of cervical cancer: Differences by race/ethnicity and income." *Med Care* **35**, 1220-1224 (1997).

18. Jemal, A. Siegel, R., Xu, Jiaquan, and Ward, E. "Cancer statistics, 2009." *CA Cancer J Clin* **59**, 225-49 (2011).

19. Ward, E., Jemal, A., Cokkinides, V., Singh, G.K., Cardinez, C., Ghafoor, A. and Thun, M. "Cancer disparities by race/ethnicity and socioeconomic status." *CA Cancer J Clin* **54**, 78-93 (2004).

20. Lacey Jr, J.V., Swanson, C.A., Brinton, L.A., Altekruse, S.F., Barnes, W.A., Gravitt, P.E., Greenberg, M.D., Hadjimichael, O.C., McGowan, L. and Mortel, R. "Obesity as a potential risk factor for adenocarcinomas and squamous cell carcinomas of the uterine cervix." *Cancer* **98**, 814-821 (2003).

21. Calle, E.E. and Kaaks, R. "Overweight, obesity and cancer: epidemiological evidence and proposed mechanisms." *Nat Rev Cancer* **4**, 579-91 (2004).

22. Key, T.J., Allen, N.E., Verkasalo, P.K. and Banks, E. "Energy balance and cancer: the role of sex hormones." *Proc Nutr Soc* **60**, 81-9 (2001).

23. Knudsen, L., Johansson, C., Philipsen, P., Gniadecka, M. and Wulf, H. "Natural variations and reproducibility of *in vivo* near-infrared Fourier transform Raman spectroscopy of normal human skin." *J Raman Spectrosc* **33**, 574-579 (2002).

24. Brookner, C.K., Utzinger, U., Staerkel, G., Richards-Kortum, R. and Mitchell, M.F. "Cervical fluorescence of normal women." *Laser Surg Med* **24**, 29-37 (1999).

25. Agrawal, A., Utzinger, U., Brookner, C., Pitris, C., Mitchell, M.F. and Richards-Kortum, R. "Fluorescence Spectroscopy of the." *Laser Surg Med* **25**, 237-249 (1999).

26. "Physical status: the use and interpretation of anthropometry. Report of a WHO Expert Committee." *World Health Organ Tech Rep Ser* **854**, 1-452 (1995).

27. Lieber, C.A. and Mahadevan-Jansen, A. "Automated method for subtraction of fluorescence from biological Raman spectra." *Appl Spectrosc* **57**, 1363-7 (2003).

28. Zou, H. and Hastie, T. "Regularization and variable selection via the elastic net." *J R Stat Soc B* **67**, 301-320 (2005).

29. Friedman, J., Hastie, T. and Tibshirani, R. "Regularization Paths for Generalized Linear Models via Coordinate Descent." *J Stat Softw* **33**, 1-22 (2010).

30. Mahadevan-Jansen, A. and Richards-Kortum, R.R. "Raman spectroscopy for the detection of cancers and precancers (Journal Paper)." *J Biomed Opt* **1**, 31-70 (1996).

31. Redd, D.C.B., Feng, Z.C., Yue, K.T. and Gansler, T.S. "Raman spectroscopic characterization of human breast tissues: implications for breast cancer diagnosis." *Applied Spectrosc* **47**, 787-791 (1993).

32. Maquelin, K., Kirschner, C., Choo-Smith, L.P., Van Den Braak, N., Endtz, H.P., Naumann, D. and Puppels, G. "Identification of medically relevant microorganisms by vibrational spectroscopy." *J Microbiol Meth* **51**, 255-271 (2002).

CHAPTER 7

NEAR-INFRARED RAMAN MICROSPECTROSCOPY DETECTS HIGH-RISK HUMAN PAPILLOMAVIRUS

This chapter contains results showing the effect of HPV infection, HPV strain and malignancy from cells and patient samples on Raman spectra obtained using a microscope system. This data was acquired from cell culture and patient samples from Vanderbilt University Medical Center. It corresponds to Specific Aim 2. A manuscript of this chapter is currently under review with the journal *Translational Oncology*.

Vargis E, Tang YW, Khabele D, A Mahadevan-Jansen. Using Near-Infrared Raman Microspectroscopy for the Detection of High-Risk Strains of Human Papillomavirus. *Translational Oncology* (In review) 2012.

7.1 Abstract

Detecting HPV infection in cervical cells is an exceedingly important part of the clinical management of cervical dysplasia. Current guidelines in women's health outline the need for both the Pap smear as well as high-risk HPV testing. Testing for HPV is expensive, time-consuming and requires experienced technicians. Two sets of experiments were conducted. First, using a Raman confocal microscope system, Raman spectra were acquired from four different cell culture lines, 2 positive for HPV (HeLa, SiHa), 1 negative for HPV but malignant (C33A) and one normal, HPV-negative cell line (NHEK). The 3 malignant lines were all derived from cervical cells. Second, Raman spectra were acquired from de-identified patient samples that were previously tested for the presence of high-risk HPV. The spectra from the cell culture lines and the patient samples contained many statistically significant differences. Using SMLR to classify

the data led to classification accuracies of 89-97% for the cell culture samples and 98.5% for the patient samples. Raman microspectroscopy can be used to detect the presence of HPV and differentiate among specific HPV strains. This technique may provide health providers with a new method for quickly testing cell samples for the presence of HPV.

7.2 Introduction

Persistent infections with sexually transmitted human papillomaviruses (HPV) are correlated with essentially all cases of cervical cancer.[1] Out of over 150 HPV strains, a limited number of high-risk strains (16, 18, 31, 33, 35, 39, 45, 51, 52, 56, 58, 59, 68, 73 and 82) have been found to cause cervical cancer..[2, 3] Of these, two high-risk HPV strains, 16 and 18, together cause 70% of cervical cancer cases worldwide. These high-risk strains predominantly infect skin and mucosal membranes to promote epithelial proliferation, resulting in uninhibited proliferation and malignant transformations. Three oncogenes, E5, E6, and E7, are found in high-risk HPV strains and cause cell damage and abnormal cell proliferation by cooperatively interfering with the functions of cellular tumor suppressor proteins, specifically p53 and pRb.[4] Since HPV infects basal layer cells and only replicates in fully differentiated cells, it can usually remain undetected by the immune system, avoiding a humoral or cell-mediated immune response for years.[5]

The Papanicolaou (Pap) test, where cells are scraped from the cervix and examined for atypical cytological features under a microscope, was introduced in the early 1920s. Since then, clinical management of cervical dysplasia has been achieved by administering regular Pap tests. However, Pap tests alone do not provide a complete picture of the possible malignant changes that occur in the cervix due to HPV infection. Since 2009, the American Society of Colposcopy and Cervical Pathology has recommended including HPV testing for the clinical management of

cervical dysplasia in women.[6] Therefore, in the past few years, testing for all high-risk HPV strains or only strains 16 and 18 has been incorporated into routine cervical cancer screening in women over 30, leading to more accurate results and a reduction in the overall number of Pap smears as women who have both a negative Pap result and a negative HPV-DNA test are only tested every 2-3 years.

Current testing methods rely on obtaining a cellular sample, fixing the cells on a slide, and then transporting the slide to a pathology lab that runs the HPV test. After 7-12 days, the test results, whether the cell sample is positive or negative for a high-risk strain of HPV, are reported. No tests currently used for routine screening report the specific high-risk strain. The HPV tests developed by Qiagen, Roche, Gen-Probe and Hologic are the most commonly used.[7, 8] Cervista® tests for HPV types 16 and 18 and is approved for use in conjunction with Pap tests in women over the age of 30.[9] In cases where the Pap smear shows malignant cells and the sample is positive for high-risk HPV, the patient then needs to return for a follow-up appointment for either another Pap smear or a colposcopy-guided biopsy. A diagnostic tool that can rapidly identify specific high-risk HPV strains *in vivo* or *ex vivo* would help medical providers determine appropriate follow-up treatment to diagnose cervical dysplasia and prevent its progression.

Two HPV vaccines, Gardasil™ and Cervarix® prevent infection from high-risk HPV strains 16 and 18.[9, 10] These vaccines are available to women ages 9-26 and some men only on a voluntary basis. However, these vaccines may not protect against the other high-risk HPV types, which are common in countries other than the United States.[11, 12] A tool for identifying cervical samples that are positive for high-risk strains of HPV remains necessary even with the increasing use of HPV vaccines.

Optical techniques, such as drug-mediated fluorescence,[13] autofluorescence,[14] Fourier transform infrared (FTIR) spectroscopy,[15] and Raman spectroscopy (RS)[16-18] have been used to detect cervical dysplasia. As the clinical management of cervical cancer has shifted more recently, some of these techniques have been extended to the detection of infection with HPV. Such methods can be used non-invasively, either directly on the cervix to detect dysplasia or to detect the presence of HPV in small volumes of *ex vivo* samples. The results from these studies have ranged from detecting the difference between HPV-positive and -negative samples with sensitivities and specificities ranging from 90-94%[13, 15] and 92-96%,[13, 15, 17] to understanding the important spectral signatures that are associated with different types of HPV infection without a diagnostic application. These optical techniques do have their drawbacks, however, as fluorescence signal increases with HPV infection, regardless of strain, and FTIR is significantly hindered by water content, a significant hurdle for potential *in vivo* applications.

In this study, we use a confocal Raman microspectroscopy system to study the biochemical characteristics of various HPV strains and malignant cervical cells. Raman spectroscopy is based on the inelastic scatter effect, where incident light is scattered from a molecular or cellular sample. This scattered light exhibits an energy shift that reports the energy of specific molecular vibrations within the sample, effectively providing a detailed biochemical composition or fingerprint. A Raman spectrum, therefore, plots the energy shift away from the incident wavelength, usually measured in relative wavenumbers, versus scattering intensity. This optical technique can objectively characterize samples from multiple tissues based solely on their biochemical constituents, without relying on specific chemical markers or exogenous agents.[19-21]

Previously, we have acquired Raman spectra from bulk cervical tissue *in vivo* using a fiber optic tool to detect and differentiate types of cervical dysplasia within a diverse patient

population.[18, 22] Recently, we have found that accounting for patient variables, such as menopausal status or previous pregnancies, can lead to an increase in disease classification accuracy.[16, 22] Infection with HPV is also an important variable that has yet to be included in these analyses because not every patient is tested for HPV and the most widely used testing standards do not differentiate between various HPV strains.

The goal of this study is to evaluate the ability of RS for detecting the presence of HPV and the differences between specific HPV strains. Therefore, in this study, two sets of experiments were conducted to determine if RS is sensitive to HPV infection. First, Raman spectra were acquired using a Raman confocal microscope from 4 different cell lines, HPV-16 positive SiHa cells, HPV-18 positive HeLa cells, HPV-negative but malignant C33A cells, and benign NHEK cells. Next, Raman spectra were obtained from HPV-positive and -negative patients samples. Logistic regression algorithms were then used to classify spectra into either specific strain categories for the cell culture studies or HPV-positive or -negative for the patient samples. Other research groups have performed similar tests acquiring Raman spectra from HPV-expressing cell lines.[23-25] However, these studies omitted either a positive or a negative control. Also, many of these studies only reported on the oncogenic component of the virus (i.e. E7), instead of a complete HPV infection. Furthermore, to our knowledge, no study has incorporated Raman spectra acquired from HPV-positive and HPV-negative patient samples into their analysis of the sensitivity of RS towards HPV.

7.3 Materials and Methods

Two sets of experiments were conducted to evaluate RS's ability to differentiate between HPV strains in cell culture lines and the presence of high-risk HPV strains in patient samples.

7.3.1. Cell Culture and Sample Preparation

In the first set of experiments, 4 cell types with different HPV strains or no HPV infection (Table 7.1) were used. First, the two HPV-expressing cells, SiHa and HeLa (ATCC, Manassas, VA), were grown in RPMI with L-glutamate media with 10% FBS and antibiotics (Gibco, Carlsbad, CA). SiHa cells express HPV-16 and HeLa cells express HPV-18, two high-risk strains. A C33A cell line (ATCC), transformed but HPV negative, was grown in DMEM with 10% FBS and antibiotics. NHEK cells (a human keratinocyte cell lines) were grown in EpiLife Media (Gibco) and antibiotics.

Cell Culture Sample	HPV Positive	Transformed (malignant)
SiHa cell culture	Yes – HPV 16, 1-2 copies	Yes
HeLa cell culture	Yes – HPV 18, 10-50 copies	Yes
C33A cell culture	No	Yes
NHEK cell culture	No	No

Patient Samples	HPV Positive	Transformed (malignant)
HPV-Positive patient samples ($n_{samples}$=25)	Yes – one or more high-risk strains	Potentially
HPV-Negative patient samples ($n_{samples}$=25)	Negative for high-risk strains	No

Table 7.1. Description of Samples Used in this study

Once the cells reached approximately 90% confluency in a T-75 flask (on average, 18.2 x 10^6 cells), the cells were washed with PBS and trypsinized (media was used to stop the trypsinization process). The cell mixture was then centrifuged at 300 g for 5 minutes. After the supernatant was removed, 10 ml of PBS was added and the mixture was centrifuged. This process was repeated 3 times. Next, 10 ml of sterile water was added and the cell-water mixture

was centrifuged at 300 g for 5-7 minutes, also repeated 3 times. Finally, the supernatant was removed and the cellular pellets were transferred onto CaF_2 slides (Crystran, Dorset, UK). The slides were allowed to air dry in a sterile environment overnight. Raman spectra were acquired the next day. This protocol was developed to minimize the effects of the different types of media used to grow each cell type.

7.3.2 Patient Samples and Preparation

After approval from the Vanderbilt University Institutional Review Board (IRB) was obtained, HPV-positive ($n_{samples}$=25) and -negative ($n_{samples}$=25) de-identified patient samples were obtained from the Molecular Infectious Diseases Laboratory at Vanderbilt University (Table 7.1). The samples were initially acquired for standard HPV testing, which includes cells from the cervix also used in liquid-based Pap smears. Vanderbilt University uses the digene HC2 HPV DNA test developed by Qiagen (Valencia, CA). After 8 weeks, when samples are typically discarded, we were able to acquire 50 samples. Each sample contained 20 µl, with an average of 9×10^4 cells (fewer than the cell culture samples). Each cell sample was centrifuged at 300 g for 5 minutes. After the supernatant was removed, 10 ml of sterile water was added and the mixture was centrifuged again. This process was repeated 3 times. Finally, the supernatant was removed and the cellular pellets were transferred onto CaF_2 slides (Crystran). The slides were allowed to air dry in a sterile environment overnight. Raman spectra were acquired the next day.

7.3.3 Raman Microspectroscopy Measurements

Confocal Raman microspectroscopy provides a platform for acquiring Raman spectra from small sample volumes. The Renishaw InVia Raman microscope (Gloucestershire, United

Kingdom, Figure 7.1) consisted of a temperature-stabilized diode near-infrared laser with a maximum power of 120 mW (Innovative Photonics, Monmouth Junction, NJ) that operates at 785 nm and delivers ~30 mW to the sample. Light was guided through a collimator onto a series of mirrors that focused the light through an open field 50x microscope lens. Dried cell pellets were illuminated with the laser beam and then light from the illuminated spot was collected with a lens and sent through a monochromator. Rayleigh scattering close to the laser line was filtered through an edge filter. The remaining inelastic (Raman) scattered light was then focused through a slit (100-μm width) and dispersed by a diffraction grating (600 grooves per millimeter) onto a CCD detector (576 x 384 pixels; each pixel is 22 × 22 μm), which then sent the detected Raman spectra to a workstation for further processing. This system yields a resolution of ~6 cm^{-1}, compared to a resolution of 8 cm^{-1} found with the portable probe-based system. For the cell culture samples, spectra were acquired with an exposure time of 30 seconds. For the patient samples, spectra were acquired with an exposure time of 45-60 seconds. Three accumulations were acquired at each acquisition point, with a binning of 3.

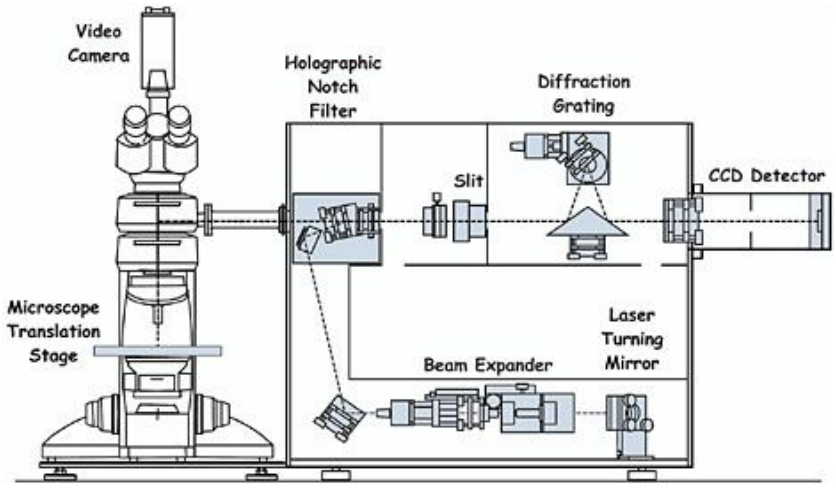

Figure 7.1. Schematic of Renishaw Confocal Raman System

The spectra were processed for fluorescence subtraction and noise smoothing using the modified polynomial fit and Savitzky-Golay methods, described previously.[26] Following data processing, each spectrum was normalized to its mean spectral intensity across all Raman bands to account for intensity variability.

7.3.4 Analysis and Classification of Raman Spectra

A Student's t-test (unpaired two-sample, equal variance) was first conducted to find regions of significant differences among the 4 cell culture samples and between the 2 patient samples. Next, classification algorithms were used to tease out subtle differences among spectra acquired from different samples. For this study, a logistic regression method called Sparse Multinomial Logistic Regression (SMLR) was used.[27] In brief, SMLR is a Bayesian machine-learning framework that computes the posterior probability of a spectrum belonging to each tissue class based on a labeled training set. For these analyses, a composite spectrum averaging Raman measurements from each cell culture or patient sample was used. A range of input parameters to SMLR was tested. The settings that provided the most accurate classification while also maximizing sparsity among the cell samples were a Laplacian prior, a direct kernel, a lambda value of 0.01, and not adding a bias term. After every analysis, a confusion matrix that displays how each spectrum classified was produced which can be presented as either the total number of spectra or a percentage. Also, each SMLR analysis provides a training algorithm that can be used for validation.

For the cell culture samples, 3 sets of SMLR analyses were used. First, HPV-positive samples (HeLa, SiHa) were compared to HPV-negative samples (C33A, NHEK). Next, malignant samples (HeLa, SiHa, C33A) were compared to the benign sample (NHEK). Finally,

SMLR was used to classify each cell line. For the patient samples, HPV-positive and HPV-negative samples were classified using SMLR. The algorithm developed from the patient samples was then applied to classify the cell samples.

7.4 Results

The goal of this study is to determine if the differences between HPV-positive and -negative samples, malignant and benign samples, and specific HPV strains from cell culture and patient samples can be detected using RS (Table 7.1). Approximately 30 Raman spectra were obtained from fifteen (15) independent samples, consisting of at least $1x10^8$ cells per sample. The power of the cell culture experiments is over 90% (two-sided statistical test, α=0.05) with an effect size of 1; the power of the human sample study is over 80% under the same criteria. Figure 7.2 displays the Raman spectra acquired with the Raman microscopy system from 4 cell culture samples: HeLa, SiHa, C33A and NHEK. Spectra acquired from the fixed HeLa cells appears to be the most different visually across the range of the spectrum, specifically around 990, 1080-1160, around 1400, and around 1670 cm^{-1}. These areas have been shown in previous work to correspond to C-C stretching in lipids and proteins, DNA content, and CH_2 deformation.[28]

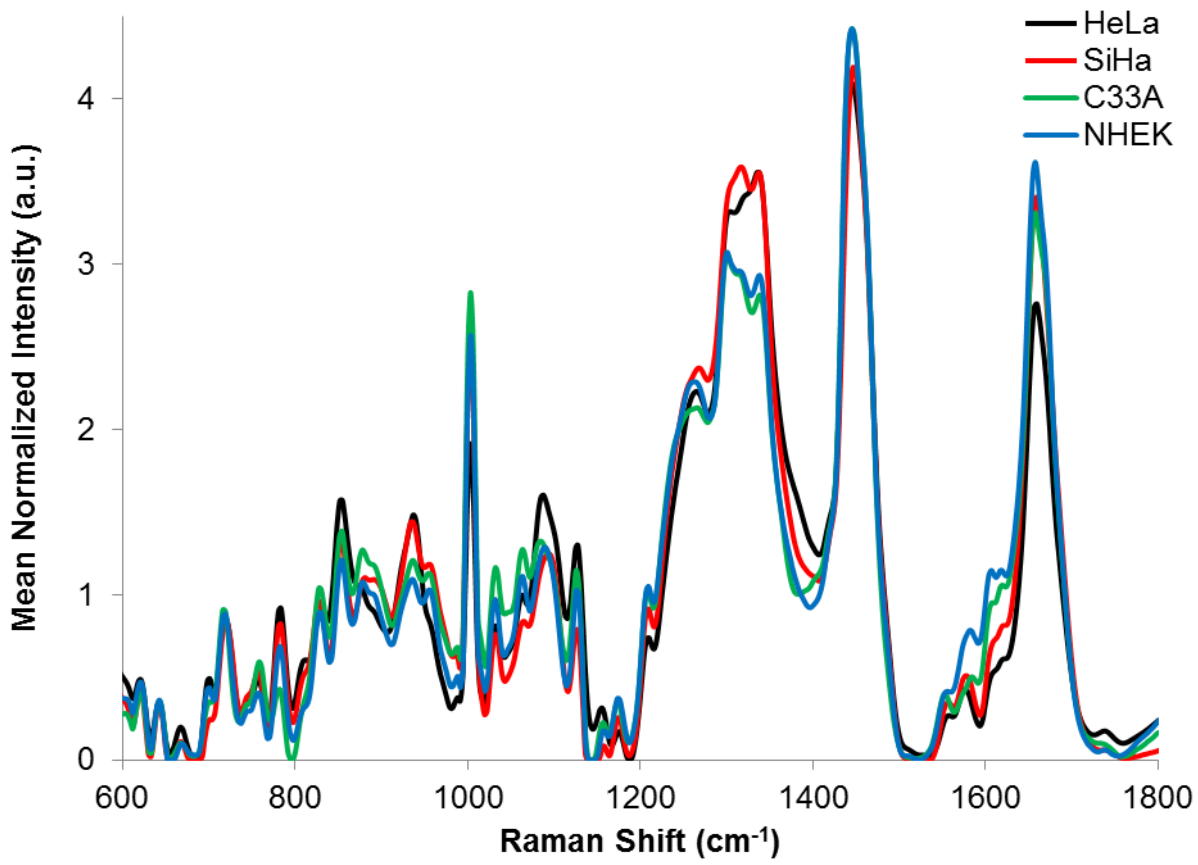

Figure 7.2. Spectra of HeLa, SiHa, C33A and NHEK cell culture samples.

In Figure 7.3, peaks and peak ratios of the spectra in Figure 7.2 are displayed to provide an in-depth view of the changes that occur in the spectra from different cell lines. Figure 7.3a and Figure 7.3b demonstrate that concentrations of molecules vary depending on cell type, HPV strain and the number of HPV copies. Specifically, wavenumber 1260 has been tentatively assigned to the deformation of CH_3 bonds and amide-III.[29] Wavenumber 1400 cm^{-1} has been shown to correspond to DNA and RNA components, such as uracil and adenine.[28] Looking at the changes among ratios of wavenumbers is another method commonly used to interpret Raman spectra. c shows the ratio of 1650 cm^{-1} to 1440 cm^{-1}, which is one way of describing the intensity of the CH_2 bending and the intensity of the C=C stretch.[30] In these samples, this ratio has a negative linear dependence on HPV infection and malignancy, leading to a decrease in the ratio.

In Figure 7.3d, the ratio of 1260 cm^{-1} to 1340 cm^{-1} or the ratio of Amide-III to amino acids is displayed.[31] In this case, as the number of copies of HPV increases in each sample (1-2 in SiHa cells, 10-50 in HeLa cells), this ratio increases, resulting in a linear correlation between HPV infection and this ratio.[32] A Student's t-test was also performed to compare the differences in the peak intensities to HeLa cells. A p-value less than 0.01 was defined as significant.

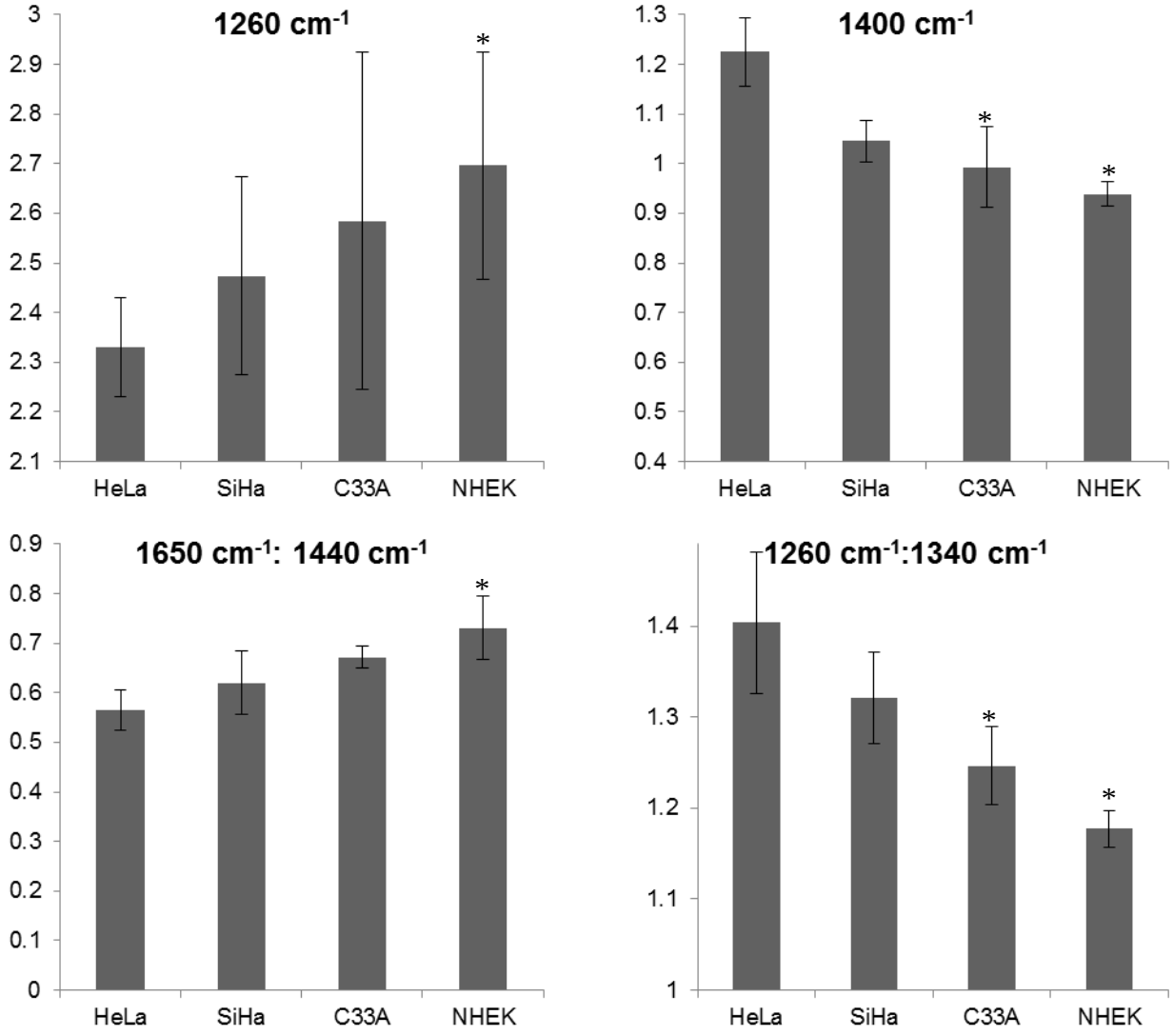

Figure 7.3. Specific wavenumbers and ratios of wavenumbers from spectra of cell culture samples with ± standard error. * represents a p-value < 0.01 when compared to HeLa cells.

The first step of this analysis to determine the clinical significance of this technique was to use SMLR to classify the cell culture samples as HPV-positive or -negative (Table 7.2). Table 7.2 shows that the presence of HPV is correctly identified using RS with a classification accuracy of 97%. Next, the analyses classified the spectra as malignant or benign (Table 7.3). Combining the malignant cell lines for comparison to the NHEK benign cell line resulted in a lower classification accuracy of 92%, with 10% of the Raman spectra obtained from malignant cells classifying as normal. Finally, SMLR was used to classify the spectra from the 4 different cell culture types with an accuracy of 89% (Table 7.4). The HeLa samples had the highest classification accuracy (98%), while the HPV-negative, malignant cells (C33A) had the lowest (84%) with 8% of its spectra classifying as normal.

Classification Accuracy: 97%		Raman Classification, output of SMLR	
		HPV Positive (HeLa, SiHa)	HPV Negative (C33A, NHEK)
Cell Culture Sample Type	HPV Positive (HeLa, SiHa, $n_{spectra}$=1365)	**98%**	2%
	HPV Negative (C33A, NHEK, $n_{spectra}$=1390)	4%	**96%**

Table 7.2. Classification Table for HPV-positive and HPV-negative cell culture samples

Classification Accuracy: 92%		Raman Classification, output of SMLR	
		Malignant (HeLa, SiHa, C33A)	Normal (NHEK)
Cell Culture Sample Type	Malignant (HeLa, SiHa, C33A, $n_{spectra}$=2075)	**90%**	10%
	Normal (NHEK, $n_{spectra}$=680)	6%	**94%**

Table 7.3. Classification Table for Malignant and Normal cell culture samples

Classification Accuracy: 89%		Raman Classification, output of SMLR			
		HeLa	SiHa	C33A	NHEK
Cell Culture Sample Type	HeLa ($n_{spectra}$=675)	**98%**	1%	1%	0%
	SiHa ($n_{spectra}$=690)	2%	**96%**	1%	1%
	C33A ($n_{spectra}$=710)	3%	5%	**84%**	8%
	NHEK ($n_{spectra}$=680)	1%	2%	9%	**88%**

Table 7.4. Classification Table for cell culture samples: HeLa, SiHa, C33A, and NHEK

Figure 7.4 shows the spectra acquired from patient samples that were tested for the presence of high-risk strains for HPV. Spectra from these two samples vary significantly across the 600-1800 cm^{-1} range, in many of the same regions listed above, but also in areas corresponding to both Amide-III and Amide-I (1200-1300 cm^{-1} and 1660 cm^{-1}, respectively).[31] P-values less than 0.001, resulting from a Student's t-test, are also shown on this graph, demonstrating that many regions of the spectra obtained from HPV-positive and -negative samples are significantly different.

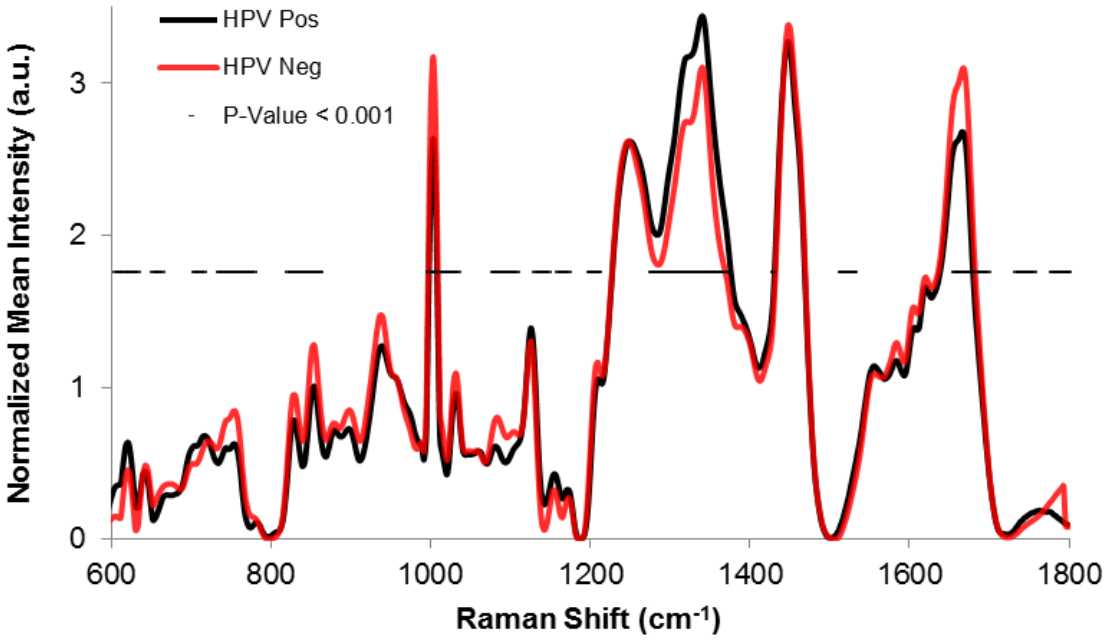

Figure 7.4. Spectra of HPV-positive vs. HPV-negative patient samples. Black line represents regions of significant difference (p-value < 0.001) when the two samples are compared.

The classification algorithm SMLR was also used to classify patient samples as HPV positive or negative and the results were compared to the HPV test result. These spectra from patient samples classified with an accuracy of 98.5% (Table 7.5). The training algorithm that resulted from using SMLR on the patient samples was then applied to both the malignant and benign classification (data not shown) and the classification of the 4 different cell culture lines. When the classification algorithm derived from the patient data was used to classify malignant and normal samples, the classification accuracy increased from 92% to 93%. For classifying the 4 cell culture lines, using the patient-sample algorithm instead of the cell-culture algorithm resulted in an increase in classification accuracy from 89% to 93% (Table 7.6). The spectra acquired from HeLa and SiHa cells maintained their previous classification accuracies, but the C33A and NHEK spectra increased their classification accuracies by 5% and 1%, respectively.

Classification Accuracy: 98.5%		Raman Classification, output of SMLR	
		HPV Positive	HPV Negative
Pathological Diagnosis	HPV Positive	**98%**	2%
	HPV Negative	1%	**99%**

Table 7.5. Classification Table for HPV-Positive and -Negative Patient Samples.

Classification Accuracy: 93%		Raman Classification, output of SMLR			
		HeLa	SiHa	C33A	NHEK
Cell Culture Sample Type	HeLa	**98%**	1%	1%	0%
	SiHa	2%	**96%**	1%	1%
	C33A	2%	4%	**89%**	5%
	NHEK	1%	2%	8%	**89%**

Table 7.6. Classification Table for cell culture samples: HeLa, SiHa, C33A, and NHEK, using algorithm derived from patient samples.

7.5 Discussion

The results of this study demonstrate that RS is able to differentiate between various cell culture samples as well as patient samples, based on the presence of HPV alone and the specific HPV strain. These results may positively contribute to screening for cervical disease by determining if cervical samples are positive for high-risk strains of HPV.

In Figure 7.2, there are certain regions that are more variable, including those corresponding to C=C stretching in lipids and proteins, DNA content, and CH_2 deformation. Also, the SiHa, C33A and NHEK spectra seem to resemble each other more than the HeLa spectra. HeLa cells have the highest number of copies of HPV 18, which may result in a more malignant cell line that has a higher concentration of DNA than the other cells types. The deformation of both proteins and lipids, found within cells and the phospholipid membrane, is observed within the Raman spectra acquired from more advanced malignant cell lines and those with a higher number of copies of high-risk strains of HPV. These changes may be associated with the increased disorganization caused by HPV infection and more advanced malignancy.

When smaller regions of the spectra are considered, differences can be observed among the cell culture samples. These differences may be related to HPV infection, the number of copies of HPV, and the transformation of the cell line. The two ratios that have been graphed (Figure 7.3c-d) demonstrate some of the biochemical changes that occur as cells with and without HPV infection advance malignantly. The 1650 cm^{-1}: 1440 cm^{-1} ratio demonstrates that as the cell develops increasingly malignant characteristics and as number of HPV copies increases, the ratio of CH_3 bending to C=C stretching decreases. This result suggests an increase in disorganization occurring at a cellular level. The 1260 cm^{-1}: 1340 cm^{-1} ratio corresponds to amide-III and the amount of amino acids (Figure 7.3d), suggesting that there are slight increases in the amount of protein as the cells become malignant and infected with HPV. It is also interesting to note that although the C33A cell line is a transformed, malignant cell line, it mostly resembles the spectra obtained from the normal NHEK cell line. This result suggests that infection with HPV is the more pertinent feature affecting Raman spectra.

The spectra obtained from patient samples appear to be dramatically different based only on infection with high-risk strains of HPV (Figure 7.4), verifying the hypothesis that RS is sensitive to HPV infection. The differences between the spectra are seen in multiple regions, such as those corresponding to lipid, amino acid, and DNA content, as well as CH stretching and bending regions that have been assigned to proteins such as albumin and collagen.[32] Many of these differences correlate with changes that occur in patient samples that are positive for at least one high-risk HPV strain. Specifically, an increased DNA content and density is found with an increased amount of phosphate and an increasing amount of disorganization, seen throughout the spectra as the deformation and breakdown of CH_x bonds.[32] Furthermore, the concentration of

lipids (tentatively assigned to 1450 cm^{-1}) seems to decrease as the number of copies of HPV increases.

Using SMLR algorithms developed from the cell culture spectra led to classification accuracy rates from 89% to 97%. Spectra of HPV-positive and HPV-negative cells classified with an accuracy of 97% (Table 7.2). As discussed, HPV infection leads to modifications within the cellular environment by circumventing normal cell growth pathways, specifically by increasing DNA synthesis. This phenomenon can be observed in the spectra, since the density or organization of DNA is lower in HPV-positive cells because the DNA is transcriptionally active, as opposed to densely packed and quiescent.[33] Next, SMLR differentiated between 3 malignant cell lines and 1 benign cell line with a classification accuracy of 92% (Table 7.3). This result is lower than the result from discriminating the HPV-positive and -negative cell lines, most likely due to the addition of the HPV-negative cell line (C33A) into the malignant category. C33A is a transformed, malignant epithelial cervical cell line, however, its spectra is closer to the spectra obtained from NHEK cells than the HPV-positive cell lines. Therefore, it is not surprising that 10% of the spectra obtained from C33A samples misclassified. It is important to note that clinically, a patient having malignant cervical cells without the presence of HPV is a very rare occurrence, accounting for approximately 0.01% of all cases of cervical dysplasia.[34] Management of such patients therefore would depend solely on the results of their Pap smears.

The lowest classification accuracy from the cell culture study was achieved when all four cell types were classified independently, resulting in an accuracy of 89% (Table 7.4). The normal NHEK cells classified correctly only 89% of the time, perhaps due to the similarities between the NHEK and C33A spectra from the lack of HPV infection, as discussed above. It is also important to note that SMLR was able to correctly classify over 95% of the spectra obtained from HeLa

and SiHa cells. The difference between these cells is likely due to the type of HPV (18 vs. 16) infection as well as the number of copies of HPV in each line (estimated 10-50 copies of HPV 18 in HeLa cells vs. 1-2 copies of HPV 16 in SiHa cells).

HPV-positive and -negative patient samples were also classified used SMLR with an accuracy of 98.5% (Table 7.5). This result corresponds with the differences observed between the two spectra, quantified by the low p-values across the spectral range. Similar to the cell culture studies, classifying patient samples based on the presence of HPV, as opposed to HPV type or copy number, leads to extremely promising results. The algorithm generated by SMLR based on the patient data set was then applied to previous data obtained from the cell culture samples to determine if the differences between the patient samples were more representative of the differences between HPV-positive and -negative cell lines. This algorithm was applied to both the malignant and benign samples (data not shown) and the 4 different cell lines (Table 7.6). Both sets of data classified with a higher accuracy when the patient-data algorithm was used. More specifically, using the patient-data algorithm lead to an increase in the classification of both the C33A and NHEK cells by decreasing their incorrect assignments to each other (i.e. C33A spectra classifying as NHEK spectra), implying that the algorithm developed from the patient data contains more accurate information about HPV-negative cells. It is also interesting to note that only a few cells needed to be infected with high-risk HPV strands to be considered HPV positive. On the other hand, it is assumed that all of the cells from HPV-negative samples were HPV negative. Future work will determine the detection limit of our RS system for detecting HPV-positive and -negative samples in patient samples in comparison to current HPV tests.

A few studies by other groups have shown that the presence of the biomarker protein $p16^{INK4A}$ has a great influence on cells infected with HPV.[35-37] $p16^{INK4A}$ is a minichromosome maintenance (MCM) protein found normally in cervical cells.[34] This protein is one of many that regulates the level of active cyclin D/CDK, part of the feedback loop involved in maintaining levels of MCM proteins, proliferating-cell nuclear antigens and cyclin E. $p16^{INK4A}$ is one of the biomarkers that corresponds to elevated E7 expression, and therefore, to high-risk HPV infection. Overexpression of $p16^{INK4A}$ has been detected in all grades of cervical lesions.[35, 37] Results from FTIR and confocal fluorescence microscopy studies on $p16^{INK4A}$ has shown that overexpression of $p16^{INK4A}$ and HPV infection result in an increase in nucleic acid levels, a decrease in lipid levels and a moderate to low change in protein levels.[36] The Raman spectra corresponds to these results, showing a biochemical increase in nucleic acid levels and a decrease in lipid levels (Figure 7.3). Current studies are focused on correlating the presence of biomarkers with HPV-positive or -negative status within the Raman data.

Recent studies have shown that combining HPV testing with the Pap test is more effective than the Pap test alone at detecting clinically relevant high-grade dysplasia early and results lead to increased prevention against more aggressive forms of cervical dysplasia in women over 30.[38] In fact, dual screening detected 25% more potentially cancerous lesions than a Pap test alone and resulted in fewer cancer cases five years later, compared to patients who were only screened with a Pap test. While previous work shows that RS is capable of detecting dysplastic areas of the cervix,[16-18] this research demonstrates that RS is capable of detecting HPV-infected cells as well. Therefore, RS could potentially be used as an alternative method to Pap tests and HPV screening to detect abnormal areas of the cervix and the presence of HPV *in vivo* and in real-time. Although *in vivo* samples were not used in this study, since HPV testing is

now recommended for women over 30, *in vivo* Raman measurements can be taken concurrently with HPV DNA testing. This work is being pursued currently.

The results from this paper demonstrate that RS is sensitive to changes occurring in cells due to HPV infection, HPV type and the number of copies of HPV. This technique can be combined with current methods used to screen for cervical dysplasia to provide a tool that can detect the presence of HPV immediately without the need for extensive sample preparation, quickly leading to accurate results. Current studies within our lab are focused on using the same technique to study the differences between low-risk and high-risk HPV strains. HPV testing is being introduced in conjunction with our ongoing *in vivo* Raman study for cervical dysplasia detection, to obtain *in vivo* measurements with the presence of HPV.

7.6 Acknowledgements

The authors acknowledge the financial support of the National Institutes of Health (Grant No. R01-CA-095405), a predoctoral fellowship (Grant No. T32-HL7751-15) and the Lai Sulin Scholarship for EV. Special thanks go to Isaac Pence and Cat Majors for their help with the upkeep of the cell culture, to Criziel Quinn for preparing the patient samples and to Amy Rudin for proofreading this paper.

7.7 References

1. Coleman, D.V., Wickenden, C. and Malcolm, A.D.B. "Association of Human Papillomavirus with Squamous Carcinoma of the Uterine Cervix." *Ciba F Symp* 120, 175-189 (1986).
2. Wright, T., Kurman, R.J. and Ferenczy, A. Blaustien's Pathology of the Female Genital Tract (Springer-Verlag, New York, 1994).
3. Rowson, K.E. and Mahy, B.W. "Human papova (wart) virus." *Bacteriol Rev* 31, 110-31 (1967).

4. Brokaw, J.L., Yee, C.L. and Munger, K. "A mutational analysis of the amino terminal domain of the human papillomavirus type 16 E7 oncoprotein." *Virology* 205, 603-7 (1994).

5. Walboomers J.M.M., Jacobs M.V., Manos M.M., Bosch F.X., Kummer J.A., Shah K.V., Snijders P.J.F., Peto J., Meijer C.J.L.M. and Munoz N. "Human papillomavirus is a necessary cause of invasive cervical cancer worldwide." *J Pathol* 189, 12-19 (1999).

6. Cox, J.T. "The clinician's view: role of human papillomavirus testing in the American Society for Colposcopy and Cervical Pathology Guidelines for the management of abnormal cervical cytology and cervical cancer precursors." *ASCCP* 1, 52-78 (2009).

7. Hesselink, A.T., van Ham, M.A., Heideman, D.A., Groothuismink, Z.M., Rozendaal, L., Berkhof, J., van Kemenade, F.J., Massuger, L.A., Melchers, W.J., Meijer, C.J. and Snijders, P.J. "Comparison of GP5+/6+-PCR and SPF10-line blot assays for detection of high-risk human papillomavirus in samples from women with normal cytology results who develop grade 3 cervical intraepithelial neoplasia." *J Clin Microbiol* 46, 3215-21 (2008).

8. Huh, W., Einstein, M.H., Herzog, T.J. and Franco, E.L. "What is the role of HPV typing in the United States now and in the next five years in a vaccinated population?" *Gynecol Oncol* 117, 481-485

9. Khan, M.J., Castle, P.E., Lorincz, A.T., Wacholder, S., Sherman, M., Scott, D.R., Rush, B.B., Glass, A.G. and Schiffman, M. "The elevated 10-year risk of cervical precancer and cancer in women with human papillomavirus (HPV) type 16 or 18 and the possible utility of type-specific HPV testing in clinical practice." *J Natl Cancer I* 97, 1072-1079 (2005).

10. Siddiqui, M.A.A. and Perry, C.M. "Human papillomavirus quadrivalent (types 6, 11, 16, 18) recombinant vaccine (Gardasil)." *Drugs* 66, 1263-1271 (2006).

11. American Cancer Society, "Cervical Cancer Resource Center." (American Cancer Society, Atlanta, 2007).

12. Au, W.W., Abdou-Salama, S., Sierra-Torres, C.H. and Al-Hendy, A. "Environmental risk factors for prevention and molecular intervention of cervical cancer." *Int J Hyg Environ Health* 210, 671-8 (2007).

13. Schneede, P., Munch, P., Wagner, S., Meyer, T., Stockfleth, E., and Hofstetter, A. "Fluorescence urethroscopy following instillation of 5-aminolevulinic acid: A new procedure for detecting clinical and subclinical HPV lesions of the urethra." *J Eur Acad Dermatol* 15, 121-125 (2001).

14. Ramanujam, N., Mitchell, M.F., Mahadevan, A., Warren, S., Thomsen, S., Silva, E., and Richards-Kortum, R. "*In vivo* diagnosis of cervical intraepithelial neoplasia using 337-nm-excited laser-induced fluorescence." *Proc Natl Acad Sci U S A* 91, 10193 (1994).

15. Cohenford, M.A. and Rigas, B. "Cytologically normal cells from neoplastic cervical samples display extensive structural abnormalities on IR spectroscopy: implications for tumor biology." *Proc Natl Acad Sci U S A* 95, 15327-32 (1998).

16. Kanter, E.M., Majumder, S., Vargis, E., Robichaux-Viehoever, A., Kanter, G.J., Shappell, H., Jones, H.W. III, and Mahadevan-Jansen, A. "Multiclass discrimination of cervical precancers using Raman spectroscopy." *J Raman Spectrosc* 40, 205-211 (2009).

17. Kanter, E.M., Vargis, E., Majumder, S., Keller, M.D., Woeste, E., Rao, G.G. and Mahadevan-Jansen, A. "Application of Raman spectroscopy for cervical dysplasia diagnosis." *J Biophotonics* 2, 81-90 (2009).

18. Vargis, E., Kanter, E.M., Majumder, S.K., Keller, M.D., Beaven, R.B., Rao, G.G. and Mahadevan-Jansen, A. "Effect of normal variations on disease classification of Raman spectra from cervical tissue." *Analyst* 136, 2981-7 (2011).

19. Haka, A.S., Shafer-Peltier, K. E., Fitzmaurice, M., Crowe, J., Dasari, R. R., and Feld, M.S. "Diagnosing breast cancer by using Raman spectroscopy." *Proc Natl Acad Sci U S A* 102, 12371-12376 (2005).

20. Chrit, L., Bastien, P., Sockalingum, G. D., Batisse, D., Leroy, F., Manfait, M., Hadjur, C. "An *in vivo* randomized study of human skin moisturization by a new confocal Raman fiber-optic microprobe: assessment of a glycerol-based hydration cream." *Skin Pharmacol Physio* 19, 207-215 (2006).

21. Bergholt, M.S., Zheng, W., Lin, K., Ho, K. Y., Teh, M., Yeoh, K. G., So, J. B., Huang, Z. "Characterizing variability in *in vivo* Raman spectra of different anatomical locations in the upper gastrointestinal tract toward cancer detection." *J Biomed Opt* 16, 037003 (2011).

22. Vargis, E., Byrd, T., Logan, Q., Khabele, D. and Mahadevan-Jansen, A. "Sensitivity of Raman spectroscopy to normal patient variability." *J Biomed Opt* 16, 117004-1-9 (2011).

23. Jess, P.R., Smith, D. D., Mazilu, M., Dholakia, K., Riches, A. C., Herrington, C. S. "Early detection of cervical neoplasia by Raman spectroscopy." *Int J Cancer* 121, 2723-8 (2007).

24. Ostrowska, K.M., Malkin, A., Meade, A., O'Leary, J., Martin, C., Spillane, C., Byrne, H. J., and Lyng, F. M. "Investigation of the influence of high-risk human papillomavirus on the biochemical composition of cervical cancer cells using vibrational spectroscopy." *Analyst* 135, 3087-93

25. Jess, P.R., Smith, D.D., Mazilu, M., Dholakia, K., Riches, A.C. and Herrington, C.S. "Early detection of cervical neoplasia by Raman spectroscopy." *Int J Cancer* 121, 2723-8 (2007).

26. Lieber, C.A. and Mahadevan-Jansen, A. "Automated method for subtraction of fluorescence from biological Raman spectra." *Appl Spectrosc* 57, 1363-7 (2003).

27. Krishnapuram, B., Carin, L., Figueiredo, M.A. and Hartemink, A.J. "Sparse multinomial logistic regression: fast algorithms and generalization bounds." *IEEE Trans Pattern Anal Mach Intell* 27, 957-68 (2005).

28. Utzinger, U., Heintzelman, D. L., Mahadevan-Jansen, A., Malpica, A., Follen, M., and Richards-Kortum, R. "Near-Infrared Raman Spectroscopy for *in vivo* Detection of Cervical Precancers." *Appl Spectrosc* 55, 955-959 (2001).

29. Miller, F.A., Mayo, D.W. and Hannah, R.W. Course notes on the interpretation of infrared and Raman spectra. (Wiley-Interscience, Hoboken, 2004).

30. Stone, N., Kendall, C., Shepherd, N., Crow, P. and Barr, H. "Near-infrared Raman spectroscopy for the classification of epithelial precancers and cancers." *J Raman Spectrosc* 33, 564-573 (2002).

31. Williams, R.W. "Protein secondary structure analysis using Raman amide I and amide III spectra." *Method Enzymol* 130, 311-331 (1986).

32. Meissner, J.D. "Nucleotide sequences and further characterization of human papillomavirus DNA present in the CaSki, SiHa and HeLa cervical carcinoma cell lines." *J Gen Virol* 80, 1725-33 (1999).

33. Arends, M.J., Buckley, C.H. and Wells, M. "Aetiology, pathogenesis, and pathology of cervical neoplasia." *J Clin Pathol* 51, 96-103 (1998).

34. Martin, C.M., Kehoe, L., Spillane, C.O. and O'Leary, J.J. "Gene discovery in cervical cancer : towards diagnostic and therapeutic biomarkers." *Mol Diagn Ther* 11, 277-90 (2007).

35. Kalof, A.N., Evans, M.F., Simmons-Arnold, L., Beatty, B.G. and Cooper, K. "p16INK4A immunoexpression and HPV in situ hybridization signal patterns: potential markers of high-grade cervical intraepithelial neoplasia." *Am J Surg Pathol* 29, 674-9 (2005).

36. Ostrowska, K.M., Garcia, A., Meade, A.D., Malkin, A., Okewumi, I., O'Leary, J.J., Martin, C., Byrne, H.J. and Lyng, F.M. "Correlation of p16(INK4A) expression and HPV copy number with cellular FTIR spectroscopic signatures of cervical cancer cells." *Analyst* 136, 1365-73

37. Dray, M., Russell, P., Dalrymple, C., Wallman, N., Angus, G., Leong, A., Carter, J. and Cheerala, B. "p16(INK4a) as a complementary marker of high-grade intraepithelial lesions of the uterine cervix. I: Experience with squamous lesions in 189 consecutive cervical biopsies." *Pathology* 37, 112-24 (2005).

38. Rijkaart, D.C., Berkhof, J., Rozendaal, L., van Kemenade, F.J., Bulkmans, N.W., Heideman, D.A., Kenter, G.G., Cuzick, J., Snijders, P.J. and Meijer, C.J. "Human papillomavirus testing for the detection of high-grade cervical intraepithelial neoplasia and cancer: final results of the POBASCAM randomised controlled trial." *Lancet Oncol* 2045, 70296-0 (2011).

CHAPTER 8

DETECTING BIOCHEMICAL CHANGES IN THE RODENT CERVIX DURING PREGNANCY USING RAMAN SPECTROSCOPY

This work in this chapter shows how Raman spectroscopy can be used to study pregnancy in normal mice and corresponds to Specific Aim 3. This study was based on the hypothesis that Raman spectra will be sensitive to changes in the cervix during pregnancy. Chapters 5 and 6 demonstrated that permanent biochemical changes occur due to pregnancy, labor and delivery. These changes are observed in the Raman spectra. It follows that the significant cervical variations that happen during pregnancy can be observed using Raman spectroscopy. The data was collected from mice housed in Dr. Jeff Reese's animal colony at Vanderbilt University. This entire chapter has been submitted to the *Annals of Biomedical Engineering.*

Vargis E, Brown N, Williams KC, Paria BC, Al-Hendy A, Reese J, A Mahadevan-Jansen. Detecting Biochemical Changes that Occur in the Rodent Cervix during Pregnancy Using Raman Spectroscopy. Annals of Biomedical Engineering (Accepted pending minor revision) 2012

8.1 Abstract

The goal of this research is to determine whether Raman spectroscopy, an optical method that probes the vibrational modes of tissue components, can be used *in vivo* to study changes in the mouse cervix during pregnancy. If successful, such a tool could be used to study cervical changes due to pregnancy, both normal and abnormal, in animal models and humans. In this study, Raman spectra were acquired before, during and after a 19-day mouse gestational period. In some cases, after Raman data was obtained, cervices were excised for structural testing and histological staining for collagen and smooth muscle. Various peaks of the Raman spectra, such

as the areas corresponding to fatty acid content and collagen organization, changed as the cervix became softer in preparation for labor and delivery. These findings correspond to the increase in compliance of the tissue and the collagen disorganization visualized with the histological staining. The results of this study suggest that non-invasive Raman spectroscopy can be used to study cervical changes during pregnancy, labor and delivery and can possibly predict preterm delivery before overt clinical manifestations, which can potentially lead to more effective preventive and therapeutic interventions.

8.2 Introduction

The physiologic changes during pregnancy that result in labor and delivery are part of complicated processes that are not fully understood. Current studies correlate maternal steroid hormonal changes and paracrine molecules with gestation and parturition (pregnancy and labor).[1-3] These small molecules regulate many of the changes in the tissues of both the mother and baby by altering the biochemical composition of the cervix to prepare for labor and delivery and by promoting fetal development. However, although pregnancy has been studied for centuries, the interactions of these molecules and the exact mechanisms governing the regulation and progression of pregnancy remain unknown. Researching human parturition is hindered since direct testing on pregnant women is limited and the hormonal pathways regulating animal pregnancy and labor vary substantially from those of humans. Much research into the maternal reproductive tract is currently focused on identifying important markers that trigger specific changes during pregnancy. Yet, it may be equally important to study the downstream effects such molecules have on maternal tissues, which change throughout pregnancy in preparation for birth.

During pregnancy, there are many well-documented physical changes in maternal tissues. The cervix, for example, is initially rigid and stays tightly closed to protect the fetus within the uterus and withstand its increasing weight. Closer to delivery, the cervix undergoes ripening, leading to its effacement (thinning) and dilation. As the uterus contracts with increasing frequency and intensity, the fetus is expelled through the softened cervix. These contractions also speed up the dilation process, with each contraction dilating the cervix as much as 30%.[4] Many of these properties require changes to the components of the extracellular matrix (ECM) of the tissues, which consists of fibrillar collagen, proteoglycans, hyaluronan, elastin and water.[4, 5] These components undergo a complex biochemical reorganizing and remodeling process throughout pregnancy, including a realignment of the collagen structure.[6, 7]

A number of small molecules have been implicated in regulating such processes.[3] Factors, such as estrogen and progesterone,[2, 3] platelet-activating factor,[8] prostaglandins[9, 10] and interleukin-8,[11] may all play a role in controlling the process that prepares the cervix for labor and delivery. Other research groups have focused on detecting changes in some of these individual factors.[12-14] However, few correlations have been found between specific molecules and biochemical changes in cervical tissues. Gestation and parturition are complex processes and it is likely that multiple interacting pathways control the progression of pregnancy, resulting in uterine contractions and cervical ripening.[3] As these pathways are discovered, health care providers may be able to more accurately determine pre-symptomatically when a woman is about to give birth and if necessary, intervene to delay preterm labor and premature birth.

Here we propose using an optical method to quantify changes downstream of small biomolecules in the cervix. Rather than removing tissue or measuring how a single molecule changes in blood or bodily secretions, optical methods can provide non-invasive, real-time,

automated measurements from bulk tissues as a whole. These measurements can contain a wide range of information, including collagen content and organization, changes due to hormonal fluctuations, and a measure of cervical length. For example, Garfield *et al*. used electromyography to measure changing action potentials of the uterus throughout pregnancy.[15] Kuon *et al.* used a collascope to measure the autofluorescence of the cervix and correlated the results with the cervical surface area, finding that during pregnancy, surface area increases as autofluorescence increases.[16] Jokhi *et al.* used electrical impedance spectroscopy to measure cervical resistivity to determine the onset of labor, with predictive values of 0.65 to 0.8.[17] Second-harmonic generation has also been used to measure changes in collagen structure during gestation.[18] Other groups have used optical methods, such as Fourier-transform infrared (FTIR),[19] resonance,[20] and light-scattering[21] spectroscopy to measure salivary changes and the presence of nitric oxide or fetal nucleated red blood cells, respectively. To our knowledge, this is the first report using Raman spectroscopy, a sensitive optical method, to study biochemical changes in tissue during pregnancy.

Raman spectroscopy (RS) is based on the Raman effect by which energy can be exchanged between incident photons and scattering molecules. When an incident photon collides with certain molecules, energy may be transferred either from the molecule to the photon or vice versa. The energy differences of the scattered photons are indicative of the molecules set into vibration. A Raman spectrum then consists of a series of peaks, which represent the different vibrational modes of the scattering molecules. These peaks are spectrally narrow and molecular-specific, such that the observed peaks may be associated with specific bonds in specific molecules. Many biological molecules have distinguishable spectra, so that one can determine a tissue's biochemical composition from its Raman spectrum. For example, one relevant

biochemical change during pregnancy is the softening and ripening of the cervix due to changes in collagen. This change, among other changes in elastin, glycogen and water content, can be detected with RS.[22-25] Other changes that RS is likely to be sensitive to are changes in collagen cross-linking, water content and hormonal variations, many of the important factors that fluctuate during pregnancy, labor and delivery, which has been seen in other studies.[26]

We have previously demonstrated the potential of RS to detect subtle changes in tissue biochemistry from the cervix.[24, 25] This technology has been applied to detect cervical precancer lesions *in vivo* and can distinguish between normal, inflammation, low-grade dysplasia and high-grade dysplasia areas with classification accuracy rates of over 97%. Also, it has been demonstrated that RS is sensitive to subtle changes in hormonal levels, the permanent effects of pregnancy and delivery, as well as malignancy-associated changes.[22] The only report on using RS for obstetrics research is for studying preeclampsia, an abnormal gestation-related increase in maternal blood pressure.[27] However, previous work indicates that the technology and knowledge exists to develop RS as a tool for studying the cervix throughout pregnancy.[15, 16, 24, 25] In this pilot study, RS was used to monitor and understand cervical changes in normal mice during pregnancy.

The goal of this paper is to characterize changes in the cervix of normal mice throughout pregnancy using Raman spectroscopy. To achieve this goal, two sets of studies were conducted. First, Raman spectra were acquired from the cervix of non-gravid (not pregnant) mice to develop a baseline of the normal cervix during murine estrus cycles. Once the effect of normal cycling was characterized, the primary study was conducted and spectra were acquired from normal mice at multiple time points before, during and after pregnancy. To verify the changes observed in the Raman spectra, after Raman data was acquired, the cervix was harvested to find the structural

properties of the tissue and to visualize cellular changes with histological staining. Logistic regression algorithms and statistical analyses were used to determine if significant differences existed in the Raman measurements, force-displacement testing and histological staining indicative of the changes related to pregnancy.

8.3 Materials and Methods

8.3.1 Animals and Tissue Collection

Adult virgin female and male mice (strain: CD1(ICR)) were purchased from Charles River Laboratories, Raleigh, NC. They were maintained in a 12 hour:12 hour light/dark cycle in the Vanderbilt University Animal Facility with unlimited access to water and food. All animal maintenance, handling and procedures were performed in accordance with National Institutes of Health guidelines for the care and use of laboratory animals and were approved by the Vanderbilt University Institutional Animal Care and Use Committee (IACUC). Before studying normal pregnancy, non-pregnant (or non-gravid (NG)) mice with normal cyclicity were first evaluated to examine the effect of hormonal changes during the estrous cycle on the cervix. Accordingly, two sets of experiments were conducted: a study to observe changes in the cervix due to hormonal changes alone and a study to examine changes due to pregnancy. Raman measurements were first obtained from 3 sets of NG mice, with 3-4 mice in each set (n=11). Measurements were taken from each set for 5 days straight over the course of 3 weeks to acquire data. The stages of the estrous cycle that were measured include proestrus, estrus, metestrus and diestrus.[28] Prior to the Raman measurements, vaginal washings were obtained by rinsing the

vaginal canal with saline and the estrous stage was determined by identifying cell types and their relative abundance present in smears under a stereo-microscope.

Timed matings were carried out by housing one normal fertile male with three normal females to study the cervical changes related to pregnancy. On the following day, females were evaluated at 0900 for the presence of a copulatory plug with gestation day 1 defined by the presence of the plug. Data from any mouse that was not visually pregnant by day 12 was not used in any of the following results. Animals in this colony typically give birth on the evening of gestation day 19. A set of mice was followed before, during and after pregnancy (n=47). Female mice were anaesthetized with isoflurane and Raman measurements were acquired prior to mating (NG), on days 1, 4, 12, 15, 18, and 19 of pregnancy, and on post-partum day 1 (PP1). At the same time points, Raman measurements were acquired and then the mouse was euthanized (overdose of isoflurane inhalation) to collect the cervix for force-displacement testing or histological staining. The cervix was dissected and trimmed to 5 mm in length to maintain consistency for the force-displacement testing. Cervices were dissected with the uterus and vaginal tissue still attached in order to control for orientation during sectioning and imaging.

8.3.2 Raman Instrumentation and Data Processing

Raman spectra were collected *in vivo* using a portable RS system consisting of a 785 nm diode laser (I0785MM0350MS, Innovative Photonic Solutions, Monmouth Junction, NJ), a beam-steered fiber optic probe without its casing (785nm, Emvision, Loxahatchee, FL), an imaging spectrograph (Holospec f/1.8i, Kaiser Optical Systems, Ann Arbor, MI), and a back-illuminated, deep-depletion, thermo-electrically cooled charge-coupled device (CCD) camera (Pixis 256BR, Princeton Instruments, Princeton, NJ), all controlled with a laptop. The fiber optic

probe (10 cm long and approximately 2.1 mm in diameter) delivered 80 mW of incident light to the tissue at an integration time of 2-3 seconds with all room lights and the computer monitor turned off. The system provided a spectral resolution of 8 wavenumbers (cm^{-1}).

Spectral calibration of the system was performed everyday using a neon-argon lamp and naphthalene and acetaminophen standards to correct for day-to-day variations. A National Institute of Standards and Technology (NIST)-calibrated tungsten lamp was used to account for the system's wavelength-dependent response. The spectra were processed for fluorescence subtraction and noise smoothing using the modified polynomial fit and Savitzky-Golay methods, described previously.[29] Following data processing, each spectrum was normalized to its mean spectral intensity across all Raman bands to account for intensity variability. The code developed to process the data minimized the error introduced by the fluorescence subtraction and the background removal. The same code with the same parameters was used for all the samples such that the same amount of minimal error was introduced to all the spectra. Finally, the spectra were normalized in order to perform relative comparisons across the data.

8.3.3 Tissue Structural Properties

Structural properties of excised cervical tissues were evaluated using modifications of the methods developed by Harkness and Harkness[30] to correlate structural tissue properties to biochemical Raman measurements. Briefly, the cervix was mounted onto two hooks inserted through the cervical canal. The hooks were made of stainless steel (22 Ga, 316L AISI grade). They were approximately 0.8mm thick and 7 mm long. One hook was attached to a stationary hook and the other hook was attached to a force transducer and a micrometer. Tissues were incubated in a water-jacketed bath containing Krebs solution at 37 °C bubbled with 95% O_2/5%

CO_2. The force transducer was calibrated using standard weights to set the minimum (~-1.03 V) to 0 g and the maximum (~9.04 V) to 50 g.

Baseline cervical dilation was determined by increasing the distance between the two hooks until a small increase (~0.1 g, constant) was detected with the force transducer. The cervix was incubated in Krebs solution and held at this displacement for 10 minutes before measurements were recorded. Then the inner diameter of the cervix was increased in 1-mm increments at 4-minute intervals to produce cervical distention. The amount of force at each 1-mm displacement and every 4 minutes was recorded (displacement rate: 0.0042 mm/s). The diameter was increased until the tissue tore. Force was plotted as a function of cervical diameter. A moving average function was used to calculate the slope of the force-displacement curve; this slope was then used as cervical stiffness. A steeper slope indicates an increased resistance to stretch or a reduced compliance. Results are displayed as mean ± standard error (S.E.) from 5 independent samples in each group.

8.3.4 Statistical Analysis

Cycling status was determined by the cells observed in vaginal smears. Pregnancy dating was determined by the presence of a cervical plug.[28] These are two gold standards often used, however, there can be errors associated with such techniques based on the expertise of the user. Measurements were excluded from any mouse originally enrolled in the study that ended up not being pregnant.

For this study, a logistic regression method called Sparse Multinomial Logistic Regression (SMLR) was used to tease out subtle differences among spectra acquired from different samples.[31] In brief, SMLR is a Bayesian machine-learning framework that computes the

posterior probability of a spectrum belonging to each tissue class based on a labeled training set. For these analyses, a composite spectrum averaging Raman measurements from each mouse at each time point was used. A range of input parameters to SMLR was tested. The settings that provided the most accurate classification while also maximizing sparsity were a Laplacian prior, a direct kernel, a lambda value of 0.01, and no additional bias term. To avoid bias, SMLR employs a leave-one-mouse-out at each time point. The algorithm uses all but one of the spectra to create a classification algorithm that is used to classify the left out spectrum. In the next iteration, a different spectrum is left out, creating a new training algorithm that is then used to classify the left out spectra. This process is completed until all of the spectra are classified. A Student's t-test was performed to compare individual peaks from d4 to all the other time points. A p-value less than 0.1 was considered significant.

For the force-displacement testing studies, a Kruskal-Wallis one-way analysis of variance (ANOVA) was performed, followed by Dunn's Method for post-hoc analysis and pairwise comparison to control for errors among the same sample group. The Kruskal-Wallis is the nonparametric alternative to ANOVA and has been used in previous tissue structural studies of the rodent cervix.[7]

8.3.5 Tissue Processing and Masson's Trichrome Staining

Cervical tissues were removed and stained to correlate the Raman spectra to important molecular and cellular changes resulting from pregnancy. First, excised cervico-uterine tissue sections were immediately snap-frozen in liquid nitrogen after removal and stored at -80 °C for later use. Next, the tissues were embedded in optimal cutting temperature (OCT) embedding medium (Tissue-Tek, Quiagen, Valencia, CA). Embedded tissues were cryosectioned into 12 μm

thick slices and thaw-mounted onto poly-L-lysine coated slides. Tissues were then fixed in Bouin's fixative, followed by Masson's trichrome staining per protocol (Sigma-Aldrich, St. Louis, MO). Trichrome staining labels collagen fibrils (blue), nuclei (black), and smooth muscle and cytoplasm (red). Tissue sections were imaged and recorded under 20x magnification.

8.4 Results

8.4.1 Cycling Study

The first step of this study was to determine if RS is sensitive to changes in the NG cervix due to hormonal cycling alone. Raman spectra ($n_{spectra}$=120) were acquired from the cervix of NG mice (n_{mice}=11) at 4 different cycling time points: proestrus, estrus, metestrus, and diestrus (Figure 8.1). Figure 8.1 shows some variations across the different time points. The majority of these differences are in the region between 1200 and 1400 cm^{-1}. This area potentially corresponds to collagen, amide-III, and lipid content.[31-34] Logistic regression analysis (SMLR) was used to determine if any significant differences existed due to cycling alone. Ninety-two of the 120 spectra or 77% classified correctly, meaning that SMLR was able to correctly classify the spectra as belonging to its corresponding time point within the estrous cycle 77% of the time (Table 8.1).

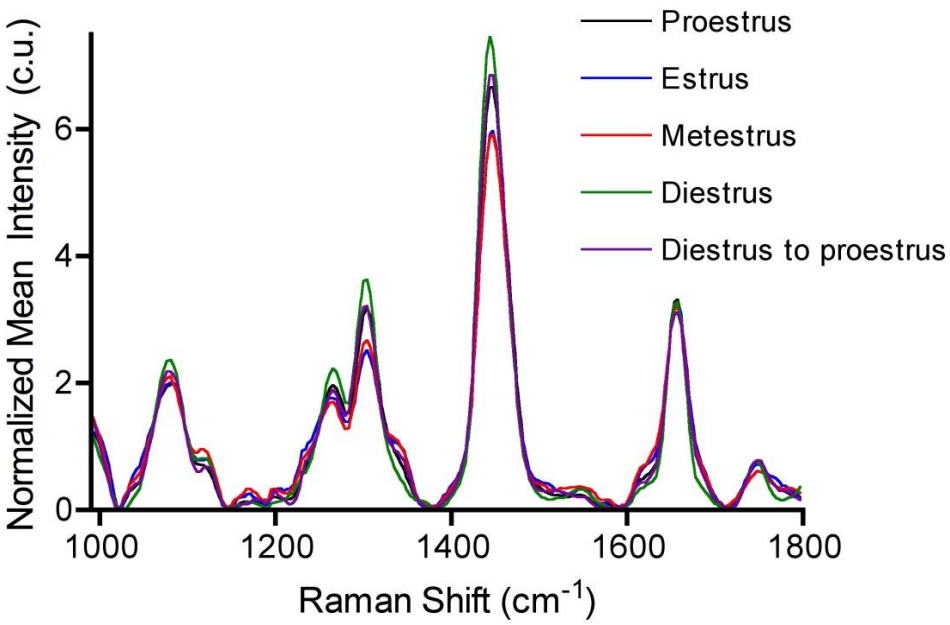

Figure 8.1. Normalized average Raman spectra of non-gravid mice at various points during the menstrual cycle.

Classification Accuracy = 77%		Raman Classification from SMLR Output				
		Proestrus	Estrus	Metestrus	Diestrus	Di to Pro
Cycling Time Point	Proestrus ($n_{spectra}$=23)	**79%**	6%	11%	-	4%
	Estrus ($n_{spectra}$=26)	14%	**78%**	7%	1%	-
	Metestrus ($n_{spectra}$=25)	-	8%	**83%**	6%	3%
	Diestrus ($n_{spectra}$=23)	2%	2%	7%	**80%**	9%
	Di to Pro ($n_{spectra}$=23)	13%	4%	5%	11%	**67%**

Table 8.1. SMLR output for cycling study. Di to pro are measurements taken between diestrus and proestrus phases. The numbers in bold represent the percentage of spectra that classified correctly.

8.4.2 Pregnancy Study

After characterizing the NG cervix using RS, Raman spectra were acquired from multiple time points during pregnancy (day 1, 4, 12, 15, 18, 19, and PP1, Figure 8.2, $n_{spectra}$=317). For some mice, acquiring spectra before mating or on day 1 (after the presence of the copulatory plug) led to miscarriage (discussed below). Accordingly, measurements were acquired starting on day 4 of the gestational period. Within these spectra, there are many regions that appear different across the entire range of 990-1800 cm^{-1}. Differences are most visible in the spectra between NG and day 19 mice.

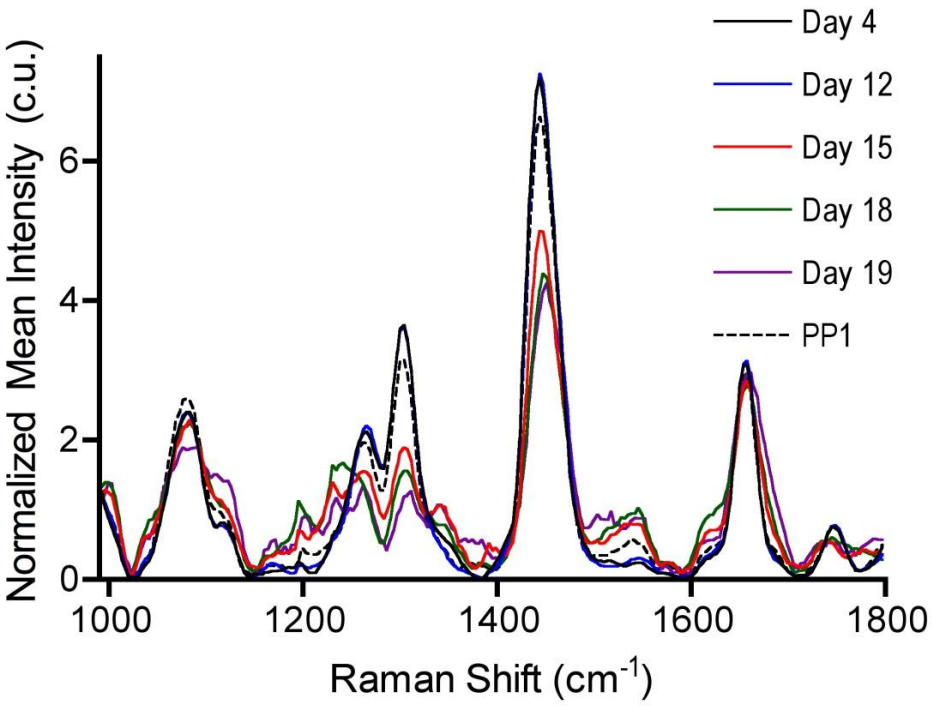

Figure 8.2. Normalized average spectra from the cervix of pregnant mice at 5 time points during their pregnancy and at 1 time point 24 hours after delivery (PP1).

Figure 8.3 shows changes in peak intensity (a-c) and peak width (d) as a function of pregnancy in four important peaks. It has been demonstrated previously that some of these regions correspond to certain biochemical structures, such as amino acids like proline and

tyrosine (Figure 8.3a, 1200 cm^{-1}),[32-34] CH_2 and lipids (Figure 8.3b, 1308 cm^{-1}),[31] and the CH_3CH_2 bending modes found in protein side chains of multiple tissue types (Figure 8.3c, 1450 cm^{-1}).[31, 33] Figure 8.3d shows the full width at half max (FWHM, ± S.E.) of the 1650 cm^{-1} peak, which has tentatively been assigned to amide-I and collagen.[34] For this region, the FWHM, as opposed to peak intensity, is a more accurate indicator of the organization and polarization of the amide-I bonds in the tissue. Performing SMLR on spectra across 6 time points: NG, early (days 1, 4 and 12), day 15, day 18, day 19 and PP1, resulted in a classification accuracy of over 94% (Table 8.2). Combining the early time points (d1, d4, d12) led to an increase in classification accuracy. Non-gravid data was used from the cycling study and day 1 data was used from any mouse that maintained its pregnancy after a day 1 measurement.

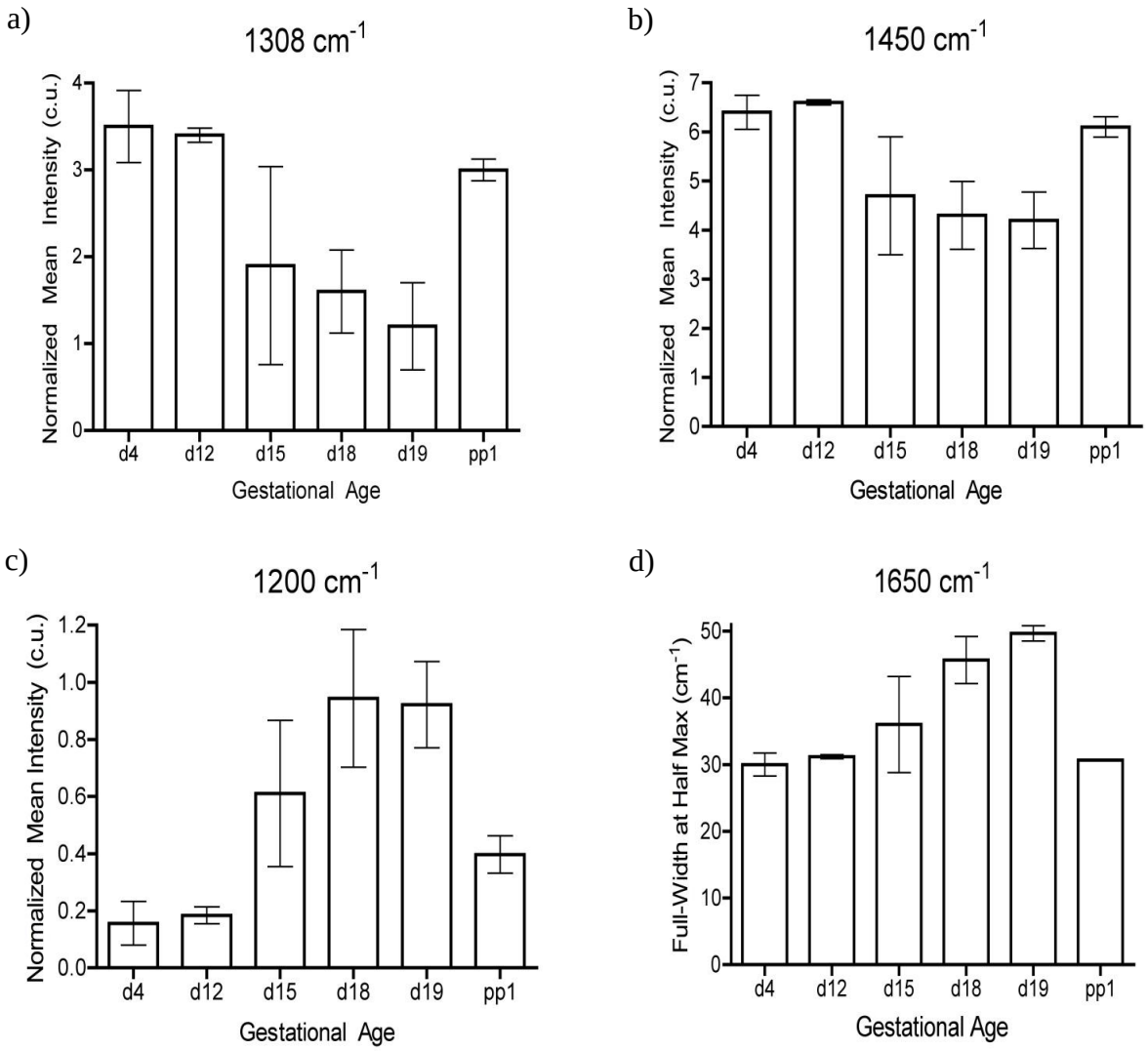

Figure 8.3. Bar graphs of specific peak intensities from Raman spectra that change over the course of pregnancy. These Raman shift peaks are potentially correlated to fatty acids and lipids (a), protein side chains (b), and amino acids (c). Bar graph of full-width at half-max shows the change of the amide-I band, which is consistent with the presence of collagen (d).

Classification Accuracy = 94%		Raman Classification from SMLR Output					
		NG	Early	d15	d18	d19	PP1
Pregnancy Time Point	NG	**99%**	1%	-	-	-	-
	Early	2%	**97%**	1%	-	-	-
	d15	-	9%	**84%**	3%	-	4%
	d18	-	-	2%	**92%**	6%	-
	d19	-	-	-	3%	**96%**	1%
	PP1	2%	3%	-	-	-	**95%**

Table 8.2. SMLR output results of pregnancy and postpartum study. The numbers in bold represent the percentage of spectra that classified correctly.

8.4.3 Stress-Strain Testing

Stress-strain testing was performed to examine the physical properties of the cervix as it changes during pregnancy. The two plots in Figure 8.4 demonstrate how the structural properties of the cervix change over the course of pregnancy and 24 hours after delivery. In Figure 8.4a, force is plotted as a function of displacement or cervical diameter, showing how samples react and resist to a specific amount of elongation. Figure 8.4a is equivalent to a stress-strain curve. For this study, cervical stiffness (g/mm), or the amount of tension (g) divided by the maximum displacement (mm) is plotted for samples at each time point (Figure 8.4b), similar to previous studies.[7] This plot corresponds to the slope of the linear portion of the Figure 8.4a or the inverse of the compliance of the cervix. Any result with a p-value less than 0.1 was defined as being statistically significant. Results from day 19 are statistically significant compared to NG, day 1, day 4 and PP1. Cervical stiffness results from both NG and PP1 mice are also significantly different ($p < 0.1$) than days 15, 18 and 19.

A

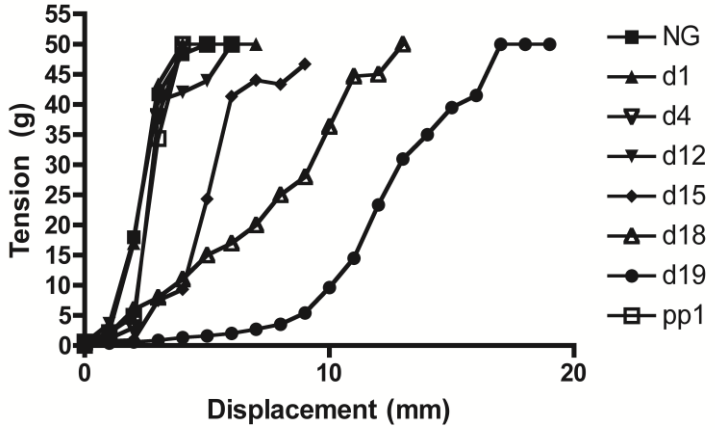

B

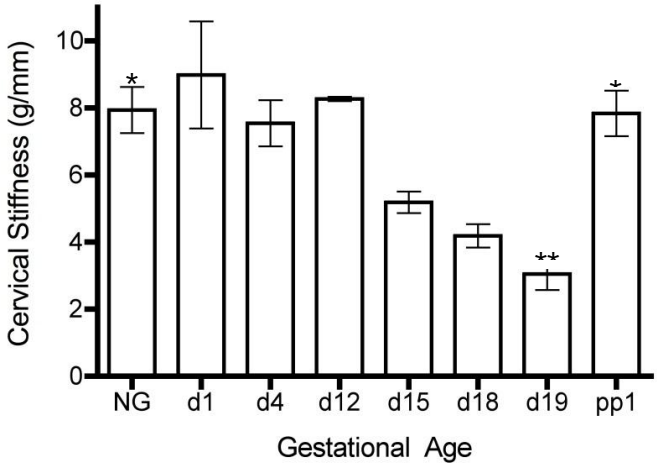

Figure 8.4. Measurements from biomechanical testing of cervical tissue. A) Tension as a function of time, displaying that the cervix can withstand increased displacement as pregnancy progresses. B) Cervical stiffness, measured from the slope of the graph in (a) showing that the cervix becomes less stiff during pregnancy and quickly regains its strength 24 hours after delivery. Day 19 is significantly different than NG, d1 and PP1. NP and PP1 are significantly different than d15, d18 and d19. * corresponds to $p < 0.1$, ** corresponds to $p < 0.05$

8.4.4 Histological Staining

Trichrome staining of samples from multiple time points (NG, d4-19, and PP1) during mouse pregnancy is shown in Figure 8.5. Before, at the start of and after pregnancy, a dense collagen network, stained blue, is the most prominent tissue component (d4, white arrow).

Smooth muscle cells, stained red, also appear to form tight bundles within the collagen and along the edges of the uterus and cervix. As pregnancy progresses, the dense collagen network becomes disorganized, especially on day 19 (d19, black arrow). While the cervix is not completely recovered by PP1, the blue-stained regions in PP1 are thicker compared to d19, signifying a reorganization of collagen within 24 hours of delivery.

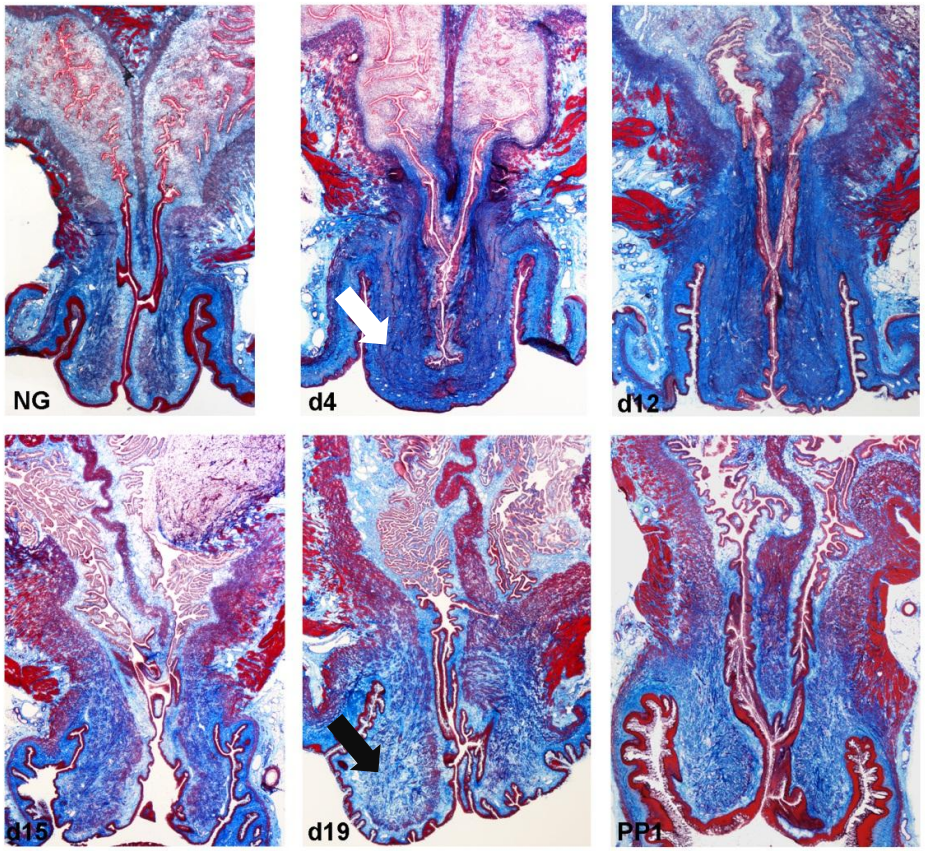

Figure 8.5. Trichrome staining images acquired at 20x from NG, d4, d12, d15, d19 and PP1 cervical tissue samples. Note the densely packed collagen structures (blue) from d4 (white arrow) compared to the disorganized areas in d19 (black arrow). Samples 24 h after delivery (PP1 resemble early time points**.**

8.5 Discussion

The goal of this research is to demonstrate the feasibility of using Raman spectroscopy to detect changes in the cervix during normal pregnancy. Before studying pregnancy, cervical changes associated with estrous cycling of NG mice were studied using RS to create a baseline

for comparison. Next, Raman spectra were acquired from the cervix of pregnant mice prior to structural testing and histological staining to study cervical changes during pregnancy using three sets of data. We found that biochemical changes correlate with the compliance of the cervical tissue and the histological results that were observed in the Raman spectra of late-stage pregnancy mice. These results will provide researchers with a better understanding of the biochemical function of the cervix during pregnancy and the mechanisms regulating pregnancy, labor and delivery.

The cycling data was obtained to determine if ovarian steroid hormonal changes during the estrous cycle would have an effect on NG data. Our prior human studies showed that the cervical changes during the menstrual cycle could be identified within Raman spectra, making it necessary to study the hormonal fluctuations of the NG cervix of mice using RS prior to comparison to a gravid cervix.[23, 24] Furthermore, prior to this study, our lab had not used RS on the cervix of mice. If the steroid hormonal effect of the cycling time point had an effect on the spectra, then multiple NG categories would need to be considered when comparing NG spectra to spectra obtained from pregnant mice. However, unlike the human data, which classified with an accuracy of over 98% based only on cycling time point,[23] the mouse cycling data classified with an accuracy of only 77% (Table 8.1), suggesting that there are few distinctions in Raman spectra from the mouse cervix due to cycling time point alone. The difference in classification accuracies between mice and humans may be due to the smaller variations that exist in the shorter 4-day mouse cycle compared to an approximately 28-day human cycle. In the human study, only two phases were considered, the proliferative and secretory phases, as opposed to the four distinct phases studied in the mouse. From these results, it was concluded that a single

category combining all the spectra acquired from NG mice could be used in the analysis that followed.

The measurements acquired during pregnancy demonstrate that many changes in the cervix can be observed in the Raman spectra (Figure 8.2). As pregnancy progresses, there is a sharp loss of spectral integrity seen by the lack of distinct peaks and valleys that is most prominent on day 19, resulting from the increasing amount of elasticity, collagen reorganization and dilation. Measurements taken on day 19 were acquired 6-12 hours prior to delivery and represent the maximum change of the cervix during pregnancy. Taken within 24 hours after delivery, the postpartum spectra (PP1) appear similar to spectra acquired from NG mice and mice early in pregnancy.

Changes in the Raman spectra associated with the changes over the course of pregnancy are observed in the four plots in Figure 8.3. Figure 8.3a-b show specific peaks decreasing in intensity as a function of gestational age. These peaks may potentially correlate to carbon bonds and lipids, as discussed previously.[31] It follows that as pregnancy continues, a decrease in the concentration of many cervical components occurs. While many of the peak intensities decrease as pregnancy continues, there are some that increase, such as the 1200 cm^{-1} peak (Figure 8.3c), which has been shown to correlate to proline, tyrosine, and amino acids.[32, 34] Amino acids play an important role in many hormonal and enzymatic pathways, and therefore may increase as labor and delivery approach.[35] The FWHM of the 1650 cm^{-1} amide-I peak provides information about the collagen content, organization and polarization (Figure 8.3d). The widening of the band may indicate an increasingly dispersed distribution of peptide carbonyl stretching during the course of pregnancy, signifying a change in the orientation of collagen fibers.[36] Many studies

have demonstrated that the total amount of collagen does not necessarily decrease during pregnancy; instead, its reorganization contributes to cervical ripening.[6, 7]

A classification accuracy of over 94% was found when SMLR was used to classify the spectra from multiple time points during pregnancy (Table 8.2), showing that the biochemical components changing during pregnancy are substantial and distinctive differences at specific gestational ages can be utilized to classify the spectra. Spectra acquired from mice at day 15 of their pregnancy had the lowest classification rate (85%). Day 15 of pregnancy marks the start of rapid changes to the cervix.[7] Although Raman measurements for each day were taken at the same time, some mice may have started the cervical ripening process before others, effectively introducing a higher amount of variation in day 15 measurements compared to other time points. Although the goal of this study is not to classify spectra based on gestational age, these results verify that the changes occurring in the Raman spectra during pregnancy can be teased out using SMLR.

The stress-strain testing verified that the cervix is able to withstand a larger displacement (Figure 8.4a) while becoming softer (Figure 8.4b) throughout pregnancy. The steep slope found in measurements taken at early time points and post-partum (Figure 8.4a) indicates an increased resistance to stretch. Many of the changes seen in the Raman data acquired during pregnancy (Figure 8.3a-b) correspond with the changes seen with the stress-strain testing (Figure 8.4). The intensities of the two Raman peaks displayed in Figure 8.3a-b correspond to fatty acids, lipids and protein side chains. These constituents play an important role in maintaining the cervix's rigidity[4, 5, 7] and the decrease in their concentration corresponds to an increase in compliance as the cervix prepares for birth. The similarities between important Raman peaks and these tests

show that RS is correctly identifying many of the important biochemical components responsible for the changes in the stiffness of the cervix.

The histological analysis shows how the collagen organization changes over the course of pregnancy. The results of the Masson's trichrome staining (Figure 8.5) provide one explanation for the changes observed in the Raman spectra and force-displacement results and are similar to previous studies that used histology to understand collagen organization in the cervix during pregnancy.[40-42] As pregnancy continues, the concentration of collagen appears to remain consistent, while its organization is altered. These results correspond to the loss of spectral integrity in the Raman measurements on days 18 and 19 (Figure 8.2). The FWHM plot of the amide-I peak from the Raman spectra (Figure 8.3d) also matches the results from the staining. Although there is no change in the intensity of the 1650 cm^{-1} peak (corresponding to the total amount of collagen), there are differences due to protein orientation, polarization and solubility. Collagen reorganization and increased solubility are two factors that result in increased elasticity of the cervix as it prepares for labor and delivery,[5, 7] an outcome which has been verified in all experiments. The parallels among the Raman measurements, the structural properties, and the histological staining indicate that RS is a quantifiable method for assessing the structural properties and cellular components of the cervix during pregnancy without excising tissue.

There were some drawbacks in this current study design that can be overcome in future studies. First, vaginal cytology was used to quickly determine the cycling point. While the results of the cycling and pregnancy studies suggest that the changes in a NG cervix are less noticeable than the changes resulting from pregnancy, it may be beneficial for future cycling studies to use serum testing to ensure that the correct cycling point is reported. Furthermore, the mouse is not the ideal model for studying estrous cycling since the phases can be shorter or longer than 24h,

as some studies have suggested.[43] Acquiring Raman data from other rodents, such as the guinea pig, may provide more accurate results.[44] Repeated *in vivo* Raman measurements of the NG cervix sometimes led to pseudopregnancy; such measurements were excluded in further analyses. Also, in the initial experimental design, data were acquired before mating and on the first day of gestation. However, taking Raman measurements at these time points sometimes resulted in the loss of the pregnancy about day 12. It was determined that starting on gestational age day 4 led to full term pregnancies without complications. Future studies may consider decreasing the size of the fiber optic probe to prevent pseudopregnancies and miscarriages.

Throughout pregnancy, the epithelium of the cervix becomes thicker. The probe used to obtain these measurements contains forward-looking optics which takes volumetric measurements approximately 1 mm in depth. For this *in vivo* study, the placement of the probe onto the mouse cervix is not known, however, each measurement is an average of at least 3 different measurements where the probe was completely removed from the cervix and vaginal canal and then replaced. Few regional variations in the spectra were found in the measurements obtained consecutively from the cervix, suggesting that data can be taken reliably without having to control from site-specificity, matching previous human studies in our lab.[45] Since this method is meant to be performed without surgery or removing tissues, knowing the placement of the probe is not essential in this initial study. Future studies will consider the effect of the thickening of the epithelium and the placement of the probe on the data.

The results from this study demonstrate that RS can be a useful tool to non-invasively and accurately study biochemical changes in the cervix during pregnancy. The impact of these results provides a new avenue for obstetrics research that does not rely on removing tissue and is not focused on one molecule. Instead, RS can be used to identify cervical changes resulting from

the interactions of multiple biomolecules, hormonal agents, feedback loops, etc., thereby providing researchers with new ways to understand the progression of pregnancy. The next steps are to use RS to study what occurs during labor and normal human pregnancy. The long-term goal of this research is not only to use RS to understand how pregnancy affects the human cervix, but to develop a method for determining patients at risk for preterm labor and delivery. Preterm birth, defined as labor prior to 37 weeks, is a serious medical complication, affecting over 1 in 8 pregnancies in the US and 75% of infants that have perinatal death are born premature.[46] Even with current advances in health care and research, there are limited diagnostics in place for predicting preterm birth.[46] Developing an effective and non-invasive method that identifies women who are at risk for preterm birth would have a tremendous impact on the medical community, enabling providers to identify patients at risk for preterm labor, thereby improving the management of these patients.

8.6 Acknowledgements

The authors acknowledge the financial support of the National Institutes of Health (Grant No. R01-CA-095405, AMJ and HD 044741, BCP) and a predoctoral fellowship (Grant No. T32-HL7751-15) for EV. Special thanks go to Stan Poole and Wais Folad for their help with the mechanical testing experiments, Xiahong Bi for conversations about Raman peak assignments and Amy Rudin for proofreading this paper.

8.7 References

1. Nathanielsz, P.W. Life before birth: the challenges of fetal development. (W. H. Freeman & Co, New York, 1996).
2. Kamel, R.M. "The onset of human parturition." *Arch Gynecol Obstet* **281**, 975-82 (2010).

3. Challis, J.R.G., Matthews, S.G., Gibb, W. and Lye, S.J. "Endocrine and paracrine regulation of birth at term and preterm." *Endocr Rev* **21**, 514-50 (2000).

4. Leppert, P.C. "Anatomy and physiology of cervical ripening." *Clin Obstet Gynecol* **38**, 267 (1995).

5. House, M., Kaplan, D.L. and Socrate, S. "Relationships between mechanical properties and extracellular matrix constituents of the cervical stroma during pregnancy." *Semin Perinatol* **33**, 300-7 (2009).

6. Yu, S.Y., Tozzi, C.A., Babiarz, J. and Leppert, P.C. "Collagen changes in rat cervix in pregnancy--polarized light microscopic and electron microscopic studies." *Exp Biol M* **209**, 360 (1995).

7. Read, C.P., Word, R., Ruscheinsky, M.A., Timmons, B.C. and Mahendroo, M.S. "Cervical remodeling during pregnancy and parturition: molecular characterization of the softening phase in mice." *Reproduction* **134**, 327 (2007).

8. Sugano, T., Narahara, H., Nasu, K., Arima, K., Fujisawa, K., Miyakawa, I. "Effects of platelet-activating factor on cytokine production by human uterine cervical fibroblasts." *Mol Hum Reprod* **7**, 475 (2001).

9. Ji, H., Dailey, T.L., Long, V. and Chien, E.K. "Prostaglandin E2-regulated cervical ripening: analysis of proteoglycan expression in the rat cervix." *Am J Obstet Gynecol* **198**, 536 e1-7 (2008).

10. Junqueira, L.C., Zugaib, M., Montes, G. S., Toledo, O. M., Krisztan, R. M., Shigihara, K. M. "Morphologic and histochemical evidence for the occurrence of collagenolysis and for the role of neutrophilic polymorphonuclear leukocytes during cervical dilation." *Am J Obstet Gynecol* **138**, 273-81 (1980).

11. Sennström, M.K.B., Brauner, A., Lu, Y., Granström, L.M.M., Malmström, A.L., Ekman, G.E. "Interleukin-8 is a mediator of the final cervical ripening in humans." *Eur J Obstet Gyn R B* **74**, 89-92 (1997).

12. Hellemans, P., Gerris, J. and Verdonk, P. "Fetal fibronectin detection for prediction of preterm birth in low risk women." *Brit J Obstet Gynaec* **102**, 207-212 (1995).

13. Polettini, J., Peraçoli, J., Candeias, J., Araújo Júnior, J. and Silva, M. "Inflammatory cytokine mRNA detection by real time PCR in chorioamniotic membranes from pregnant women with preterm premature rupture of membranes." *Eur J Obstet Gyn R B* **144**, 27-31 (2009).

14. Erez, O., Gotsch, F., Mazaki-Tovi, S., Vaisbuch, E., Kusanovic, J.P., Kim, C.J., Chaiworapongsa, T., Hoppensteadt, D., Fareed, J., Than, N.G. "Evidence of maternal platelet activation, excessive thrombin generation, and high amniotic fluid tissue factor immunoreactivity and functional activity in patients with fetal death." *J Matern-Fetal Neo M* **22**, 672-687 (2009).

15. Garfield, R.E., Maul, H., Maner, W., Fittkow, C., Olson, G., Shi, L., and Saade, G.R. "Uterine electromyography and light-induced fluorescence in the management of term and preterm labor." *J Soc Gynecol Investig* **9**, 265-75 (2002).

16. Kuon, R.J., Shi, S. Q., Maul, H., Sohn, C., Balducci, J., Shi, L., and Garfield, R.E. "A novel optical method to assess cervical changes during pregnancy and use to evaluate the effects of progestins on term and preterm labor." *Am J Obstet Gynecol* **205**, 82.e15-82.e20 (2011).

17. Jokhi, R., Brown, B. and Anumba, D. "The role of cervical Electrical Impedance Spectroscopy in the prediction of the course and outcome of induced labour." *BMC Preg Child* **9**, 40 (2009).

18. Akins, M.L., Luby-Phelps, K. and Mahendroo, M. "Second harmonic generation imaging as a potential tool for staging pregnancy and predicting preterm birth." *J Biomed Opt* **15**, 026020 (2010).

19. Sultana, R.R., Zafarullah, S.N. and Kirubamani, N.H. "Saliva signature of normal pregnant women in each trimester as analyzed by FTIR spectroscopy." *Indian J Sci Technol* **4**, (2011).

20. Suzuki, T., Mori, C., Yoshikawa, H., Miyazaki, Y., Kansaku, N., Tanaka, K., Morita, H. and Takizawa, T. "Changes in nitric oxide production levels and expression of nitric oxide synthase isoforms in the rat uterus during pregnancy." *Biosci Biotech Bioch* **73**, 2163-2166 (2009).

21. Lim, K.-H., Salahuddin, S., Qiu, L., Fang, H., Vitkin, E., Ghiran, I.C., Modell, M.D., Takoudes, T., Itzkan, I., Hanlon, E.B., Sachs, B.P. and Perelman, L.T. "Light-scattering spectroscopy differentiates fetal from adult nucleated red blood cells: may lead to noninvasive prenatal diagnosis." *Opt Lett* **34**, 1483 (2009).

22. Vargis, E., Kanter, E. M., Majumder, S. K., Keller, M. D., Beaven, R. B., Rao, G. G., and Mahadevan-Jansen, A. "Effect of normal variations on disease classification of Raman spectra from cervical tissue." *Analyst* **139,** 2981-2987 (2011).

23. Kanter, E.M., Majumder, S., Kanter, G.J., Woeste, E.M. and Mahadevan-Jansen, A. "Effect of hormonal variation on Raman spectra for cervical disease detection." *Am J Obstet Gynecol* **200**, 512 e1-5 (2009).

24. Kanter, E.M., Vargis, E., Majumder, S., Keller, M. D., Woeste, E., Rao, G. G., and Mahadevan-Jansen, A. "Application of Raman spectroscopy for cervical dysplasia diagnosis." *J Biophotonics* **2**, 81-90 (2009).

25. Vargis, E., Byrd, T., Logan, Q., Khabele, D. and Mahadevan-Jansen, A. "Sensitivity of Raman spectroscopy to normal patient variability." *J Biomed Opt* **16**, 117004-1-9 (2011).

26. Akins, M.L., Luby-Phelps, K., Bank, R.A. and Mahendroo, M. "Cervical softening during pregnancy-regulated changes in collagen cross-linking and composition of matricellular proteins in the mouse." *Biol Reprod* **84**, 1053-62 (2011).

27. Basar, G., Parlatan, U. and Seniak, S. "Investigation Of Preeclampsia By Raman Spectroscopy." *Proc SPIE* **1267**, 378 (2010).

28. Deb, K., Reese, J. and Paria, B.C. "Methodologies to study implantation in mice." *Meth Mol Med* **121**, 9-34 (2005).

29. Lieber, C.A. and Mahadevan-Jansen, A. "Automated method for subtraction of fluorescence from biological Raman spectra." *Appl Spectrosc* **57**, 1363-7 (2003).

30. Harkness, M.L. and Harkness, R.D. "Changes in the physical properties of the uterine cervix of the rat during pregnancy." *J Physiol* **148**, 524-47 (1959).

31. Krishnapuram, B., Carin, L., Figueiredo, M.A. and Hartemink, A.J. "Sparse multinomial logistic regression: fast algorithms and generalization bounds." *IEEE Trans Pattern Anal Mach Intell* **27**, 957-68 (2005).

32. Frank, C.J., McCreery, R.L. and Redd, D.C.B. "Raman spectroscopy of normal and diseased human breast tissues." *Anal Chem* **67**, 777-783 (1995).

33. Arp, Z., Autrey, D., Laane, J., Overman, S.A. and Thomas Jr, G.J. "Tyrosine Raman signatures of the filamentous virus Ff are diagnostic of non-hydrogen-bonded phenoxyls: Demonstration by Raman and infrared spectroscopy of p-cresol vapor." *Biochemistry* **40**, 2522-2529 (2001).

34. McColl, I.H., Blanch, E.W., Hecht, L., Kallenbach, N.R. and Barron, L.D. "Vibrational Raman Optical Activity Characterization of Poly(l-proline) II Helix in Alanine Oligopeptides." *J Am Chem Soc* **126**, 5076-5077 (2004).

35. Miura, T. and Thomas Jr, G. "Raman spectroscopy of proteins and their assemblies." *Sub-Cell Biochem* **24**, 55 (1995).

36. Palejwala S. Stein, D.E.W., G., Monia, B.P.,Tortoriello D., and Goldsmith L.T. "Relaxin positively regulates matrix metalloproteinase expression in human lower uterine segment fibroblasts using a tyrosine kinase signaling pathway." *Endocrinology* **142**, 3405-3413 (2001).

37. Wang, Y.N., Galiotis, C. and Bader, D. "Determination of molecular changes in soft tissues under strain using laser Raman microscopy." *J Biomech* **33**, 483-486 (2000).

38. Reinwald, S., Li, Y., Moriguchi, T., Salem, N. and Watkins, B.A. "Repletion with (n-3) Fatty Acids Reverses Bone Structural Deficits in (n-3)-Deficient Rats." *J Nutr* **134**, 388-394 (2004).

39. Puskas, J.E. and Chen, Y. "Biomedical application of commercial polymers and novel polyisobutylene-based thermoplastic elastomers for soft tissue replacement." *Biomacromolecules* **5**, 1141-1154 (2004).

40. Fosang, A.J., Handley, C., Santer, V., Lowther, D. and Thorburn, G. "Pregnancy-related changes in the connective tissue of the ovine cervix." *Biol Reprod* **30**, 1223 (1984).

41. Zhao, L., Samuel, C.S., Tregear, G.W., Beck, F. and Wintour, E.M. "Collagen studies in late pregnant relaxin null mice." *Biol Reprod* **63**, 697-703 (2000).

42. Zhao, L., Roche, P.J., Gunnersen, J.M., Hammond, V.E., Tregear, G.W.,Wintour, E.M., Beck, F. "Mice without a functional relaxin gene are unable to deliver milk to their pups." *Endocrinology* **140**, 445 (1999).

43. Nelson, J., Felicio, L., Randall, P., Sims, C. and Finch, C. "A longitudinal study of estrous cyclicity in aging C57BL/6J mice: I. Cycle frequency, length and vaginal cytology." *Biol Reprod* **27**, 327-339 (1982).

44. Croix, D. and Franchimont, P. "Changes in the serum levels of the gonadotrophins progesterone and estradiol during the estrous cycle of the guinea pig." *Neuroendocrinology* **19**, 1-11 (1975).

45. Robichaux-Viehoever, A., Kanter, E., Shappell, H., Billheimer, D., Jones III, H. and Mahadevan-Jansen, A. "Characterization of Raman Spectra Measured *in vivo* for the Detection of Cervical Dysplasia." *Appl Spectrosc* **61**, 986-993 (2007).

46. Behrman, R.E. and Butler, A.S. Committee on Understanding Premature Birth and Assuring Healthy Outcomes: Preterm birth: causes, consequences, and prevention. (National Institue of Medicine, Bethesda, 2007).

CHAPTER 9

SUMMARY AND CONCLUDING REMARKS

9.1 Summary and Integration

This dissertation focused on the continued development using Raman spectroscopy (RS) to detect changes in the uterine cervix. The first part of this work carried on the research using RS to detect cervical dysplasia but in a more diverse population and with the consideration of the role of HPV infection. The second part of this work used concepts and techniques developed from the cervical dysplasia project to monitor the changes in the cervix due to pregnancy. Demonstrating the success of RS to detect cervical dysplasia in diverse populations brings this method one step closer to being utilized in lower-resource settings. This research has also shown for the first time that RS can be used to monitor the changes in the cervix during pregnancy, potentially leading to a method that can alert health care providers to patients at risk for preterm labor or other complications during pregnancy, labor or delivery.

The preliminary studies in Chapters 2-3 laid the background and foundation for the work that followed within this dissertation. These studies looked at normal and malignant cervical tissue, both *in vivo* and as excised tissue. Understanding contributions to the Raman spectra was also pursued by acquiring data from mimicked cervical tissue (raft cultures) containing stromal and epithelial layers of cultured cells.[1] In the first set of *in vivo* studies, the Raman spectra classified with an accuracy of 88% across 4 disease categories (normal, inflammation, low-grade and high-grade dysplasia).[2] It was then determined that when hormonal status (specifically menstrual cycle and menopausal state) was accounted for, the classification of diseased tissues

increased to over 94%.[3-5] While these results were promising, they were all performed at Vanderbilt University and a private medical practice in northern Kentucky. Accordingly, the majority of the patients recruited to the previous studies was Caucasian and had health insurance.

The first step of this PhD dissertation, therefore, was to verify the results of the previous study in a more varied patient population. In the course of doing so, it became apparent that a study of the sensitivity of RS to patient variables was also necessary in order to translate this method to a clinical setting. Further, it became clear that if RS is sensitive to subtle changes in the cervix due to previous disease, for example, it would also be able to detect the changes that occur in the cervix during pregnancy. This is the first report, to our knowledge, using RS to study the biochemical changes that occur in the cervix of pregnant mice and humans.

As discussed above, previous studies examining the sensitivity of RS first looked at the effect of normal hormonal variations due to menstrual cycle and menopausal state.[5] The next step, described in Chapter 4, looked at the permanent and localized effects of disease. To observe their impact, data were acquired from normal cervical areas from patients who had no cervical disease (currently or in the past) and from patients who currently presented with cervical malignancies. After the Raman spectra were processed, combined MRDF-SMLR was used to classify the data. In this study, it was found that accounting for previous disease increased the classification accuracy to 97%. Previous studies that did not separate true normal, currently normal, and adjacent-to-disease normal tissue resulted in classification accuracies at a maximum of 94%. This study was conducted at the same private practice in northern Kentucky, with a largely Caucasian population who had health insurance. At this point within the cervical dysplasia project, it was determined that hormonal status, previous disease and proximity to

disease are important variables that must be accounted for in order to maximize the disease classification accuracy of RS.

The next two chapters, 5 and 6, deal with normal patient variables that may have an effect on both the normal cervix as well as the classification of disease. For this part of the research, the cervical dysplasia study was conducted at the Nashville General Hospital at Meharry Medical College, which is a county hospital in middle Tennessee serving a more diverse population. Four common patient variables that were considered for these studies were body mass index (BMI), previous pregnancies (parity), race/ethnicity and health insurance status. These four variables can be readily found while obtaining a patient's history. The sensitivity of other optical methods, like fluorescence spectroscopy, to patient variables has been previously tested. Such techniques, however, are not affected by these types of variables.[6, 7] BMI may correlate with the level of hormones circulating through the body. A previous pregnancy may have a permanent impact on the cervix. Race/ethnicity may have an effect on the baseline makeup of the cervix and needed to be studied since there is an increase rate of cervical cancer incidence in black and Hispanic women compared to white and Asian.[8] Having health insurance is one indicator of socioeconomic status and may be correlated with diet, exercise and other lifestyle factors. These four variables were used for the following studies due to their potential impact on the physiology of the cervix and to compare Raman to other optical techniques.[9]

In Chapter 5, normal patients were studied to determine the importance and the role of the four variables. In this study, Raman spectra were acquired from 75 premenopausal women with no history of cervical disease.[5, 10] Next, SMLR was used to classify the data by these four variables alone, i.e. would the data be classified into two categories based on whether or not the patient was pregnant previously? If the variable had no effect on the data, a classification

accuracy rate of close to 50% would have been found. For the variables race/ethnicity (white, black, Hispanic) and health insurance status, the spectra classified with accuracies of 58% and 61% respectively. For BMI (normal, overweight and obese) and parity, the spectra classified at 78% and 75% respectively. These results suggest that race/ethnicity and health insurance status are factors that do not affect Raman spectra acquired from the cervix. Incorporating BMI and obstetric history into algorithms prior to classification may increase the sensitivity and specificity rates of the results. At this study's completion, we concluded that hormonal status, previous disease, BMI and obstetric history were all important factors that should be included in any algorithm using RS to detect cervical dysplasia.

In Chapter 6, previous results were combined to assess the effect of each variable on classifying disease spectra. Patients coming to Nashville General Hospital for a colposcopy-directed biopsy, after an abnormal Pap test, were recruited to this study, regardless of menopausal status, previous disease, BMI, etc. Iterations of SMLR were then performed to determine which combination of variables resulted in the highest classification accuracy. Results showed that combining menopausal status, obstetric history and BMI led to classification accuracies of over 99% across 4 different pathologies. Raman spectroscopy is therefore sensitive to these patient variables, and it does not seem necessary to include other variables such as menstrual cycle, race/ethnicity or health insurance status to achieve maximal classification.

More recently, the pivotal role of high-risk HPV infection in the initiation and progression of cervical cancer has been elucidated.[11] While HPV testing is now recommended to be performed in conjunction with routine cervical exams, not every facility runs the time-consuming and costly test. Therefore, to understand the impact of high-risk HPV infection on Raman spectra, four cell culture lines were grown and patient samples that were negative and

positive for HPV were obtained, summarized in Chapter 7. Two of the cell lines were positive for high-risk strains of HPV, one was malignant and HPV-negative, and one was a benign cell line. Raman microspectroscopy was used to acquire data from these small samples. SMLR was then used to classify the data, leading to accuracies of 89-97% for the cell culture samples, depending on how the spectra were combined, and 98.5% for the patient samples. Therefore, HPV is another factor that has a significant impact on Raman spectra and the results of this study show that Raman microspectroscopy can be used to detect the presence of high-risk HPV.

The results from studying these variables in cervical dysplasia and their effect on Raman data show that RS is a highly sensitive technique. The changes that occur in the cervix during pregnancy are significant and many times greater than those that are associated with cervical disease. Using RS to study the cervix of pregnant patients may lead to a method of detecting preterm labor and other complications associated with labor by understanding the biochemical changes that occur within the tissue.

The World Health Organization estimates that 1000 women per day die from complications related to pregnancy and childbirth.[12] Even with an increase in research in the last 20 years, over half of all patients who experience problems during pregnancy are never suspected to be at risk for such difficulties. During pregnancy, the changes that occur in the cervix become more obvious as the body prepares for labor and delivery. However, there may be biochemical changes at the cellular level potentially indicative of problems associated with pregnancy that cannot be easily detected.. These subtle changes may be observed using RS. To assess if RS can diagnose at-risk pregnant women, the first step is to obtain and analyze data from normal pregnancies in mice and women.

Chapter 8 describes the Raman data acquired from mice during their 19-day gestational period (*in vivo* and *ex vivo*) and its correlation to mechanical testing and Masson's trichrome staining (collagen, smooth muscle). Various peaks of the Raman spectra, such as the areas corresponding to fatty acid content and collagen organization changed significantly as the cervix became softer and more elastic in preparation for labor and delivery. These results correspond to the increased amount of stretch with an increased amount of strain found with the mechanical testing, as well as the collagen disorganization visualized with the histological staining. These findings suggest that non-invasive RS can be used to study the cervical changes during pregnancy, labor and delivery in mice.

In the appendix that follows, the results from a pilot human pregnancy study are reported. Patients were recruited to this study during their 1^{st} trimester and six measurements were obtained throughout the pregnancy, one from the 1^{st} trimester, 1 from the 2^{nd}, 3 from the 3^{rd} and 1 post-partum from a total of 41 patients. A smaller study was conducted on 5 patients where weekly measurements were obtained during their 3^{rd} trimester. The Raman data shows that biochemical changes occur in the cervix of these patients. Using SMLR to classify the data led to an accuracy of 87%, suggesting that significant changes are occurring throughout pregnancy and that these changes are significantly different between measurements. Further work must be pursued to see if RS can be developed as a tool for monitoring women during pregnancy.

There were a number of challenges that were overcome during the course of this PhD. Moving the cervical dysplasia study to Meharry Medical College, a hospital in a more urban environment, presented a new set of obstacles. Minority populations in a lower socioeconomic setting proved difficult to recruit to research studies. While only 2 patients out of 168 asked to

participate refused, they frequently did not show up for their appointments, making it difficult to consistently obtain measurements.

Even so, the majority of obstacles came from the clinic administration itself, which caused this study to last longer than the other cervical dysplasia studies. However, I found that by maintaining a routine twice-weekly schedule, befriending the clinical staff, and having at least one doctor who was committed to recruiting patients I was able to recruit a high number of patients.

Initially, the human pregnancy study (Appendix 1) began at Meharry Medical College where it proved difficult to retain patients in the study for the full 5 measurements during pregnancy and the 1 postpartum measurement. Because of this, a small grant was obtained from the Vanderbilt Institute for Clinical and Translational Research (VICTR) to provide up to $100 compensation for each patient participating in the study. About this same time, however, the care of pregnant patients at Meharry moved under the control of a midwife who was uncooperative and intentionally put up barriers between researchers and patients. Therefore, the study was moved to Vanderbilt's 100 Oaks site, where there were still some difficulties in recruiting and retaining patients. However, posting flyers throughout the clinic, mailing them to new patients, , and, as with the cervical dysplasia study, consistently checking the schedule for new patients were all vital to recruiting patients to the study. Working with our research nurse, Amy Rudin, was essential to accomplishing this study.

9.2 Major Conclusions

- Previous disease as well as the current presence of disease leaves a permanent effect on the cervix, altering the biochemical fingerprint of such tissues. Accounting for previous disease

and proximity to disease prior to spectral classification leads to higher classification accuracy when using RS to detect cervical dysplasia.

- Two patient variables, BMI and parity, which can both be easily obtained from the patient, were determined to be important variables to incorporate into classification algorithms in order to maximize disease classification accuracy.
- Almost 100% classification accuracy of diseased spectra can be obtained when menopausal status, obstetric history and BMI are considered before classifying Raman data. Menstrual cycle, race/ethnicity and health insurance status do not have as great an effect on Raman spectra and do not need to be incorporated in the classification algorithm.
- Raman spectroscopy may be more sensitive than other optical methods like fluorescence spectroscopy or optical coherence tomography (OCT), which is why normal variations have a significant effect on its spectra. While this may seem like a disadvantage, Raman's sensitivity is also the reason why it can be used to classify diseased areas of the cervix with a much higher success rate than similar optical methods.
- Raman spectra obtained from pregnant mice show consistent and extreme change during the 19-day gestational period, verified with standard tissue testing and staining for collagen. RS can be used as often as needed, *in vivo* to monitor the changes without affecting the pregnancy or sacrificing mice.
- The biochemical changes that occur in the cervix of women during pregnancy can also be monitored non-invasively using RS. A lot of information is within these spectra, however, at this time, it is not clear if these changes are consistent or if they can be used to indicate the onset of preterm labor or other complications associated with pregnancy.

9.3 Recommendations

The conclusions presented in this dissertation lead to many recommendations for current research goals and more long-term plans. Presently, there are a number of studies in both the cervical dysplasia and the pregnancy research that should be pursued. With the cervical dysplasia research, the immediate need is to acquire Raman data from patients and test the same patients for infection with high-risk strands of HPV. The results from such a study would provide a direct correlation between the *in vivo* data, the pathology report from a Pap test or a colposcopy-guided biopsy, and the results of the HPV test. Definitive conclusions on the effect of HPV infection on Raman spectra acquired directly from cervical tissue can then be made. Also, the analysis in this work used a woman's health insurance status as a loose measure of her socioeconomic status. Surveying patients for their education, eating habits, etc., may be a more accurate method of correlating the Raman data with a patient's true socioeconomic status.

The cervical dysplasia study should also be moved to lower-resource settings, so that the ability of RS to diagnose women in other environments can be tested. Such settings can include free clinics (e.g. the Shade Tree Family Clinic run by Vanderbilt University's Medical School) or rural clinics that are temporarily set up to provide isolated populations easier access to medical care. A goal for the future would be to take the RS system to Zambia or India to use RS as a tool for accomplishing real-time diagnosis of cervical cancer, or as a "see and treat" tool.

The results from the pregnancy study presented in this dissertation were only the beginning of this work and many avenues of further research can be pursued in the future. The most pressing need is to determine if RS can be used to detect changes that occur during labor and delivery. This could be accomplished by designing a study that acquires data during labor on day 19 in mice and over the course of labor and delivery in women. Correlating this data with

current standards of care, such as measurements of cervical length or ultrasound, would also demonstrate the feasibility of using RS for monitoring pregnancy and labor.

This dissertation only contained Raman data from normal mice and low-risk pregnant patients. Another step for the pregnancy study includes using models of preterm labor and at-risk patients. Injecting mice with lipopolysaccharide (LPS) to initiate preterm labor after infection or with mifepristone (RU486), an anti-progesterone that causes abortion, are two ways to mimic preterm birth using mice. Raman data acquired from mice that undergo preterm labor and delivery (between days 15-18) can then be compared to data obtained from mice who gave birth on day 19 to determine what changes are different between the 3 sets of mice. Similarly, the human *in vivo* study should be conducted on at-risk patients referred to the maternal-fetal medicine clinic. Data acquired from at-risk patients should then be compared to the data acquired from lower-risk patients, again to determine if the changes are similar or different between the two groups. Many of these at-risk patients are prescribed progesterone to prevent preterm labor. However, the mechanism that makes progesterone work and its effect on the cervix are unknown. Raman spectroscopy can be used to non-invasively observe the biochemical changes that occur in the cervix under progesterone therapy.

The more long-term goals of this research include designing a side-firing probe and a more portable Raman system. The current probe is front-facing and all the data collected *in vivo* has been obtained from the front surface of the cervix. A side-firing probe would be beneficial for detecting cervical dysplasia and indicators of preterm labor. There are a number of circumstances, such as when a woman gets older or as the cervix prepares for labor, that the cervical squamo-columnar junction (or transformation zone) recedes into the cervical os or the small opening of the cervix. This area contains a large amount of information, since it is the

junction between the squamous and columnar (glandular) epithelium. Samples from this area are currently obtained with a more invasive endocervical curettage (ECC) or a scraping of the inner cervix, which is never performed on pregnant patients. To obtain a complete analysis of the cervix, Raman data must also be obtained from inside the os, which may be achieved by the development of a side-firing probe that can be used to non-invasively acquire such information. Finally, beyond cervical dysplasia and preterm labor detection, RS could be used in the cervix for other purposes, such as fertility treatments. The results from the mouse work demonstrate that the differences among the 4 hormonal stages that non-pregnant mice experience can be detected with RS. It is possible that similar differences may be seen in women if more than 2 phases of the ovulation cycle were considered. Raman spectroscopy could be developed as a tool used by doctors or patients to detect ovulation or monitor a woman's ability to conceive. My PhD work has demonstrated that RS may be sensitive enough to detect the right time for implantation.

Ultimately, translating RS for detecting abnormal cervical changes to any setting will depend on the system's portability and ease of use. While the cart system is practical for clinical work, using it in lower resource settings may be cumbersome or unfeasible. Developing a Raman system that is smaller and more energy efficient, such as utilizing a cell phone to obtain Raman spectra may make the system's worldwide use a reality. The current design requires two people, one to place the probe on the patient and one to collect the data. Future plans should strive to allow the patient to make measurements by herself. Also, when designing a new system, efforts should be pursued to make the probe easy to sterilize and eliminate the need for obtaining data in a dark room.

9.4 Contributions to the Field and Societal Impact

Throughout the course of my PhD work, I have made many contributions to optical, cancer and obstetrics research areas. To my knowledge, I am the first person to use RS to examine the cervical changes in both mice (n_{mice}=19) and humans ($n_{patients}$=46) during pregnancy. This is an innovative use and a new application of RS as a tool to non-invasively monitor the changes in the cervix during pregnancy. Over 1 in 8 pregnancies results in a preterm birth, a rate that has risen by over 36% in the last 25 years.[13] Using RS as a method to prevent preterm labor has the potential to curtail this increasingly important challenge in health care. As outlined in Appendix 1, successfully implementing this technique would have a significant benefit for all pregnant patients and their health care providers.

Raman spectroscopy has been applied with moderate success to detect malignancies and other abnormal tissue sites; however, its translation to the medical field has not occurred. One reason for this may be Raman's sensitivity to factors that have not previously been accounted for. This dissertation provides the most detailed account of variables that may influence Raman spectra obtained from the cervix *in vivo*, leading to much higher and consistent classification accuracy rates. I was able to draw these conclusions from the data collected from over 175 patients at Nashville General Hospital and 40 patients at the private practice in Kentucky. By determining the factors that affect the data, the classification algorithms focused on the changes in the spectra that were most likely to correspond to disease. I suggest that other Raman researchers consider normal variations that may impact their data, which may result in higher success rates when using Raman.

To my knowledge, my work is also the first report that correlates structural properties of cervical tissue to Raman spectra. The only mechanical measurements that have been correlated

to Raman data have been obtained from bone, therefore these are the first soft tissue stretching measurements correlated to Raman spectra. Such measurements provide another approach for describing and understand the Raman data. The system and protocol for measuring the structural properties of tissue samples was developed and redesigned by me, with the guidance from members of Dr. Jeff Reese's lab. It is currently being used by other students to perform similar studies.

9.5 Protection of Research Subjects

As stated in the methods sections of the relevant chapters, all patient samples were collected after having been de-identified, with approval from the Vanderbilt Institutional Review Board (#100668). For clinical measurements, informed written consent was obtained by a participating doctor or nurse practitioner in a process approved by the Vanderbilt IRB (#010245 – cervical dysplasia; #100544 – human pregnancy) and the Meharry Medical College IRB. The mouse studies were performed with the approval of the Vanderbilt University Institutional Animal Care and Use Committee (Protocol M/10/051).

9.6 References

1. Viehoever, A.R., Anderson, D., Jansen, D. and Mahadevan-Jansen, A. "Organotypic raft cultures as an effective *in vitro* tool for understanding Raman spectral analysis of tissue." *Photochem Photobiol* **78**, 517-524 (2003).
2. Robichaux-Viehoever, A., Kanter E.M., Shappell H., Billheimer D., III Jones H., and Mahadevan-Jansen A. "Characterization of Raman spectra measured *in vivo* for the detection of cervical dysplasia." *Appl Spectrosc* **61**, 986-93 (2007).
3. Kanter, E.M., Majumder S., Vargis E., Robichaux-Viehoever A., Kanter G., Shappell H., III Jones H., and Mahadevan-Jansen A. "Multiclass discrimination of cervical precancers using Raman spectroscopy." *J Raman Spectrosc* **40** (2009).

4. Kanter E.M., Vargis E., Majumder S., Keller M.D., Beaven R.B., Rao G.G. and Mahadevan-Jansen A. "Application of Raman spectroscopy for Cervical Dysplasia Diagnosis." *J Biophotonics* **2**, 81-90 (2009).

5. Kanter, E.M., Majumder, S., Kanter, G.J., Woeste, E.M. and Mahadevan-Jansen, A. "Effect of hormonal variation on Raman spectra for cervical disease detection." *Am J Obstet Gynecol* **200**, 512-512 (2009).

6. Chang, S.K., Mirabal, Y. N., Atkinson, E. N., Cox, D., Malpica, A., Follen, M. and Richards-Kortum, R. "Combined reflectance and fluorescence spectroscopy for *in vivo* detection of cervical pre-cancer." *J Biomed Opt* **10** (2005).

7. Utzinger, U., Trujillo, E.V., Atkinson, E.N., Mitchell, M.F., Cantor, S.B., and Richards-Kortum, R. "Performance estimation of diagnostic tests for cervical precancer based on fluorescence spectroscopy: Effects of tissue type, sample size, population, and signal-to-noise ratio." *IEEE T Bio-med Eng* **46**, 1293-1303 (1999).

8. Jemal, A. Siegel, R., Xu, Jiaquan, and Ward, E. "Cancer statistics, 2009." *CA Cancer J Clin* **59**, 225-49 (2011).

9. Krantz, K.E. The Biology of the Cervix (The University of Chicago Press, Chicago, 1973).

10. Vargis, E., Kanter, E. M., Majumder, S. K., Keller, M. D., Beaven, R. B., Rao, G. G., and Mahadevan-Jansen, A. "Effect of normal variations on disease classification of Raman spectra from cervical tissue." *Analyst* **139,** 2981-2987 (2011).

11. Schiffman, M., Castle, P.E., Jeronimo, J., Rodriguez, A.C. and Wacholder, S. "Human papillomavirus and cervical cancer." *Lancet* **370**, 890-907 (2007).

12. Villar, J., Purwar, M., Merialdi, M., Zavaleta, N., Anthony, J., De Greeff, A., Poston, L., and Shennan, A. "World Health Organisation multicentre randomised trial of supplementation with vitamins C and E among pregnant women at high risk for pre-eclampsia in populations of low nutritional status from developing countries." *Brit Med J* **116**, 780-788 (2009).

13. MacDorman, M.F. "Race and ethnic disparities in fetal mortality, preterm birth, and infant mortality in the United States: an overview." *Semin Perinatol* **35**, 200-8 (2011).

APPENDIX 1

EVALUATION OF THE CERVIX DURING PREGNANCY USING RAMAN SPECTROSCOPY

This chapter includes work from a pilot *in vivo* study examining the usefulness of Raman spectroscopy to detect changes in the cervix during pregnancy. The manuscript corresponding with this chapter is currently in preparation.

A1.1 Abstract

Preterm birth is the second leading cause of neonatal mortality and leads to a number of complications including delayed development and cerebral palsy. Currently, there is no way to accurately predict preterm labor, making its prevention and treatment virtually impossible. While there are some at-risk patients, over half of all preterm births do not fall into any high-risk category. This study seeks to prevent preterm labor by using Raman spectroscopy to detect changes in the cervix during pregnancy indicative of the onset of labor. Since Raman spectroscopy has been used to detect cancers *in vivo* in organs like the cervix and skin, it follows that spectra will significantly change over the course of pregnancy. Previous studies have shown that fluorescence, due to collagen organization, decreased during pregnancy and increased during post-partum exams to pre-pregnancy levels. We believe important changes will occur in the Raman spectra obtained during the course of pregnancy. In this study, Raman spectra from the cervix of women undergoing a low-risk pregnancy were acquired. Specific changes that occur due to cervical softening and ripening were observed within the spectra.

A1.2 Introduction

Almost half a million - or one in eight - babies born in the US are preterm, leading to complications for the mother and the baby, both during birth and through further development.[1] Currently, there are no accurate ways to predict preterm labor, making its prevention and treatment virtually impossible.[2] While there are some at-risk populations for preterm birth (for example, women who have had a previous preterm birth, are pregnant with more than one child, or have uterine/cervical abnormalities), over half of all preterm births do not fall into any high-risk category.[3] Therefore, an accurate and non-invasive method of identifying women who are at risk for preterm birth is greatly needed. The impact of a successful approach would lead to fewer preterm births and an improved outcome for at-risk patients and their children.

Preterm birth is the leading cause of infant mortality, causing over 17% of all infant deaths and 75% of infants that have perinatal death are premature.[4] A successful preterm birth can still result in a wide array of complications for the mother and baby (if living), including cerebral palsy, developmental delay, visual and hearing impairment, and chronic lung disease.[5] Even with current advances in medical knowledge and an increase in research funding, the rate of preterm labor has steadily increased over the last few decades. Furthermore, the reasons for preterm labor remain vague. Various factors, from an insufficient change in collagen content in the cervix to unregulated hormone levels or infection, have been implicated to occur during preterm labor, but none have been determined as the major cause. A fundamental change must occur in the way we approach the problem of preterm labor. The immediate need is to improve the ability of physicians to recognize the onset of labor early, before physical signs are apparent, giving the physician sufficient time to implement preventive treatment options.

An accurate and non-invasive method that identifies women who are at risk for preterm birth early would have a tremendous impact on the management of care for these patients. This tool would need to incorporate many factors since it appears that a combination of factors, not just one or two, lead to preterm labor. The impact of a successful approach would result in fewer preterm births and an improved outcome for at-risk patients and their children. Preventing preterm labor even for a day is beneficial. When doctors can accurately diagnose preterm labor, they then have the option of prescribing corticosteroids or tocolytics to increase the time a fetus spends in the womb, which can greatly help brain and lung development, thus improving the odds of survival. These drugs, given at the earliest sign of preterm labor, can delay delivery from 2-7 days and reduce infant death by 30%.[5] They can also reduce the two most serious complications of preterm birth: respiratory distress syndrome (RDS) and bleeding in the brain. However, these drugs cannot be maximally utilized unless the physician is able to accurately diagnose preterm labor. A tool for decreasing the incidence of preterm birth must be able to do so regardless of the patient's race, ethnicity, or socioeconomic status.

We have demonstrated the potential of Raman spectroscopy (RS), an optical technique, to detect subtle changes in tissue biochemistry, *in vivo*, in patients, in the cervix.[6, 7] While the technology thus far has been applied primarily for cancer and precancer detection, the sensitive nature of RS indicates that it has the potential to be applied towards the specific problem of predicting cases of preterm birth. Further, RS has been applied to humans *in vivo* to detect subtle changes in tissue biochemistry associated with changes to cervical hormonal status.[6-8] Two groups of patients were recruited to this pilot study. In the first group ($n_{patients}$=41), patients were recruited during the 1st trimester of their pregnancy. One measurement was acquired during the 1st trimester, 1 during the 2nd trimester and 3 during the 3rd trimester. A final measurement was

taken at the patient's postpartum visit. A smaller group of patients ($n_{patients}$=5) was recruited for weekly measurements during their 3rd trimester and one measurement at their postpartum visit. Initial results show that many changes that occur in the cervix during pregnancy can be observed using RS. To our knowledge, this is the first report using RS to monitor pregnant patients.

A1.3 Methods

Raman spectroscopy is based on the Raman effect where energy is exchanged between incident photons and scattering molecules. When an incident photon collides with certain molecules, energy may be transferred either from the molecule to the photon or vice versa. The energy differences of the scattered photons are indicative of the molecules set into vibration. A Raman spectrum consists of a series of peaks, which represent the different vibrational modes of the scattering molecules. These peaks are spectrally narrow and molecular-specific, such that the observed peaks may be associated with specific bonds in specific molecules. Many biological molecules have distinguishable spectra, so the biochemical composition of a tissue can be determined from its Raman spectra. One particularly relevant biochemical change that occurs during pregnancy is the ripening or the softening of the cervix due to changes in collagen. This change, among other changes in elastin and glycogen, can be detected with RS.[8, 10] Other changes that RS is likely to be sensitive to are changes in collagen cross-linking, water content, and hormonal variations. In addition, biochemical changes that are triggered in preparation for labor are likely to be picked up by RS.

A1.3.1 Human Subjects

Raman spectra were collected from low-risk pregnancy patients to evaluate the ability of RS to detect the early signs of labor in a human population. Adult patients of any race or ethnicity at the Vanderbilt Clinic and Meharry Medical College Women's Clinic were included in the study. Informed written consent was obtained from each patient studied. Patient information such as age, parity, race, and obstetric and gynecological history was noted. The protocol was approved by the both Institutional Review Boards prior to the study and the physician determined if the patient is eligible to participate. A total of 41 full pregnancy and 5 weekly measurement patients were recruited to this study.

A1.3.2 Raman Data Acquisition and Instrumentation

A portable RS system (Figure A1.1, left) was used to collect Raman spectra *in vivo*. It consisted of a 785 nm diode laser (I0785MM0350MS, Innovative Photonic Solutions, Monmouth Junction, NJ), a beam-steered fiber optic probe (Figure A1.1, right, 400 μm excitation fiber, 7 200-μm collection fibers, 2.1 mm inner diameter, 785nm filtering, Emvision, Loxahatchee, FL), an imaging spectrograph (Holospec f/1.8i-NIR, Kaiser Optical Systems, Ann Arbor, MI), and a back-illuminated, deep-depletion, thermo-electrically cooled CCD camera (Pixis 256BR, Princeton Instruments, Princeton, NJ), all controlled with a laptop computer (Figure A1.1, left). The fiber optic device delivered 80 mW of light onto the tissue with an integration time of 2-3 seconds. During the measurements, all room lights and the computer monitor were turned off. A spectral resolution of 8 wavenumbers (cm^{-1}) was achieved.

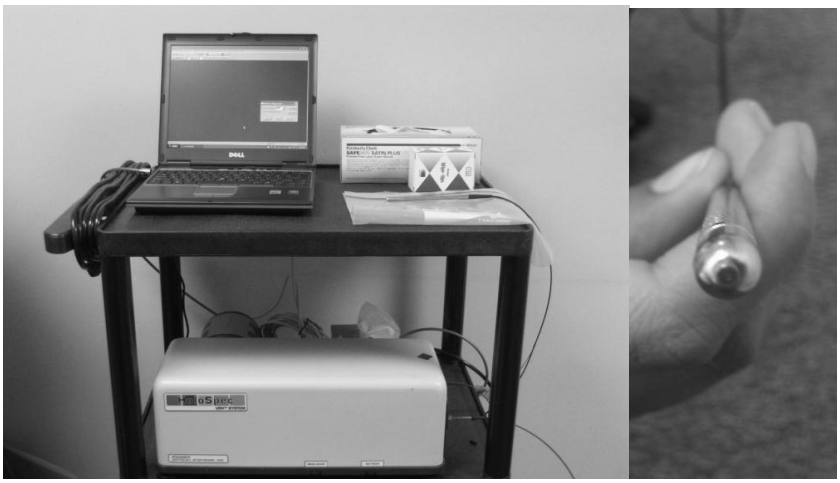

Figure A1.1. Picture of RS system used for *in vivo* measurements (left) and close-up of Raman probe (right).

Spectral calibration of the system was performed daily with a neon-argon lamp and naphthalene and acetaminophen standards to correct for day-to-day variations. A National Institutes of Standards and Technology (NIST)-calibrated tungsten lamp was used to adjust for the wavelength-dependent response of the system. Spectra were processed for fluorescence subtraction and noise smoothing using the modified polynomial fit and Savitzky-Golay methods, described previously.[12] Following data processing, each spectrum was normalized to its mean spectral intensity across all Raman bands to account for intensity variability.

The following protocol was used to acquire the Raman data: first, the cervix was exposed using a speculum and wiped with a cotton swab to remove any discharge. All *in vivo* spectral measurements (i.e. placement of the probe) was performed by the participating clinician or health care provider to maintain consistency. No additional tissue was removed. These measurements were performed during 5 prenatal visits (1 during the 1st trimester, 1 during the 2nd, 3 during the 3rd) until term and 1 postpartum visit. Patients were classified based on when they delivered their baby. Probes were disinfected completely between each measurement using standard protocols for cervical instruments. Raman spectra were measured from 3-5 areas on the

cervix, with each measurement taking 3 seconds. All spectra were calibrated and processed using methods described above. Spectral differences observed as a function of time and with the onset of labor were then characterized.

A1.3.3 Data Analysis

Sparse multinomial logistic regression (SMLR) was used to extract the important features from the Raman spectra across the various time points and use those features to classify the data. SMLR is a Bayesian machine-learning framework that computes the posterior probability of a spectrum belonging to each pregnancy time point on a labeled training set. For these analyses, a composite spectrum averaging Raman measurements from each patient at each time point was used. A range of input parameters to SMLR was tested. The settings that provided the most accurate classification while also maximizing sparsity were a Laplacian prior, a direct kernel, a lambda value of 0.01, and no additional bias term. Leave-one-patient-out analysis was performed to minimize bias.

A1.4 Results

A total of 7 patients from Meharry Medical College and 34 patients from Vanderbilt's Clinic were recruited into this study and measurements were acquired across their pregnancy. Five patients from Vanderbilt's Clinic were recruited for weekly measurements in their 3rd trimester. A representative set of spectra from one patient is shown in Figure A1.2.

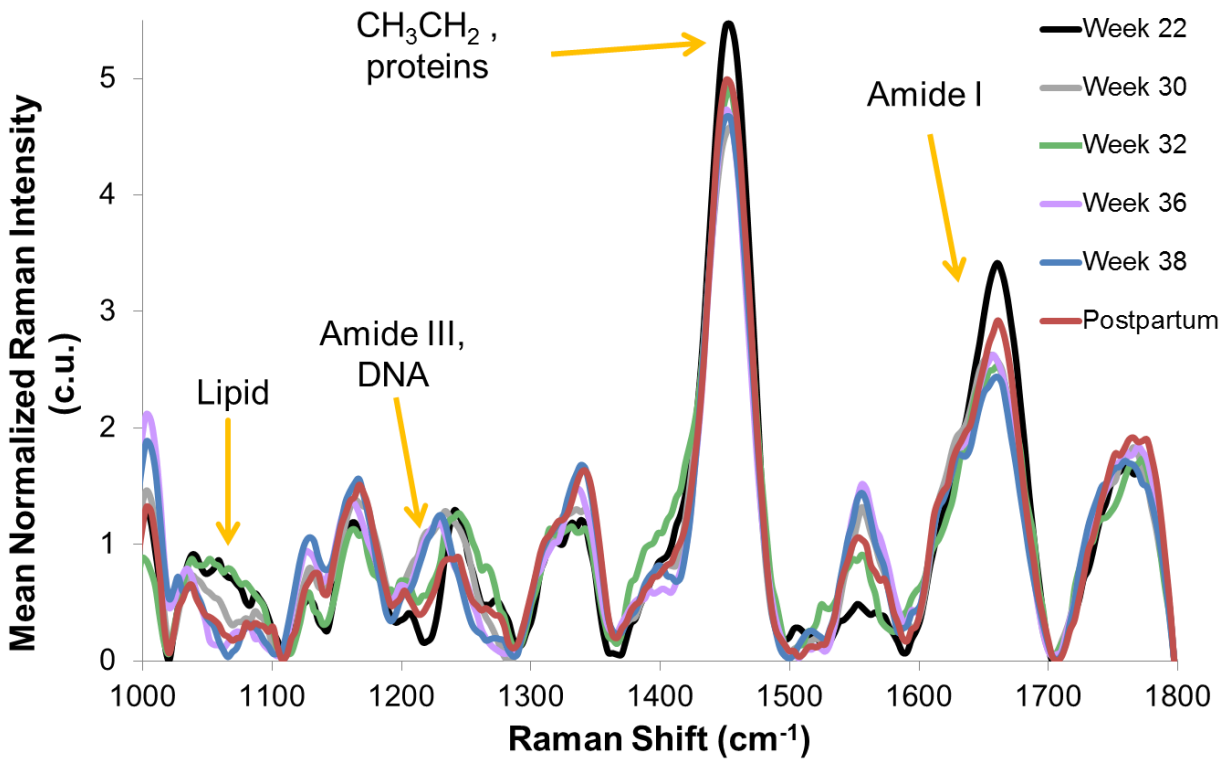

Figure A1.2 Spectra obtained from one representative patient over the course of her pregnancy.

Similar to the mouse data (Chapter 8), a spectral disintegration can be observed in the spectra acquired at later time points within pregnancy. These differences are the most prominent in the regions around 1200 cm^{-1} and around 1650 cm^{-1}. Based on previous work, these regions have been labeled as potentially corresponding to proteins, amide-I and amide-III.[8,9] All of these are important constituents of the cervix which drastically change during pregnancy, as the cervix begins to prepare for labor and delivery.[13] Many of these differences are similarly seen across the patient population to various extents (data not shown).

The classification algorithm SMLR was used to classify data across the patient group who were recruited for measurements throughout their pregnancy ($n_{patients}$=41) to determine if the regions of difference among the various time points were significant enough to be used to classify the data based on the time point during pregnancy (Table A1.1). The best classification

was obtained when all data obtained during the 3rd trimester was combined. Classifying the data based on the 4 separate time points resulted in a classification accuracy of 87%.

		Raman Classification, Output of SMLR			
		1st Trimester	2nd Trimester	3rd Trimester	Postpartum
Pregnacy Time Point (Based on Delivery Date)	1st Trimester	**82%**	6%	4%	8%
	2nd Trimester	7%	**87%**	2%	4%
	3rd Trimester	4%	5%	**88%**	3%
	Postpartum	6%	2%	1%	**91%**

Table A1.1. Confusion matrix when all data from pregnant patients was classified by SMLR. A classification accuracy of 87% was achieved.

With the weekly measurement patient population ($n_{patients}$=5), an initial analysis was conducted to visualize any important changes that occur close to the onset of labor. Spectra from multiple time points from one patient which have been subtracted from the patient's postpartum measurement are shown in Figure A1.3. There are a few areas (~1050, ~1250, and ~1610 cm^{-1}) where the measurement acquired prior to labor and delivery are significantly different compared to other time points.

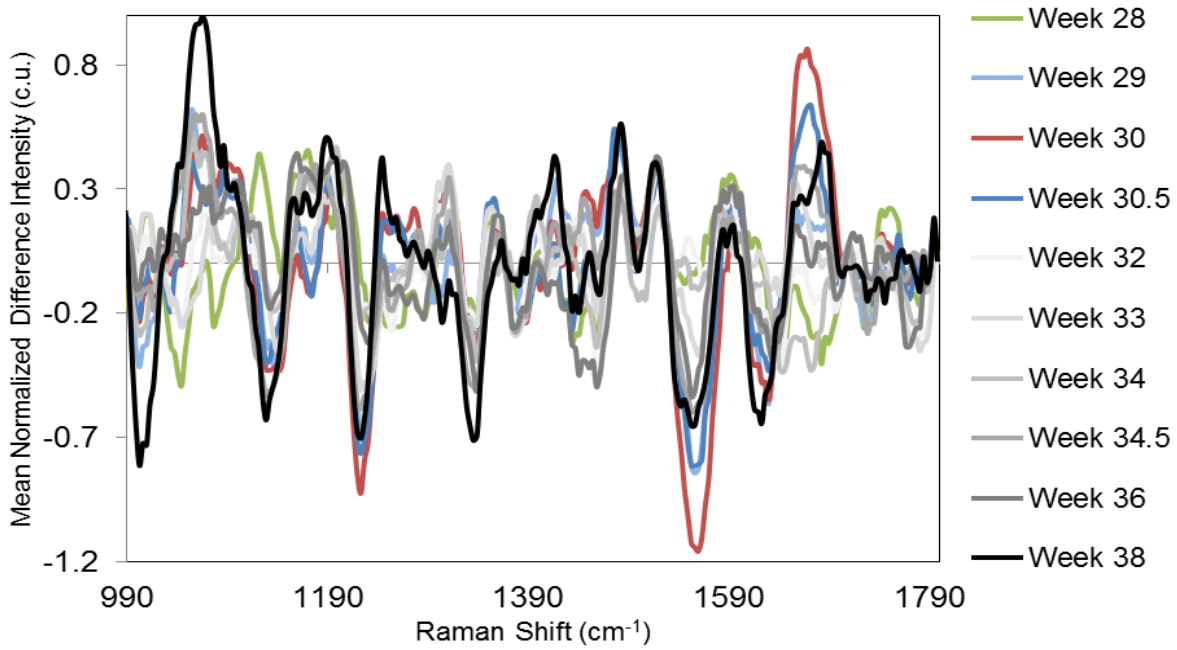

Figure A1.3. Weekly measurements from one representative patient. Each measurement was subtracted from the patient's postpartum measurement.

A1.5 Discussion

Preterm labor is a common problem in obstetrics and prenatal care, affecting over 12% of all births in the United States.[5] Even with the steady increase in research funding, this rate has not decreased. In fact, some reports are showing a slight increase in the rate of preterm births, particularly in lower socioeconomic communities.[1] A paradigm shift in how preterm labor is studied has to occur to decrease its incidence rate. Instead of looking for one or two particular biomarkers that may indicate the onset of labor, it is possible that looking at the complete picture of downstream effects may be a more useful method for recognizing symptoms of preterm labor. Using RS, we are able to see multiple factors, such as collagen, DNA, and fat content of the cervix can be measured. This wide array of data is something that cannot be found by doing assays or even looking at autofluorescence; those techniques are limited to analyzing only one or at least a few biomarkers at a time. This study was the first step in utilizing RS for detecting the onset of labor in humans.

Looking at the spectra, a lot of information is contained in the Raman data that may be useful for monitoring the changes in the cervix throughout pregnancy (Figure A1.2 and Figure A1.3). Many of the important constituents that are involved in cervical ripening as the cervix prepares for birth, such as collagen crosslinking (Amide-III) and water content (disorganization of the spectra), are significant factors that can be visualized in the spectra.[11,13] These changes are so dramatic that they are noticeable after standard processing, prior to any statistical analysis.

However, to see if these changes are indeed statistically significant, SMLR was needed to classify the data. An overall classification of 87% was achieved when the algorithm was used to classify the data as 1st, 2nd, 3rd trimester or post-partum (Table A1.1). This high classification rate demonstrates that changes are consistent across multiple patients. The 1st trimester measurements

classified with the lowest amount of accuracy. They were obtained from patients at their first visit. It is possible that this initial measurement is more affected by the patient's history, for example, if the patient had a previous cervical disease or if she had been pregnant recently. It is also important to note that measurements from the 3rd trimester were combined because patients returned at various times. Combining all the measurements from the 3rd trimester may have led to a lower classification across all categories, since it is clear that the cervix is rapidly changing as labor and delivery become closer (Figure A1.3). Nonetheless, these results suggest that the cervix in the 3rd trimester remains significantly different compared to other time points, no matter when the 3rd trimester measurement is obtained.

In this study, 80mW of light was delivered with a 400 μm excitation fiber with an integration time of 3 seconds. The thickness of the cervix at the beginning of the 1st trimester is between 4-5 cm, thinning to approximately 2.5 cm towards the end of the 3rd trimester. Previous work has shown that such a fiber optic probe interrogates approximately 1-1.5 mm into the tissue, suggesting that all photons will be absorbed by the cervix.[14] When the probe is applied to the cervix, approximately 63.7 W/cm^2 of 785 nm light is delivered. The maximum permissible exposure (MPE) of the skin is 0.3 W/cm^2; the MPE of the cornea is 1.9 mW/cm, as published by the American National Standards Institute (ANSI). While we are orders of magnitude above the MPE, we do not believe the eyes of the infant are being harmed. These MPE values are for direct exposure to either tissue site, i.e. if the probe was placed on the cornea. As the light penetrates the cervix, it becomes scattered and absorbed, which dramatically decreases the power of the light and the amount of photons that continue to the placenta and to the infant. Also, damage due to the laser has never been observed on the cervix. If data is ever acquired from the cervix during later time points in pregnancy when the cervix is thinner, we will need to ensure that light is not

reaching the retina of the fetus. Possible alternatives to the current design are to increase the size of the excitation fiber and to decrease the power of the laser.

Ideally, this system will be used to find indicators of the abnormal progression of pregnancy prior to what can be seen by health care providers. These studies and the studies that will follow, however, are focused on determining the important changes that occur during the latter part of pregnancy and during labor and delivery (future work) in low-risk patients. It is necessary to start with these later time points in low-risk pregnancies to ascertain what happens normally and which changes are the most important. Certainly, to determine if this method has any success, studies must be moved to an at-risk preterm labor patient population and data must be acquired early during pregnancy, where the maximum benefit of diagnosis and intervention can be attained. These future studies will determine how early abnormal changes can be detected. In this cohort of patients, there were no preterm births because any patient who was suspected of going into preterm birth was removed from the study. In the future, it will also be helpful to study patients who are low risk, but end up going through preterm birth.

At the time, measurements from a controlled population are still necessary to determine if the regions found in this pilot study are indicators of the onset of labor and delivery. The first step is to acquire data from more patients, both throughout pregnancy and during weekly measurements during the 3rd trimester. Next, data should be acquired from patients during labor and delivery, both when induced and naturally, to determine the most significant changes that occur. Finally, as discussed above, at-risk patients will be recruited, especially those who are currently being given progesterone treatment to delay the onset of labor and birth. Similar to the mouse studies, further analysis into the mechanical properties of the human cervix and the hormonal background of the patients should be pursued in order to correlate the Raman data to

other forms of data. The results of these studies will provide insight into the biochemical and medical basis of Raman spectra in order to have a better understanding of the role of the cervix during pregnancy and to come closer to identifying factors indicative of preterm birth.

A1.6 Acknowledgements

The authors acknowledge the National Institutes of Health (Grant No. R01-CA-095405) and a fellowship (Grant No. T32-HL7751-15) and the Lai Sulin Scholarship for EV. Special thanks go to the staff and nurses at Meharry Medical College and at the 100 Oaks Clinic at Vanderbilt University.

A1.7 References

1. Mathews, T. J. and MacDorman, M. F. "Infant mortality statistics from the 2005 period linked birth/infant death data set." *Natl Vital Stat Rep* **57**, 1-32 (2008).

2. Goldenberg, R. L., Cliver, S. P., Mulvihill, F. X., Hickey, C. A., Hoffman, H. J., Klerman, L. V. and Johnson, M. J. "Medical, psychosocial, and behavioral risk factors do not explain the increased risk for low birth weight among black women." *Am J Obstet Gynecol* **175,** 1317-1324 (1996).

3. Martin, J. A., Hamilton, B. E., Sutton, P. D., Ventura, S. J., Menacker, F., Kirmeyer, S. and Munson, M. L. "Births: final data for 2005." *Natl Vital Stat Rep* **56**, 1-103 (2007).

4. Goldenberg, R. L. and Rouse, D. J. "Prevention of premature birth." *N Engl J Med* **339**, 313-320 (1998).

5. Iams, J. D. "Prediction and early detection of preterm labor." *Obstet Gynecol* **101**, 402-412 (2003).

6. Kanter, E., Majumder, S., Kanter, G., Woeste, E. and Mahadevan-Jansen, A. "Effect of hormonal variation on Raman spectra for cervical disease detection." *Am J Obstet Gynecol* **200**, 512-512 (2009).

7. Kanter, E. M., Vargis, E., Majumder, S., Keller, M. D., Woeste, E., Rao, G. G. and Mahadevan-Jansen, A. "Application of Raman spectroscopy for cervical dysplasia diagnosis." *J Biophotonics* **2**, 81-90 (2009).

8. Mahadevan-Jansen, A. and Richards-Kortum, R. "Raman spectroscopy for the detection of cancers and precancers," *J Biomed Opt* **1**, 31-70 (1996).

9. Maul, H., Saade, G. and Garfield, R.E. "Prediction of term and preterm parturition and treatment monitoring by measurement of cervical cross-linked collagen using light-induced fluorescence." *Acta Obstet Gynecol Scand* **84**, 534-6 (2005).

10. Mahadevan-Jansen, A. Raman Spectroscopy: From Benchtop to Bedside (CRC Press, Washington DC, 2003).

11. Timmons, B. C. and Mahendroo, M. "Processes regulating cervical ripening differ from cervical dilation and postpartum repair: insights from gene expression studies." *Reprod Sci* **14**, 53-62 (2007).

12. Lieber, C.A. and Mahadevan-Jansen, A. "Automated method for subtraction of fluorescence from biological Raman spectra." *Appl Spectrosc* **57**, 1363-1367 (2003).

13. Olson, D. M., Mijovic, J. E. and Sadowsky, D. W. "Control of human parturition." *Semin Perinatol* **19**, 52-63 (1995).

14. Keller, M.D., Vargis, E., de Matos Granja, N., Wilson, R.H., Mycek, M.A., Kelley, M.C. and Mahadevan-Jansen, A. "Development of a spatially offset Raman spectroscopy probe for breast tumor surgical margin evaluation." *J Biomed Opt* **16**, 077006 1-8 (2011).

APPENDIX 2

EXPLANATION OF MATLAB TOOLS AND STATISTICAL ANALYSIS

GLMnet[1] – Generalized Linear Models with elastic net penalties

This method for classifying the Raman data relied on sparsity-promoting criterion to select the values within the spectra that contribute most highly to discriminating between classes. Multiple linear methods (linear regression, logistic regression, and multinomial regression) are used to model the Raman spectra. GLMnet then uses penalties, L1 (the lasso) and L2 (ridge regression) and the mixture of the 2 (also known as the elastic net) to separate the data into specific categories.

The advantage of GLMnet is that it incorporates multiple methods and multiple types of penalties into one algorithm. It is currently being used instead of SMLR (described below) because it utilizes many regression methods including logistic regression which is the basis of SMLR. GLMnet is more suitable for large amounts of data with higher dimensions to solve complex optimization problems.

A GLMnet package is available for download to use in R. This method was used in Chapter 6.

MRDF[2] –Maximum Representation Discrimination Feature

MRDF is a method of feature extraction that maximally extracts the diagnostic information that tends to be hidden in a set of measured spectral data. It achieves this by reducing its dimensionality through a set of mathematical transforms. Given a set of input data with spectra from different tissue types, MRDF finds a set of nonlinear transforms (restricted order polynomial mappings) of the input data that optimally discriminate between the different classes in a reduced dimensionality space. First, the input spectral data $\mathbf{x} = [x_1, x_2, ...x_N]^T$ (intensities corresponding to wavenumbers of the spectra) from each tissue type are raised to the power p' to produce the associated nonlinear input vectors $\mathbf{x}_{p'} = [x_1^{p'}, x_2^{p'}, ..., x_N^{p'}]$, which are then subject to a transform Φ'_M such that $\mathbf{y}'_M = \Phi'^T_M \mathbf{x}_{p'}$ are the first stage output features in the nonlinear feature space of reduced dimension $M << N$. In the second stage, the reduced M-dimensional output features $\mathbf{y}'_M$ for each tissue type are transformed nonlinearly to the power p to produce higher order features $\mathbf{y}'_{Mp} = [y'^p_1, y'^p_2, ..., y'^p_M]$, and a second transform Φ_K is computed so as to yield the final output features $\mathbf{y}_K = \Phi^T_K \mathbf{y}'_{Mp}$ in the nonlinear feature space of dimension K ($K \leq M$).[2]

This method was used prior to SMLR in Chapters 3 and 4.

Savitzky-Golay filter[3] – determines the smoothed value for each point in the Raman spectrum by performing a moving polynomial fit or a local polynomial regression (of degree k) on a series of values (of at least k+1 equally spaced points).

The advantage of this filter compared to other techniques (i.e. moving average filter) is that it preserves the features of the distribution such as relative maxima, minima and width, which can be reduced with other averaging techniques. In our case, using this filter preserves the Raman features while minimizing the noise within the signal.

When I processed my Raman data, I used the MATLAB function *sgolayfilt* with a polynomial order 3 and a frame size of 11.

SMLR[4] – Sparse Multinomial Logistic Regression

SMLR is a method of supervised classification that also promotes sparsity. It is a probabilistic multi-class model based on a sparse Bayesian machine-learning framework of statistical pattern recognition. SMLR's goal is to separate a set of labeled input data into its classes by predicting the posterior probabilities of their class-membership. It computes the posterior probabilities using a multinomial logistic regression model and constructs a decision boundary that separates the data into its constituent classes based on the computed posterior probabilities, following Bayes' rule. Data is assigned to a class for which its posterior probability is the highest.

For my analysis, I used the following range of input parameters: a Laplacian prior, a direct kernel, a lambda value of 0.01, and no additional bias term.

This algorithm can be downloaded directly from www.cs.duke.edu/~amink/software/smlr/ and was used in Chapters 3, 4, 5, 7, 8 and Appendix 1.

1. Tibshirani R., Hastie T, and Friedman J. "Regularization Paths for Generalized Linear Models via Coordinate Descent." *J Stat Softw* **33**, 1-24 (2009).

2. Talukder A. and Casasent D. "General methodology for simultaneous representation and discrimination of multiple object classes," *Opt Eng* **37**, 904-913 (1998).

3. Savitzky A. and Golay M.J.E. "Smoothing and Differentiation of Data by Simplified Least Squares Procedures." *Anal Chem* **36**, 1627-1639 (1964).

4. Krishnapuram B., Carin L., Figueiredo M.A.T., and Hartemink A.J. "Sparse multinomial logistic regression: Fast algorithms and generalization bounds," *IEEE T Pattern Anal* **27**, 957-968 (2005).

APPENDIX 3

ROLE OF THE STUDENT IN THE MANUSCRIPTS

Chapter 3 (summary of preliminary studies) – I am the 2nd author and 3rd author on 2 of the full-lengths manuscripts summarized in this chapter. They were published in the *Journal of Biophotonics* and the *Journal of Raman Spectroscopy* respectively, both in February 2009.

Chapter 4 – I am the co-1st author of this paper, and am responsible for a majority of the data collection and the writing. It was published in *Analyst* in June 2011.

Chapter 5 – I am the 1st author of this paper, which was published in the *Journal of Biomedical Optics* in November 2011.

Chapter 6 – I am the 1st author of this paper, currently being prepared for submission.

Chapter 7 – I am the 1st author of this paper, which is under review with the editors of *Translational Oncology*.

Chapter 8 – I am the 1st author of this paper, which has been accepted pending minor revision to the *Annals of Biomedical Engineering*.

Appendix 1 – I am the 1st author of this paper, which is currently in preparation.